EXPERIMENTAL AND NUMERICAL STUDY ON MANUFACTURING

GALLIUM NITRIDE THIN FILMS IN MOCVD PROCESS

by

OMAR DHANNOON JUMAAH

A dissertation submitted to the

School of Graduate Studies

Rutgers, The State University of New Jersey

In partial fulfillment of requirements

for the degree of

Doctor of Philosophy

Graduate Program in Mechanical and Aerospace Engineering

Written under the direction of

Yogesh Jaluria

and approved by

_____

_____

_____

_____

New Brunswick, New Jersey

October, 2019

ABSTRACT OF THE DISSERTATION

EXPERIMENTAL AND NUMERICAL STUDY ON MANUFACTURING

GALLIUM NITRIDE THIN FILMS IN MOCVD PROCESS

By Omar Dhannoon Jumaah

Dissertation Director:

Yogesh Jaluria

Gallium nitride (GaN) thin film is an attractive material for manufacturing optoelectronic device applications due to its wide band-gap and superb optoelectronic performance. The reliability and durability of the devices depend on the quality of thin films. Metal-organic chemical vapor deposition (MOCVD) process is a common technique used to fabricate high-quality GaN thin films. The deposition rate and uniformity of thin films are manipulated by controlling operating conditions and reactor geometry configurations. In this study, the epitaxial growth of GaN thin films on sapphire substrates (AL_2O_3) was carried out in two commercial MOCVD systems, a vertical rotating disk MOCVD reactor, and a close-coupled showerhead MOCVD reactor. Material characterizations have been done using Atomic Force Microscopy (AFM), X-ray diffraction (XRD), Scanning Electron Microscope (SEM), and Raman scattering to examine the surface morphology and crystal quality of GaN thin films. The growth rate and uniformity of GaN thin films are simulated based on a three-dimensional computational fluid dynamics (CFD) model. Transport phenomena and chemical kinetics of the GaN growth process are performed using a reduced chemistry model, which contains 17 gas phase, and 8 surface species participating in 17 gas phase and 17 surface reactions. Numerical simulation of the single wafer and multi-wafers

reactors have performed. A comprehensive study of the influence of operating variables, including rotation rate of the susceptor, susceptor temperature, inlet velocity, the reactor pressure, and precursor concentration ratio, on the GaN growth process is carried out. Operating parameters that have significant effects on the growth rate and uniformity of GaN thin films are identified. The reactor pressure and flow rate of trimethylgallium (TMG) have a significant effect on the deposition rate. A high-quality thin film is obtained when pure H_2 is used as a carrier gas. The high flow rate of pure N_2 gas enhances the growth of GaN thin films at high reactor pressure. However, it decreases the uniformity of the GaN thin film and promotes carbon contaminations. Thus, using an appropriate mixture of H_2 and N_2 as a carrier can improve the deposition rate and quality of GaN thin films. The inlet design has a significant effect on improving the reactant species utilization and increases the growth rate. The proper distance between the inlet and the susceptor aids to decrease the temperature gradient and improve the stability of the flow above the rotating susceptor.

The optimization of GaN deposition rate and uniformity in the MOCVD process have represented in a surrogate model. Surrogate-based optimization is an effective technique to alleviate expensive computation experiments with fewer sample points. The response surface from simulation data with minimum error variance estimation is generated using the Kriging method. The optimization of GaN deposition is performed as a deterministic problem, without taking into consideration the uncertain input parameters and the corresponding output response. Also, the optimization under uncertainty of design variables is considered. Multi-objective optimization using a multi-objective genetic algorithm carried out to find optimal solutions. The results reveal that the proposed optimization formulation can generate Pareto frontier of conflicting objectives, thus providing reliable trade-off solutions for decision-makers.

Acknowledgment

Dedication

To whom always on my mind, and forever in my heart
my dear brother, Mohammed

Table of contents

List of Tables

List of Figures

List of Acronyms and Symbols

TMG	Trimethyl-gallium	$(GaCH_3)_3$
MMG	Monomethyl-gallium	$GaCH_3$
V/III	The volumetric ratio of NH_3 to TMG	
SLM	Standard liter per minute	
$\dot{R}_1$	Volumetric rate of species	$(kg/m^3/s)$
M_i	The molecular weight of the species	$(kg/kmol)$
D_i^T	Thermal diffusion coefficient	(m^2/s)
ρ	Density	(kg/m^3)
M	Dynamic viscosity	$(kg/m.s^{-1})$
R	Gas constant	$(j/kmol.K)$
K	Thermal conductivity	$(W/m/K)$
Ea	Activated energy	$(kj/kmol)$
T	The temperature	(K)
ω_i	Mass fraction of species	
D_{ij}	Multicomponent diffusion coefficient	(m^2/s)
A	Pre-exponential factor (consistent unit)	

Chapter 1

INTRODUCTION

1.1 Background

Gallium nitride (GaN) is an attractive material for manufacturing optoelectronic devices due to its large direct band-gap, high thermal stability, high breakdown voltage, and superb optoelectronic performance. The reliability and durability of the devices depend on the quality of thin films. Various manufacturing techniques such as molecular beam epitaxy (MBE) [1], pulsed laser deposition (PLD) [2], and metal organic chemical vapor deposition (MOCVD) [3] have been used for growing GaN thin films

MOCVD is an essential technique in the semiconductor industry for manufacturing unique materials and electric devices. It has many advantages such as faster growth rate, good reproducibility, large deposition area, and conformal deposition [4]–[6]. Many studies have been performed by using CVD to study the deposition rate of different semiconductor materials such as silicon [7], silicon carbide [8], diamond [9] and recently GaN [10]. The growth rate and uniformity of GaN thin films are important factors in the design of MOCVD systems.

Much work has been done to improve the MOCVD process to carry out mass production at low cost, but there is a compromise between quality and the quantity. Many industries are integrating geometric reactor design to get higher quality and higher deposition rate of thin films. However, growth rate, uniformity, and throughput of GaN thin films are still some of the major problems that industry is facing nowadays [6], [11], [12]. These factors are related to operating conditions such as substrate temperature, inlet flow rate, reactor pressure, susceptor rotation, carrier gas, and precursors concentration, as well as the design of the MOCVD reactor. The flow characteristic and thermal field in the MOCVD reactor can be manipulated by controlling operating conditions and

reactor geometry. Thus it is required to control these parameters precisely to obtain an undisturbed laminar flow, uniform temperature distribution along the wafer, and even distribution of precursors inside the MOCVD reactor.

1.2 Overview of Gallium nitride (GaN) applications

Recently, wide band-gap (WBG) semiconductor materials, such as Gallium nitride (GaN), Silicon carbide (SiC), and related materials, have attracted strong attention for microelectronic and optoelectronic device applications. The electronic bandgap represents the energy gap between the valence band and the conduction band in solid materials. WBG-based devices have a smaller size than the equivalent silicon-based device, and they are capable of tolerating high operating temperatures. GaN has sophisticated properties such as high thermal stability, robustness in harsh environments, high electron velocity, high breakdown voltage field (5×10^6 V/cm) and direct wide bandgap (3.39 eV)[16,17]. GaN thin films are used for many electronic applications that operate at high frequency and high-temperature environments, as well as for high electronic power devices [2,3]. It is recognized as an essential material to produce promising and high value-added products such as light emitting diodes (LEDs), field effect transistors (FETs), laser diodes (LDs) [1].

LEDs are compact light sources that consume low power and thus dissipate a small amount of heat. Compared to conventional lighting devices, LEDs deliver several hundred-lumen outputs with a cost-effective and safe alternative. Different sizes and shapes size of LED chips can be sliced from the wafer that is produced by the MOCVD process [17], see Figure 1.1. In 1993, Nakamura et al. [1] deposited a high-quality GaN thin film which was later used in various electronic devices such as a short wave LD, and a blue LED. LED depends on the p-n junction that is an active interface layer used to provide holes and electrons layers from the p-type and n-type layers. During the growth process, GaN layers are doped by silicon (Si) as a donor or magnesium (Mg) as an acceptor to fabricate n-type or p-type GaN layer, respectively [2].
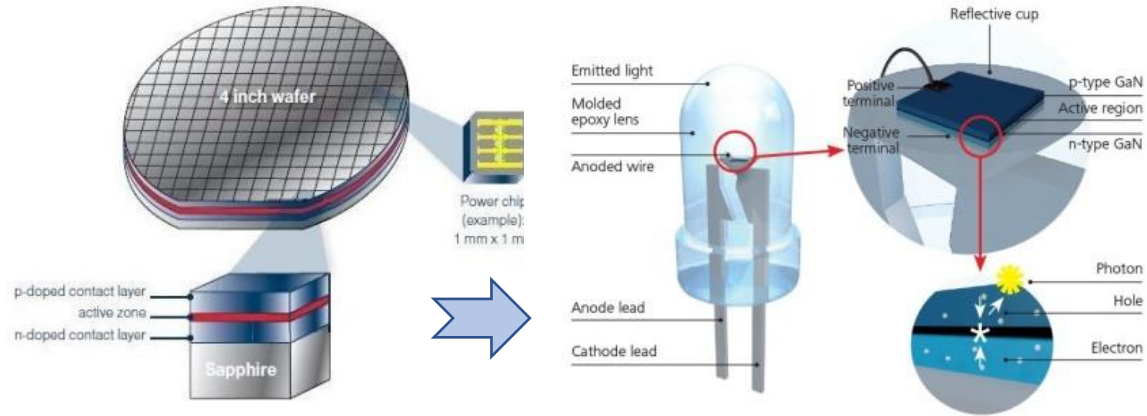
Figure 1.1. Schematic diagram of the structure of a light emitting diode (LED) [17]

Currently, many efforts are going on to develop and produce high brightness and efficient white LED. The III-V nitrides are suitable for optoelectronic applications. GaN and its alloy systems are characterized by large direct band-gaps which makes them suitable for manufacturing LEDs that are capable of emitting light over a wide range of wavelengths covering most of the range of the electromagnetic spectrum, from blue to ultraviolet (UV). GaN can be alloyed with indium (In) and aluminum (Al) to form ternary alloys that have wide bandgap values. The bandgap and the electrical properties of GaN can be tunable by forming continuous alloy systems with Indium (In) and Aluminum (Al) to produce a wide range of bandgaps (1.9–6.2 eV) [19]. The produced wavelength (λ) of light is inversely proportional to the band gap energy (Eg) as given by the following equation [18]:

$$\lambda\ (nm) = \frac{1.243}{E_g(e.V)} \qquad\qquad 1\text{-}1)$$

The storage capacity is increased by decreasing the spot size of the laser diode (LD) beam, which depends on the wavelength. That means that GaN-based LDs help to store more data on storage devices, as shown in Figure 1.2. These features are essential for enhancing the storage capacity of high-density optical storage applications (CD, DVD, and Blue-ray) [19]. Blue LD has high brightness, good directionality, and excellent monochromaticity. It is used in the 3D printing

technique instead of the traditional UV light source. Blue LD enhances the polymerization efficiency and deep penetrations in photosensitive composite resins containing particles. Furthermore, the outstanding advancements of application of blue LDs for visible light curable resin-based 3D printing will provide lots of applications in various fields [20].
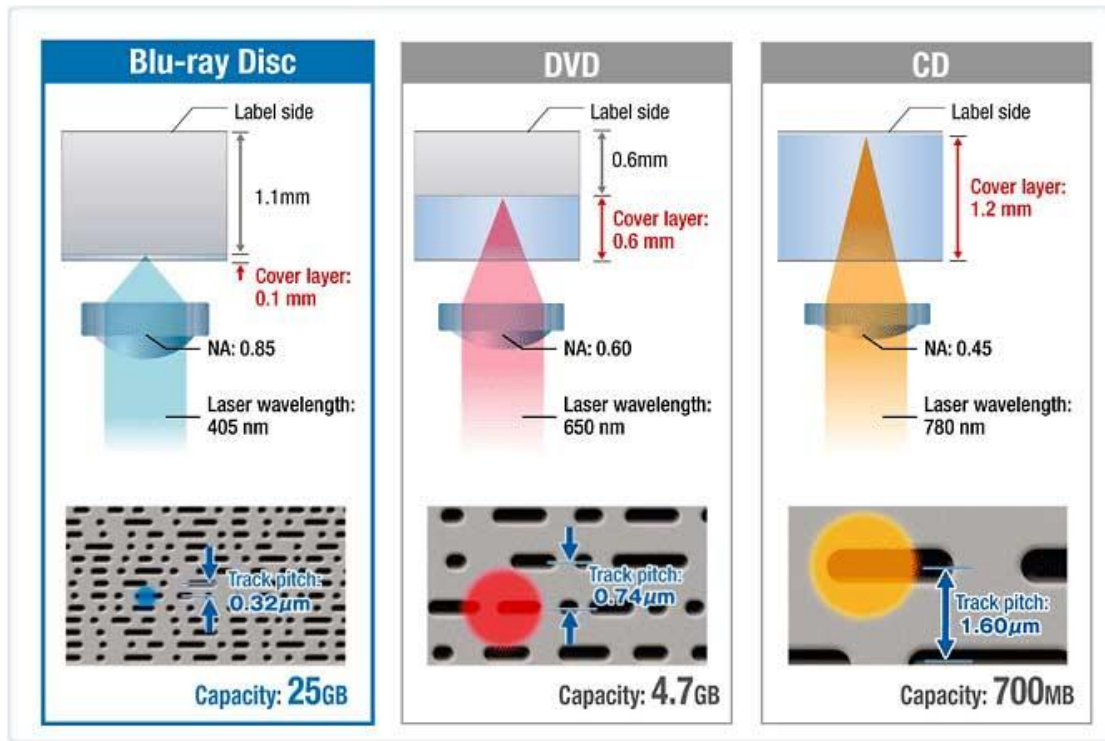
Figure 1.2 Comparison of spot size for CDs, DVDs, and Blu-Ray Discs [19]

GaN Nanowires (NWs) have attracted much interest because of their potential for the fabrication of optoelectronic devices. GaN NWs are produced by the MOCVD process [21]. So far, MOCVD is a widely used technique for GaN thin film deposition. The MOCVD process has many advantages such as controllable in-situ doping, large area deposition, and high growth rate. Also, by changing growth conditions, the MOCVD process is used for growing different types of layers, including epitaxial, amorphous, polycrystalline films, and nanostructures. The performance of semiconductor devices crucially depends on the quality of the produced thin film.

1.3 Metal-organic chemical vapor deposition (MOCVD)

MOCVD involves the formation of a thin film on a heated substrate surface via chemical reactions of vapor-phase precursors. MOCVD provides control and flexibility to grow high-quality GaN thin films. In general, MOCVD includes complex chemical reactions coupled with heat transfer, mass transport, and gas flow dynamics. Figure 1.3 shows fundamental aspects involved in a CVD process such as thermodynamics and chemical kinetics. Thermodynamics describes the driving mechanisms behind epitaxial growth and maximum growth rate of the thin film. Chemical kinetics determines the rate of chemical reactions during the process. Also, the figure describes the chemical reactions that occur both in the gas phase and at the solid surface [22].
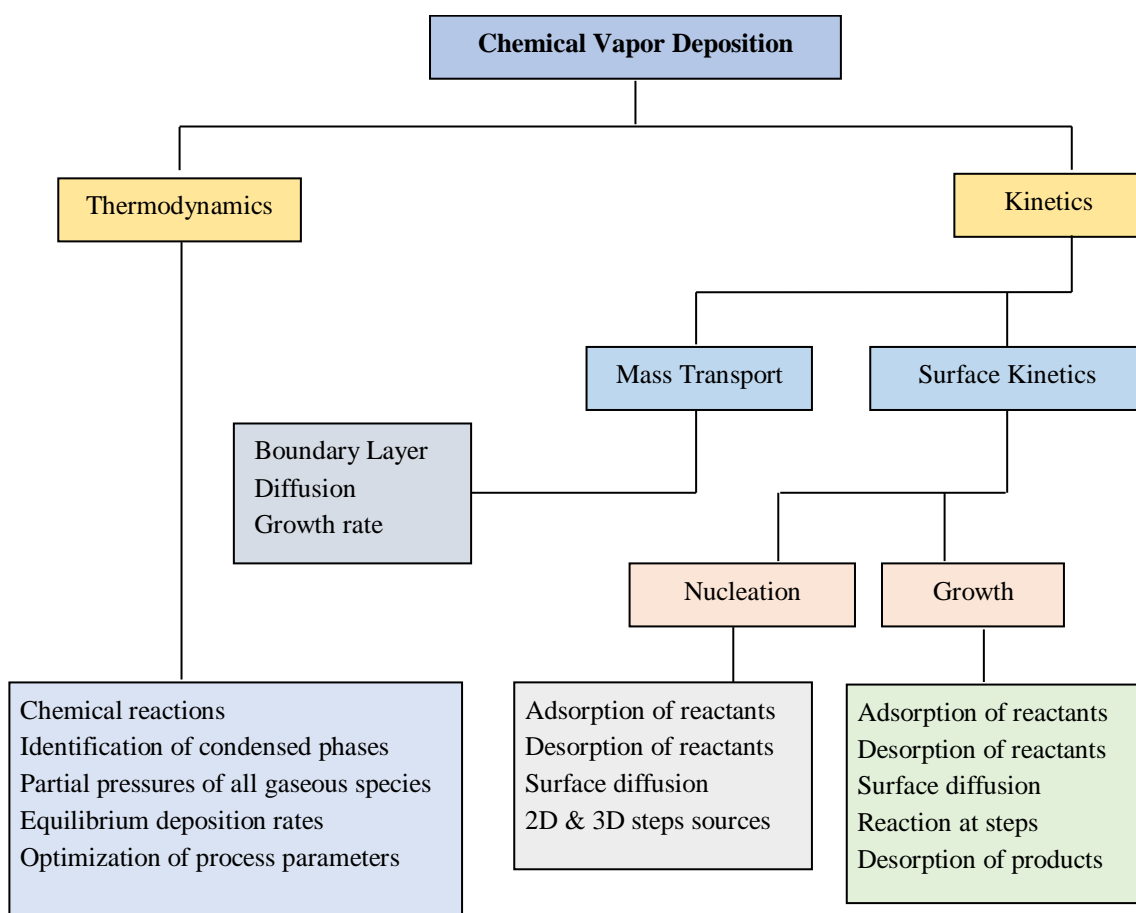
Figure 1.3 Basic principles involved in Chemical Vapor Deposition [22].

Various ways are used to classify the CVD process such as low and high temperature, low and high pressure, cold and hot wall, close and open system [22]. Moreover, CVD can be categorized according to the reactor configurations such as a horizontal reactor, vertical stagnation flow reactor, pancake reactor, and barrel reactor, as shown in Figure 1.4 [23].
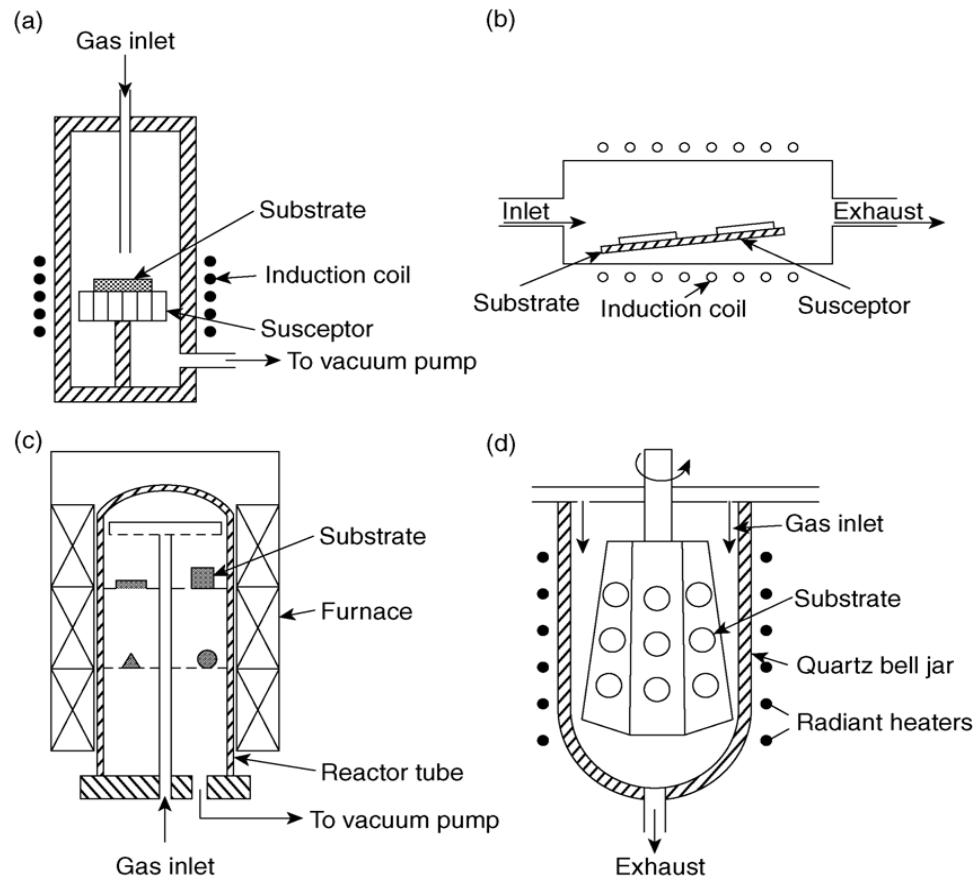
Figure 1.4 Examples of configuration reactors: (a) vertical reactor, (b) horizontal reactor vertical hot-wall reactor, and (d) barrel reactor, adapted from [23]

1.4 Growth mechanisms

Irrespective of the type or the configuration, Figure 1.5 shows a fundamental transport process and reaction steps that occur during the deposition in the MOCVD process. In typical GaN-based MOCVD reactor, N_2, H_2, and NH_3 are major gas species. A carrier gas is used to bring metal-organic (MO) precursors into the reaction chamber and deliver products of reactions out the system.

The metal-organic (MO) precursors such as trimethyl-gallium TMG will diffuse through the mixed atmosphere to reach the wafer surface. Near to the wafer surface, the MO precursor starts decomposing into various reactant species that diffuse laterally on the surface and incorporated in suitable crystal sites. These steps are summarized as follows [13], [14]:

➤ Homogenous chemical reactions in the gas phase from precursors.

➤ MO precursors diffuse through the gaseous boundary layer to the substrate surface.

➤ Reactive gas species are absorbed on the substrate surface.

➤ Surface diffusion occurs on the substrate surface lead to growing the thin film.

➤ Desorption of gaseous byproducts.
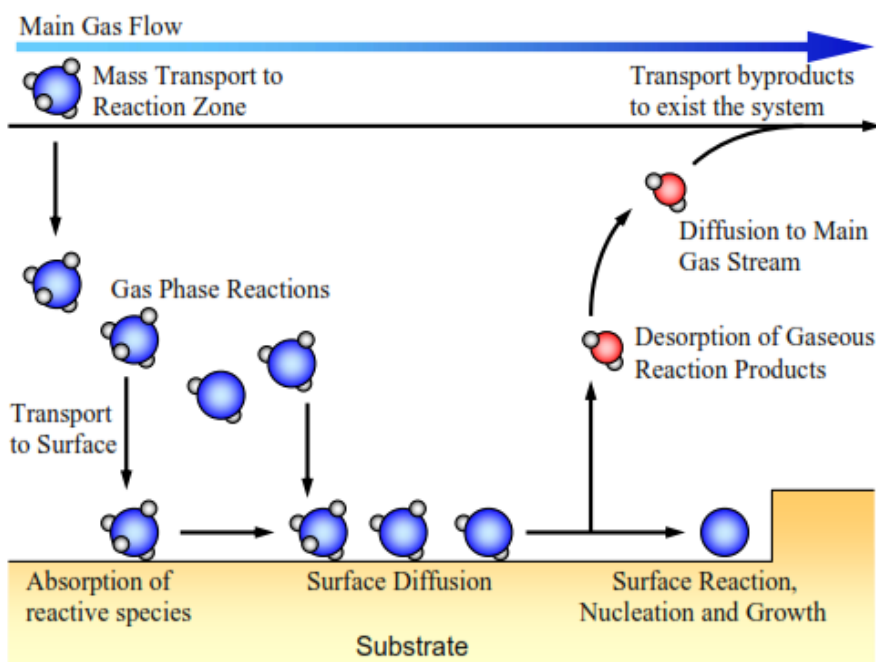
Figure 1.5 Schematic diagram represents fundamentals steps in a horizontal CVD reactor, adapted from [23]

1.5 Growth modes

Thermodynamic and chemical kinetics mechanisms control the growth of thin films. The thin film is produced via the heterogeneous gas-solid chemical reactions that take place at the substrate's

surface. The film grows epitaxially where a single-crystal film formation is extended on top of a crystalline substrate. The term "epitaxy" comes from the Greek "epi" meaning "above", and "taxis" meaning "in an ordered manner". Epitaxy can be classified into homoepitaxy and heteroepitaxy growth. The homoepitaxy where the film and substrate are the same material. The heteroepitaxy where the film and substrates are composed of different materials [25]. When the thin film is grown on a foreign substrate wafer, it can be classified into three main categories modes [26]:

➢ 2D layer-by-layer growth mode where film atoms strongly bound to the substrate rather than to each other.

➢ 3D island growth mode where film atoms are more strongly bound to each other than to the substrate.

➢ Layer-by-layer plus island growth mode where 3D islands grow on top of 2D layers.
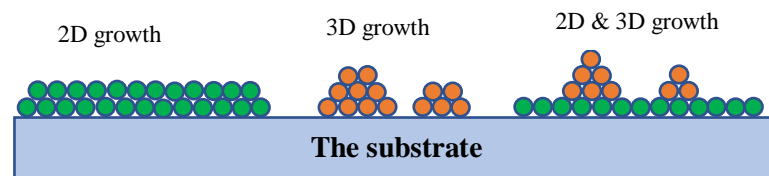
Figure 1.6 Schematic sketch represents the main growth modes

The substrate is a single crystal wafer that is manufactured from single-crystal ingots that are pulled or cast from molten material. The crystallographic direction of the wafer is determined by the cutting direction of the ingot related to the major axis of the ingot, see Figure 1.7 (a). Substrate wafers are described as having their surface parallel to a given crystallographic plane or surface orientation [27]. GaN has a stable wurtzite crystal structure that is described by two interpenetrating hexagonal close-packed lattices (HCP) with parameters c = 5.185 Å, and a = 3.189 Å, as shown in Figure 1.7 (b). When the thin film and substrate crystal are identical, the lattice parameters are perfectly matched, and there is no interfacial bond straining [25].
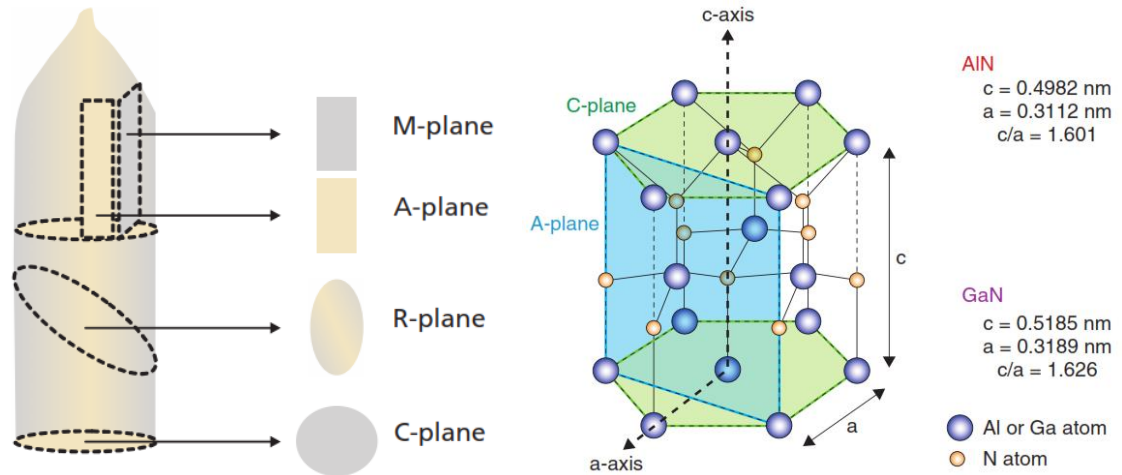
Figure 1.7 (a) Schematic diagram shows wafer cutting from ingots [27] and (b) Crystal structure of Gallium Nitride (GaN) [18].

1.5.1 The lattice mismatch

The lattice mismatch describes the relationship between the thin film and the wafer substrate across the interface. When GaN thin film is epitaxially grown on foreign substrates including silicon carbide (SiC), Silicon (Si), and Sapphire (Al_2O_3), there is a lattice mismatch between GaN crystal structure and substrate wafer crystal structures, see Figure 1.8. There are significant lattice mismatch (17%) and an incompatible thermal behavior between the GaN thin film and Si substrate, making the GaN crystal structure strain locally to match the Si structure in the early stages of growth.

As a result, it is difficult to grow high-quality GaN thin films on Si substrates. SiC is a promising substrate with its 3.5% lattice parameter mismatch, but the high cost hinders it to be a commonly used substrate. On the other hand, Sapphire (Al_2O_3) is by far the most common commercially used substrate for GaN thin films based devices [28]. However, it is required to compensate the 16% lattice mismatch between GaN and c-plane (Al_2O_3) wafer to get high crystalline quality. Figure 1.8 compares the material properties of GaN with those of the prospective substrate materials, together with the lattice mismatch and the thermal expansion mismatch [29].
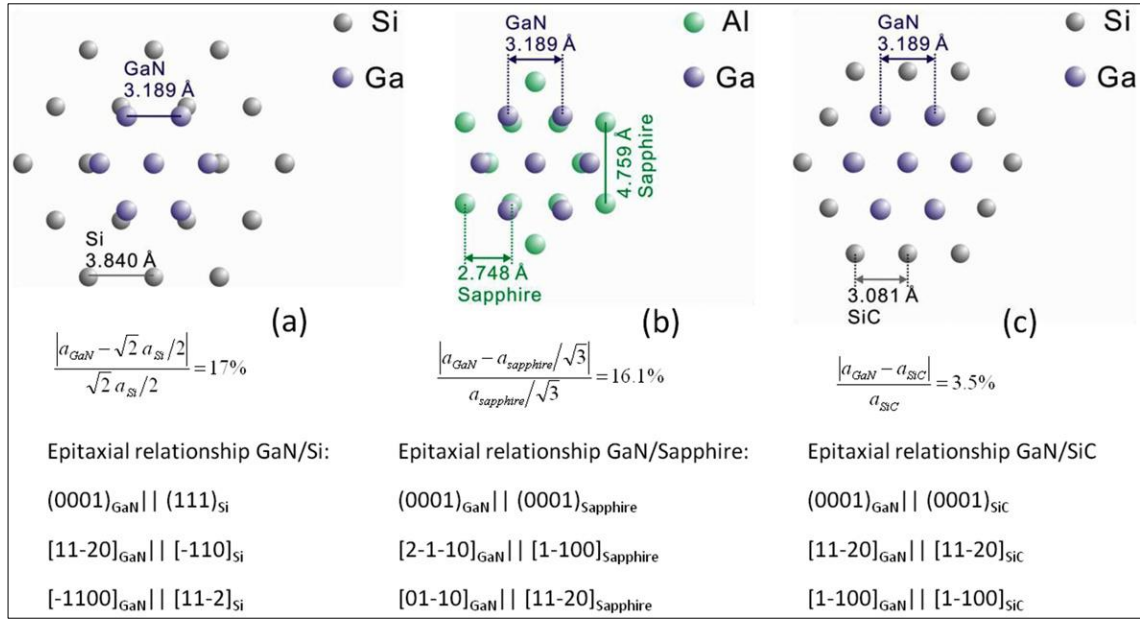
Figure 1.8 Schematic diagram shows the lattice mismatch between GaN layers and substrates (a) Si, (b) Al$_2$O$_3$, and (c) 6H-SiC [29].

Table (1-1) The lattice and thermal properties of GaN and the prospective substrates, adapted from [29].

Material	GaN	AlN	Sapphire	6H-SiC	Si
Lattice constant (°A)	a=3.189 c=5.185	a=3.112 c=4.982	a=4.759 c=12.991	a=3.081 c=15.117	a=5.431
Lattice mismatch	--	-2.5%	-16%	-3.5%	+17%
Thermal expansion coefficient (10^{-6}K^{-1})	a=5.59 c=3.17	a=5.27 c=4.15	a=7.3 c=8.5	a=4.46 c=4.16	a=2.6 c=2.6
Thermal expansion mismatch (a)	--	-34.7%	-23.4%	-25.3%	-115%
Thermal conductivity (W cm^{-1}K^{-1})	4.1	5.9	0.41	4.9	1.3
Melting point (K)	2791	3487	2303	3102	1690

Due to incompatibility in lattice parameters and thermal expansion coefficients many defects such as vacancies, threading dislocations (TDs), stacking faults, twins, cracking in layers, grain boundaries, micropipes in addition to biaxial strains, are generated during the heteroepitaxial growth [30]. The presence of defects in GaN thin films is undesirable because it degrades both the electrical and optical properties of devices.

1.6 Buffer layers

When GaN thin films are grown directly on sapphire (Al_2O_3), a three-dimensional island growth mode occurs which degrades the thin film quality. In this situation, film atoms bond to each other more than the bond to the substrate. Furthermore, GaN does not wet the sapphire (Al_2O_3) at the high growth temperature. Some techniques such as two-step deposition process and epitaxial lateral overgrowth (ELO) [31] have been used to improve the quality and minimize the structural defects in the thin film growth. Two-step deposition process [32] involves depositing intermediate layers such as GaN buffer layer [33], AlN buffer layer [5], or SiNx buffer layer [34] on the sapphire (Al_2O_3) substrate at low-temperature. Then the GaN thin film grows at high-temperature on the top of the buffer layer. When an intermediate layer of GaN is grown onto the substrate, it may promote the wetting of the sapphire (Al_2O_3) substrate surface, and this reduces the mismatch between both lattices [27].

The basic idea of ELO is to filter out the defects by employing the dielectric mask. Figure 1.9 shows the schematic diagram of the ELO process. First, a thin planar GaN template is grown on substrates followed by deposition of a dielectric (SiO_2 or SiNx) mask by plasma-enhanced chemical vapor deposition (PECVD) reactor. By using standard photolithography, a set of parallel stripes is defined on the GaN template [35]. From the openings (window) between the set of parallel SiO_2 strips, the GaN layer is regrown vertically and laterally over the SiO_2 strips until the lateral growth fronts coalesce to form a continuous layer as shown in Figure 1.9. Then a high-temperature GaN thin film is grown. The dislocation density reduces dramatically in the portion of the thin film that is grown laterally over SiO_2 strips [31]. However, ELO requires an extra procedure for preparing a dielectric mask.
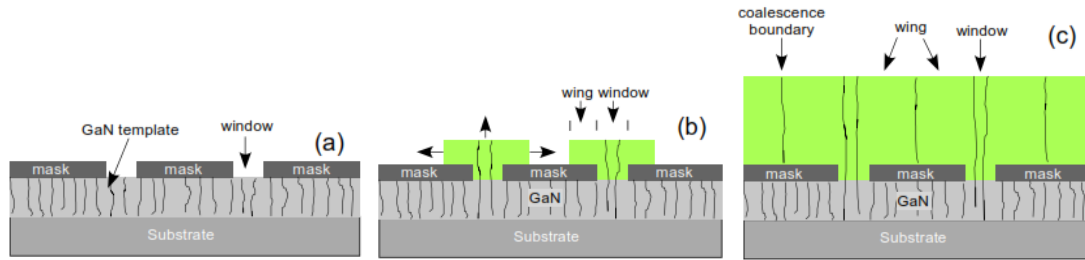
Figure 1.9 Schematic for an ELO process: (a) stripe-shaped mask, (b) the GaN thin film starts growth at the window regions, and (c) GaN thin film expands both vertically and laterally adapted from [35]

1.7 Threading Dislocations

During the deposition process, threading dislocations (TDs) usually are initiated in the thin film due to incompatible lattice constants and thermal expansion coefficients between GaN and foreign substrates. Dislocations disrupt the long-range order of the crystal lattice. Dislocations are considered to have misfit components that form an array propagates through the thin film from the layer-substrate interface to the surface [27]. Dislocations can be characterized by using Burgers vector (**b**). Thus, **b** represents the magnitude and direction of the lattice distortion resulting from a dislocation in a crystal lattice. There are three types of TDs are associated with a local lattice distortion: edge, screw, and mixed dislocations.

➢ edge dislocations (**b** = 1/3 <11-20>) lattice twist;

➢ screw dislocations (**b** =<0001>) lattice tilt;

➢ mixed dislocations (**b** = 1/3 <11-23>) both.

In edge dislocations, Burgers vector (**b**) is perpendicular to the line direction of dislocation. In screw dislocations, **b** is parallel to the line direction of dislocation. Burgers vector (**b**) lies at an acute angle related to the line direction of dislocation in mixed type dislocations [36]. Usually, the edge dislocation is predominant in the GaN thin film growth. The edge dislocations have a state of plane strain so they will distort the lattice plane indices (hkl) with either h or k nonzero. The pure

screw dislocations have a pure shear strain field so they will distort all (hkl) planes with l nonzero. High dislocation density is undesirable for high-performance devices [29]. The high dislocation density in the GaN thin films can affect the performance and the life of GaN-based optoelectronic devices by three mechanisms [37]:

➢ serving as nonradiative recombination centers for electrons and holes leading to heat generation instead of optical emission;

➢ introducing fast diffusion along the dislocation lines, smearing out quantum wells and shorting p–n junctions;

➢ disturbing the epitaxial growth front, so that atomically flat structures cannot be obtained.

Analyzing the growth mechanism of GaN films helps to interpret the relationship between thin film quality and threading dislocations (TDs). The nature of TDs in thin films can be ascertained using the diffraction contrast analysis such as diffraction contrast imaging in transmission electron microscopy (TEM) and dislocation selective etching techniques. However, these techniques have limited capacity for investigating the influence of dislocations on electronic materials/devices due to the required time-consuming, destructive sample preparation, and limited information on the spatial mapping of dislocations [31]. XRD-method has nondestructive nature, high strain sensitivity. It is considered a rapid analysis tool to represent the results and to estimate the density of TDs [32–34]. The density and distribution of defects in GaN thin films are related to substrate types, growth techniques, growth conditions, flow field characteristics, and thermal distribution.

1.8 Growth conditions

The MOCVD process involves transport phenomena such as momentum, heat transfer, and mass diffusion, as well as chemical reactions [7]. Thus, controlling operating conditions and reactor geometry configurations can affect the quality of the thin film. The high structural quality, fewer defects, and very smooth surface of GaN thin films are critical factors for high-performance GaN-

based devices. In the market, there is a trend toward producing large wafer diameter of thin films with high uniformity and deposition rate. Although many efforts have been made to control the growth rate and uniformity of GaN thin films, it is still a challenge in the semiconductor industry [19]–[21].

Many studies have investigated the influence of growth parameters such as the susceptor temperature [46], the growth pressure [36], [37] the rotating speed of substrate [49], NH_3 flow rate [38], V/III ratio [50] on the quality of thin films structures in MOCVD process. Therefore, there is a need to understand the effects of changes in growth conditions in the MOCVD process the surface morphology and microstructure of GaN thin films.

1.8.1 Effect of susceptor temperature

The temperature is one of the critical parameters in the MOCVD process, as all species properties and chemical reactions are highly dependent on it [17]. Surender et al. [46] have studied the effect of growth temperature (680-760 °C) on the systematic variation of material characterization of InGaN/GaN samples that are grown in a horizontal MOCVD reactor. Increase in the growth temperature from 680 °C to 760 °C was found to lead to a high crystalline quality and smooth surface. Yu et al. [51] studied the effect of growth temperatures (370-1050 °C) on the crystallinity and surface morphology of GaN thin films grown in an atmospheric, horizontal MOCVD reactor using a low flow rate of triethylgallium (TEG) and ammonia (NH_3) as precursors and helium (He) as the carrier gas. The surfaces of GaN thin films deposited on sapphire (Al_2O_3) substrate at a temperature below 500 °C were smooth and specular, but they degraded at higher temperatures. The temperature range (527-977 °C) is typical for growing GaN thin films in most MOCVD [52]. Empirical studies have identified three regions of GaN growth by MOCVD process: surface kinetically-limited, mass transport-limited (diffusion-limited), and desorption-limited regimes [53]. The kinetically-limited regime at temperatures below 530 °C, the diffusion-limited regime at

moderate temperatures ranging from 530 °C to 970 °C, and the desorption-limited regime at temperatures above 970 °C. With low temperature, the growth rate is limited by the surface reaction rate.

For example, the growth rate of the GaN buffer layer that is grown at a temperature range (450-550 °C), will increase significantly for the same amount of precursors by increasing the temperature. When the temperature increases further, the surface reaction rate will be high enough where the growth rate becomes limited by the diffusion rate of the reactant species onto the wafer surface [54]. At higher temperature, reactants species desorb from the wafer surface due to decomposing the GaN layer and thus declines the growth rate. Furthermore, higher substrate temperature increases homogenous reactions in the gas phase resulting in the degradation of surface morphology.

1.8.2 Effect of reactor pressure

At low reactor pressure, the gas inlet velocity increases results in increasing the mass diffusion coefficient of the reactant gases. Under moderate pressure (150-760 Torr), where the deposition is limited by the mass transport of reactants, reactants need to diffuse through the boundary layer before arriving at the deposition surface [55]. Xian et al. [47] observed an improvement in the electrical and optical properties of the p-GaN layer that is grown on 2-inch c-plane sapphire (Al_2O_3) substrates by increasing growth pressure up to 300 Torr in closed coupled showerhead (CCS) MOCVD system. When the growth pressure is increased, the concentration of magnesium (Mg) is reduced and leads to high carrier mobility. Increasing pressure provides more active precursors atoms on the wafer surface. However, when it increased to near the atmospheric pressure, this leads to form more gas-phase adducts and decrease the growth rate [56].

In general, the growth rate of GaN is a function of growth pressure due to the cluster formation in the vapor-phase [57]. Ra et al. [21] revealed that the diameter and size of GaN nanowires (NWs)

could be controlled by changing growth pressure. Increasing the growth pressure up to 600 Torr leads to growing regular shape of GaN NWs that are normally orientated on the substrate. GaN NWs would be more useful for the manufacturing of electronic devices. From the above observations, it is concluded that the variation in the reactor pressure influences the growth rate and the uniformity of the thin film. Further investigations are required to optimize the reactor pressure.

1.8.3 Effect of rotation rate

The rotation rate is beneficial to enhance growth rate due to decreasing the residence time of species in the gas phase, and more rapid arrival of the species at the rotating susceptor surface. Following the concept of the boundary layer, the gas in contact with the susceptor's surface is assumed to move at the same rotation speed as the spinning susceptor. Hence as the gas flows vertically toward the rotating susceptor, it is dragged by the susceptor to spiral down and eventually rotate outward horizontally. Mostly, the downward pulling force of the susceptor helps to overcome the natural convection effect of a heated susceptor surface [55]. Mitrovic et al. [11] recommended that either reduce the chamber pressure or raise the susceptor rotation speed, to make GaN thin film growth rate more even. Wang et al. [49] investigated the influence of rotation speed of substrate on the growth mechanism of InGaN/GaN multiple quantum wells (MQWs) grown by MOCVD system. Different Indium (In) concentration layers within one well of the MQWs were observed at low-speed rotation (5) rpm. Increase in the rotation speed to (20) rpm enhanced the uniformity of (In) concentration layer and led to a good crystal structure.

The high rotation speed of the susceptor increases the axial velocity magnitude and reduces the thermal boundary layer thickness. The thinner the boundary layer, the larger the gradient and diffusion flux of metal-organic species onto the wafer [54]. As a result, the rotation rate is essential

for improving the stability of flow pattern and suppressing the vertical vortices that are induced by the high-temperature gases near the hot susceptor surface.

1.8.4 Effect of V/III concentration ratio

The (V/III) is the volumetric ratio of ammonia (NH_3) flow rate to metal-organic precursors flow rate, such as trimethylgallium (TMG), or triethylgallium (TEG). It is a crucial factor in the growth mechanism of GaN thin films in the MOCVD process. The growth of high-quality GaN thin films requires adequate amounts of Ga and active N species near the heated substrate surface. Niebuhr et al. [50] studied the effect of variation of V/III ratio in the range (150-2500) on the growth rate of the GaN thin film on the sapphire substrate using horizontal MOCVD reactor at atmospheric pressure. At low V/III ratio where TMG is kept constant, while the NH_3 flow rate is varied. At low NH_3 flow rate, both the GaN growth rate and carbon content at the substrate interface were increased. Briot et al. [58] showed that for all the samples grown at 980°C, the morphologies were smooth, mirror-like, except at the lowest V/Ill molar ratio (equal to 1000), where the layer exhibited a hazy surface. Besides, the growth rate is increased by increasing V/III ratio up to 5000; then it slightly decreases with increasing the ratio further. The lowering of growth rate may be due to the dilution effects as high NH_3 flow rate leads to decrease in the partial pressure of triethylgallium (TEG), and also homogeneous reactions in the gas phase which consumes TEG precursors.

Suresh et al. [48] investigated the effect of variations NH_3 flow rate on the concentrations of defects and dislocations of the GaN layer grown by MOCVD. The results showed that increasing NH_3 flow rate leads to an increase in both the density of edge dislocations and gallium vacancy related defect points, and decrease the density of screw dislocations. Typically, the growth rate depends on the TMG flow rate as NH_3 is oversupplied. The surface reaction rate is assumed to be large enough, so the vapor pressure of the MO precursor is zero on the wafer surface. This will result in a gradient of MO concentration from the high-concentration region in the gas phase toward the low-

concentration region at the wafer surface. The gradient generates a diffusion force of TMG species [54]. The convection of the total reactor gas flow is another driving force for the MO precursor, which pushes the MO precursors from the gas inlet, which is the high-pressure region, toward the exhaust, which is the low-pressure side. Decreasing the V/III ratio has a significant influence on the growth rate and the surface morphology of GaN thin films. Thus, it is indicated that the growth rate is strongly affected by the V/Ill molar ratio. It is necessary to study the influence of changing of TMG flow rate to get a better understanding of its effect on properties of GaN thin films.

1.9 Numerical modeling

Numerical simulation is developed to be a significant approach to analyze the transport phenomena and predict the growth rate of the thin film in MOCVD. Until recently, the reactor design and process optimization of CVD were done by means trial and error [59]. Many theoretical and experimental studies have been conducted to explore the reaction mechanisms, transport phenomena, and the effect of operating conditions of the MOCVD process [5,6]. Using a computational model can reduce the cost and the effort of experimental study.

The GaN deposition in the MOCVD process has been performed numerically using a 2D or 3D model for many reactors, such as a vertical rotating disk and a horizontal reactor [8–10]. Fotiadis et al. [61] used 2D and 3D models based finite element method (FEM) to study the effect of heat transfer characteristics on the flow pattern and deposition rate of GaAs thin film in a vertical rotating disk CVD reactor. The results demonstrate that natural convection effects can be minimized by increasing both the inlet flow rate and the rotating rate of the susceptor while reducing the reactor pressure.

Modeling of the MOCVD process depends on the unraveling of detailed chemical reaction mechanisms in the gas phase and surface reaction. Sun et al. [62] proposed a simple reaction mechanism which includes five gas-phase reactions and one surface reaction. Modeling of surface

reactions assumed to be very rapid, so it is not sufficient to predict the deposition rate of GaN thin films. Theodorpoulos et al.[63] utilized a chemical mechanism model involved six gas-phase reactions and seven surface reactions to investigate the influence of different process parameters on the growth rate of GaN thin films. Some reaction parameters in the chemical model were estimated using collision theory, which is useful for a dilute gas mixture. Sengupta et al. [64] used the *ab initio* quantum chemistry method to derive a complicated chemistry model for predicting the growth of GaN thin films. The model has sufficient accuracy, but it has an exceptionally high computational cost. Hu et al. [65] simplified the comprehensive reaction model of the previous study [64], to predict GaN thin film efficiently with a low computational cost.

1.10 Optimization

Numerical simulations give flexibility and versatility to be used widely for the optimization of thermal systems, but it consumes much time. The optimization of the MOCVD process can give further clarification regarding the growth rate and uniformity of thin films. Many efforts have been done regarding getting an optimal growth rate and a uniform thin film. However, the optimization of the MOCVD process is still a challenge. Zhang et al.[66] used orthogonal test analysis to examine the growth process of GaN in a close-coupled showerhead (CCS) MOCVD reactor. The study is based on 3D numerical modeling. Mitrovic et al.[6] studied the optimization of operating parameters on the maximum growth rate and uniformity of InP within a 2D model. George et al.[67] introduced a compromise response surface method (CRSM) to investigate the optimization of silicon deposition from saline in a vertical impinging CVD reactor. The optimal growth conditions of GaN thin films in the MOCVD reactor still requires further computational experiments to find optimal solutions. Surrogate-based optimization provides more efficient prediction than that with a numerical analysis [68]. It appears as an effective method to alleviate the expensive computations for design optimization with the least possible number of sample points.

1.11 Motivation

It must be stressed that a uniform film thickness means more uniform distribution of components and higher quality of the thin film. The effect of operating parameters on the GaN growth rate, film uniformity, surface morphology, and crystal quality requires investigations to enhance MOCVD performance. Moreover, further research is needed in the development and optimization of the MOCVD system to find optimal operating conditions that enhance the growth rate and quality of GaN thin films. Limited experimental studies of multi-wafer MOCVD reactors, coupled with 3D simulations modeling are available in the literature [69], [70], [71]. Also, predicting optimal operating conditions of producing GaN thin films using iterative numerical analyses usually require massive iterations and high computational cost. Therefore, understanding the essential characteristic of the MOCVD process will support optimization the operating variables for improving the uniformity and deposition rate of GaN thin films

The current study aims to investigate the manufacturing of GaN thin films using a vertical rotating disk MOCVD reactor and to examine material characterizations of the specimens, including the crystal quality and surface morphology. Also, the study would develop three-dimensional models for single wafer and multi-wafer reactors to describe various operating conditions that are related to morphology and uniformity of thin films. It would also utilize optimization-based surrogate models to predicate optimal operating parameters for high deposition rate and excellent uniformity of GaN thin films. Optimized computational results can be used as inputs to modify the operating conditions of practical MOCVD system. These major areas will be considered to discuss growing GaN thin films in the MOCVD reactor that consistent with growth operating conditions and reactor configurations.

1.12 Outline of the dissertation

The study is organized in many chapters. Chapter 1 presents the technical background of the fundamental properties of gallium nitride (GaN), MOCVD process, and operating conditions followed by the motivation and objectives of this research. Chapter 2 describes the experimental work of growing GaN thin film samples in two different MOCVD systems. Chapter 3 presents the material characterization of GaN thin film samples grown in the MOCVD reactor. Chapter 4 presents the detailed numerical modeling of the GaN growth by MOCVD process and investigation of GaN thin films growth under different boundary conditions in a single-wafer MOCVD reactor. Chapter 5Chapter 6 investigates GaN growth in a multi-wafer MOCVD reactor. Chapter 6 presents an optimization study to obtain the optimal deposition rate and uniformity of GaN thin films in the rotating disk MOCVD reactor. Finally, the conclusions of this study and the future work needed in this area are presented in chapter 7.

Chapter 2

EXPERIMENTAL WORK

2.1 Introduction

In this chapter, growth experiments have been performed under different operating conditions in MOCVD reactors. Major components and subsystems that support the MOCVD reactor are highlighted. The epitaxial growth of GaN thin films was carried out in two commercial MOCVD systems. A vertical rotating disk MOCVD system at Valence Process Equipment Inc., and a close-coupled showerhead MOCVD system at Structured Materials Industries Inc, in New Jersey, USA.

2.2 MOCVD system

MOCVD is a vapor-phase deposition process, where metal-organic precursors are used to growing a solid thin film. Figure 2.1 shows the schematic diagram of the typical MOCVD system. It consists of the reactor unit, gas supply system, computer control system, and filtering and vacuum pump system. In addition to measurement systems of the temperature, pressure, mass flow rate controller, and the growth rate of the thin film during the growth process. In the reactor unit, the substrate, which is a sapphire wafer, is placed on the susceptor. The susceptor is coated by silicon carbide to increase the conductivity. Concentric heaters are used to heat the susceptor and achieved a uniform temperature distribution on the substrate surface. The susceptor is set on the top of a shaft, which is driven by a motor. A high vacuum loading unit is interfaced to the reactor chamber to keep a clean environment during wafer loading-unloading process. Figure 2.2 shows the vertical rotating disk MOCVD reactor at Valence process equipment Inc. It used to grow samples of GaN thin films on 4-inch c-plane sapphire (Al_2O_3) wafers. A mixture of hydrogen (H_2) and nitrogen (N_2) as a carrier gas, is used to deliver trimethylgallium (TMG) and ammonia (NH_3), which are reactant precursors into the reactor. The injector system consists of combined several inlets that produce an

adequate uniform inlet velocity. The inlet, inner and outer walls of the reactor are maintained at a

constant temperature using cooling water.
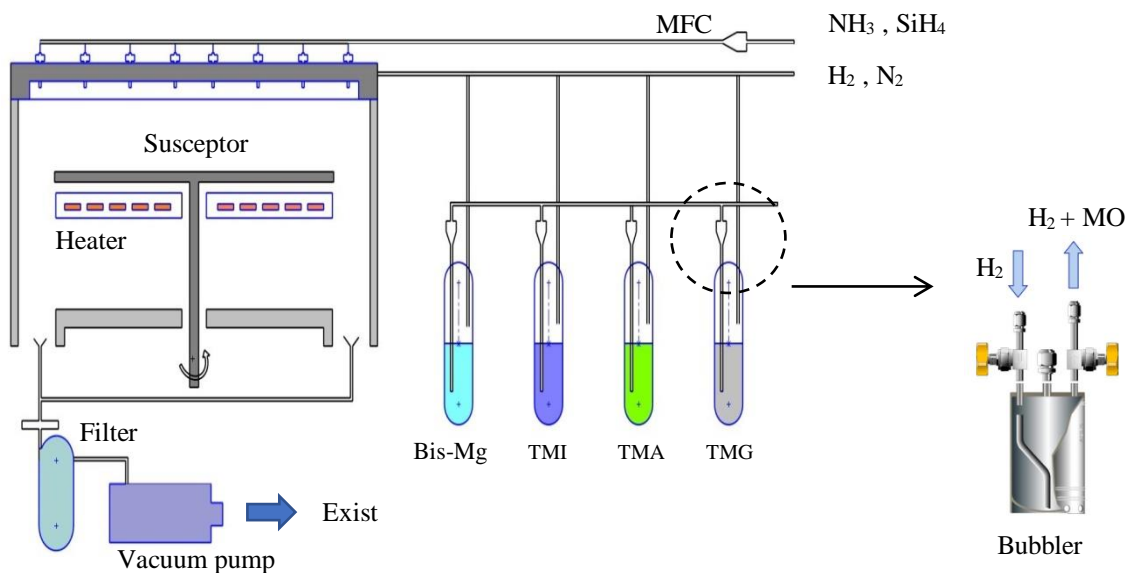
Figure 2.1 Schematic diagram of main units of the MOCVD system.
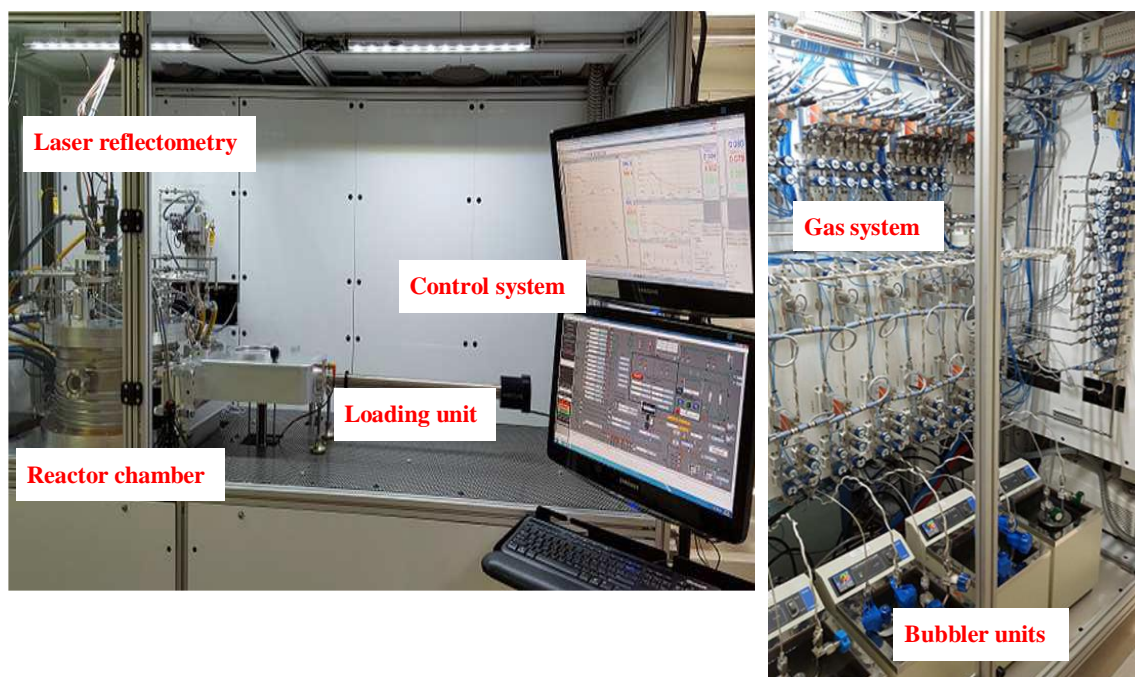
Figure 2.2 Views of (a) the vertical rotating disk MOCVD reactor in Valence process
equipment Inc. and (b) The gas supply system and bubbler units.

Figure 2.3 shows a view of the close-spaced reactor MOCVD reactor in Structure materials industries, Inc. It used to grow samples of GaN thin films on 2-inch c-plane sapphire (Al_2O_3) wafers. Pure hydrogen (H_2) or pure nitrogen (N_2) as a carrier gas, is used to deliver reactant precursors from the shower-head inlet into the reactor.
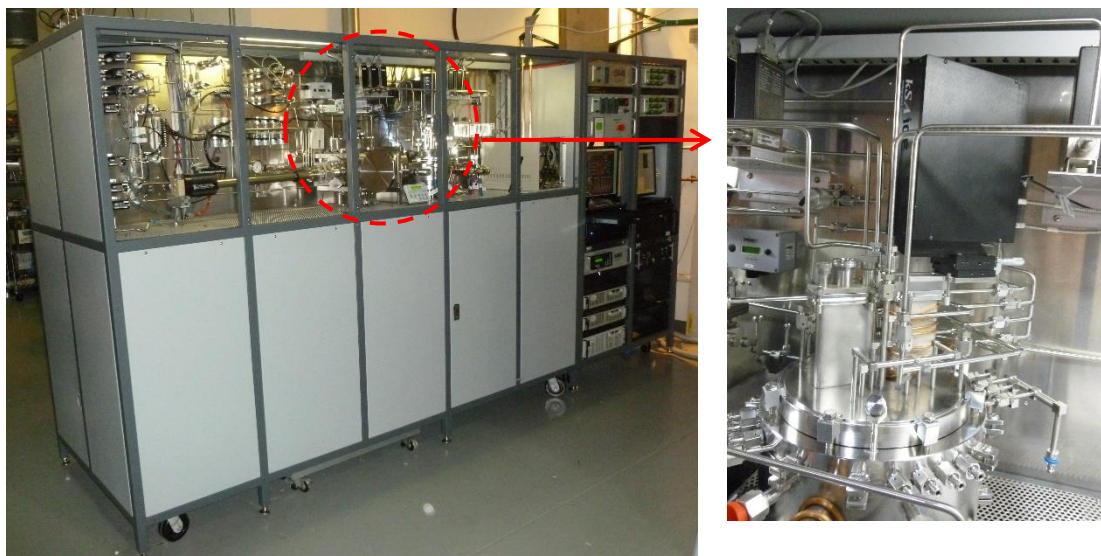
Figure 2.3 (a) View of the multi-wafer MOCVD system in Structure materials industries, Inc. and (b) View of the main reactor.

2.2.1 Gas Supply System

The gas supply unit is composed of mass flow controllers (MFCs), control valves, pneumatic valves, throttle valves, pressure monitor, extensive pipes network, and other connections components. The flow rate is typically measured in standard cubic centimeter per minute (sccm) or standard liters per minute (slm). The MFC regulates precisely the flow rate of delivering gases through the gas supply unit. During the growth process, the gas mixture is delivering into the reactor chamber from the inlet. Generally, H_2 or N_2, or a mixture of both gases is used as a carrier gas, which is injected to deliver reactant precursors into the MOCVD reactor. Metal-organic (MO) precursors such as TMG, TEG are kept in liquid form in a sealed container is called bubbler. Figure

2.4 shows the schematic diagram of gas supply and the main reactor of the MOCVD system in

Structure materials industries, Inc.
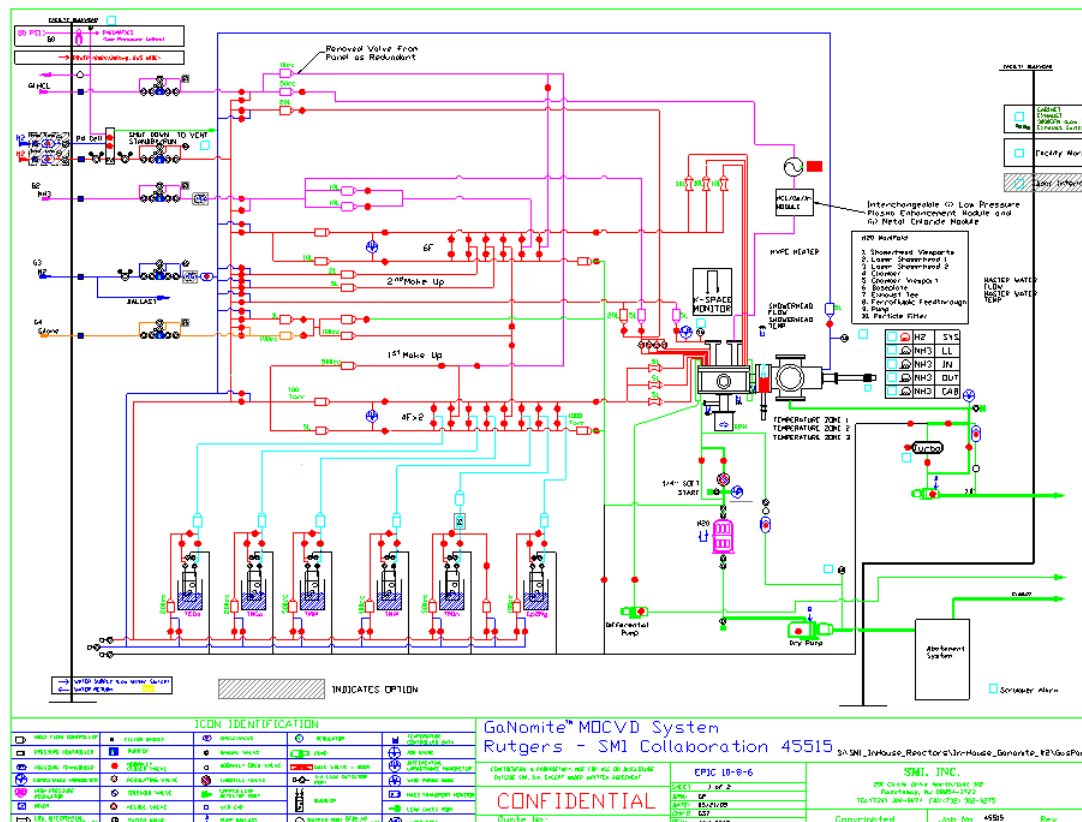
Figure 2.4 Schematic diagram of the gas supply system of the MOCVD process in Structure materials industries, Inc.

The metal-organic precursors are heated to a relatively moderate temperature so that their vapor can be carried by the carrier gas into the reactor chamber. The H_2 gas is injected into the bubbler to transport the precursor vapor into the reactor, as shown in Figure 2.5. The bubbler is kept in a temperature-controlled bath, where the temperature is set in the range of (0 - 10 °C). The concentration of metalorganic precursors entering the reactor determines the growth rate of the thin film. The flow rate of TMG F_{TMGa} is controlled by three factors the vapor pressure P_{TMGa} of TMG, the flow rate of H_2 gas F_{H2}, and the bubbler pressure $P_{bubbler}$. The flow rate of TMG is adjusted

by flowing H_2 gas through the bubbler vessel according to the following equation, which is assumed both the H_2 gas and the vapor of the precursors are ideal gases:

$$F_{TMGa}\left(\frac{mol}{min}\right) = \frac{P_{TMG}}{P_{bubbler} - P_{TMG}} \cdot \frac{F_{H2}\left(\frac{sccm}{min}\right)}{22400\left(\frac{sccm}{mol}\right)} \tag{2-1}$$

$$\log(P_{TMG}) = A - \frac{B}{T_b(K)} \tag{2-2}$$

Where $P_{bubbler}$ is the bubbler pressure, which is set at 900 Torr, the P_{TMGa} is the vapor pressure of TMG, which depends on the bubbler temperature $T_b(K)$, and A and B are constants related to the properties of metalorganic compounds. The constants A and B of some metalorganic precursors commonly used in the MOCVD system are listed in Table (2-1.
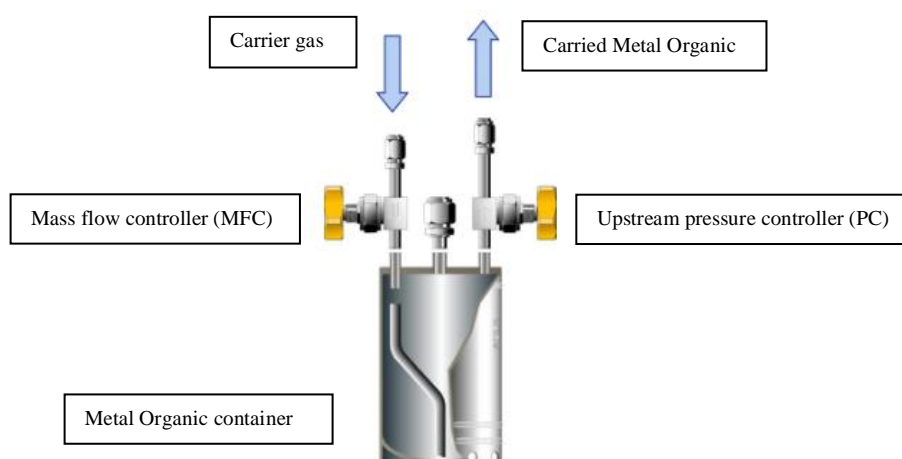
Figure 2.5 Schematic diagram of the MO source bubbler used in the MOCVD system.

Table (2-1) The constants A and B of common metal-organic precursors used in the MOCVD process.

Metal-organic	A	B	Vapor pressure (Torr)	Melting point (°C)
Trimethylaluminium Al(CH3)3	10.475	2780	9.7	15
Triethylaluminium Al(C2H5)3	10.784	3625	0.026	-46
Trimethylgallium Ga(CH3)3	8.495	1825	64.5	-15.8
Trimethylgallium Ga(C2H5)3	9.165	2530	3.4	-82.3
Trimethylindium In(CH3)3	9.375	2830	1.2	88
Triethylindium In(C2H5)3	8.935	2815	0.44	-31.9

2.2.2 Measurement systems

Measurement systems involve various monitoring equipment such as pressure transducers, thermocouples, and non-intrusive measuring devices. Pressure sensors are placed in many areas to monitor and regulate the pressure throughout the MOCVD systems. Thermocouples and pyrometer are used to monitor the temperature in the reactor and the susceptor surface, respectively. At higher temperature, thermocouples have errors due to conduction and radiation.

The pyrometer can be emissivity corrected to measure the temperature of the susceptor surface accurately during the growth process. Measuring the temperature helps to give a quite good indication for adjusting the growth temperature. Closed-loop control and precise measurement of the temperature assist in keeping the surface temperature of the wafer more uniform and stable. All of the measuring systems are connected to the main computer, which controls, monitors, and records data. The growth process can be processed automatically by running the recipe after growth conditions are correctly set up.

2.2.3 The optical reflectance

The optical reflectance is a non-intrusive device used in-situ to monitor the film growth in real-time. The reflectance intensity is recorded and displayed as a function of time. The intensity of reflectance depends on the refractive index of the layer, interference at interfaces, absorption of light by material and scattering at the layer surface. During the growth process, an increase of thickness of the thin film layer leads to multiple oscillations occur on the reflectance and transmittance curves due to interferences among multiple reflected waves, which results in peaks and valleys in the reflectance curve. The oscillation characteristics are strongly dependent on the surface morphology of the thin film. Figure 2.6 shows the oscillation period of typical surface morphologies, including flat, wavy, and rough. The amplitude of the reflectance curve for the flat

surface oscillates periodically while for the wavy surface it shrinks gradually. On the other hand, the rough surface scatters the light and reduces, the amplitude of the reflectance curve further.[54].
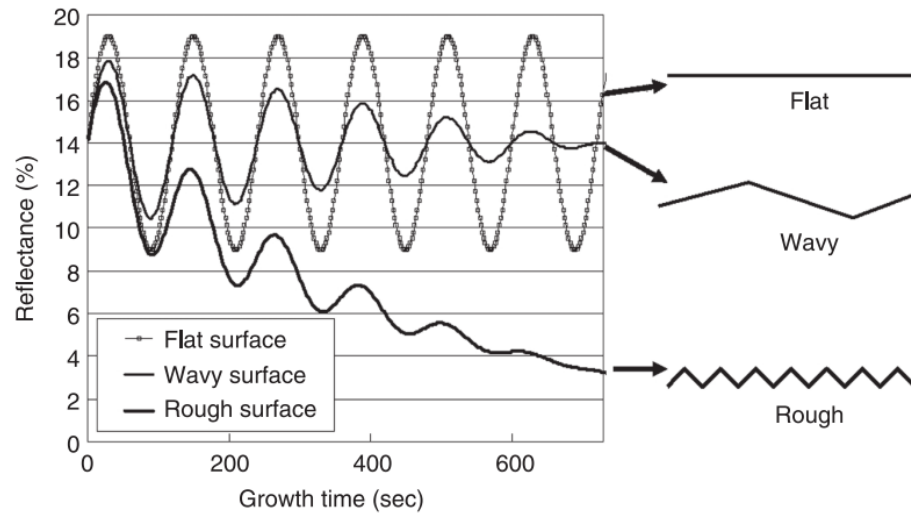
Figure 2.6 Reflectance signal related to the surface morphology [54].

The optical reflectance has usually monitored the growth of the thin film on the wafer during the growth process. Nowadays most MOCVD reactors are using in-situ optical monitor KSA ICE metrology system which is capable of measuring real-time temperature, reflectivity, growth rate, film thickness, substrate curvature, see Figure 2.7
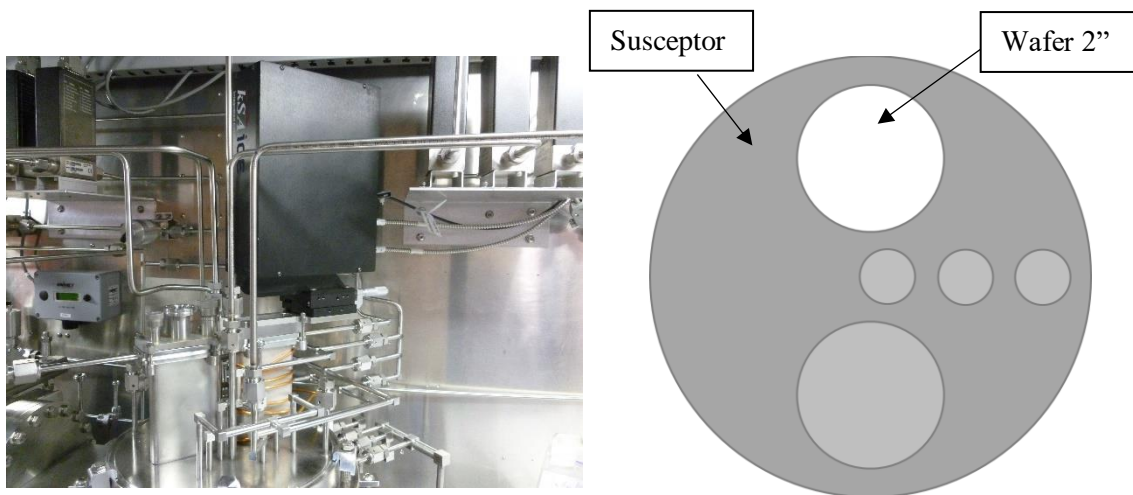
Figure 2.7: (a) In-situ optical monitor KSA ICE device of the MOCVD system in SMI, Inc. (b) Schematic diagram of the wafer carrier (susceptor).

2.3 Film thickness measurement

Single-spot thickness measurements are general-purpose film thickness measurement instruments and are frequently used for optical device characterization, see Figure 2.8 (a).
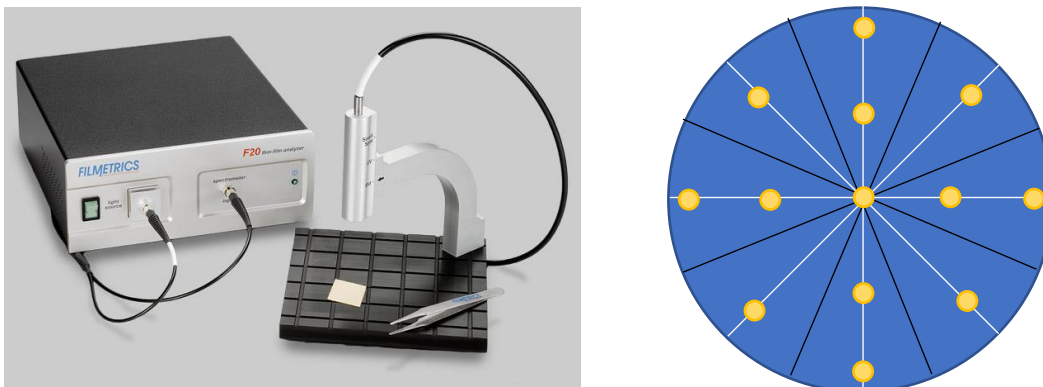
Figure 2.8 (a) Single-Spot Thickness Measurements, and (b) distribution of measured points on the wafer surface.

The spectrophotometric measurements are direct and non-destructive allow the simultaneous determination of the film thickness and refractive index. The thickness of GaN thin films is measured by analyzing how the film reflects light. The thickness mapping is performed on multiple points, that are distributed evenly on the wafer surface, as shown in Figure 2.8 (b).

2.4 Growing GaN thin films

Experimental deposition runs of GaN thin film samples have been performed in different commercial MOCVD systems. GaN thin film samples are grown with different values of TMG flow rate have been deposited by MOCVD reactor in Valence process equipment Inc. The other samples were grown by changing the reactor pressure and the type of the carrier gas in a close-coupled showerhead (CCS) MOCVD reactor in Structured materials industries, Inc. In both systems, the growth process runs with a sequential task that is called a recipe. It is a list of commands to control operating conditions in the MOCVD system. The recipe defines the

processing sequence including the flow rate of precursors, the flow rate of carrier gas, chamber pressure, a setpoint temperature of the wafer, etc.

The experiments started by loading the sapphire (Al_2O_3) wafer on the susceptor. The growth process can proceed automatically by running the recipe. Figure 2.9 shows the schematic diagram of the temperature history of the growth process, which including clean the substrate at a high temperature of (900 -1010 °C) under H_2 atmosphere, followed by a two-step growth process of GaN thin films. The first step involves growing a buffer layer on the substrate surface at a temperature of 550 ° C. The second step starts by supplying more TMG, while NH_3 is kept constant to deposit GaN at a high temperature of (1030 -1080 °C). Finally, the supplying of precursors switched off, and any remaining gases are driven out of the system and then expelled through the vent. When the temperature is decreased to room temperature, the sample takes out the reactor for further material characterization
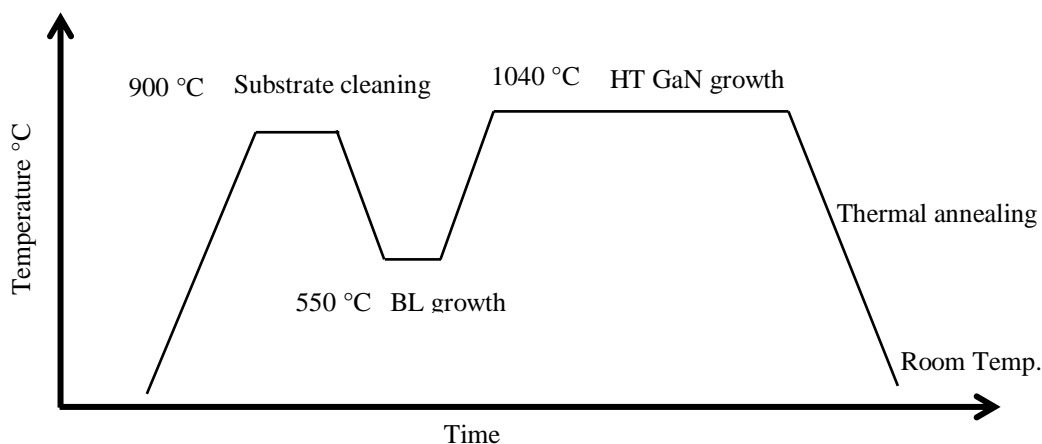
Figure 2.9 Schematic diagram shows the temperature history of growing GaN thin films in the MOCVD system

2.4.1 The V/III ratio

The flow rate of metal-organic precursors is a critical parameter in the MOCVD process. It determines the concentration of metalorganic precursors entering the reactor, and subsequently, the

growth rate of the thin film. The growth rate and the microstructure of GaN thin films were investigated under different values of the V/III ratio in the range of (487-1220). GaN thin films were grown on 4-inch sapphire (Al_2O_3) wafer by MOCVD system. The flow rate of TNG is varied while the NH_3 flow rate is kept constant at 16.67 slm with a mixture of N_2 and H_2 as a carrier gas. The total inlet flow rate of gases is set at 61.012 slm. The first step of growth is growing a buffer layer at 550 °C; then it is annealed at temperatures 1060°C for 3-5 min to enhance the recrystallization. The second step of growth is increasing the flow rate of TMG, while NH_3 is kept constant to deposit the GaN thin film at a temperature of 1040 °C. During the growth process, the reactor pressure and the rotation rate of the susceptor are set at 200 Torr and 300 rpm, respectively. Table (2-2) lists the summary of operating conditions used to grow GaN samples. The optical reflectance technique is used to monitor the GaN thin film growth as a function of elapsed time.

Table (2-2) Summary of all the operating conditions

Sample (V/III)		Temperature (C)		Flows (slm)				Pressure (Torr)
		in	out	TMG	NH_3	H_2	N_2	
487	Bake	900	900		16.670	16.670	16.670	500
	Buffer	550	550	3.25e-03	16.670	16.670	16.670	500
	N-layer	1040	1030	3.422e-02	16.670	16.670	16.670	200
	U-GaN	1040	1030	3.422e-02	16.670	16.670	16.670	200
615	Bake	900	900		16.670	16.670	16.670	500
	Buffer	550	550	3.25e-04	16.670	16.670	16.670	500
	N-layer	1040	1030	2.712e-02	16.670	16.670	16.670	200
	U-GaN	1040	1030	2.712e-02	16.670	16.670	16.670	200
820	Bake	900	900		16.670	16.670	16.670	500
	Buffer	550	550	3.25e-04	16.670	16.670	16.670	500
	N-layer	1040	1030	2.033e-02	16.670	16.670	16.670	200
	U-GaN	1040	1030	2.033e-02	16.670	16.670	16.670	200
1220	Bake	900	900		16.670	16.670	16.670	500
	Buffer	550	550	3.25e-04	16.670	16.670	16.670	500
	N-layer	1040	1030	1.366e-02	16.670	16.670	16.670	200
	U-GaN	1040	1030	1.366e-02	16.670	16.670	16.670	200

Figure 2.10 (a) shows a typical reflectance curve of GaN grown on a sapphire substrate measured by in situ monitoring system. At the first stage of growth, a nucleation layer (NL) is grown on a bare substrate surface at low temperature 550 C°, followed by annealing the NL for a short time.

The annealing process enhances the surface to be rough and form nucleation islands. During the GaN growth at high temperature, nucleation islands grow in lateral and vertical directions [31]. After that, the islands start to coalesce with each other to form a quasi 2D layer to establish a smooth surface [32]. Finally, The reflectance curve starts to increase periodically until the GaN islands fully coalesce into the smooth surface and form a continuous thin film.

The thickness of the GaN layer can be deduced from the increase in the reflectance, which acts as an indirect tuning parameter for the layer thickness. At a high value of the V/III ratio, fewer oscillations are observed over a given range of time, which indicated growing a thinner film, as shown in Figure 2.10 (b). When the V/III ratio reduced, more TMG precursor is introduced into the reactor, which increases the growth rate. Thus, many oscillations are observed at the low value of V/III ratio, which indicated growing a thicker film, as shown in Figure 2.10 (d).
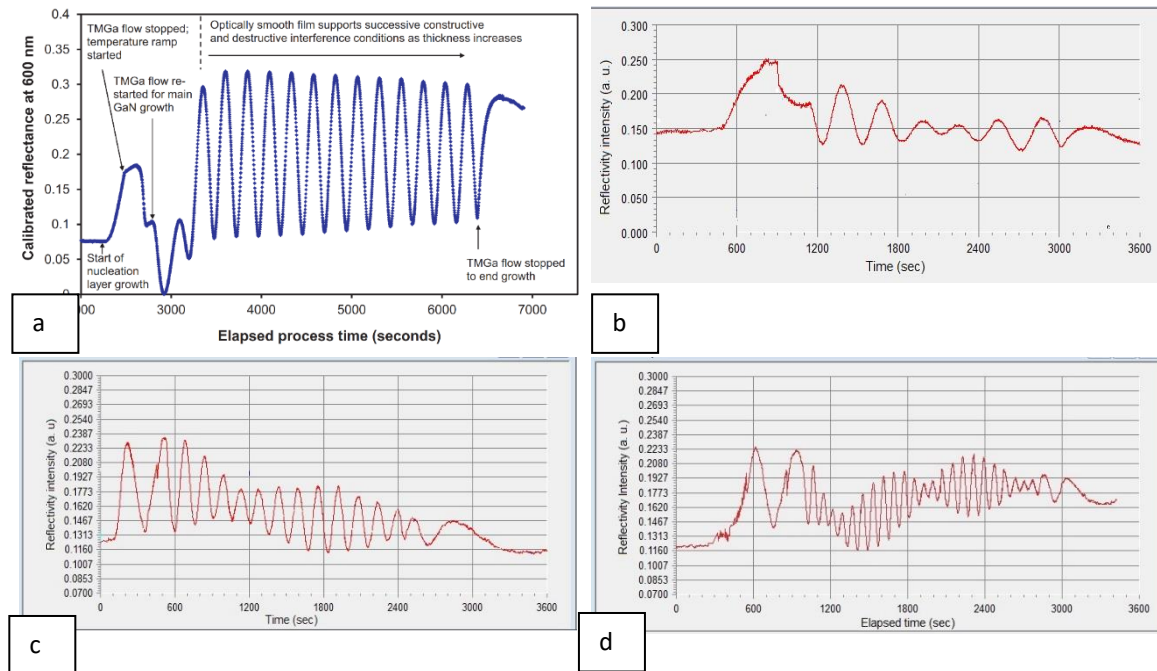
Figure 2.10 (a) Typical in situ reflectivity records of the GaN growth on sapphire wafers as a function of growth time. In situ records at different V/III ratios (b) 1220, (c) 615, and (d) 487.

Figure 2.11 shows photoluminescence (PL) of thickness mapping of GaN thin films on the sapphire substrate at different values of the V/III ratio. The PL system scans the wafer surface then it maps

variations in the intensity, wavelength, and width of the PL spectra at each point. It is observed that

high thickness is obtained with low V/III ratio, while low thickness is obtained at high V/III ratio.
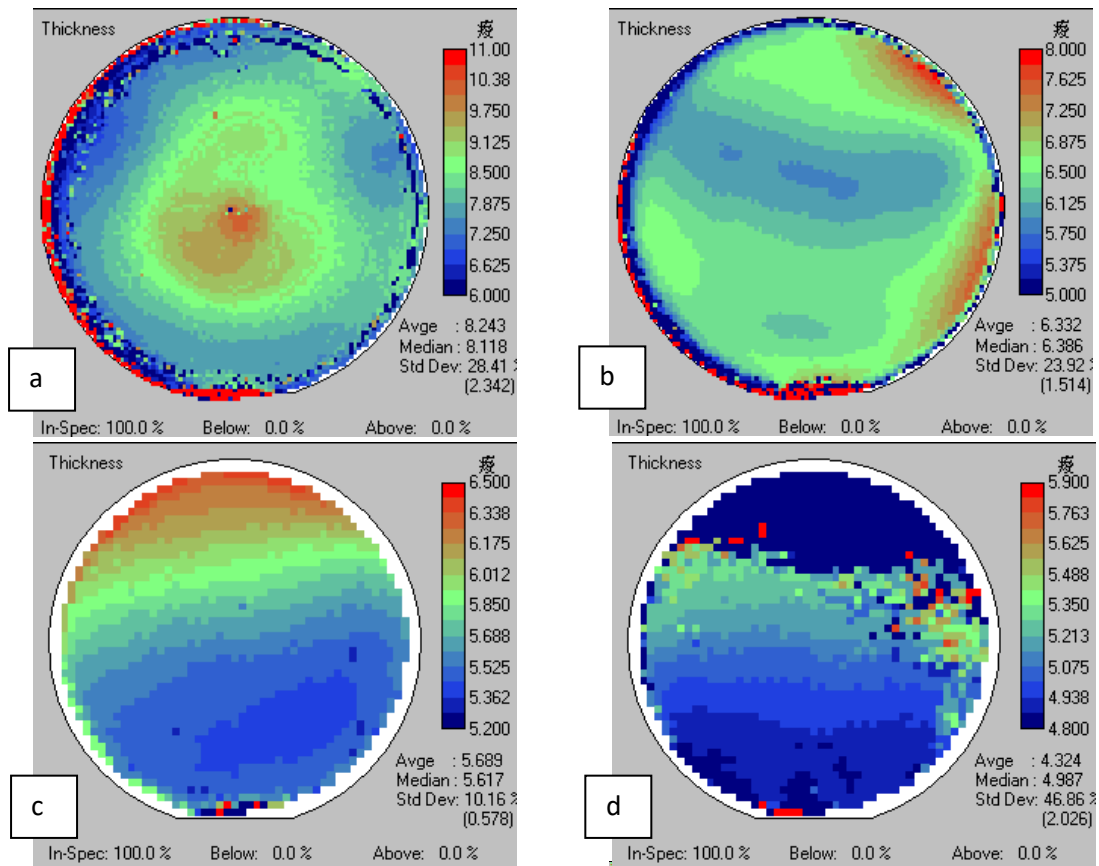
Figure 2.11 Photoluminescence thickness map of the GaN thin film grown on the 4-inch sapphire wafer at different values of the V/III ratio (a) 487, (b) 620, (c) 815, and (d) 1220.

In summary, one can see that the deposition rate increases significantly with decrease the V/III

ratio, while other operating parameters are kept constant.

2.4.2 The reactor pressure

The influence of varying the reactor pressure on the growth rate and uniformity of GaN thin films

has been investigated. The reactant precursors TMG and NH_3 are delivered from the shower-head

inlet into the reactor chamber using pure H_2 as a carrier gas with a constant flow rate. The total inlet

gas flow rate is set at 20.003 slm. GaN thin films were grown on the 2-inch sapphire (Al_2O_3) wafer

using CCS MOCVD system, see Figure 2.3. The wafer and susceptor were cleaned thermally (baking) for 10 minutes at 1010 C° in H_2 ambient; then the temperature is lowered down to 550 C° to deposit a buffer layer of GaN on the substrate surface. This is followed by growing a thick GaN layer at a high temperature of 1065 C° under the same growth conditions, except the flow rate of TMG is increased. Detailed growth conditions used to grow GaN thin film samples are summarized in Table 2-3. Figure 2.12 shows reflectance curves measured by in situ monitoring system for GaN thin films grown on a sapphire substrate at different values of the reactor pressure.

Table 2-3) Processing conditions of GaN thin film samples deposited in the CCS MOCVD system.

Sample (P)		Temperature (C°)			Flows (SLM)				Pressure (Torr)		
		shaft	In	out	TMG	NH_3	H_2	N_2			
100	bake	770	1086	880			14	0	500		
	buffer	480	530	470	7.55e-05	4	14	0	500		
	N-layer	730	1040	830	2.25e-04	6	14	0	200		
	U-GaN	730	1040	830	2.25e-04	6	14	0	100		
200	bake	770	1075	880			14	0	500		
	buffer	480	530	470	7.55e-05	4	14	0	500		
	N-layer	740	1040	830	2.25e-04	6	14	0	200		
	U-GaN	740	1040	830	2.25e-04	6	14	0	200		
300	bake	770	1075	880			14	0	500		
	buffer	480	533	470	7.55e-05	4	14	0	500		
	N-layer	740	1032	830	2.25e-04	6	14	0	200		
	U-GaN	740	1032	830	2.25e-04	6	14	0	300		
500	bake	770	1075	880			14	0	500		
	buffer	480	533	470	7.55e-05	4	14	0	500		
	N-layer	740	1064	830	2.25e-04	6	14	0	200		
	U-GaN	740	1064	830	2.25e-04	6	14	0	500		
700	bake	770	1075	880			14	0	500		
	buffer	480	530	470	7.55e-05	4	14	0	500		
	N-layer	740	1040	830	2.25e-04	6	14	0	200		
	U-GaN	740	1062	830	2.25e-04	6	14	0	700		
200	bake	770	1075	880			14	0	500		
,500	buffer	480	530	470	7.55e-05	4	14	0	500		
,700	N-layer	740	1040	830	2.25e-04	6	14	0	200		
	U-GaN	740	1062	830	2.25e-04	6	14	0	200	500	700
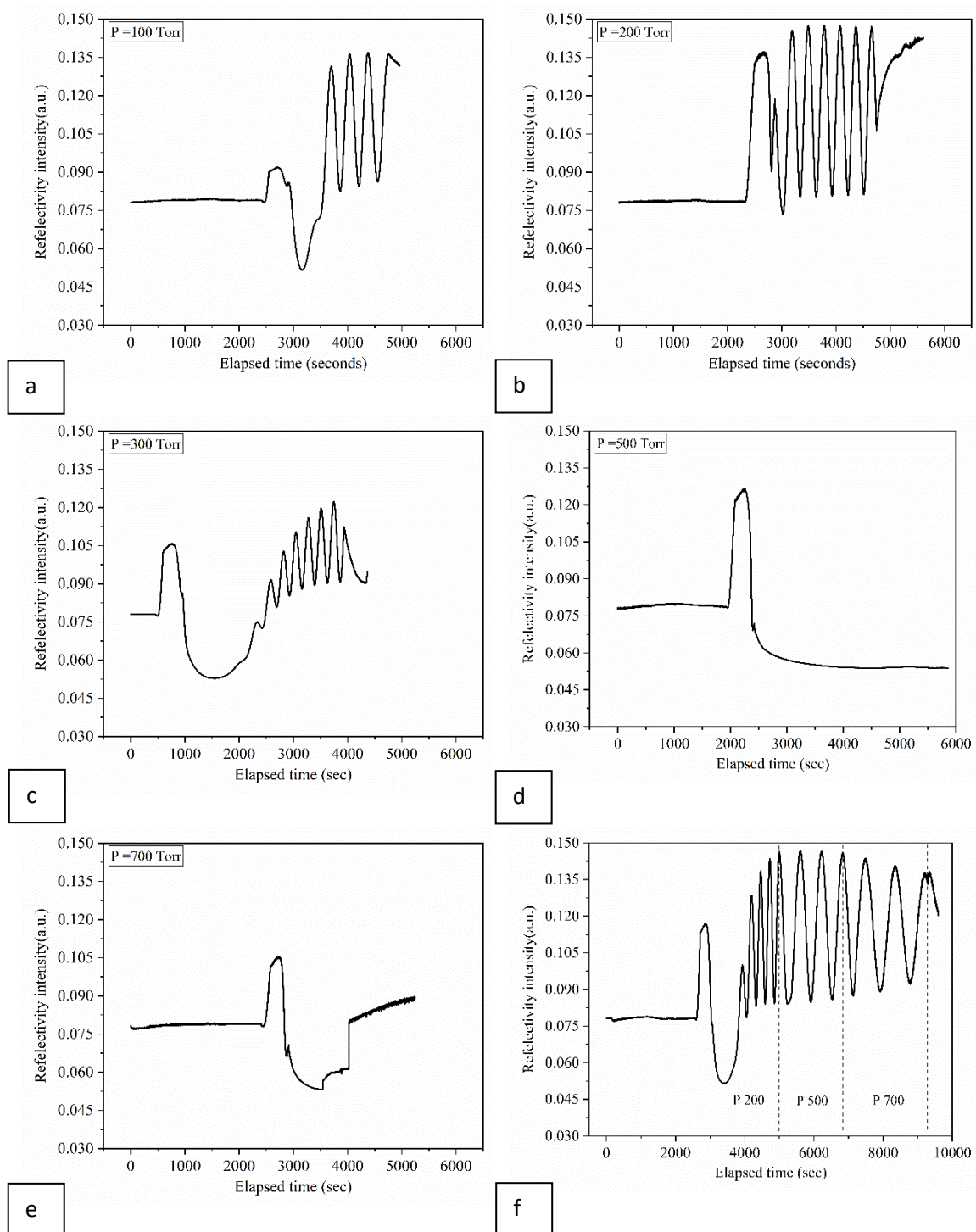
Figure 2.12 In situ reflectivity records of the GaN growth on sapphire wafers at different values of the reactor pressure (a) 100, (b) 200, (c) 300, (d) 500, (e) 700, (f) 200-700 Torr.

At low reactor pressure, the reflectance curve starts to oscillate periodically, which indicates a smooth surface is obtained. The thickness maps of GaN thin films at different reactor pressure are illustrated in Figure 2.13. At low reactor pressure, low thickness GaN thin film is obtained. When the reactor pressure increases, the thickness of GaN thin films increases, as shown in Figure 2.13 (c).
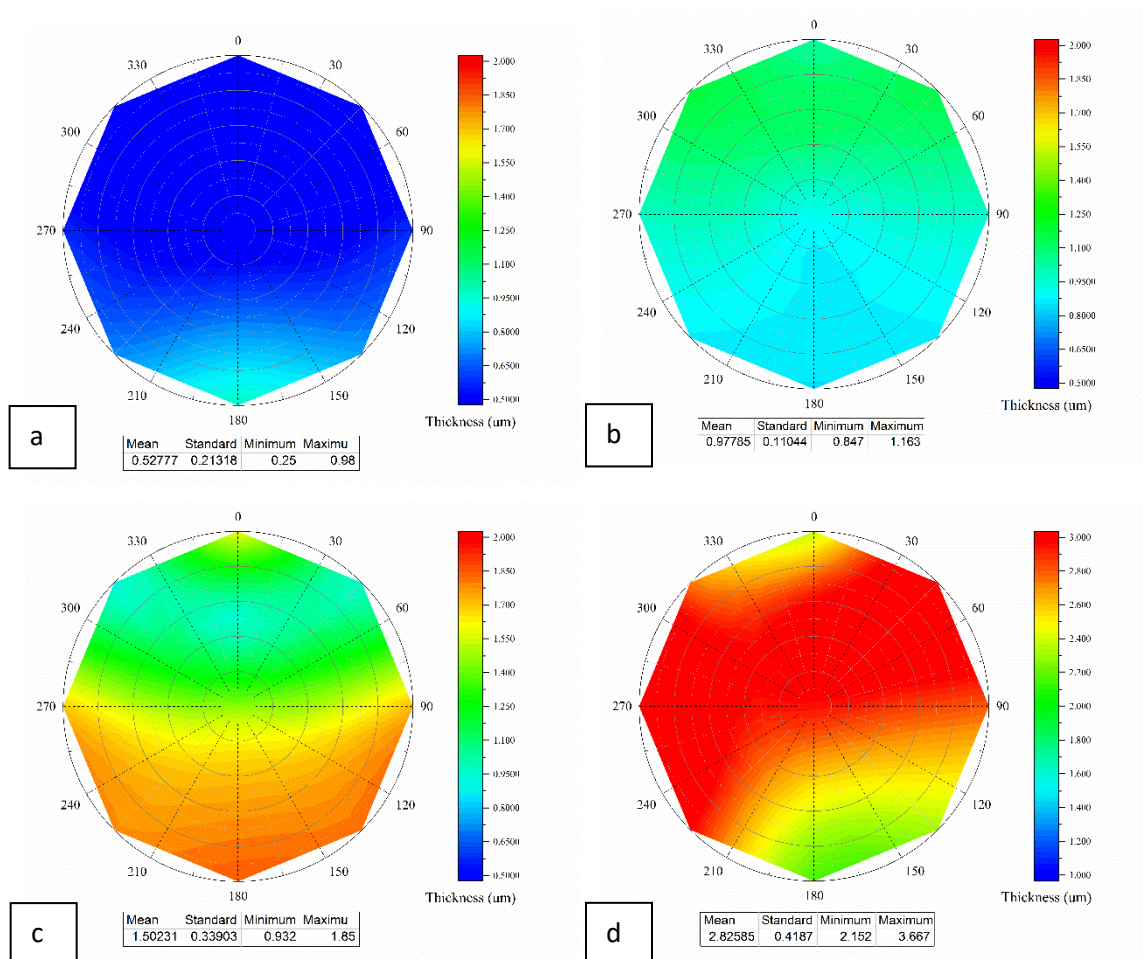
Figure 2.13 Thickness mapping of GaN thin films grown on the 2-inch sapphire wafer under reactor pressure of (a) 100 Torr and (b) 200 Torr (c) 300 Torr and (d) 200 to 700 Torr.

When the reactor pressure increased to 500 and 700 Torr, respectively, a rough surface of GaN thin film is obtained. The thickness maps of GaN thin film were not captured by IR fringes light at 500 and 700 Torr, respectively. The light is scattered significantly, and this results in almost zero

reflectance, as shown in Figure 2.12 (d and e). It is expected that a rough surface occurs due to the growth of the GaN islands three-dimensionally. Figure 2.14 shows the microstructure of GaN thin films grown under reactor pressure of 200 and 700 Torr, respectively. It is shown that a continuous GaN thin film obtained with the reactor pressure of 200 Torr, while a discontinuous thin film is grown under the reactor pressure of 700 Torr. Sasaki and Matsuoka [75] reported that continuous GaN thin films could not grow under atmospheric pressure, while under low-pressure increasing the flow rate of carrier gas will change the morphology of GaN thin film from pyramid-like to truncated pyramid-like. However, the reactor pressure of 200 Torr enhances the nucleation layer and improves the recovery to produce GaN thin films at elevated pressure. As a result, it is difficult to grow GaN thin films at high reactor pressure directly because GaN layers do not have enough recovery time to grow on the buffer layers. However, increasing the reactor pressure gradually from 200 to 700 Torr helps to grow a continuous GaN thin film successfully, as shown in Figure 2.12 (f).
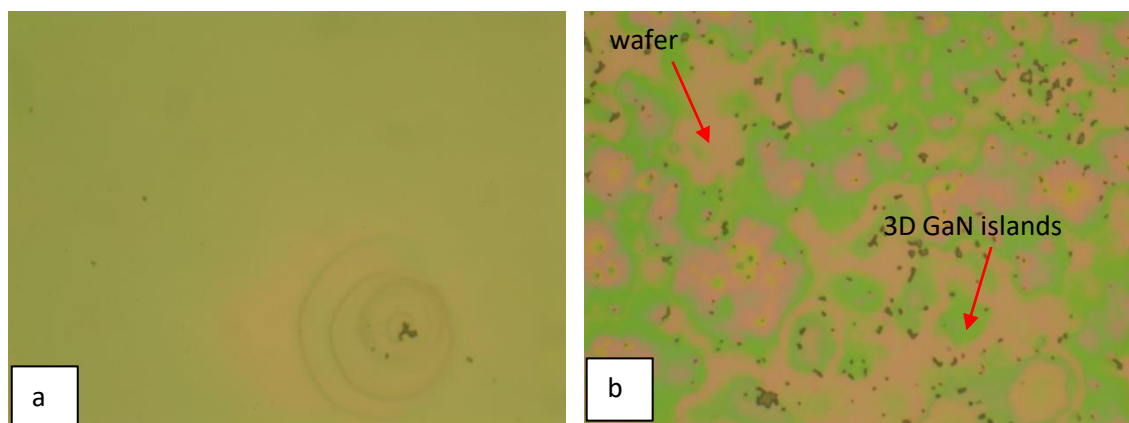
Figure 2.14 Microstructure of GaN thin films grown on the 2-inch sapphire wafer under reactor pressure of (a) 200 Torr and (b) 700 Torr.

Also, it is observed that the thickness map of the GaN thin film increased when the reactor pressure increased, as shown in Figure 2.13 (d). However, the interference fringe spacing is clearly expanding, as shown in Figure 2.12 (f), which indicates a lower deposition rate is obtained at the

high pressure. At near atmospheric pressure 700 Torr, the growth efficiency of GaN is reduced due to gas-phase reactions, which result in reducing the uniformity and growth rate of thin films. It is concluded that abrupt change of the reactor pressure to high values affect the forming of GaN thin films. Moreover, it promotes gas-phase reactions, which reduce the deposition rate. Thus, it is required to grow a GaN nucleation layer at low pressure, which enhances the recovery time then grow GaN thin films gradually at high values of the reactor pressure.

2.4.3 The carrier gas

The deposition rate of GaN thin films is influenced by the flow rate of the carrier gas. Pure H_2 is the typical gas selected as a carrier gas in the deposition of GaN thin films. GaN thin films grow under pure N_2 as the carrier gas with different values of the reactor pressure. GaN thin films were grown on 2-inch sapphire (Al_2O_3) wafer by CCS MOCVD system. The wafer and susceptor were cleaned thermally (baking) for 10 minutes at 1010 C° in H_2 ambient; then the temperature is lowered to 525 C°. A buffer layer of GaN is deposited onto the substrate surface. This is followed by a thick GaN layer grown at high temperature 1065 C° under a continuous flow of pure N_2 as the carrier gas. Detailed growth conditions used to grow GaN samples are summarized in Table 2-3. Figure 2.15 shows reflectance curves measured by in situ monitoring system for GaN thin films grown on a sapphire substrate at different values of the reactor pressure using pure N_2 as the carrier gas.

When the reactor pressure is increased, the amplitude of the reflectance curve oscillates periodically and shrinks gradually. When the N_2 is employed as the carrier gas, the number of oscillations is increased while the recovering time is decreased with increasing the reactor pressure, as shown in Figure 2.15-(c). On the other hand, almost zero reflectance is obtained at the reactor pressure of 500 Torr, when H_2 is used as a carrier gas, as shown in Figure 2.12-d. The changing in peak spacing of the interference fringes indicate how the deposition rate changes with the reactor pressure.

Table (2-4) processing conditions of GaN samples deposited in the CCS MOCVD system.

Sample (P)		Temperature (C°)			Flows (SLM)				Pressure (Torr)
		shaft	In	out	TMG/H$_2$	NH$_3$	H$_2$	N$_2$	
100	bake	770	1086	880			14	0	500
	buffer	480	560	470	7.55e-05	4	0	14	500
	N-layer	730	1080	830	2.25e-04	6	0	14	200
	U-GaN	730	1040	830	2.25e-04	6	0	14	100
200	bake	770	1073	880			14	0	500
	buffer	480	560	470	7.55e-05	4	0	14	500
	N-layer	740	1080	830	2.25e-04	6	0	14	200
	U-GaN	740	1040	830	2.25e-04	6	0	14	200
300	bake	770	1072	880			14	0	500
	buffer	480	563	470	7.55e-05	4	0	14	500
	N-layer	740	1082	830	2.25e-04	6	0	14	200
	U-GaN	740	1032	830	2.25e-04	6	0	14	300
500	bake	770	1095	880			14	0	500
	buffer	480	563	470	7.55e-05	4	0	14	500
	N-layer	740	1084	830	2.25e-04	6	0	14	200
	U-GaN	740	1064	830	2.25e-04	6	0	14	500

Utilizing pure N$_2$ as the carrier gas instead of using H$_2$ leads to an increase in the potential flow. N$_2$ is heavier than H$_2$ gas, which results in increasing the inlet mass flow rate. It is observed that the deposition rate increased by increasing the reactor pressure from 100 our 300 Torr, while a slight increase is observed at 500 Torr. The CCS MOCVD reactor has a short distance between the inlet and the susceptor surface. The high flow rate of N$_2$ aids to deliver the metal-organic efficiently towards the susceptor surface and consequently enhances the thickness of GaN thin films, as shown in Figure 2.16. When the reactor pressure is increased from 100 Torr to 300 Torr, the thickness of a GaN thin film is increased. Increasing the pressure further up to 500 Torr leads to grow a continuous thin film, but decrease the thickness of GaN thin films.

Moreover, the results of the thickness map show a high value of the standard deviation is obtained. It indicates that a rough surface of GaN thin films is obtained at different values of the reactor pressure with N$_2$ as a carrier gas. Moreover, it is observed that using pure N$_2$ as the carrier gas promotes carbon contamination, which affects the quality of GaN thin films.
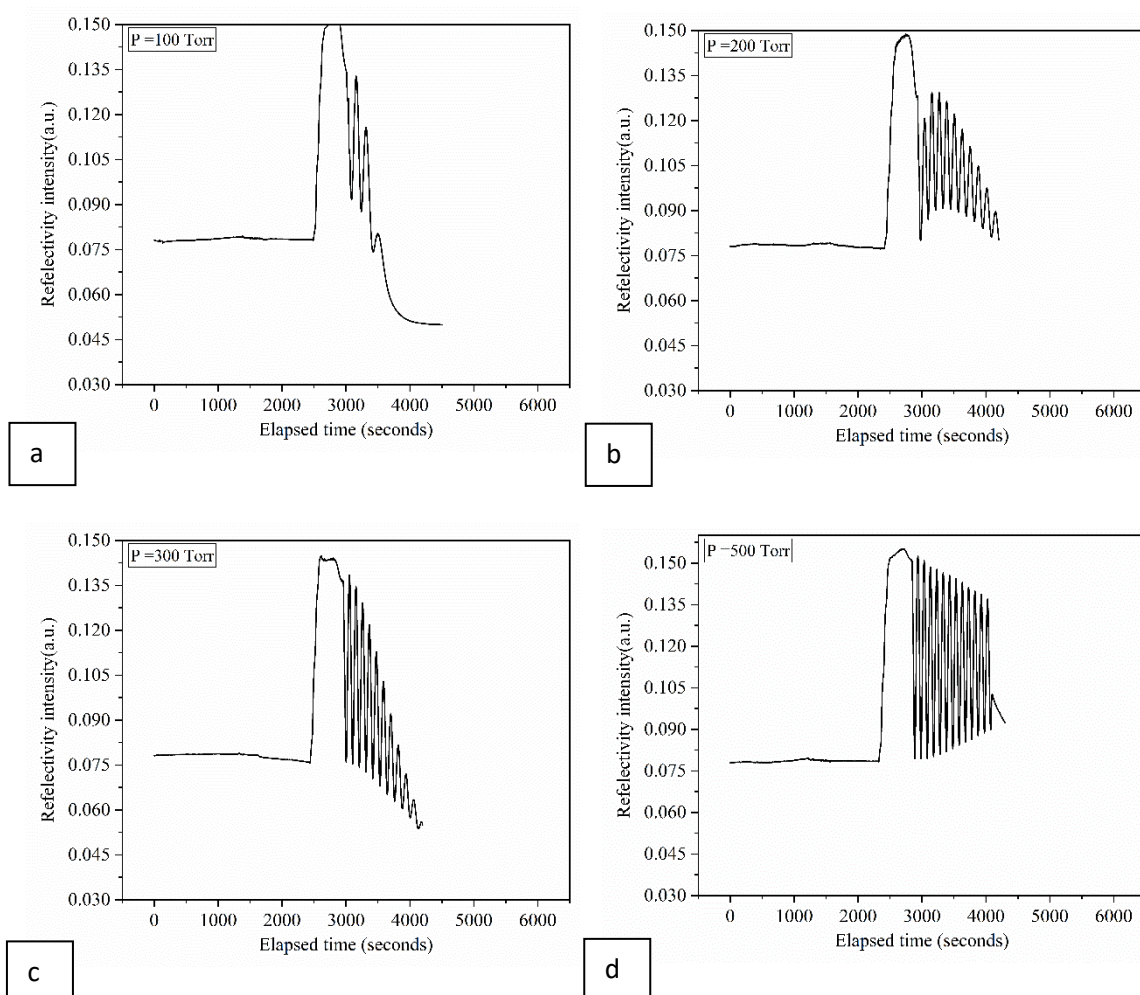
Figure 2.15 In situ reflectivity records of the GaN growth on sapphire wafers at different values of the reactor pressure with N_2 as carrier gas (a) 100, (b) 200, (c) 300, (d) 500 Torr.

At a low reactor pressure, carbon contaminations are distributed near the edge of the wafer, as shown in Figure 2.17. The surface of GaN thin films is light yellow and looks dull, which reveals that it is contaminated. Interestingly when the reactor pressure is increased to 500 Torr, the amount of carbon contamination is decreased. Increasing the reactor pressure promotes the gas-phase reaction between TMG and NH_3 in the gas phase, which leads to a decrease in the deposition rate. When pure N_2 is used as a carrier gas, the GaN thin film grown has a light yellow and dull surface. Therefore, the quality of the GaN crystal can be improved by increasing the reactor pressure. ,
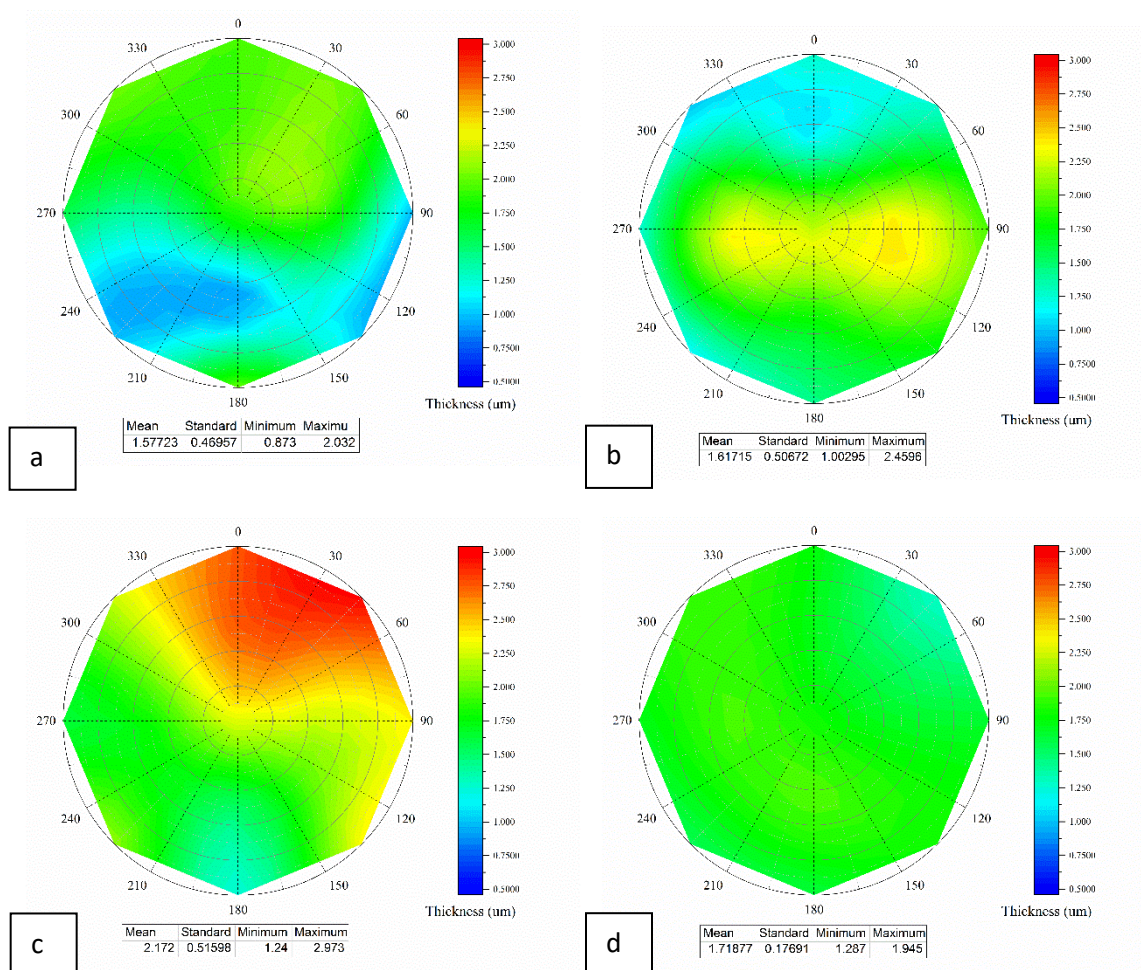
Figure 2.16 Thickness mapping of GaN thin films grown on the 2-inch sapphire wafer at the reactor pressure of (a) 100, (b) 200, (c) 300, and (d) 500 Torr with N_2 as the carrier gas.
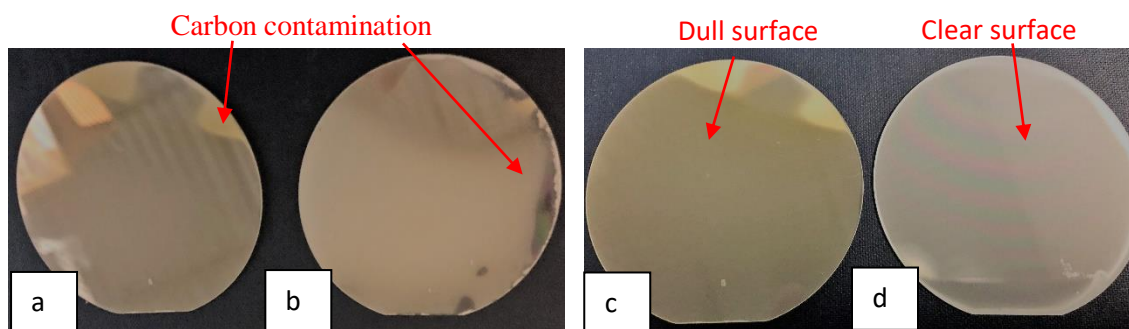
Figure 2.17 View of GaN thin films grown on the 2-inch sapphire wafer at the reactor pressure of (a) 100, (b) 200, (c) 300 Torr with N_2 as the carrier gas respectively, and (d) 300 Torr with H_2 as the carrier gas.

Pure H_2 as a carrier gas plays an important factor in GaN growth by neutralizing other contamination or impurities. Figure 2.17-(c and d) shows a comparison between two samples of the GaN thin film grown with pure N_2, and H_2 as a carrier gas respectively at the reactor pressure of 300 Torr. Thus, controlling of H_2 flow rate precisely can enhance the growth rate and the quality of GaN thin films. As a result, using an appropriate mixture of N_2 and H_2 as the carrier gas enhances the deposition rate and uniformity of GaN thin films.

2.5 Conclusions

In this chapter, three sets of GaN thin film samples have been deposited using the MOCVD reactor under different operating conditions. The first set samples are grown under different values of the V/III ratio, the second set samples are grown under different values of the reactor pressure, and third set samples are grown using pure N_2 as a carrier gas. The results indicate that the average deposition rate increases with increase the reactor pressure, but it decreases with increasing the precursor concentration ratio. At high V/III ratio, the low deposition rate is obtained due to the low flow rate of TMG. When the V/III ratio is decreased, the flow rate of TMG has increased leads to involve more species in chemical reactions, which increase the deposition rate.

On the other hand, increasing the reactor pressure can increase the deposition rate. However, high reactor pressure can promote the reaction between the metal-organic precursors and NH_3 in the gas phase. When pure H_2 is used, a high-quality thin film is produced. Utilizing a high flow rate of pure N_2 as a carrier gas enhances the deposition rate. However, it decreases the uniformity of the thin film, and also it deteriorates the quality of GaN thin films as more carbon contamination is involved. It is worth to note that using an appropriate mixture of H_2 and N_2 as a carrier can improve the deposition rate and quality of GaN thin films.

Chapter 3

MATERIAL CHARACTERIZATION

3.1 Introduction

This chapter describes the equipment and techniques used to study the material characterization of GaN thin film samples. The characterization analysis provides a clear understanding of the effect of changing growth conditions on the properties of the GaN thin film. The structural quality and surface morphology of GaN thin films grown under different values of V/III ratios, and also the carrier gas type have been discussed.

3.2 Atomic Force Microscopy (AFM)

Surface morphology and roughness of GaN thin films grown in the MOCVD process were evaluated using Park NX10 AFM system. This system has three operation modes, contact, non-contact, and tapping. In this study, contact mode is chosen to scan the surface morphology of GaN thin films samples. In contact mode, the AFM probe, which consists of a very tiny cantilever that is ended by a sharp cone-shaped tip, makes a soft contact with the sample surface. When the distance between the tip and the sample surface becomes shorter, an interaction force between these surfaces will exist. The interatomic force as a function of the distance will deflect the cantilever upward or downward when it scans a convex region or concave region, respectively. The probe deflection is used as a feed feedback loop to produce an image of the surface topology.

The surface roughness is quantified by the root mean square (RMS) values over an area of (5 x 5 um2) of the sample. GaN thin films were grown under different values of the V/III ratio with a mixture of 60 % N_2 and 40 % H_2 as the carrier gas. Figure 3.1 shows that the RMS value of GaN thin film samples increases when the V/III ratio decreases. It reveals that the surface tends to have

larger grains size and rough surface morphology. On the other hand, one can see that increasing the V/III ratio leads to a decrease in the RMS value.
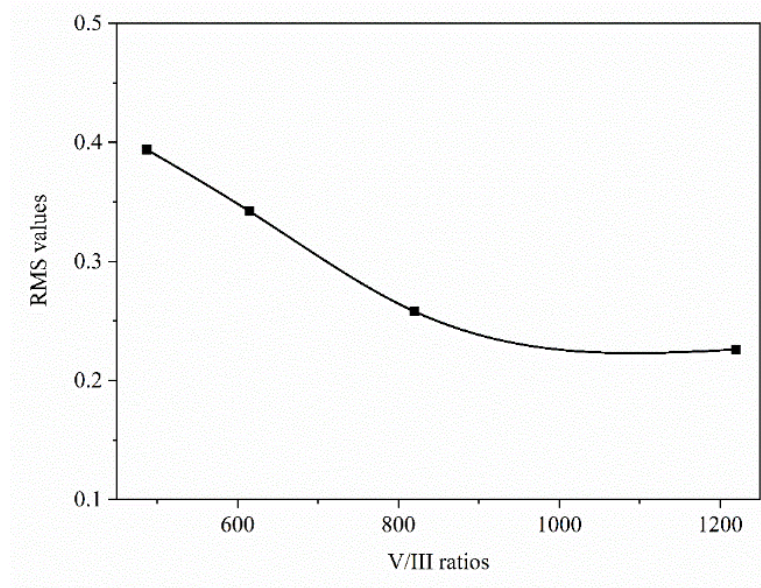
Figure 3.1 Surface roughness of GaN thin films at different values of the V/III ratio.

The surface morphologies of GaN thin films samples exhibit a "step-flow" pattern, which indicates the growth of two-dimensional monolayer. A clear step-flow pattern with nano-pits is observable on the surface of the sample grown at high V/III ratio, as shown in Figure 3.2. However, at high V/III ratio, a step-flow pattern is visible that indicates a smooth surface morphology of GaN thin films. Step terminations on a single crystal surface correspond to the intersection of a threading dislocation with the free surface. When V/III ratio is decreased further, a rough surface morphology produced and several small pits observed on the surface as shown in Figure 2.10-(a). It is observed that the increase in the V/III ratio more than 820 has a slight effect on the RMS value. Thus, the GaN thin film sample was grown at the high V/III ratio has a low RMS value, which indicates a smooth surface is obtained.
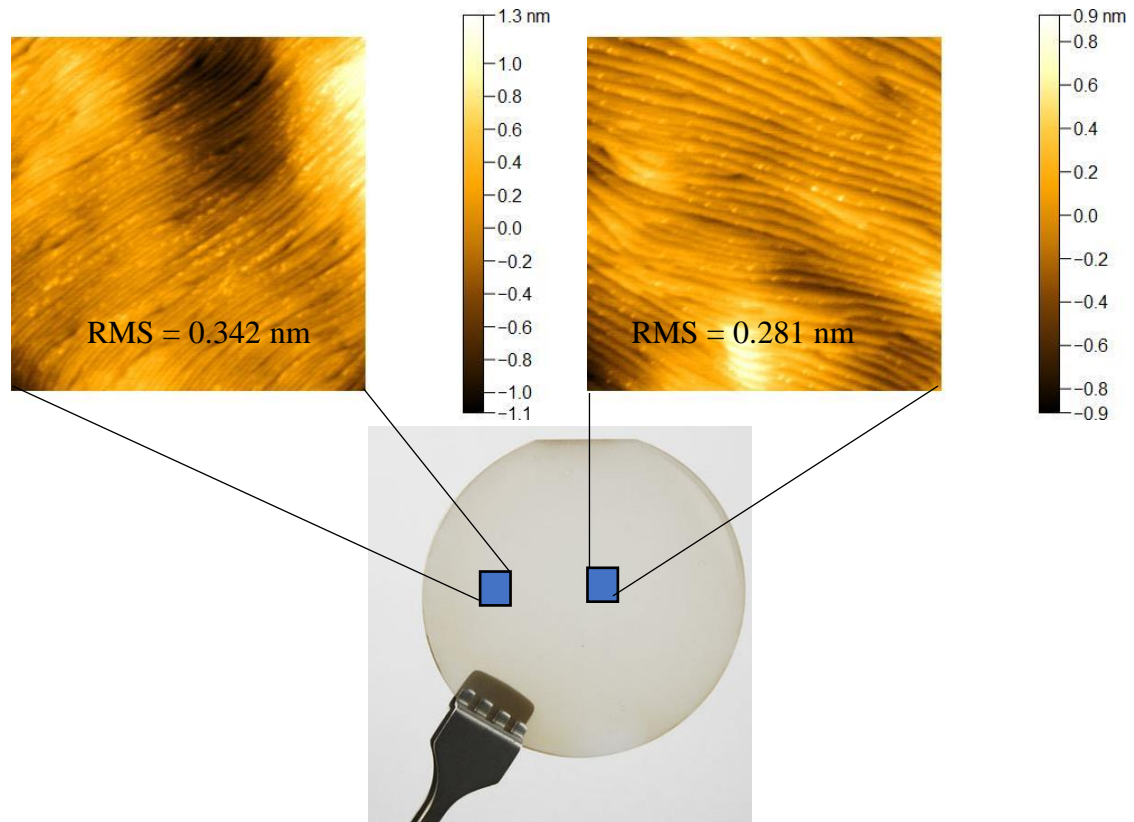
Figure 3.2 AFM image of surface morphology of GaN thin films grown on the c-plane sapphire substrate at the V/III ratio of 615.

The high density of nano-size spots is most likely tended to merge together and develop into larger ones. These pits are inevitably terminated the flow steps and pinned the threading dislocations resulting in nonparallel growth steps at the GaN surface. Tarsa et al. reported similar results for GaN samples grown under different V/III ratios in the MBE process [76].

At low V/III ratio, results showed that the surface of the GaN thin film was rough and the structure was titled columnar with a high density of stacking faults. To promote a 2D growth mode and improve structural quality, H_2 is used as a carrier gas. The diffusion rate of Ga-containing species in H_2 is higher than in N_2, so it leads more deposition on the reactor walls and less deposition on the wafer. Using H_2 as carrier gas results in layers with better morphologies, but it can affect electrical characteristics [77].
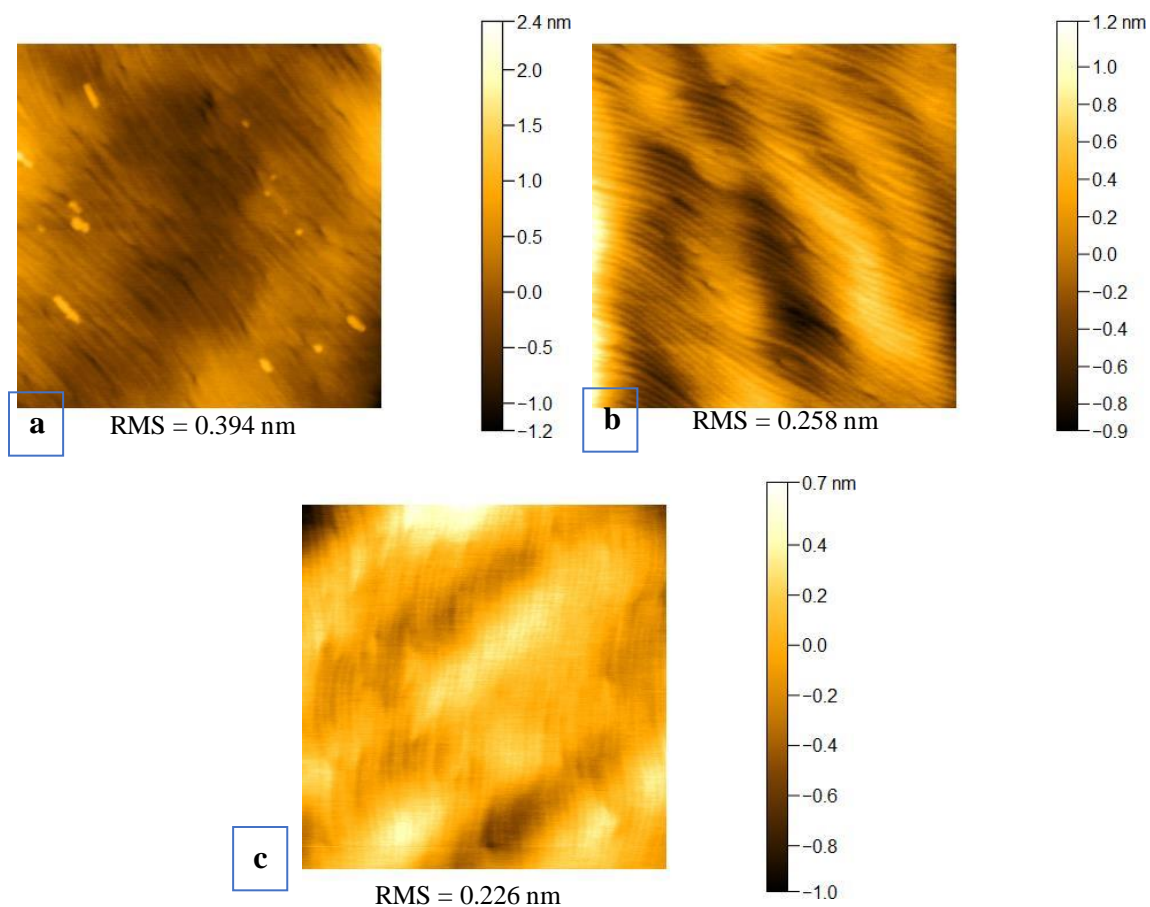
Figure 3.3 AFM images of surface morphology of GaN thin films grown on the sapphire substrate at different values of the V/III ratio (a) 487 (b), 820, (c) 1220
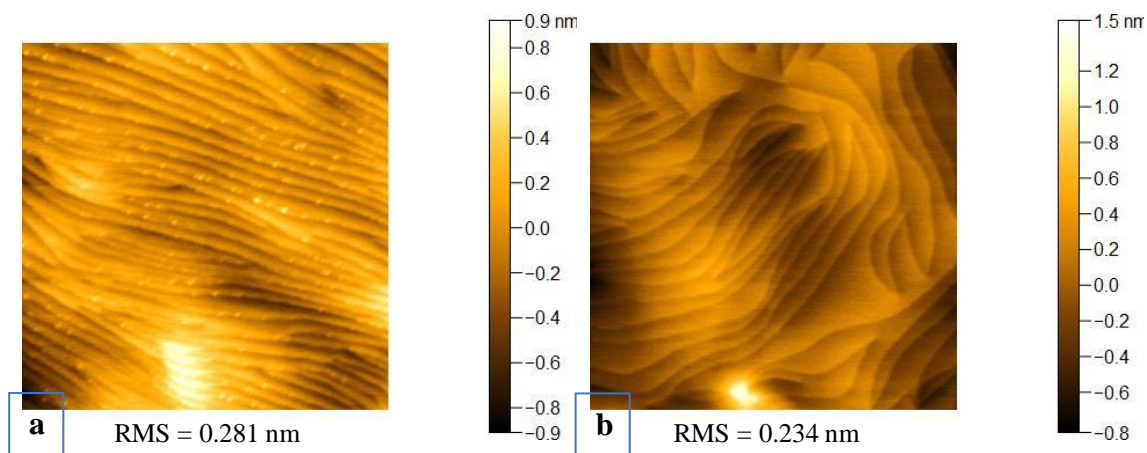
Figure 3.4 AFM images of surface morphology of GaN thin films grown on the sapphire substrate at the V/III ratio of 615 with (a) a mixture of 60 % N_2 + 40 % H_2, and (b) pure H_2 as a carrier gas.

Figure 3.4-(b) shows steps flow on the surface with no visible nano-pits, demonstrating the high quality of GaN thin film. Thus, utilize pure H_2 as a carrier gas instead of the mixture of 60 % N_2 and 40 % H_2, enhances the surface morphology of GaN thin films. Wang et al. [78] also observe a change in surface morphology with changing $N_2/(N_2+H_2)$ ratio. Increasing the ratio led to a rough surface and a decrease in the structural quality of the material, while using pure H_2 led to mirror-like surface morphology. They attribute this change in surface morphology to a decrease in diffusion length of the reactants on the growth surface caused by increasing of the density of carrier gas. The high diffusivity of metal-organic precursors in H_2 leads to undesired deposited material on inner walls of the reactor and consequentially increase repairing maintenance cost. In this study, an appropriate mixture of H_2 and N_2 as carrier gases used to improve the quality of GaN and reduce the residual strain.

3.3 X-ray Diffraction (XRD)

The crystal quality of GaN thin film samples evaluated by using XRD Bruker Vantec-500 system which is equipped with a 3-circle Azlan goniometer, and it is operating at 40 kV and 35 mA with $CuK_{\alpha 1}$ radiation. X-ray diffraction involves probing a crystal with x-ray radiation having a wavelength (λ) close to the crystal lattice spacing. XRD system uses short-wavelength radiation (λ=1.54 Å) to probe the structural properties of a material and extract information such as strain, grain size, and defect density. X-rays are generated by bombarding a metal typically copper with electrons in an evacuated tube, and monochromatic x-rays are usually selected. These x-rays are scattered by the electron cloud surrounding each atom in the crystal. Constructive interference occurs between the scattered x-rays according to Bragg's law [40]:

$$n\lambda = 2dsin\theta$$

3-1)

where d is the spacing between the atom planes, and θ is the angle at which the incident beam must probe the plane.

The diffraction of X-rays from a crystal can be described by Bragg's law [79]. It states the relationship of the atomic spacing d_{hkl} in crystals to the angle of diffraction at a given X-ray wavelength is given in the following equation:

$$d_{hkl} = \frac{2\lambda}{2\sin(\theta_{2h2k2l} + \Delta\theta)} \qquad \text{3-2)}$$

Where λ is the X-ray wavelength, θ_{hkl} is the measured angular position of the (hkl) reflection planes, $\Delta\theta$ is the error of the instrument which is ignored here. The d-spacing value is related to the lattice parameters (c and a) of hexagonal systems as illustrated in the following equation:

$$d_{hkl} = \frac{1}{\sqrt{\frac{3}{4}\left(\frac{h^2 + hk + k^2}{a}\right)^2 + \left(\frac{l}{c}\right)^2}} \qquad \text{3-3)}$$

Different peaks at symmetric and asymmetric reflections in multi-diffraction ω-2θ scan have been measured to determine rocking curves. The crystallite size broadening is most pronounced at large angles 2θ.
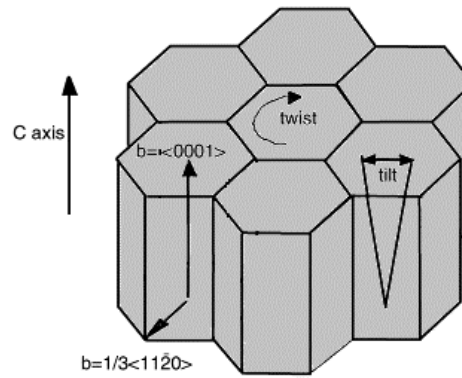
Figure 3.5 Schematic diagram of GaN subgrains with tilt and twist angles on the sapphire wafer.

The on-axis reflection is related to the tilt of the subgrains concerning the substrate, whereas the off-axis reflection results from a combination of the tilt and twist of the subgrain, as shown in Figure 3.5.
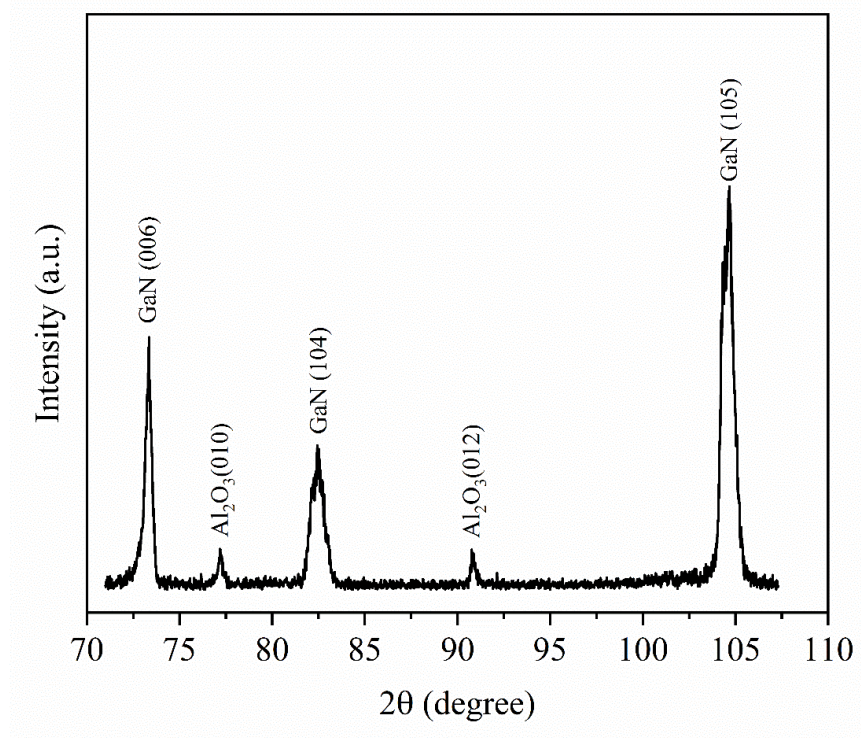
Figure 3.6 XRD intensity-2θ diffraction curve of GaN thin film obtained at V/III ratio equals 615.

Burger vector (b) for pure edge dislocations is $b = \frac{a}{3} < 11\bar{2}0 >$, and for pure screw dislocations is $b = c < 0001 >$ whereas $b = a + \frac{c}{3} < 11\bar{2}3 >$ for mixed dislocations in GaN crystal. Pure edge dislocations have no component in c-direction, so they are emerging in terraces. Pure screw and mixed dislocations have components in c-direction, which are related to step terminations. Figure 3.6 shows the XRD intensity-2θ scan of GaN films grown on the sapphire substrate at the V/III ratio of 615, while other growth conditions are kept constant. It is observed narrow and strong emission peak, indicating the deposited GaN thin film is a single crystal.

The XRD intensity-2θ scan of other samples grown under different V/III ratios show the same behavior. Figure 3.7 shows the measured FWHM of rocking curves for the symmetric (006) and asymmetric (105) reflection planes of GaN thin films grown at different V/III ratios. The symmetric reflection (006) is affected by screw dislocations, while the off-axis reflection (105) is affected by both edge and screw dislocations. At the low V/III ratio where the flow rate of TMG is varying, and the flow rate of the NH_3 is kept constant, the deposition rate of GAN thin films is increased. Increasing of GaN growth rate can be the source for the generation of threading dislocations at interfaces [80]. Figure 3.8 shows FWHMs values of rocking curves of GaN thin films grown on a sapphire substrate at different values of the V/III ratio. It is observed a slight decrease in FWHM of the GaN (006) reflection plane with reducing the V/III ratio in the range of (815-1220); then it is obviously increased with a further decrease in the V/III ratio.

On the other hand, the FWHM of GaN (105) reflection plane is increased with reducing V/III ratio due to the effect of both edge and screw dislocation. Suresh et al. [48] reported that asymmetric GaN rocking curve is broadening with increasing V/III ratio showing the opposite trend of GaN (105) in this study, as shown in Figure 3.8. In their work, the flow rate of TMG was kept at 0.1075 sscm, while the NH_3 flow rate is varied from 4 to 7 slm. Therefore, high NH_3 flow rate promotes GaN islands to merge, and forming a 2D quasi thin layer. From Figure 3.7, it observed that the value of GaN (006) is increased from 320 arcsec to 325 arcsec when the V/III ratio is increased from 820 to 1220. Heying et al. [64] confirmed that the asymmetric (105) reflection plane is sensitive to pure edge dislocations, and its FWHM is broadening due to rapid islands coalescence.
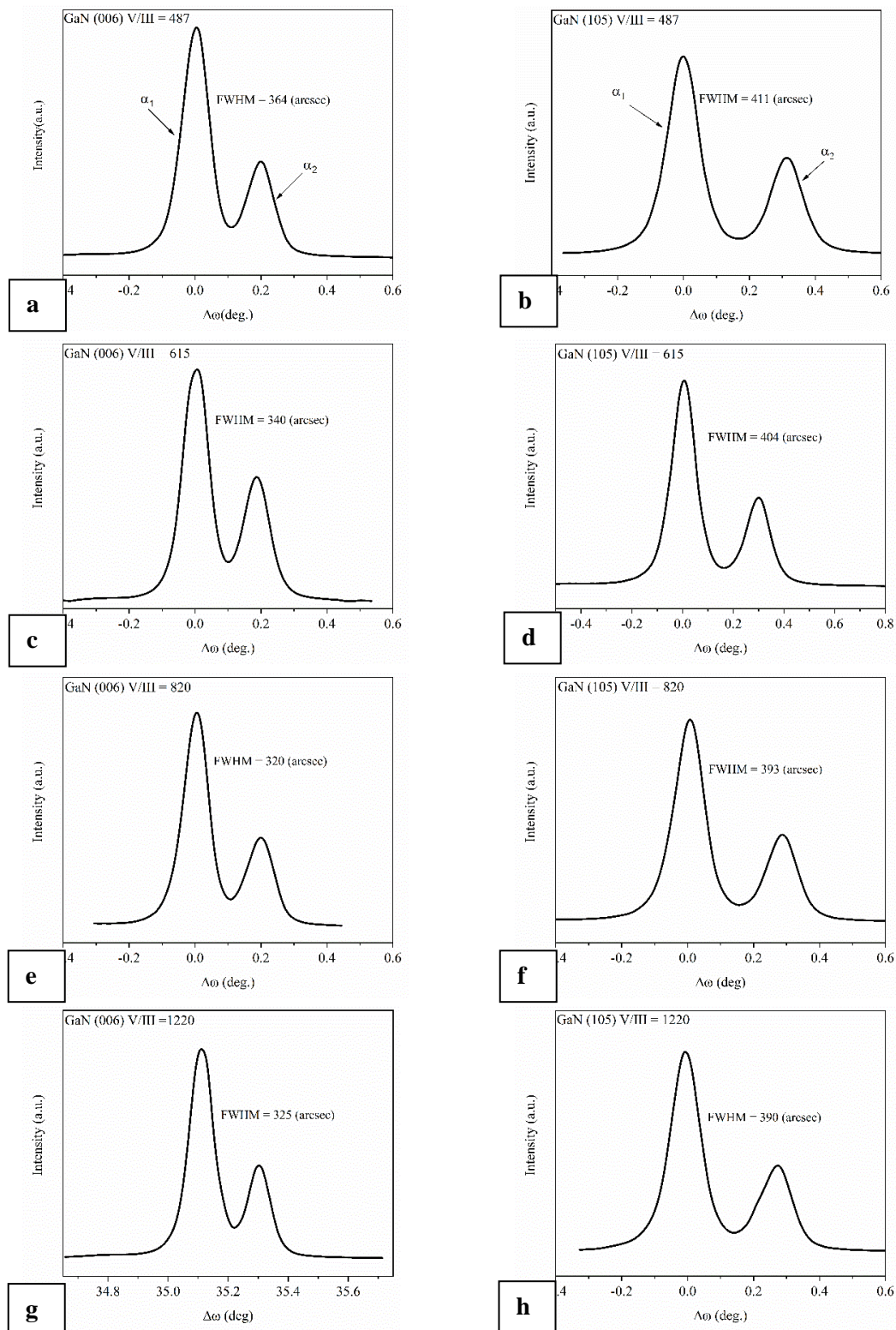
Figure 3.7 FWHM of the rocking curve for GaN (006) and (105) reflection planes at different V/III ratios: (a,b) 487 (c,d) 615 (e,f) 820 and (g,h) 1220.
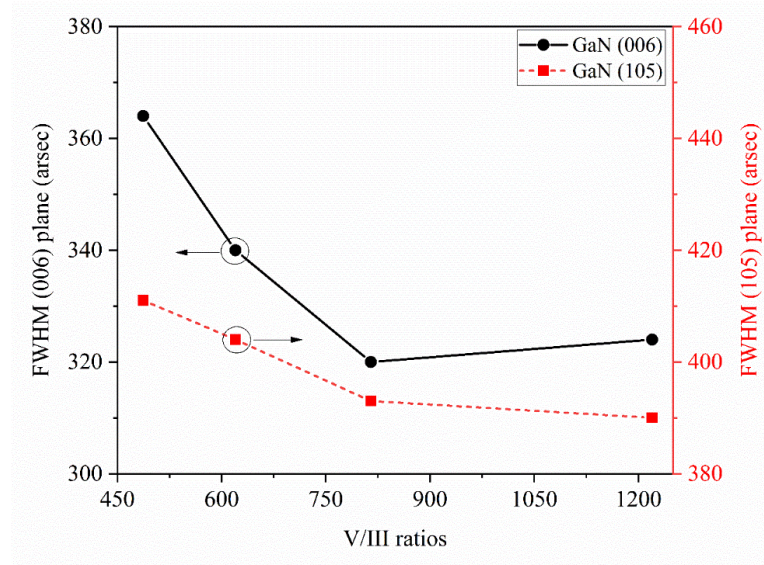
Figure 3.8 FWHMs of the rocking curve for GaN thin films that are grown at different V/III ratios.

In this work, GaN thin films samples grown at high V/III ratio showed better qualities than those samples grown at low V/III ratio. The broad FWHMs of rocking curves related to the threading dislocation density in the thin film. When the line width of the sample grown at high V/III ratio is decreased, it indicates a decrease in the density of threading dislocations. Experimental results show that the GaN thin film deposited with the V/III ratio of 820 has the best results in surface morphology and the FWHM of the rocking curve.

Figure 3.9 shows measured rocking curves of (006) and (105) reflection planes using pure H_2 carrier gas. When the molar rate of H_2 is increased, the broad FWHM at GaN (105) and (105) planes is increased due to the effect of the screw and mixed dislocations, as shown in Figure 3.10. Mixed dislocations are associated with the step terminations in (105) planes. The resulting AFM image in Figure 3.3-d reveals that the screw and mixed dislocation ascribe step termination.
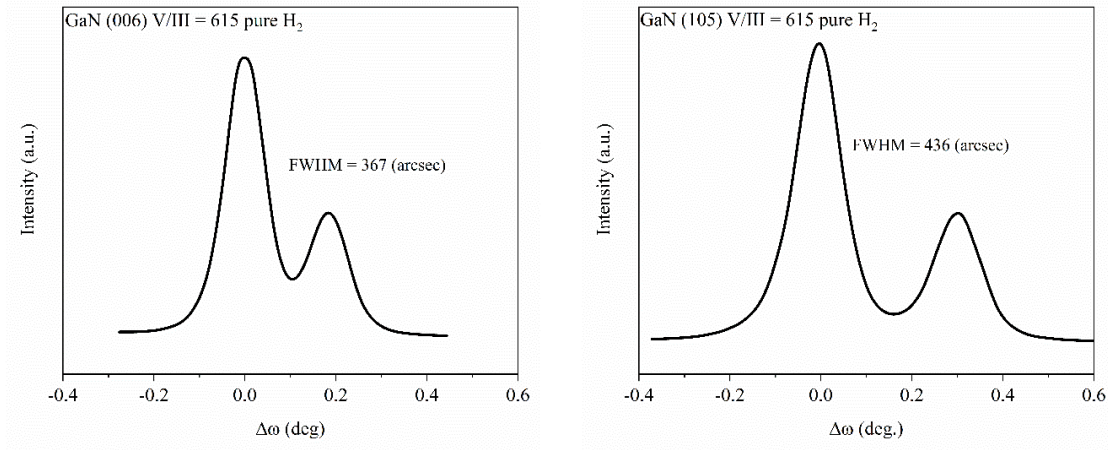
Figure 3.9 Measured rocking curves of ω scans for GaN (006) and (105) planes at pure H_2 carrier gas.
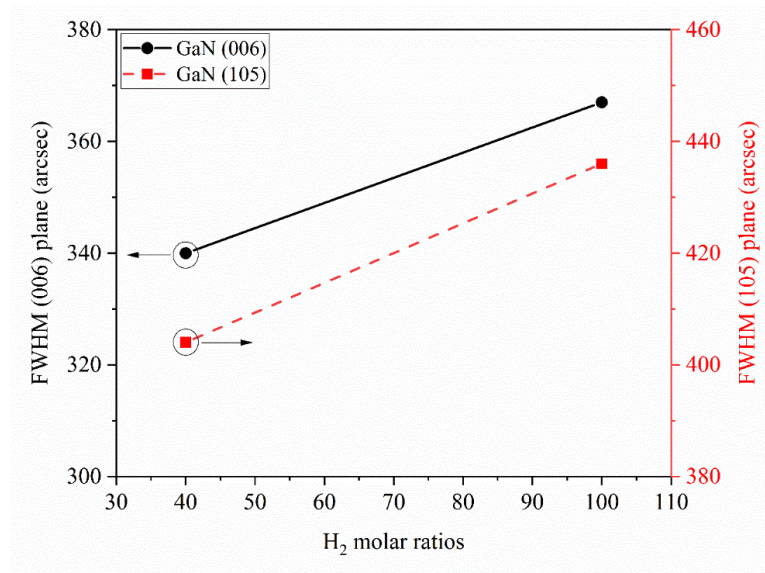
Figure 3.10 FWHMs of the rocking curve for GaN (006) and (105) at different H_2 molar ratios where the V/III ratio of 615.

3.3.1 Dislocation density

To evaluate the crystal quality of GaN thin films, FWHM of rocking curves can provide valuable information about TDs in the lattice structure. FWHM is a direct measure of the mosaicity in the thin film. Chierchia et al.[36] proposed relation of estimating the dislocation density D_d, using the

FWHM values of rocking curves. It is assumed that TDs are distributed randomly at grain boundaries.

$$D_d = \frac{\beta^2}{2\pi \ln(2)\ b^2} \tag{3-4}$$

$$\beta^2 = \beta_{edege}{}^2 + \beta_{screw}{}^2 \tag{3-5}$$

Where β is is the line broadening at FWHM of the rocking curve, which is fitted by Gaussian peak shapes, and b is the Burgers vector magnitude. *βedge* and *βscrew* are the contributions of screw and edge dislocations, respectively. Figure 3.11 shows the edge and the screw dislocation density for GaN thin films samples grown at different V/III ratios. The edge-dislocations density decreased from $(8.9\ x\ 10^8\ cm^{-1})$ to $(8.07\ x\ 10^8\ cm^{-1})$ with the increase of V/III ratio. On the other hand, the screw dislocation density decreased from $(2.65\ x\ 10^8\ cm^{-1})$ to $(2.16\ x\ 10^8\ cm^{-1})$.
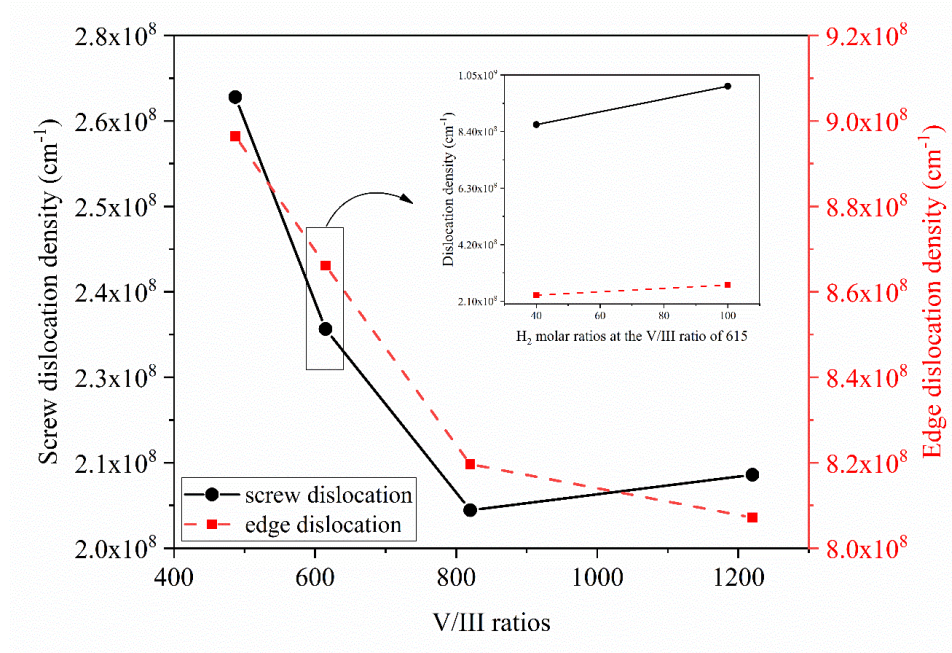
Figure 3.11 Effect of varying the V/III ratio and H_2 molar ratio on the dislocation density of GaN thin films.

Results show that the edge dislocation is more sensitive to the V/III ratio than the screw dislocation. This result agrees well with the smooth surface morphology indicated by AFM images. As a result, the surface morphology of GaN thin films grow with a high V/III ratio is improved as the screw-type dislocations, and density of pinned steps is reduced. The results of the estimated threading dislocation densities in Figure 3.11 show that further increases in V/III ratio leads to decrease both screw and edge dislocations. On the other hand, increasing H_2 molar ratio leads to rising the off-axis dislocation obviously while the on-axis dislocation increases slightly. These XRD measurement results agree well with the surface morphology of GaN thin films. Since the FWHM of the XRD diffraction peak is relative to the average crystalline grain size in the film [81]. According to XRD results it is concluded that changing V/III ratios affect the quality of the GaN thin film, and further decreasing V/III ratio can deteriorate the quality of thin film significantly.

3.4 Scanning electron microscope

For further investigation of the effect of varying the V/III ratio on the surface morphology and the crystalline structure of GaN thin films, examinations were carried out on the GaN samples using Zeiss Sigma field emission scanning electron microscope (FESEM). Figure 3.12 shows the cross-section of GaN thin films grown on sapphire (Al_2O_3) wafers with different values of the V/III ratio. It is observed that the thickness of GaN thin films increases with the increase in the TMG flow rate during the growth process. It means that the growth rate increases with decreasing the V/III ratio. It has been revealed that the thickness of the GaN thin films depends on the TMG flow rate. This can be ascribed to sufficient supply of the flow rate of metal-organic TMG precursors to the substrate surface and consequently increase the growth rate. However, some micro-cracks are found in the cross-section of GaN thin films, as shown in Figure 3.12.

Micro-cracks result from plastic relief of tensile strain the consequence of growing grain coalescence. These micro-cracks are induced in the surface morphology may be due to the strain

between the buffer layer and the GaN thin film grow at high temperature. At the low value of the

V/III ratio is observed, subsurface cracks oriented nearly perpendicular to the substrate surface, as

shown in the cross-sectional SEM image in Figure 3.12 (a).
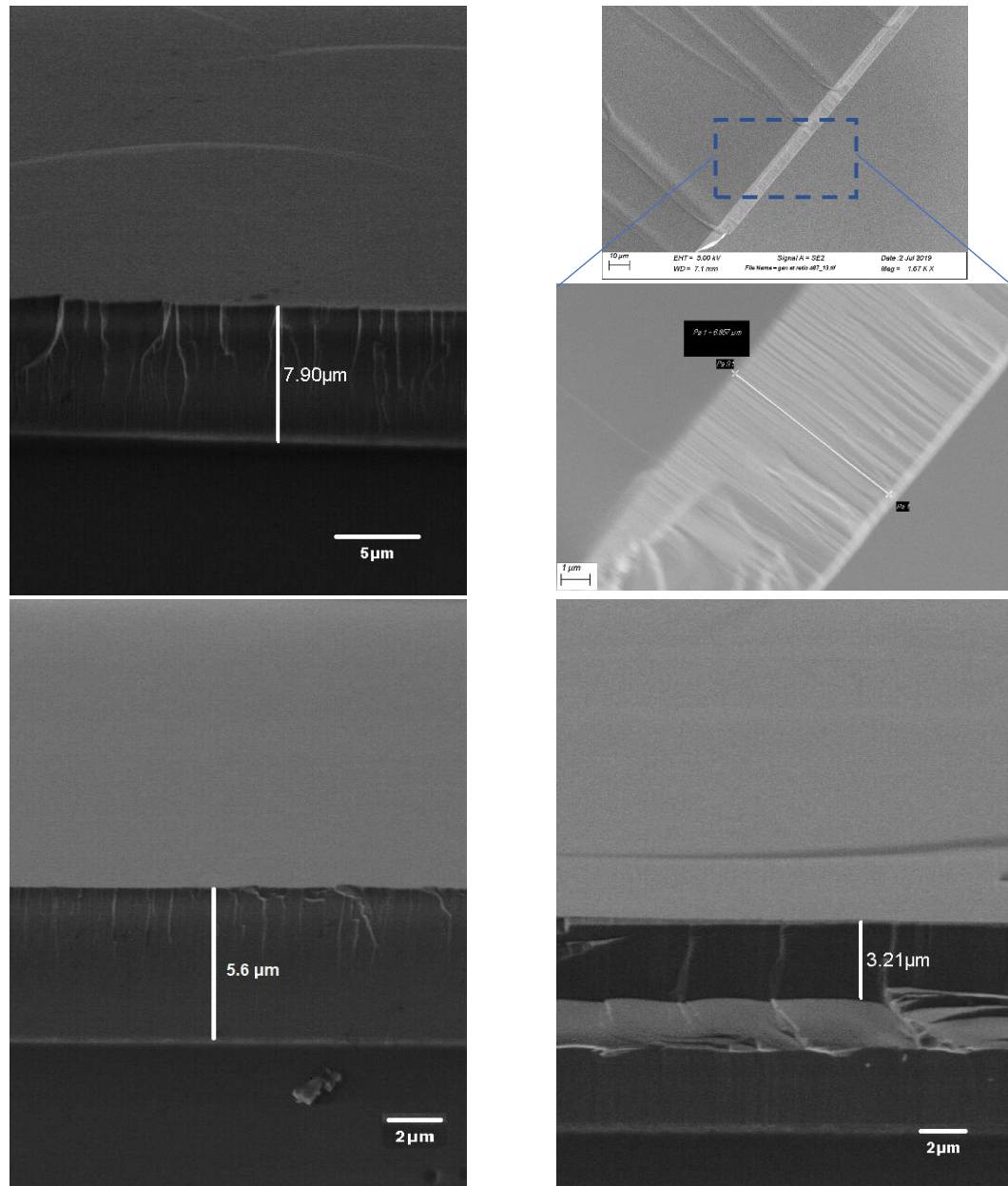
Figure 3.12 cross-sectional SEM images of the GaN thin film deposited on the sapphire wafer with different values of the V/III ratio (a) 487, (b) 625, (c) 815, and (d) 1220 with a mixture of 40%H_2 and 60%N_2 as the carrier gas at reference conditions.
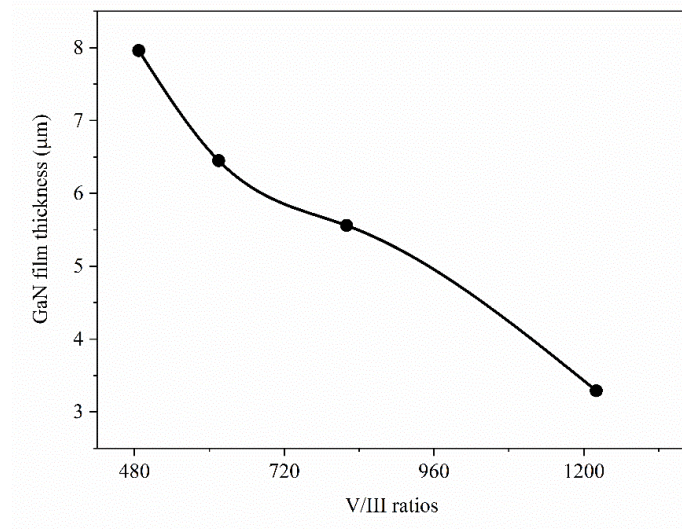
Figure 3.13 Varying the thickness of GaN thin films with different values of the V/III ratio.

When the V/III ratio is increased, these internal cracks did not reach the substrate surface during. For thick layers, cracks may occur, resulting from the build-up of tensile stress [86]. The thickness of the GaN thin film is observed to increase gradually when the V/III ratio is decreased. The thickness is varied between 3.2 µm to 7.9 µm with reducing the V/III ratio from 1220 to 487, respectively, as shown in Figure 3.13.

3.5 Raman Microscopy

Raman spectroscopy is a non-destructive test used to investigate strain state in the material by measuring the inelastic scattering of an incident photon. The incident photon can be scattered elastically (Rayleigh scattering) at the same frequency as the incident photons, inelastically (Stokes scattering) if the scattered photons have a frequency less than the incident photons. To the contrary, if the scattered photon has a higher frequency than the incident photons, it is called Anti-Stokes scattering [82]. The Raman measurements were performed by Renishaw spectrometer at room temperature, using 514 nm wavelength of Helium-Neon laser. All samples of GaN thin films are prepared in consistence dimensions to fit the device. The common phonon modes in hexagonal

GaN crystal structure are the E_2 near 566 cm-1 and A1 near 735 cm-1, as shown in Figure 3.14. [83]. It is known that the value of E_2 phonon mode is 566.2 in unstrained GaN thin film. [84]
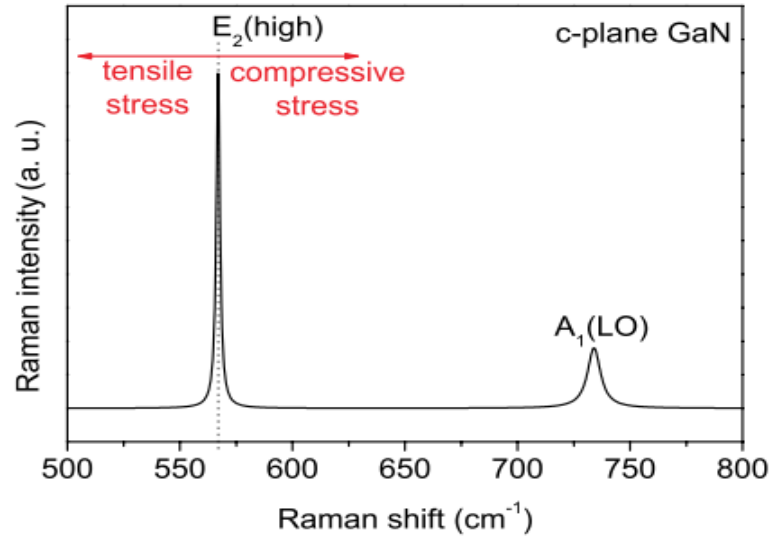
Figure 3.14 Typical Raman phonon frequencies (cm^{-1}) observed at 300 K for epitaxial GaN [83].

Figure 3.15 shows the peak position of E_2 phonon mode is slightly shifted to higher wavenumber with reducing the V/III ratio. Shifting E_2 phonon mode to a higher number indicates that GaN thin film under compressive strain compared to the unstrained position. The residual compressive stress can be estimated from Raman shift by the following formula [85]:

$$\sigma = \frac{\Delta\omega}{2.56} \quad (GPa^{-1}cm^{-1}) \tag{3-6}$$

Where **$\Delta\omega$** is the Raman frequency shift. The results reveal that the residual compressive stress increases with decreasing V/III ratio as shown in Figure 3.16
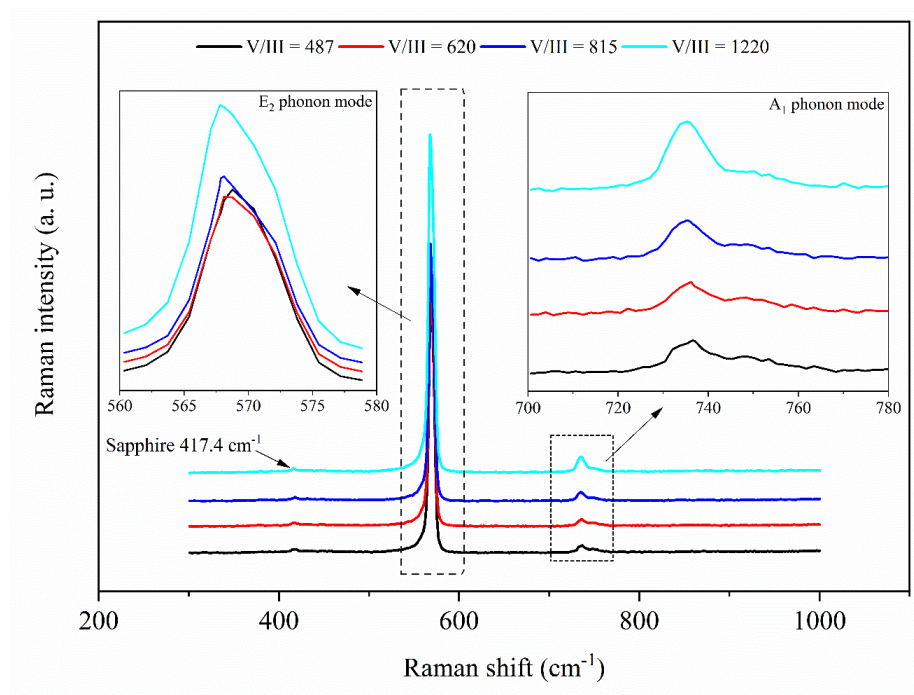
Figure 3.15 Raman spectrum of GaN GaN thin films grown at a different value of the V/III ratio with a mixture of 40%H_2 and 60%N_2 as the carrier gas at reference conditions.
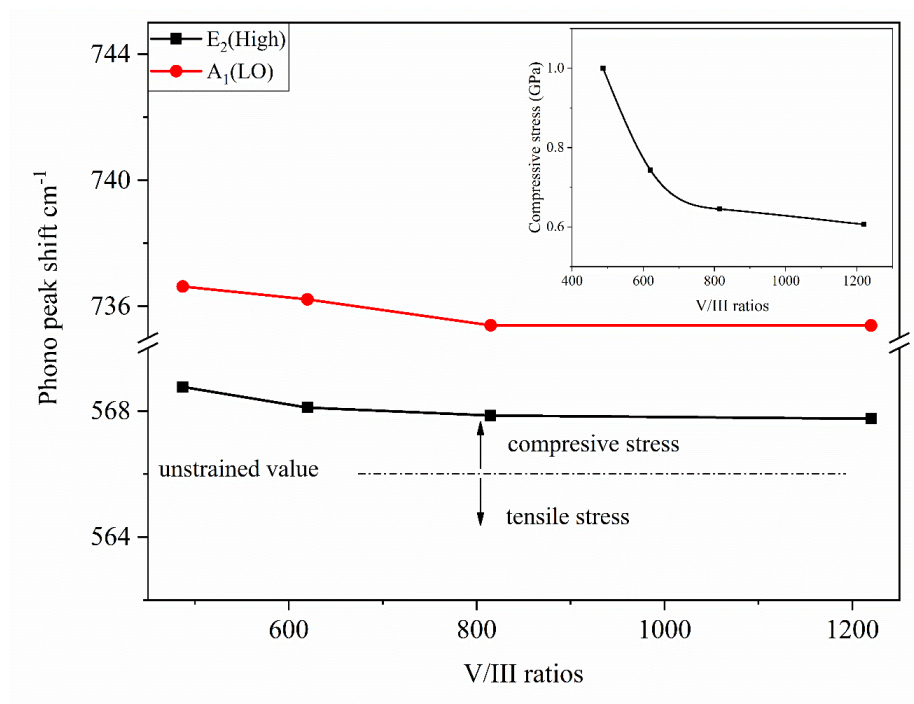
Figure 3.16 Raman phonon frequencies (cm^{-1}) of GaN thin films grown at a different value of the V/III ratio with a mixture of 40%H_2 and 60%N_2 as the carrier gas at reference conditions.

As electrical resistivity of the thin film is inversely proportional to the carrier concentration, the strong A_1 (LO) mode is an indication of a low free carrier concentration which affects the electrical properties of the material.[82]. Figure 3.16 shows that A_1 (LO) mode increases with decreasing V/III ratio indicates that incorporation of impurities or formation of defects in the thin film. This behavior is consistent with XRD results.

3.6 Conclusions

In conclusion, the crystal structure and surface morphology of GaN thin films grown on sapphire substrates in the MOCVD reactor was found to be strongly dependent on the varying of the V/III ratio, while other growth conditions are kept constant. The AFM results indicate that the GaN thin film deposited at the high V/III ratio has a smooth surface. Using a mixture of carrier gases (H_2 and N_2) promotes getting a smooth surface with high crystal quality. Thereby, a higher flow of nitrogen in III-carrier gas resulted in a GaN layer with a hillock surface. In contrast, the GaN layer grown with smaller nitrogen (higher hydrogen flow) in III-carrier gas showed a mirrorlike surface. XRD results show that GaN thin films grown at low V/III ratio have high dislocation density, and that can affect the quality of the thin film. Moreover, some-micro cracks were observed on the cross-sectional image of GaN thin films grown at low V/III ratio. On the other side, Raman scattering results show that GaN thin films that are grown at high V/III ratio have less residual stress and high crystalline quality. In conclusion material, characterizations can shed light on the optimization of GaN thin films in the MOCVD process.

Chapter 4

NUMERICAL SIMULATION OF GAN GROWTH

4.1 Introduction

The MOCVD process is demonstrated to accomplish a successful transition from traditional processes to mass production and high throughput. This chapter presents the mathematical model that describes the steady-state transport phenomena in the MOCVD reactor. It consists of a set nonlinear, coupled, and partial differential equations that are based on conservation of mass, momentum, energy, and chemical species. The chemical kinetics model is coupled with the transport processes in the single MOCVD reactor. These equations are employed to simulate the process to study the growth rate and uniformity of GaN thin films under different boundary conditions.

4.2 Governing Equations

The governing equations for the MOCVD process are derived from the principles of conservation of mass, momentum, energy, and chemical species. Some assumptions are made to reduce the complexity of modeling the CVD process. In the MOCVD, the process involves convective transport, diffusive transport, and chemical reactions. The gas flow in the reactor is assumed to be laminar, so it is not necessary to consider turbulent flow [3]. Typically, the MOCVD process runs at low inlet velocity and low reactor pressure that result in low Reynolds numbers. For the given pressure and temperature, the gas mixture is treated as a continuum and as an ideal gas, which satisfies Newton's law of viscosity [24]. Some reactant species absorb infrared heat radiation. Usually, these species are present in very low molar ratio. Therefore, the gas mixture to be assumed non-participating for heat radiation. The viscous dissipation in the gas mixture is negligible due to the low inlet flow velocity and low viscosity.

(1) Conservation of mass.

$$\frac{\partial \rho}{\partial t} + \nabla.(\rho V) = 0 \qquad \text{4-1)}$$

(2) Momentum force balance.

$$\partial \frac{\rho V}{\partial t} = -\nabla P + \nabla.(\rho V V) + \nabla \left\{ \mu[\nabla V + (\nabla V)^T] - \frac{2}{3}\mu I \nabla.V \right\} + \rho g \qquad \text{4-2)}$$

(3) Conservation of energy.

$$Cp \, \frac{\partial(\rho T)}{\partial t} = -Cp\nabla.(\rho V T) + \nabla.(k\nabla T) + \nabla.\left(RT \sum_{i=1}^{N} \frac{D_i^T}{M_i} \frac{\nabla x_i}{x_i} \right) + \sum_{i=1}^{N} \frac{H_i}{M_i} \nabla.j_i - \sum_{i=1}^{N} \frac{H_i}{M_i} \dot{R}_i \qquad \text{4-3)}$$
$$+ S$$

$$\dot{R}_i = M_i \sum_{i=1}^{N} v_{in}(R_n^i - R_{-n}^i) \qquad \text{4-4)}$$

(4) Conservation of species.

$$\frac{\partial \rho \omega_i}{\partial t} = -\nabla.(\rho V \omega_i) - \nabla.j_i + \sum_{j=1}^{k} \dot{R}_j^i \qquad \text{4-5)}$$

Where $\dot{R}_j$ is the net volumetric rate of generating of species j, ω_i is the mass fraction of species i, and j_i is the diffusion mass flux vector of species i, and S is an external heat source. The diffusion fluxes of concentration and temperature gradients are given by:

$$j_i = \rho \frac{M_i}{M} \sum_{i=1}^{N} D_{ij} \left(\nabla \omega_j + \omega_j \frac{\nabla M}{M} \right) - D_i^T \frac{\nabla T}{T} \qquad \text{4-6)}$$

Where M_i is the molecular weight of the species, D_{ij} is the multi-component diffusion coefficient between species i and j, D_i^T is the multi-component thermal diffusion coefficient of species. The remaining symbols are defined in the nomenclature.

The growth rate of the thin film is determined by two factors: the collision rate of the gas species on the substrate surface and the diffusion of active reactants to the surface [53]. Therefore, the GaN deposition rate is controlled by the transferring Ga-containing species to the wafer surface. The growth rate GR of GaN thin films is given by:

$$GR = \frac{M_{GaN}}{\rho_{GaN}} \sum_i \frac{J_i}{M_i}$$

4-7)

4.2.1 Transport properties of gaseous species

Due to the large temperature gradients inside the MOCVD reactor, and the large difference in molecular weights (g/mol) between precursors (trimethylgallium M_{TMG} = 114.83, ammonia M_{NH3} = 17) of GaN and the carrier gas (hydrogen M_{H2}=2), the dilute mixture approximation in laminar flow is not adequate. The effect of coupling between heat transfer and mass diffusion becomes significant. Therefore, the gas mixture is treated as a multi-component species system. Temperature-dependent transport properties of the gas mixture such as D diffusion coefficients (m^2/s), dynamic viscosity μ (kg/m/s), heat capacity Cp (J/kg/K), and thermal conductivity k (W/m/K), have significant effect on the accurate prediction of the growth rate in most MOCVD processes.

The kinetic theory of gases is used to estimate the transport properties of the gas mixture. These depend on properties and compositions of the reactant species [86].

(a) The ideal gas law describes gas mixture density:

$$\rho = \frac{P}{RT \sum \omega_i / M_i}$$

4-8)

where ω_i is the mass fraction and M_i is the molecular weight of species i.

The constraint on the mass fraction is:

$$\sum_{i=1}^{N} \omega_i = 1 \qquad \text{4-9)}$$

(b) The dynamic viscosity of chemical species i, is calculated using the kinetic theory

$$\mu_i = 2.67E - 06 \frac{\sqrt{M_i T}}{\sigma_i^2 \Omega_D} \qquad \text{4-10)}$$

where Ω_D is the collision integral of the species, and σ_i is Lennard-Jones parameters of species. [21]. The viscosity of the gas mixture is given by:

$$\mu = \sum_{i=1}^{N} \frac{x_i \mu_i}{\sum_j x_j \varphi_{ij}} \qquad \text{4-11)}$$

$$\varphi_{ij} = \frac{\left[1 + \left(\frac{\mu_i}{\mu_j}\right)^{\frac{1}{2}} \left(\frac{M_i}{M_j}\right)^{\frac{1}{4}}\right]^2}{\left[8\left(1 + \frac{M_i}{M_j}\right)^{\frac{1}{2}}\right]} \qquad \text{4-12)}$$

where x_i, x_j and M_i, M_j are mole fractions and molecular weight of species i, j respectively.

(c) The specific heat capacity of chemical species is calculated using Gordon-McBride polynomial function of temperature and NIST-JANAF thermodynamic tables to calculate the coefficients [69], [70]:

$$\frac{C_{Pi}}{R_i} = c_1 + c_2 T + c_3 T^2 + c_4 T^3 + c_5 T^4 \qquad \text{4-13)}$$

Where R_i is the gas constant of species i. The specific heat capacity of the gas mixture is computed as the average of mass fraction of the specific heat capacity of species:

$$C_p = \sum_i \omega_i C_{p,i}$$

4-14)

(d) The thermal conductivity of chemical species i, is computed using Eucken correlation [22]:

$$k_i = \mu_i \left(c_{pi} + \frac{5}{4} R_i \right)$$

4-15)

The thermal conductivity of the gas mixture is estimated as follows:

$$k = \sum_{i=1}^{N} \frac{x_i k_i}{\sum_j x_j \varphi_{ij}}$$

4-16)

(e) The binary mass diffusion coefficient is computed using the modified Chapman-Enskog theory since the diffusion behavior of gas mixture species depends on the growth temperature and reactor pressure.

$$D_{ij} = 1.88 * 10^{-2} \frac{\sqrt{T^3 \left(\frac{M_i + M_j}{M_i * M_j} \right)}}{P \sigma_{ij}^2 \Omega_D}$$

4-17)

All quantities in equation 4-17) are in SI units except σ_{ij} (°A).

(f) The thermal diffusion coefficient of species is computed using empirical-based composition-dependent expression

$$D_i^T = -2.59E - 07T^{0.659} \left[\frac{M_i^{0.511} x_i}{\sum_{i=1}^{N} M_i^{0.511} x_i} - \omega_i \right] \cdot \left[\frac{\sum_{i=1}^{N} M_i^{0.511} x_i}{\sum_{i=1}^{N} M_i^{0.489} x_i} \right]$$

4-18)

This equation will impact species diffusion such that heavy molecules diffuse less rapidly while light molecules will diffuse more rapidly towards the heated surface [88].

4.2.2 Chemistry model

The MOCVD process involves chemical reactions between metal-organic vapors group III and gaseous group V in the periodic table. These precursors are diluted in a carrier gas and passed over a heated substrate to form a solid thin film. In growing of the GaN thin film, trimethylgallium TMG (group III) and the ammonia NH_3 (group V) are typical precursors of the gallium (Ga) and the nitrogen atom (N), respectively. The overall reaction between TMG and NH_3 precursors to form the GaN thin film and release methane (CH_4) can be simplified and represented as follows:

$$TMG\ (gas) +\ NH_3(gas) \rightarrow GaN(solid) + 3CH_4(gas)$$
4-19)
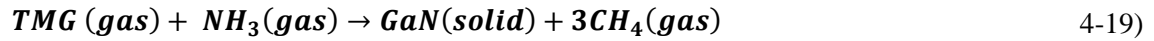
However, there are many intermediate chemical reactions take place during the deposition process. The chemical reactions in the MOCVD growth process are divided into two types, the gas phase, and the surface phase. Sengupta et al. [64] investigated comprehensive reaction mechanisms for the deposition of GaN thin films in the MOCVD process. Their model involved gas phase and surface reactions, adsorption of surface species at the substrate surface, and growth of GaN thin films. The reaction mechanism included 17 gas phase and 23 surface species that participate in 17 gas phase and 52 surface reactions, respectively. Hu et al. [65] simplified the comprehensive model, proposed by Sengupta et al. [64], using the rate of production (ROP) analysis to identify dominant chemical reaction paths.

The reduced model involves 17 gas-phase species and 7 surface species that participate in 17 gas-phase reactions and 17 surface reactions, respectively. The reduced model is adapted in this study to investigate the effects of boundary conditions in the MOCVD process. Table (2-4) summarizes equations of gas-phase reactions and surface phase reactions. The corresponding reaction rate constants for these reactions in the gas and at the surface are estimated by using thermochemical methods and thermodynamic data of existing experimental observations [70,74]. It is assumed that

precursors are decomposed homogenously to intermediate species that react on the wafer surface to form a solid thin film.

4.2.3 Gas-phase reactions

The chemical reactions of the gas phase involve two pathways that describe the formation and decomposition of species, as shown in Figure 4.1. The first pathway is adduct formation between TMG and NH_3 at the inlet gas. Such adducts may condense on the cold reactor surface to form particulates that degrade the film quality [89]. A split inlet design of the precursors can exclude the formation of stable adduct [63]. Adducts start to decompose in the high-temperature zone of the reactor. The second pathway is the decomposition of trimethylgallium (TMG) into dimethylgallium (DMG), and monomethylgallium (MMG) by eliminating methyl groups (CH_4, CH_3), and reacting with NH_3. Under high temperature near the substrate surface, MMG and COMPM1(s) are expected to be dominant Ga-containing precursors that contribute to the deposition of GaN thin films [65].
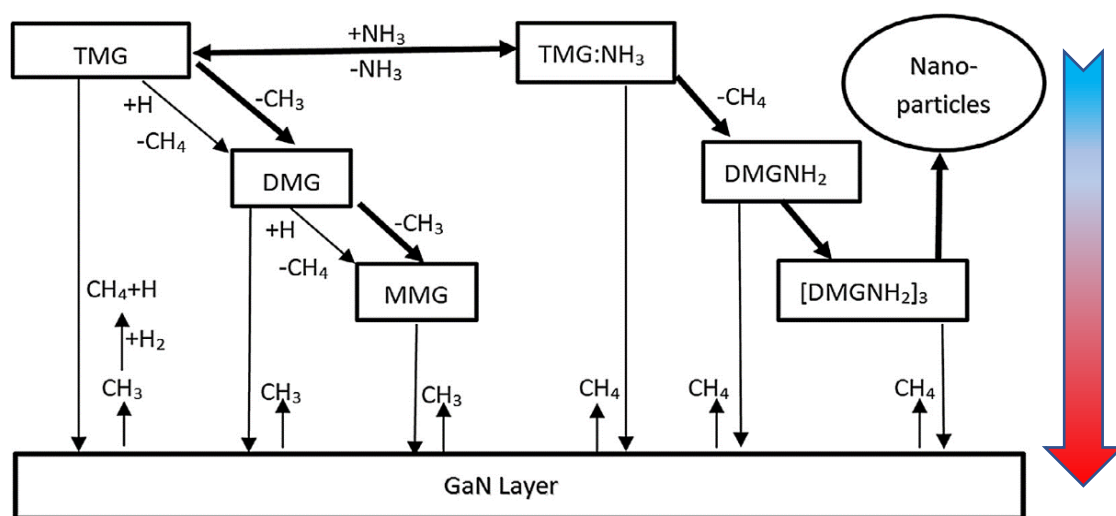
Figure 4.1 Schematic diagram of chemical pathways for the GaN deposition and growth, adapted from [90].

In the high-temperature zone, the conversion of TMG into MMG is rapid, and the concentration of MMG is expected to be high. When the energy is sufficient, the MMG in the gas phase is absorbed by the substrate to form the surface site MMG(s) which then interacts with NH_3 to form COM1(s). Finally, CH_4 and CH_3 are released to produce GaN. The finite rate chemistry model has solved the chemical reaction, and the Arrhenius equation defines reaction rate constants in the gas phase and surface reactions:

$$k = AT^n e^{-Ea/RT} \qquad \qquad \text{4-20)}$$

where A_i and Ea_i are the pre-exponential factor and the activation energy, respectively, R is the gas constant and T is the inlet temperature.

Table (4-1) Gas-phase reactions in GaN deposition

	$k = AT^n e^{-Ea/RT}$	A	N	Ea (kj/mol)
G1	TMG $\longleftrightarrow$ DMG + CH_3	1.0e+47	-9.18	76996
G2	DMG $\longleftrightarrow$ MMG + CH_3	7.67e+43	-9.8	34017
G3	MMG $\longleftrightarrow$ Ga + CH_3	1.68e+30	-5.07	84030
G4	TMG +NH_3 $\longrightarrow$ TMG:NH_3	2.28e+34	-8.31	3115
G5	TMG +NH_3 $\longrightarrow$ DMG:NH_2 + CH_4	1.7e+04	2.0	19969
G6	DMG +NH_3 $\longrightarrow$ DMG:NH_3	4.08e+31	-7.03	3234
G7	DMG +NH_3 $\longrightarrow$ MMG:NH_2 + CH_4	530e+03	1.56	20744
G8	MMG +NH_3 $\longrightarrow$ MMG:NH_3	7.95e+24	-5.21	2094
G9	MMG +NH_3 $\longrightarrow$ $GaNH_2$ + CH_4	8.1e+05	1.3	17722
G10	NH_3 + CH_3 $\longrightarrow$ NH_2 + CH_4	3.31e+03	2.51	9859
G11	CH_3 + H_2 $\longrightarrow$ CH_4 + H	1.2e+12	0	12518
G12	TMG + H $\longrightarrow$ DMG + CH_4	5.0e+13	0	10036
G13	DMG + H $\longrightarrow$ MMG + CH_4	5.0e+13	0	10036
G14	$TMGNH_3$ $\longrightarrow$ MMG + $2CH_3$ + NH_3	1.33e+44	-8.24	77791
G15	CH_3 + H + M $\longrightarrow$ CH_4 + NH_3	2.4e+22	-1	0
G16	CH_3+ CH_3 $\longrightarrow$ C_2H_6	2.0e+13	0	0
G17	2H + M $\longleftrightarrow$ H_2 + M	1.0e+16	0	0

4.2.4 Surface reactions

Surface reactions take place at the heated substrate surface and involve gas adsorption and desorption, diffusion, deposition, and etching of the solid thin film [91]. The mechanism of surface reactions involves three types of species: gas phase, surface, and bulk species, as shown in Figure 4.2. The gas-phase species denoted by (g) exist above the substrate surface in the flow stream. The surface species denoted by (s) exist at the gas-solid interface layer on the top of the substrate surface. Bulk species is a solid species denoted by (b) that is located below the surface of the previous layer. Besides, there is an open site denoted by N(s), which is used to conserve both sites and elements in surface reaction.
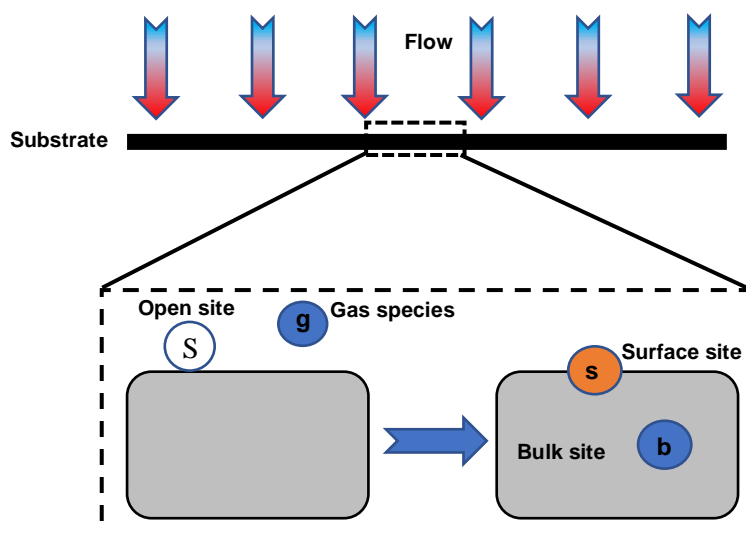
Figure 4.2 Schematic diagram illustrates the types of species in the surface reaction.

For example, consider the reaction (S1) in Table (4-2), where the gas-phase (MMG) is reacting with a free site (Ns) leading to formation of an adsorbed species (MMG(s)) at the substrate surface. The desorption of surface species (COMPM2(s)) leads to deposit GaN (solid species) and leave an open site (Ns) as well as release H_2 (gas species) back to the gas phase, as seen in reaction (S6).

Table (4-2). Surface phase reaction in GaN deposition				
	$k = AT^n e^{-Ea/RT}$	A	N	Ea (kj/mol)
S1	MMG+N(s) ⟶ MMG (s)	1.16e+05	2.98	0
S2	MMG(s) ⟶ MMG + N(s)	1.12e+14	0.55	107673
S3	NH3 + MMG(s) ⟶ COMPM1(s)	3.35e+07	3.33	0
S4	COMPM1(s) +MMG ⟶ NH3 + MMG(s)	5.7e+13	-0.16	8146
S5	COMPM1(s) ⟶ CH_4 + COMPM2(s)	1.23e+10	3.22	23446
S6	COMPM2(s) ⟶ $2H_2$ + 2GaN(B) + N(s)	3.68e+09	2.05	59610
S7	TMG+N(s) ⟶ TMG (s)	1.16e+05	2.98	0
S8	TMG(s) ⟶ TMG + N(s)	1.12e+14	0.55	49675
S9	TMG(s) + NH_3 ⟶ TCOM1(s)	3.35e+07	3.33	0
S10	TCOM1(s) ⟶ NH_3 + TMG(s)	5.7e+13	-0.161	11922
S11	TCOM1(s) ⟶ CH_4 + TCOM2(s)	1.49e+11	0.609	32785
S12	TCOM2(s) ⟶ $2CH_4$ + GaN(B) + N(s)	1.49e+11	0.609	49675
S13	$TMGNH_3$ + N(s) ⟶ TCOM1(s)	1.16e+05	2.98	0
S14	TCOM1(s) ⟶ $TMGNH_3$ + N(s)	1.12e+14	0.55	49675
S15	TCOM1(s) ⟶ $2CH_3$ + MMG +NH_3 + N(s)	1.12e+14	0.55	107673
S16	$MMGNH_3$ + N(s) ⟶ COMPM1(s)	1.16e+05	2.98	0
S17	COMPM1(s) ⟶ $MMGNH_3$ + N(s)	1.12e+05	0.55	107673

Table (4-3). Compositions of the chemical compounds exist in the surface phase reactions.		
1	COMPM1(s)	NH_3.MMG(s)
2	COMPM2(s)	Ga.NH_2.MMG(s)
3	TCOM1(s)	NH_3.TMG(s)
4	TCOM2(s)	NH_2.DMG(s)

4.3 Computational techniques of solution

The mathematical model of the MOCVD process involves a complex interaction of transport phenomena, chemistry, thermodynamic properties, and process conditions, so it is not possible to solve it analytically. Numerical techniques are used to convert the coupled nonlinear partial differential equations of the mathematical model to algebraic equations that can be solved. The solution domain is divided into many small control volumes or cells. The governing equations are integrated numerically over each of these cells, and the numerical solution gives the values of the variables at the center of each computational cell. The computational mesh should be well defined to obtain a convergent solution that reflects reasonably the physical reality. A coarse mesh is used in locations that have small changes of the variable, while a fine mesh is used near areas that have

large gradients to achieve a proper resolution. Common discretization approaches are employed in the modeling of the CVD process as following:

➢ Finite difference method (FDM) is used for the numerical solution of complex models of CVD [92]. FDM treats the solution region as a collection of discrete grid points by using Taylor series.

➢ Finite element method (FME) is used to model complex geometries of highly diluted gas systems of the CVD process [61]. FME treats the solution region as a buildup of many small, interconnected sub-regions that form the grid.

➢ Finite volume method (FVM) is used for modeling 2D and 3D transport phenomena in the diluted and undiluted CVD process [24]. FVM discretizes the integral form of conserved equations directly in the physical domain without transforming the governing equations to the computational domain. Since FLUENT solver employs FVM in the discretization of the governing equations, here is a brief description of FVM. This method is described in more details elsewhere [59].

4.3.1 Finite Volume Method

This method employs structured and unstructured grids, so it has the flexibility to solve a complex geometry by defining the shape and location of the control volumes. The mathematical model of transport governing equations is written as unsteady convective-convection type for a variable $\emptyset$ as follows:

$$\zeta_\emptyset \frac{\partial}{\partial t}(\rho\emptyset) = -\zeta_\emptyset \nabla.(\rho\emptyset u) + \nabla.(\Gamma_\emptyset \nabla\emptyset) + S_\emptyset \qquad \text{4-21)}$$

where $\zeta_\emptyset$, $\Gamma_\emptyset$ are generalized diffusion coefficients and $S_\emptyset$ is a source term per unit volume. The computational domain is discretized into a set of finite control volumes; each of them surrounding a grid point. Scalar quantities (temperature, pressure, mass fraction of species, and material properties) are stored and calculated typically at the center of each control volume. Vector

quantities (velocity and diffusion flux of species) are calculated in points that are located at the cell surface by interpolated local and adjacent cell values.

Equation	$\emptyset$	$\zeta_\emptyset$	$\Gamma_\emptyset$	$S_\emptyset$
(4-1)	1	1	0	0
(4-2)	$\boldsymbol{V}$	1	M	$\nabla\left\{\mu[\nabla\boldsymbol{V}+(\nabla\boldsymbol{V})^T]-\dfrac{2}{3}\mu I\nabla.\boldsymbol{V}\right\}+\rho g$
(4-3)	T	C_p		$\nabla.\left(RT\displaystyle\sum_{i=1}^{N}\dfrac{D_i^T\,\nabla x_i}{M_i\ x_i}\right)+\displaystyle\sum_{i=1}^{N}\dfrac{H_i}{M_i}\nabla.j_i-\displaystyle\sum_{i=1}^{N}\dfrac{H_i}{M_i}\dot R_\iota$
(4-5)	ω_i	1		$\nabla.j_i+\displaystyle\sum^{k} R_j^i$

The general equation form is the volume integral over the control volumes that are surrounding the grid point **P**, which has four sides for the 2D process, see Figure 4.3.

$$\zeta_\emptyset\frac{\partial}{\partial t}\int \rho\emptyset dV + \zeta_\emptyset\int \rho\emptyset u.\,dV = \int \Gamma\nabla\emptyset.\,dV + \int S_\emptyset dV \qquad\text{4-22)}$$

The volume integral of the convection and diffusion terms is transformed into a surface integral by using the Gauss-divergence theorem.

$$\zeta_\emptyset\frac{\partial}{\partial t}\int \rho\emptyset dV + \zeta_\emptyset\int \rho\emptyset u.\,dA = \int \Gamma\nabla\emptyset.\,dA + \int S_\emptyset dV \qquad\text{4-23)}$$
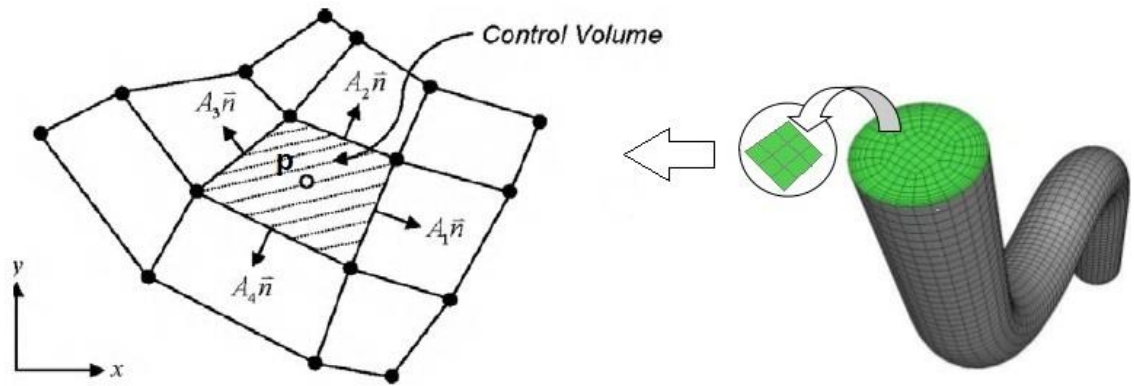
Figure 4.3 Schematic diagram of the control volume surrounding the grid point.

Replacing the surface integral by a summation over the faces that are enclosed the element, equation 4-23) becomes:

$$\zeta_\emptyset \frac{\left(\rho\emptyset_p\right)^{\Delta t+t} - \left(\rho\emptyset_p\right)^t}{\Delta t} \Omega_a + \zeta_\emptyset \sum_{i=1}^{f} \rho\emptyset_i u . A_i = \sum_{i=1}^{f} \Gamma\nabla\emptyset_i . A_i + S_\emptyset\Omega_a \qquad \text{4-24)}$$

where Δt indicates the value of incremental time at the next step, $\emptyset_i$ indicates the value of variables at the external sides of the control volume Ω_a, and the f denotes for the number of bounding surfaces. The discretized form in equation (4-24) can be expressed simply in a set of the algebraic form for every control volume in the domain:

$$a_p\emptyset_p + \sum_{nb} a_{nb}\emptyset_{nb} = b_p \qquad \text{4-25)}$$

where a_p and a_{nb} are coefficients derived from the discretized equation, and $\emptyset_{nb}$ is the summation over the surrounding sides of neighbor grid points (nb). This equation shows that the local grid point **P** is related to its adjacent cell values and the residual term b.

4.4 Solution procedure

The algebraic equations are nonlinear and coupled, so the iterative method is used in the solution procedure until the converged solution is obtained. Ansys- Fluent provides two kinds of basic solver algorithms:

➢ Density-based coupled solver (DBCS) solves the coupled system equations of fluid dynamic (continuity, momentum, and energy).

➢ The pressure-based solver has two algorithms:

❖ The segregated solver solves the pressure correction and momentum equation sequentially.

❖ The coupled solver solves the pressure and momentum equations simultaneously.

Pressure based (Segregated)   Pressure based (Coupled)   Density based (Coupled)

Solve U-momentum

Solve V-momentum

Solve W-momentum

Solve Mass continuity Update velocity

Solve Mass, Momentum,

Solve Mass, Momentum, Energy, Species

Solve Energy

Solve Species

Solve Turbulence Equations

Solve Other Transport Equations as required
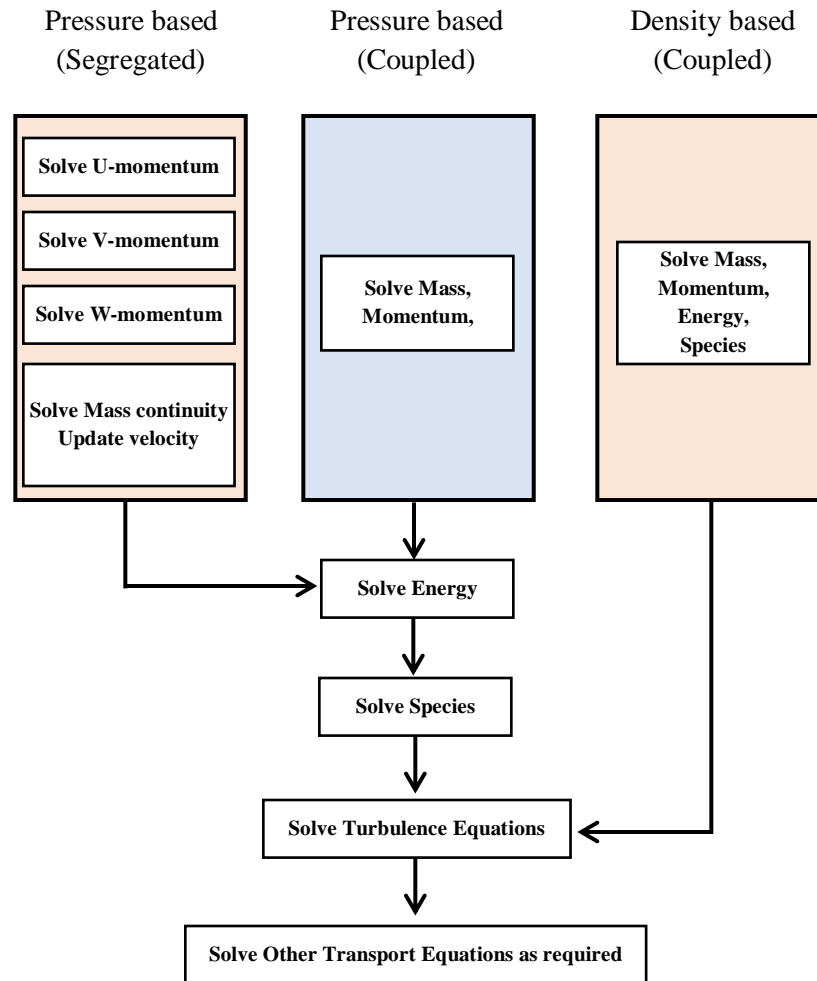
Figure 4.4 Schematic diagram of solvers in Ansys-Fluent.

The pressure-based algorithm is proved as robust and versatile. Thus, it is utilized for a wide range of physical models, including multi-phase flows, conjugate heat transfer, and combustion [93]. However, there is a fundamental difficulty in the calculation of the velocity field, related to the pressure gradient term in the momentum equation. There is no apparent equation for obtaining the pressure distribution [94]. Thus, pressure-velocity coupling refers to the numerical algorithm, which uses a combination of continuity and momentum equations to derive the pressure correction equation. Then the pressure correction is used to obtain the velocity correction. The corrected pressure and velocity are used with an initial guess iteratively until the convergence is achieved. The pressure-velocity coupling algorithm PISO (pressure-implicit with the splitting of operators)

is used in this study. PISO has a higher order of the approximate relation for pressure and velocity corrections, and also it also performs neighbor correction and skewness correction.

4.5 Validation of Numerical model

Figure 4.5 shows a sketch of a vertical CVD reactor, which is considered in detailed in this study. We first consider a reactor employed by Sandia Labs. The wafer with a diameter of 50.8 mm is placed on the rotating susceptor inside a quartz tube with an inner diameter of 114.3 mm. The distance from the gas inlet and the susceptor surface is 100 mm [63]. It involves precursors and carrier gases impinging on a heated, rotating susceptor. The boundary conditions for the MOCVD reactor are stated as follow: the mixture of metal-organic precursors TMG and NH_3 is diluted in the carrier gas H_2, which provides the bulk flow inside the reactor. This mixture of gases enters from the top of the vertical rotating disk MOCVD reactor and impinges on the heated wafer surface that rotates at a high-speed rate of 1200 rpm. The initial total volume flow rate at standard conditions is (13.1003 slm), specified at the inlet. The temperatures of the inlet flow and of inner and outer walls are set at 300 K. Table (4-4) shows a range of parametric values employed at the inlet of the reactor.

Table (4-4) Parametric values used for the GaN growth in the MOCVD process considered.

Symbol	Factors	Reference values	Range
ω	Susceptor rotating rate (rpm)	1200	0 – 1400
T	Wafer temperature (K)	1273	773 – 1473
u	Velocity inlet of the mixture (m/s)	0.127	0.0254-0.4563
P	Pressure (Torr)	140	20-760
NH_3	Flow rate of NH3 (slm)	6	2 – 10
TMG	Flow rate of TMG (slm)	0.003	0.001 - 0.01

Some assumptions are made for the model as follow: the flow is laminar, and the mixture of gases is treated as a continuum and as an ideal gas. Non-slip, impermeable conditions apply on velocity, and zero species gradient are employed for non-reacting walls. The flow at the outlet is taken as

fully developed. The temperature distribution at the susceptor is taken as uniform. The heating system is located directly below the susceptor so the heat radiation between walls can be neglected. The effect of viscous dissipation in the flow is neglected.

The numerical simulation is carried out by using the commercial CFD code ANSYS-FLUENT that utilizes the finite volume method [93]. Grid independence is examined by using different mesh sizes to get consistent results. A quarter of the reactor is used for the simulation with an axial symmetry condition. The reactor model is validated by comparing the predicted results with available experimental data in the literature [63]. Numerical results agree quite well with the experimental results, as shown in Figure 4.5 (b). It is observed that the predicted results in the proposed model are slightly higher than experimental results, around 5 %. This is within the acceptable range as provides validation for model.
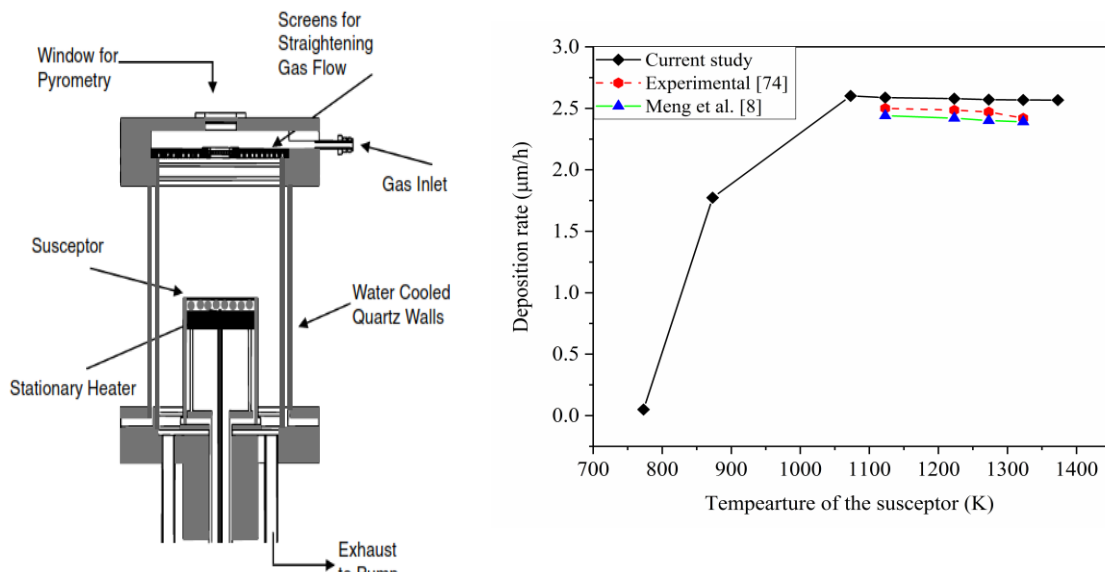
Figure 4.5 (a) Schematic diagram of the vertical rotating susceptor reactor considered in this study (b) Comparison of predicated GaN growth rate by computational model and experimental results [63]

The temperature distribution and magnitude of velocity components inside the reactor at the given conditions are shown in Figure 4.6(a). The flow spreads over the susceptor, and then turns

downward at the edge, as expected. The vertical velocity of the gas flowing downward is reduced as it approaches the susceptor and is redirected radially, reaching a stagnation point of zero vertical velocity at the susceptor surface. A "hump" is seen on the axial velocity component (**u**) because the gas heats up and expands due to the thermal effect of the high temperatures near the susceptor. On the other hand, the temperature increases monotonically from the inlet to the susceptor surface. Further results are obtained for this CVD reactor using the validated numerical model.
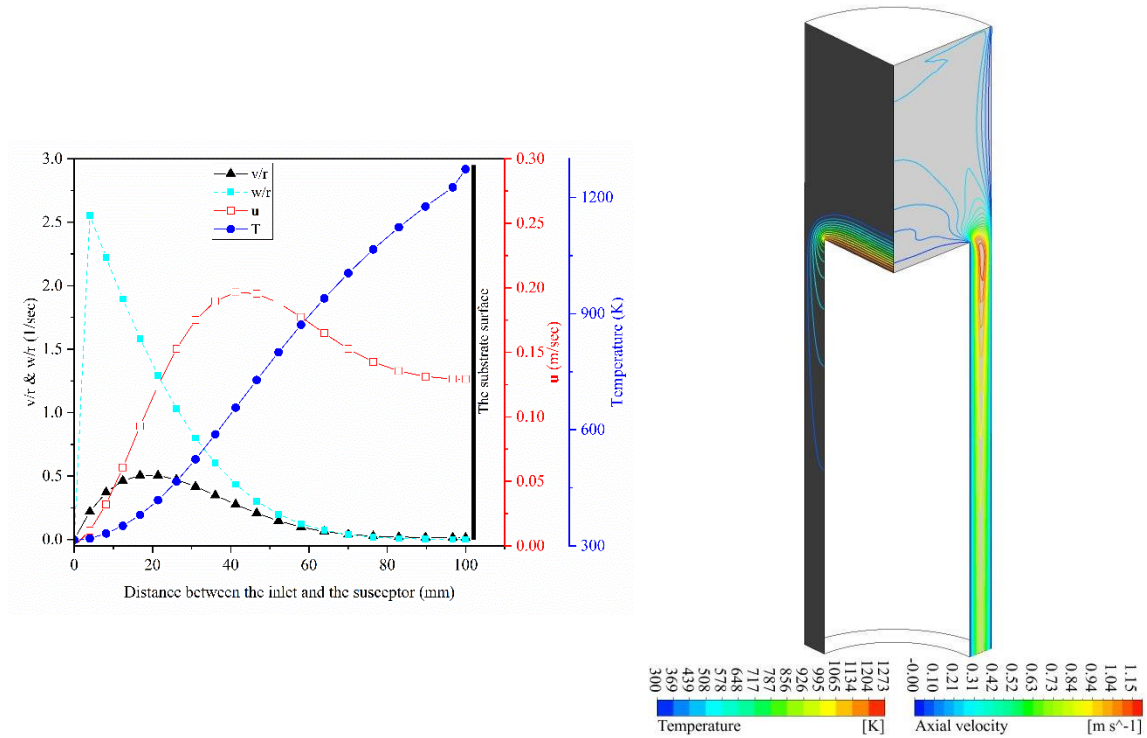
Figure 4.6 (a) Velocity and temperature profiles as a function of height above the susceptor at initial conditions. (b) The contour plot of the thermal field and flow field.

4.6 Results and discussion

This section presents a comparative study of GaN thin films grown on c-plane sapphire (Al_2O_3) wafers in the MOCVD process. Results for samples under different growth conditions are discussed. The effect of critical operating conditions on the growth rate and uniformity of GaN thin films in the MOCVD process is investigated. This gives a greater insight into the reactor

performance and process optimization. One parameter is varied every time while the others are kept constant at reference values. The average deposition rate (GR) and standard deviation (St) are used to evaluate the growth rate and uniformity of GaN thin films on the wafer surface. The area-weighted average of the growth rate is computed by dividing the summation of the product of the total local growth rate GR_i and surface element area S_i, by the total area of the wafer surface S, as follows:

$$GR = \frac{1}{S}\int GRdS = \frac{1}{S}\sum GR_i|S_i| \tag{4-26}$$

$$S_t = \sqrt{\frac{\sum_{i=1}^{N}(GR - \overline{GR})^2}{N}} \tag{4-27}$$

where $\overline{GR}_m$ is the average deposition rate on the wafer surface. S_t is the standard deviation of the growth rate used to evaluate the uniformity of the thin film.

4.6.1 Rotation rate.

The rotation rate creates a centrifugal pumping effect, which is beneficial to increase the growth rate and improve the uniformity on the wafer surface. Centrifugal pumping pulls the gas species towards the rotating susceptor along the axis of rotation and throws them out along susceptor edges [61]. Figure 4.7 shows the influence of varying the rotation on the deposition rate and uniformity of GaN thin films on the wafer surface. For a stationary susceptor, the buoyancy-driven recirculation prevents precursors from reaching the heated substrate surface efficiently. Thus, the low deposition rate and non-uniform growth rate are obtained, as shown in Figure 4.8 (a). On the other hand, increasing the susceptor rotation rate enhances the downward flow and increases the magnitude of the downward velocity, as shown in Figure 4.8 (b). This aids in suppressing the natural convection-driven recirculation.

Figure 4.7 (a) Variation of average growth rate and standard deviation profiles of GaN thin films at different values of the susceptor rotation rate. GaN deposition rate at (b) 0 rpm and (c) 1400 rpm
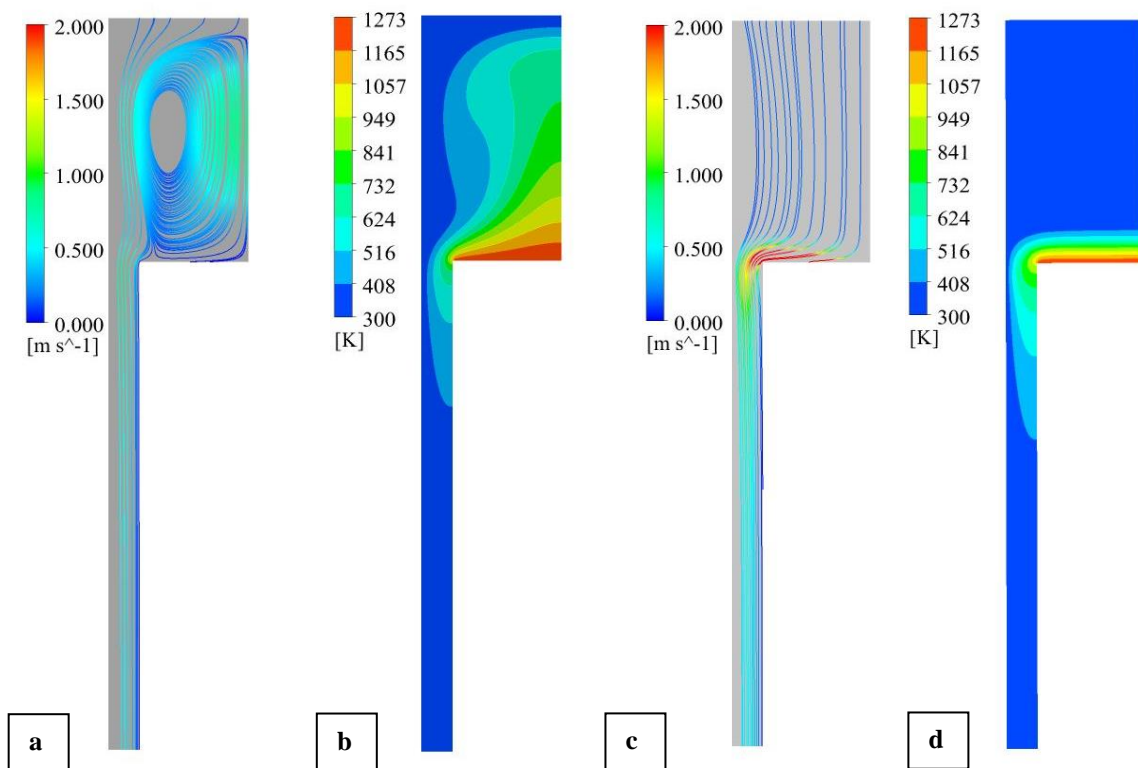
Figure 4.8 Flow and thermal field at the susceptor rotation rate of 0 rpm (a, b) and 1400 rpm (c, d).

These results are consistent with the conclusion revealed by Coltrin et al. [95]. They deduced that increasing the susceptor rotation rate reduces the thermal boundary layer thickness that leads to a consistent growth rate on the wafer surface. Furthermore, the high susceptor rotation rate decreases the residence time of gaseous species to decompose at the gas phase and enhances the transport of reactant species in reaching the substrate surface. As a result, the uniformity of GaN thin films becomes better, and the deposition rate is increased.

4.6.2 Susceptor temperature

The effect of susceptor temperature on the growth rate and uniformity of GaN thin films is investigated. Figure 4.9 shows the growth rate and standard deviation for temperatures range of 773-1423 K. At low temperature (below 900 K), which is a rate-limited (surface kinetic) regime, a very low deposition rate occurs.

Figure 4.9 (a) Variation of average growth rate and standard deviation profiles of GaN thin films at different values of the susceptor temperature. GaN deposition rate at (b) 773 K and (c) 1323 K

In the rate-limited region, the energy is not enough to overcome the activation barriers of reactants species. The activation energy is the maximum energy required to start the chemical reactions. The

growth rate increases when the temperature increases above 900 K, see Figure 4.9. In the diffusion-limited regime (900-1300 K), the surface diffusion energy is higher than the activation energy of the surface chemical reactions. Thus, the growth rate is limited by the mass transfer of reactant species across the boundary layer to the substrate surface. Due to the high susceptor rotation rate and low reactor pressure, the high-temperature gradient has a slight effect on the flow characteristic, as shown in Figure 4.10.

It is observed that increasing the temperature beyond the diffusion-limited regime, the growth rate decreases, and the uniformity profile decline slightly. At high temperature more than 1373 K, the growth rate decreases due to desorbing of some reactants species from the substrate surface. Moreover, a significant dissociation of the deposited film occurs due to the libration of Nitrogen (N) atoms (desorption) from the GaN lattice structure.
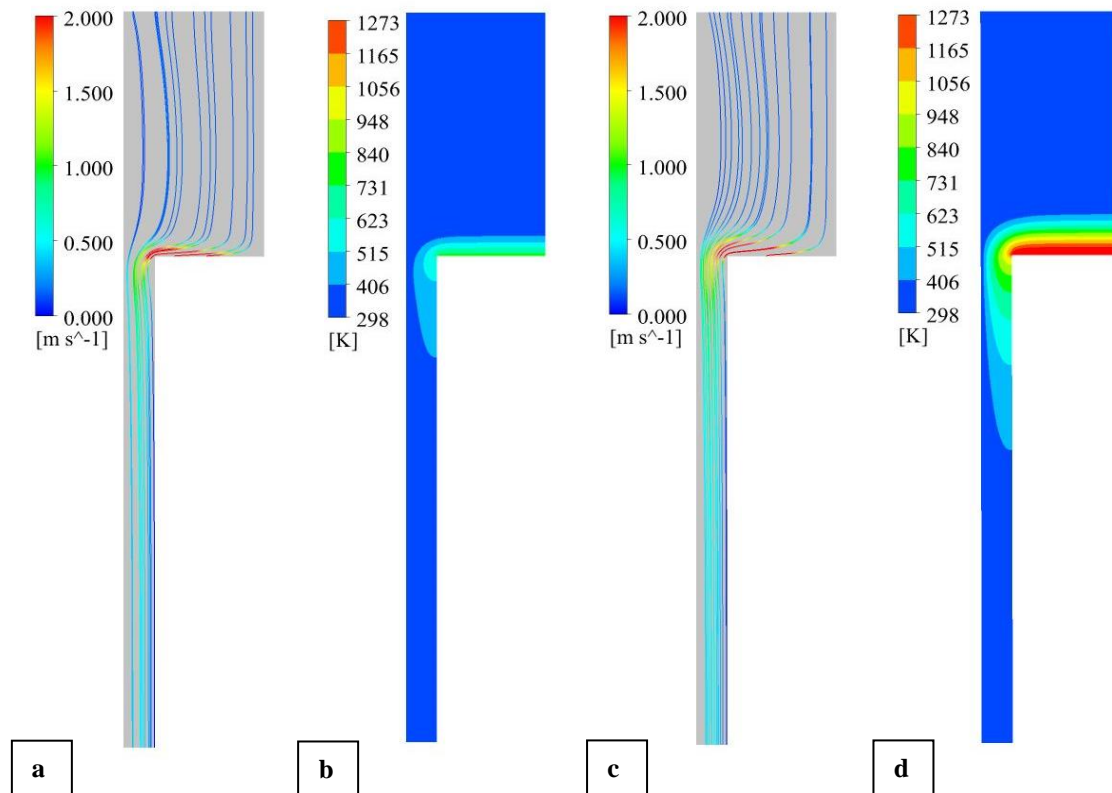
Figure 4.10 Flow and thermal field at the susceptor temperature of 773 K (a, b) and 1473 K (c, d).

As a result, to enhance the growth rate and crystal quality of GaN thin films for the practical growth process, the susceptor temperature should be located in the range of (1220-1350 K).

4.6.3 Velocity inlet.

The effect of inlet velocity on the growth rate and uniformity of GaN thin films is investigated. At low inlet velocity, both the deposition rate and standard deviation are low, as shown in Figure 4.11. Low inlet velocity enhances the reactant species to reside for sufficient time inside the reactor. However, at low inlet velocity, recirculation flow appears due to the effect of thermal driven buoyancy. This alters the growth rate and uniformity of thin films, as shown in Figure 4.12. The higher total flow rate provides more fresh reactants species for mixing before reaching the wafer surface and suppresses the flow recirculation, as shown in Figure 4.12.
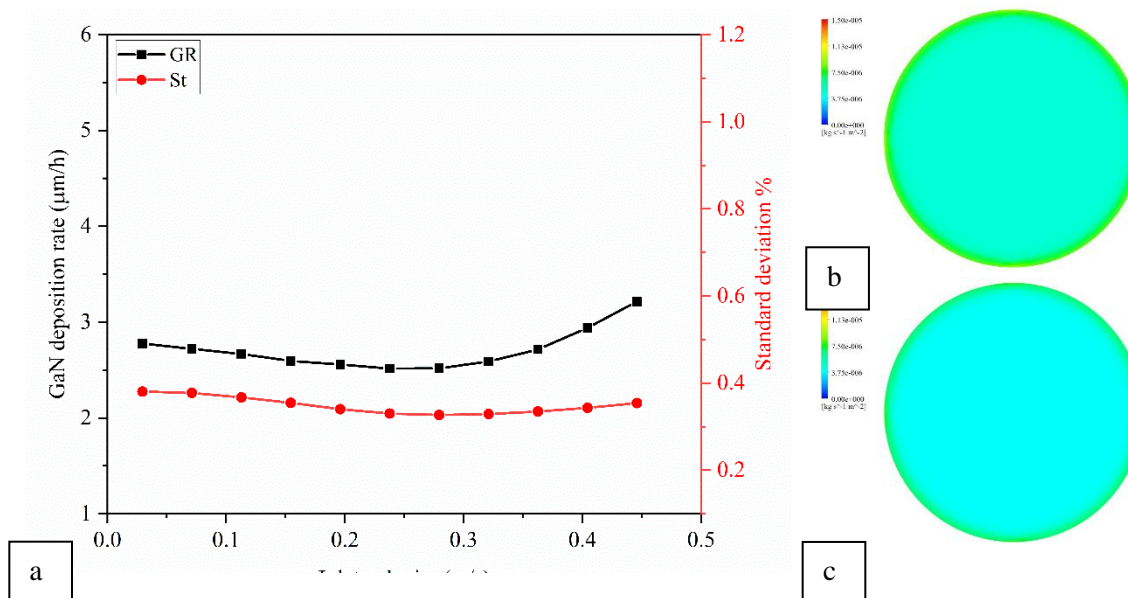
Figure 4.11 Variation of average growth rate and standard deviation profiles of GaN thin films at different values of the gas inlet velocity. GaN deposition rate at (b) 0.025 m/s and (c) 0.45 m/s

Increasing the inlet velocity from 0.03 m/s leads to a slight decrease in the deposition rate but improves the uniformity by decreasing the standard deviation, St profile. Also, it is observed that

increasing the inlet velocity of more than 0.25 m/s would further improve the deposition rate of
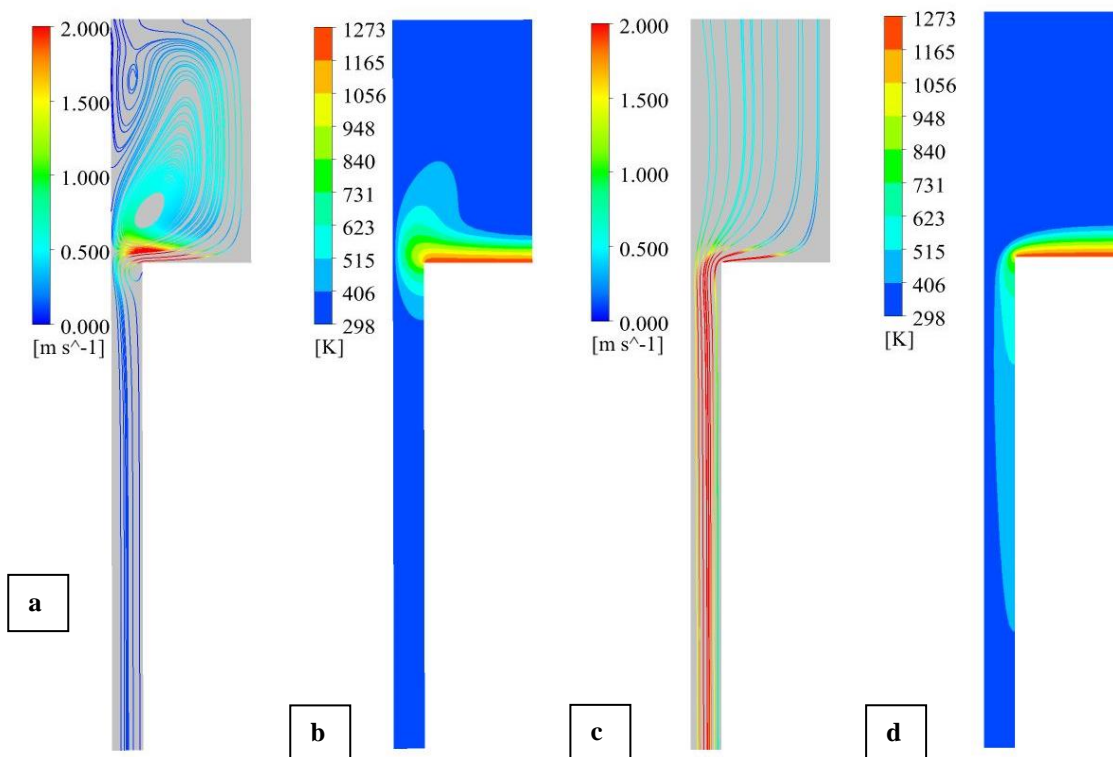
GaN thin films.

Figure 4.12 Flow and thermal field at a gas inlet velocity of 0.025 m/s (a, b) and 0.45 m/s (c, d).

4.6.4 Reactor pressure.

The effect of varying the reactor pressure on the deposition rate and uniformity of GaN thin films

is shown in Figure 4.13. The growth rate is increased with increasing the reactor pressure up to 600

Torr; then it slightly increases near the atmospheric pressure. Interestingly, the uniformity profile

of the thin film is improved with increasing the pressure up to 400 (Torr). However, increasing the

pressure further leads to an increase in the standard deviation and consequently decrease the

uniformity near the atmospheric pressure. When the mass inlet flow rate is kept constant, higher

pressure leads to a higher density of gas mixture due to the ideal gas behavior and provide more

reactants species into the reactor, but the inlet velocity decreases.
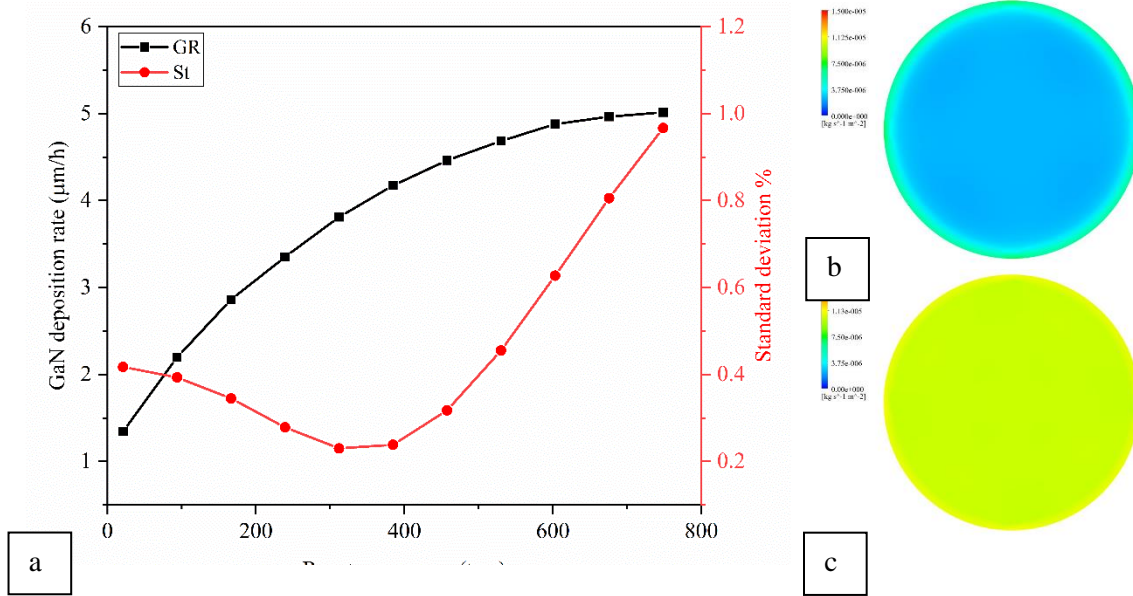
Figure 4.13 Variation of average growth rate and standard deviation profiles of GaN thin films at different values of the reactor pressure. GaN deposition rate at (b) 20 Torr and (c) 700 Torr.

Under high rotation rate (1200 rpm), the thermal boundary layer above the susceptor will be thinner that improves deposition rate. The standard volume flow rate depends on reactor pressure difference and rotation rate as follow:

$$Q \propto \sqrt{\omega \Delta P} \tag{4-28}$$

However, increasing the reactor pressure causes a decrease in the mass diffusion coefficient of reactant species, as indicated in equation 4-29), which becomes very small near the atmospheric pressure. Both the concentration of precursors and the mass diffusion coefficient can determine the deposition rate. Thus, at high-pressure, insufficient reactants reach the susceptor to achieve a uniform growth of the thin film. The residence time of the species in the gas phase becomes longer at high pressure. Long residence time enhances the parasitic reaction in the gas phase to form undesired nano-particles [70]. Further increase in the reactor pressure leads to the flow recirculation, which deteriorates the uniformity of the thin film, as shown in Figure 4.14. Such

circulating flow patterns have to be avoided, since small particles formed due to gas-phase reactions may stay in the reactor and grow, and degrade the quality of the films.
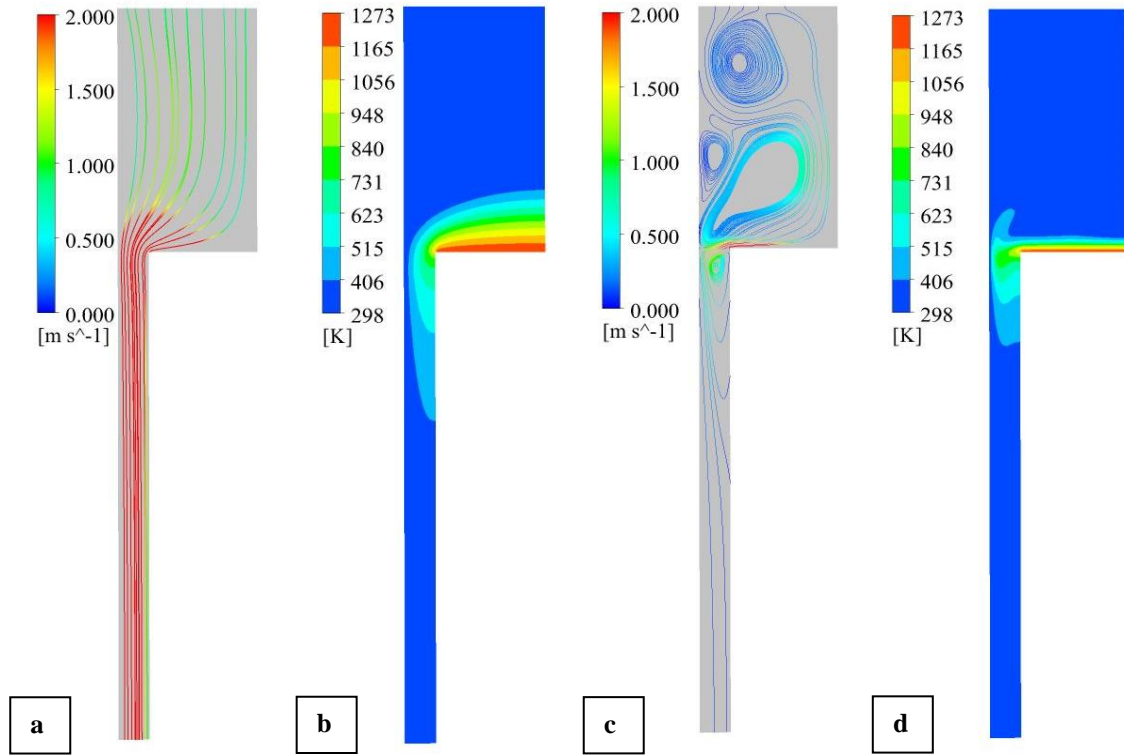
Figure 4.14 Flow and thermal field at the reactor pressure of 20 Torrs (a, b) and 760 Torrs (c, d).

As a result, the reactor pressure in the range of (200 to 400) Torr is preferable to obtain uniform and high-quality GaN thin films for optoelectronic devices.

4.6.5 V/III ratio

Figure 4.15. Shows the effect of changing the V/III ratio on the growth rate of GaN thin films. The flow rate of TMG is varied from 0.001 to 0.01 slm, while the flow rate of NH_3 is kept constant at 6 slm. It is observed that the GaN growth rate increases with decreasing V/III ratio since the TMG flow rate is increased. When the V/III ratio is decreased down, more TMG molecules are involved in the reactions, resulting in a significant increase in the deposition rate. A high growth rate of up

to 11 µm/h can be achieved at V/III ratio of 487, where other conditions are kept constant. On the other hand, keeping the TMG flow rate constant at 0.003 slm and increasing the NH_3 flow rate from 2 to10 slm leads to a decrease in the deposition rate. At a constant total flow rate, reducing the flow rate of NH_3 will increase the flow rate of H_2 in the gas mixture. Low amount of available NH_3 at the substrate results in a decrease in the growth rate. Moreover, the high-quality GaN thin film requires an adequate amount of Ga and active N species near the substrate.
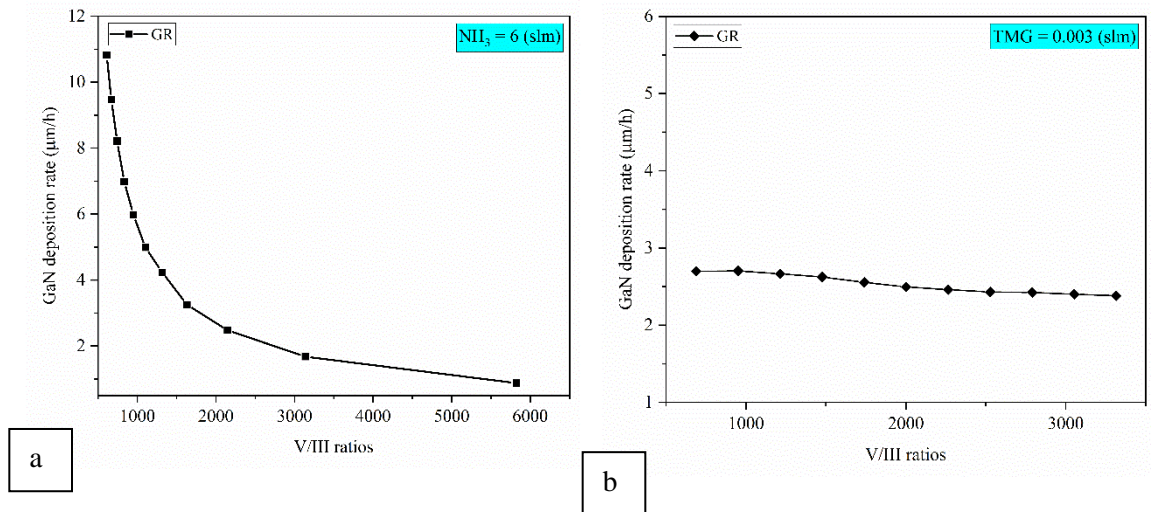
Figure 4.15 Variation of average growth rate and standard deviation profiles of GaN thin films at different values of the V/III ratio (a) NH_3 is constant and (b) TMG is constant at reference conditions.

Figure 4.16 shows the deposition rate and the standard deviation of GaN thin films at different values of the flow rate of TMG. Both GR and St are increased proportionally when the flow rate of TMG is increased. The GaN deposition rate is limited by the diffusion of Ga-containing species at the heated substrate surface. The boundary layer is caused by developing velocity, temperature fields, and the concentration of the reactants [96]. The flow rate of TMG has a slight effect on the flow and thermal fields, as shown in Figure 4.17. However, increasing the flow rate of TMG leads to a high concentration of Ga-containing species in the gas phase.
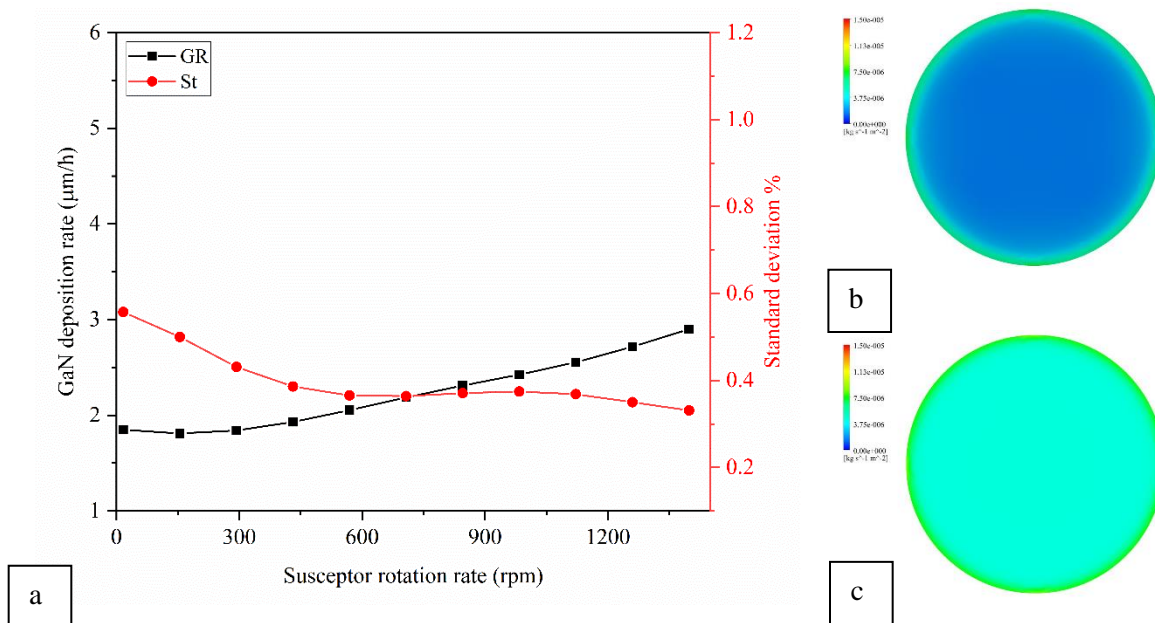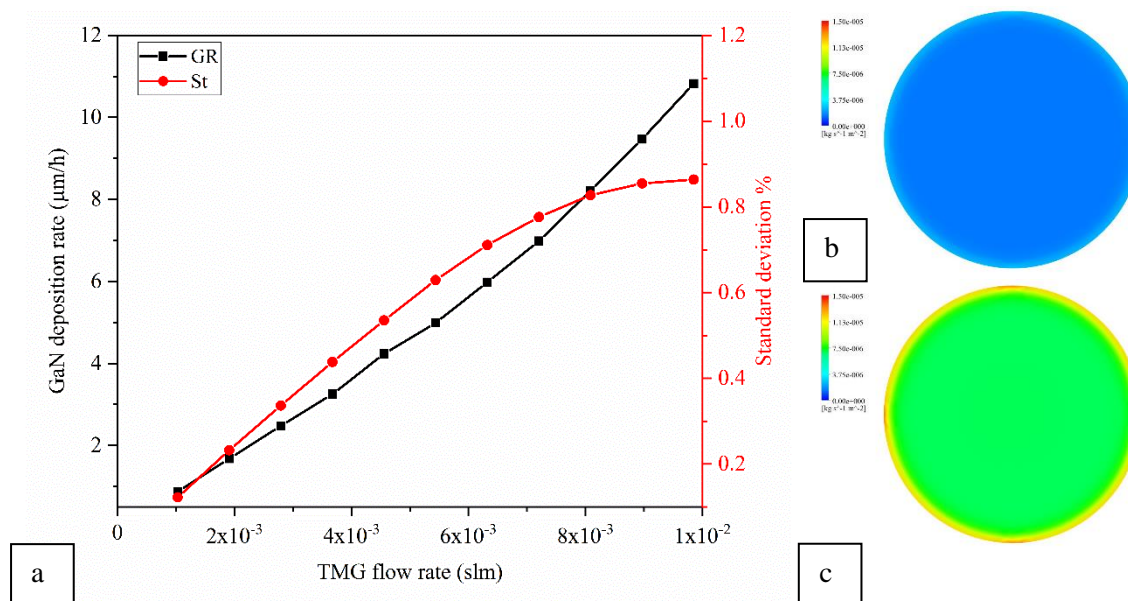
Figure 4.16 Variation of average growth rate and standard deviation profiles of GaN thin films at different values o f (a) NH$_3$ and (b) TMG at reference conditions. GaN deposition rate at (b) 0.001 slm and (c) 0.01 slm.
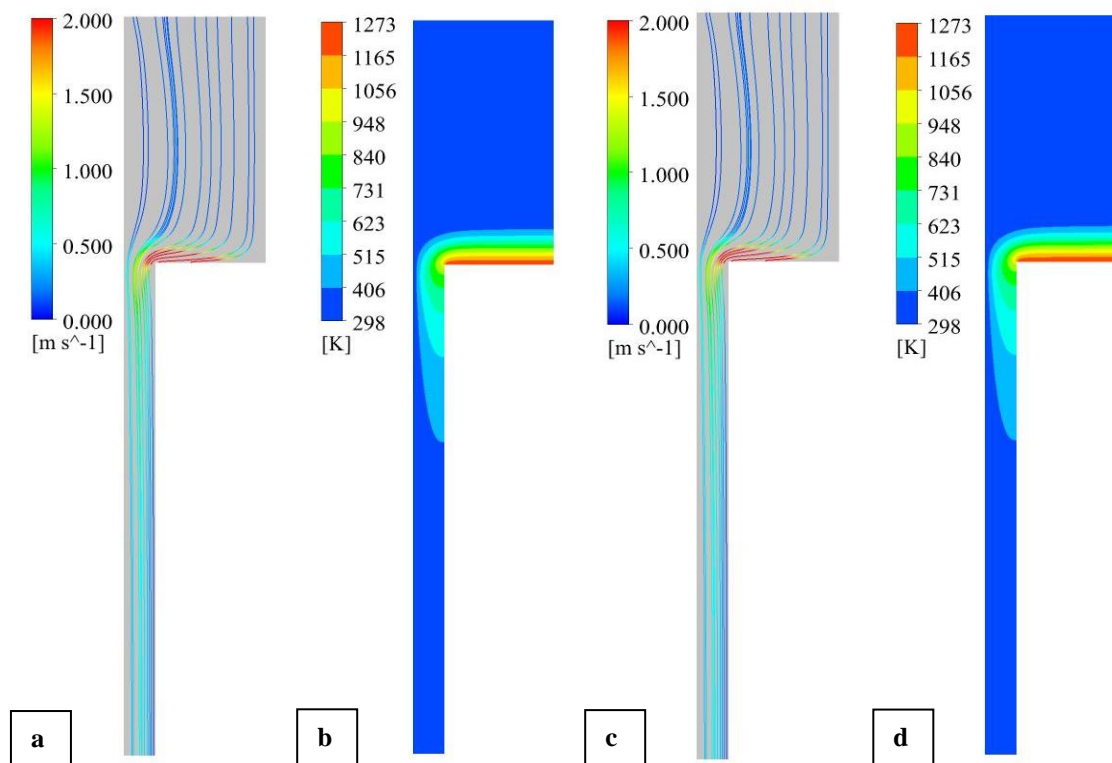
Figure 4.17 Flow and thermal field at the TMG flow rate of 0.001 slm (a, b) and 0.005 slm (c, d).

The chemical boundary layer is defined as the distance from the maximum concentration of Ga-contain species in the gas phase to the wafer surface.

$$GR \propto D_{ij} \frac{C_{Ga}^{max} - C_{Ga}^{surface}}{\delta}$$

4-30)

Where D_{ij} is the diffusion coefficient, and δ is the boundary layer thickness. The growth rate is enhanced by the high concentration of Ga-containing species and thin boundary layer above the susceptor. At high temperatures close to the wafer surface, TMG decomposes rapidly into intermediate species leading to MMG.
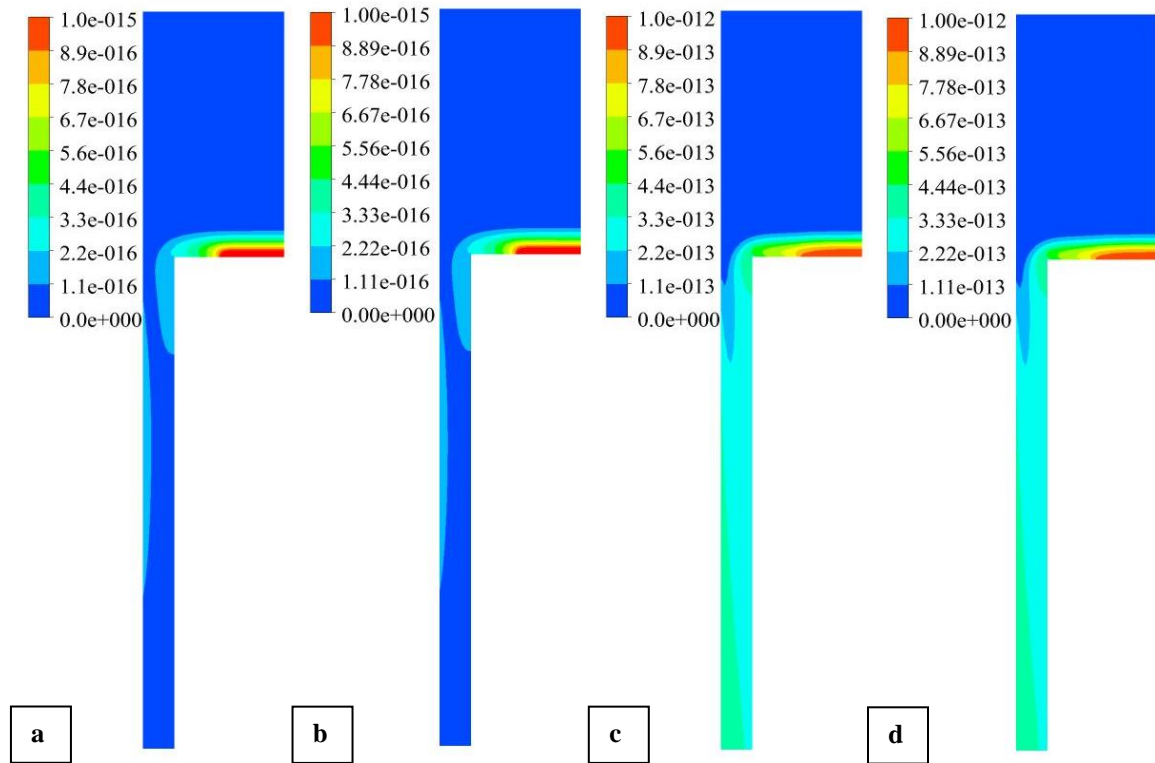
Figure 4.18 Distribution of (a) MMG and (b) MMG: NH_3 mass fraction with pure H_2 as the carrier gas at TMG flow rate of 0.001 slm (a, b) and 0.005 slm (c, d).

The deposition process is controlled mainly by diffusion of MMG and MMG: NH_3 at a high temperature near the substrate surface. MMG and MMG-NH_3 dominate Ga-containing species at a high temperature near the substrate surface. Figure 4.18 shows the mass fraction distribution of

MMG and MMG:NH$_3$ with pure H$_2$ as the carrier gas at different values of TMG flow rate. The results show that not as much of the mass fraction of MMG and MMG:NH$_3$ remain near the substrate surface because they are consumed in the surface reactions to form the GaN thin film.
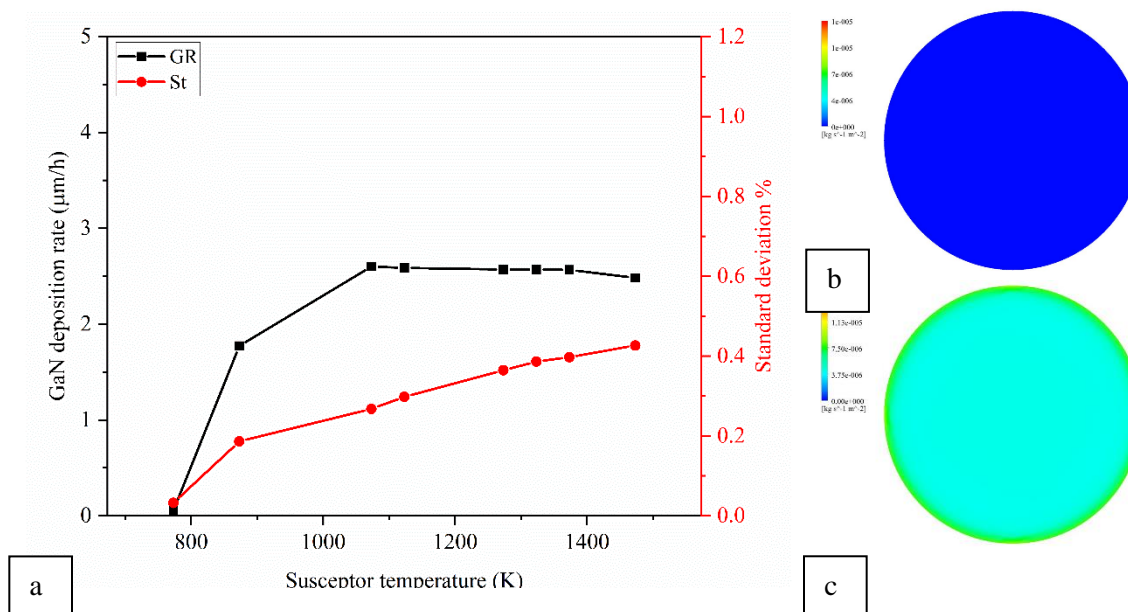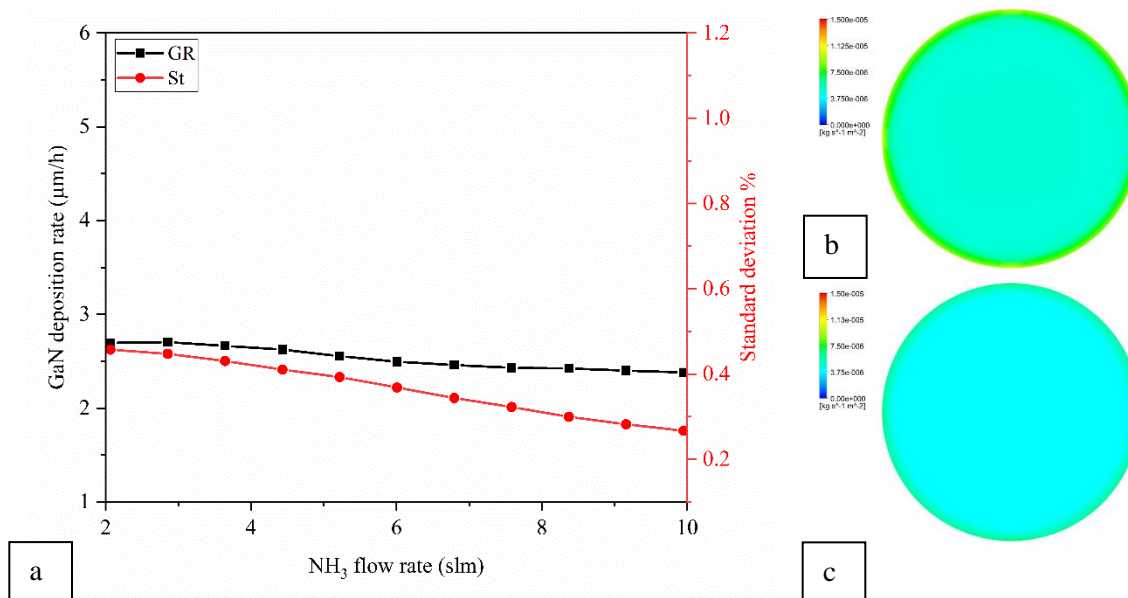

Figure 4.19 Variation of average growth rate and standard deviation profiles of GaN thin films at different values of (a) NH$_3$ and (b) TMG at reference conditions.

When the flow rate of NH$_3$ is increased, the uniformity of GaN thin film is improved, but there is a slight decrease in the growth rate, as shown in Figure 4.19. The flow rate of NH$_3$ affects the flow characteristics and thermal field. High NH$_3$ flow rate leads to reducing the thermal boundary layer, as shown in Figure 4.20. Moreover, the high flow rate of NH$_3$ pushes the intermediate species to leave the region above the substrate surface more quickly, resulting in fewer surface reactions due to a decrease of species residence time. TMG has a lower diffusion rate to the substrate in the NH$_3$ atmosphere [53]. Thus, increasing the flow rate of NH$_3$ results in increasing the NH$_3$ concentration near the substrate.
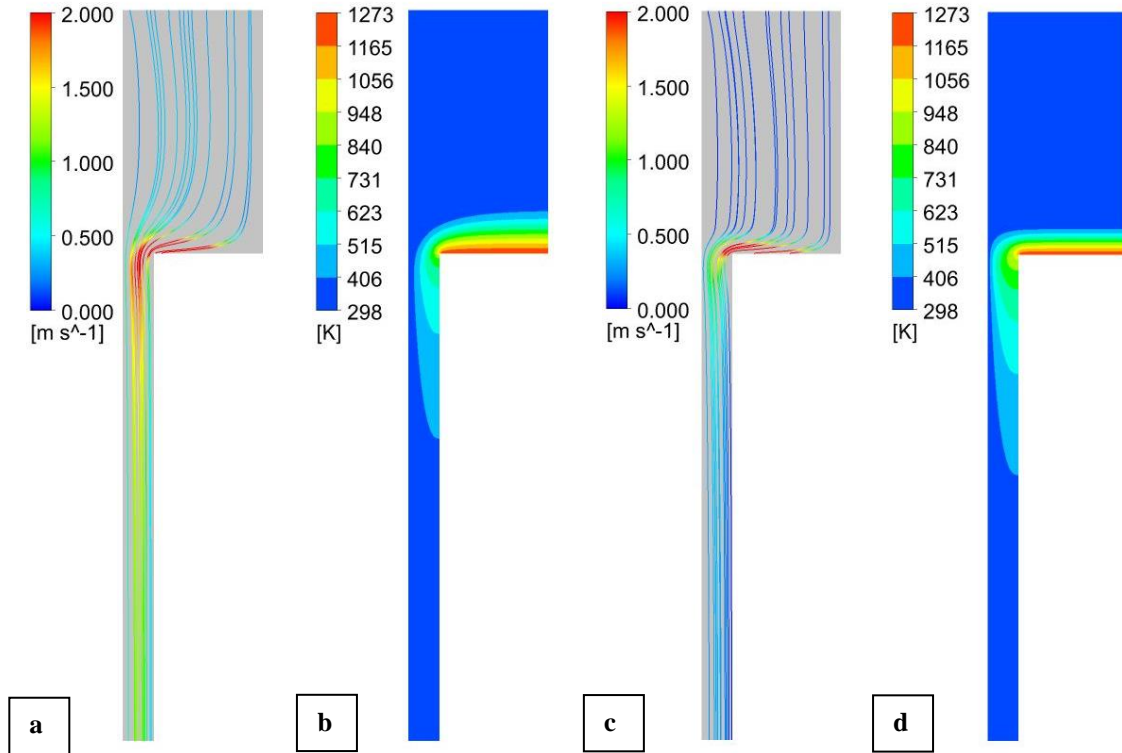
Figure 4.20 Flow and thermal field at the NH$_3$ flow rate of 2 slm (a, b) and 8 slm (c, d).

Figure 4.21 shows the mass fraction distribution of MMG and MMG:NH$_3$ with pure H$_2$ as the carrier gas at different values of NH$_3$ flow rate. The results show that a large amount mass fraction of MMG and MMG:NH$_3$ remain near the substrate surface. Consequently, an excess of the amount of NH$_3$ prevents Ga-containing species to diffuse properly to the substrate and leads to a low growth rate. In summary, changing the V/III ratio has a significant effect on the growth rate of GaN thin films. When the flow rate of NH$_3$ is kept constant, increases the TMG flow rate results in deposition rate, but with lower quality. On the other hand, when the flow rate of NH$_3$ is increased, and flow rate of TMG is kept constant, the uniformity of GaN thin film is improved, but there is a slight decrease in the growth rate. It is concluded that higher film thickness is obtained by controlling the flow rate of TMG, but with lower quality.
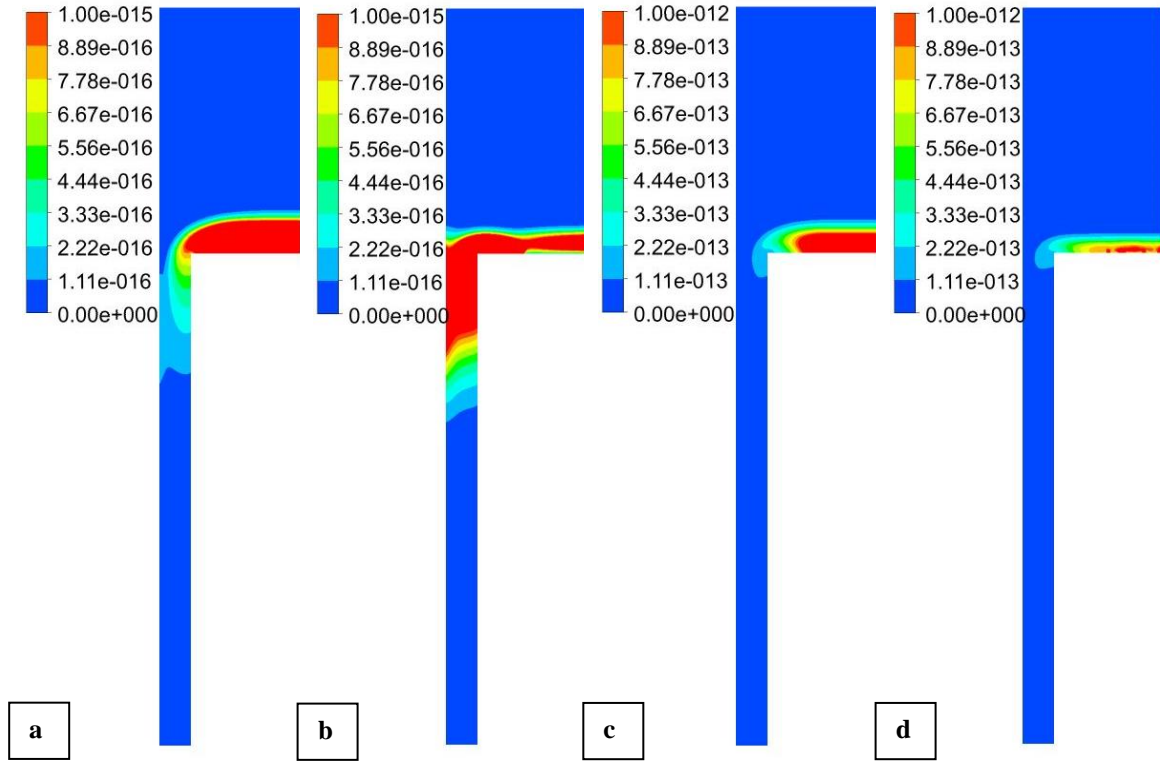
Figure 4.21 Distribution of MMG and MMG:NH$_3$ mass fraction with a pure H$_2$ as the carrier gas at the NH$_3$ flow rate of 2 (a, b) and 10 (c, d) (slm).

4.7 Dimensionless numbers

Dimensionless numbers such as Reynolds number (Re), rotational Reynolds number (Re_w), and Grashof number (Gr) are crucial parameters to give a better understanding of flow and thermal field variation in the MOCVD reactor, Table (4-5. These numbers play significant roles in controlling the growth rate and uniformity of thin films. However, the use of dimensionless numbers in MOCVD process is rather complicated due to the complex dependence of the gas properties, chemical reactions, and boundary conditions, the temperature, reactor pressure, and the mixture composition. Moreover, the main flow in a vertical MOCVD reactor is in the same direction as the gravity, so the nonlinear coupling between the buoyancy, viscous, inertia effects leads to further complications [97]. Thus, in the current study, the use of dimensionless numbers is considered for some cases to examine the stability of flow in the reactor.

Table (4-5) Dimensionless numbers

$Re = \dfrac{2R_s\rho_0 v_0}{\mu_0} = \dfrac{inertial\ forces}{viscous\ forces}$	4-31)
$Re_w = \dfrac{2R_s^2\omega\rho_0}{\mu_0} = \dfrac{inertial\ forces}{viscous\ forces}$	4-32)
$Gr = gH^3\beta_T(T-T_0)\left(\dfrac{\rho_0}{\mu_0}\right)^2 = \dfrac{heat\ buoyancy}{viscous\ force}$	4-33)

Where R_s is the susceptor radius, H is the distance between inlet and susceptor, g is the magnitude of gravitational acceleration, and β_T is coefficient of volumetric thermal expansion. The Re_ω is a measure of the significance of the forced convection due to the susceptor rotation. The Re is a measure of the significance of the forced convection, while the Gr characterizes the significance of the natural convection in the reactor. The buoyancy-to-inertia ratio (Gr/Re^2) indicates the flow stability of the mixed convection, where both natural and forced convection processes are important. The ratio $\dfrac{Gr}{Re^2}$ depends on the reactor shape and the temperature gradient between the susceptor and inlet gas flow, so it controls the flow stability inside the reactor chamber. Note that when $\dfrac{Gr}{Re^2}$ is large, the buoyancy-driven flow occurs in the reactor, which results in a decrease in the film growth performance [98]. Conversely, if it is small, buoyancy forces have a small effect on the stability of the flow.

Table (4-6) Some sample runs

Case	$P\ (torr)$	$Q\ (slm)$	$\omega\ (rpm)$	Gr	Re	Re_ω	$\dfrac{Gr}{Re_\omega Re}$	$\dfrac{Gr}{Re^2}$
1	300	10.5	100	3.872E05	62.1	273.6	----	100.2
2	300	14	100	3.872E05	83.14	273.6	----	56.01
3	300	17.5	100	3.872E05	98.07.8	273.6	----	46.6
4	300	21	100	3.872E05	103.8	273.6	----	35.93
5	300	14	100	3.872E05	83.14	273.6	17.01	----
6	300	14	200	3.872E05	83.14	547.28	8.515	----
7	300	14	300	3.872E05	83.14	821.08	5.67	----
8	300	14	400	3.872E05	83.14	1094.7	4.25	----

Due to the complexity of the chemistry model, some cases have been investigated at different values of the total inlet flow rate and susceptor rotation rate, respectively without the effect of chemical reactions on the deposition rate. Figure 4.22 shows the flow field at different values of the total inlet flow rate. It is observed that increases the total inlet flow enhances the flow stability and suppresses the buoyancy-driven recirculation in the reactor
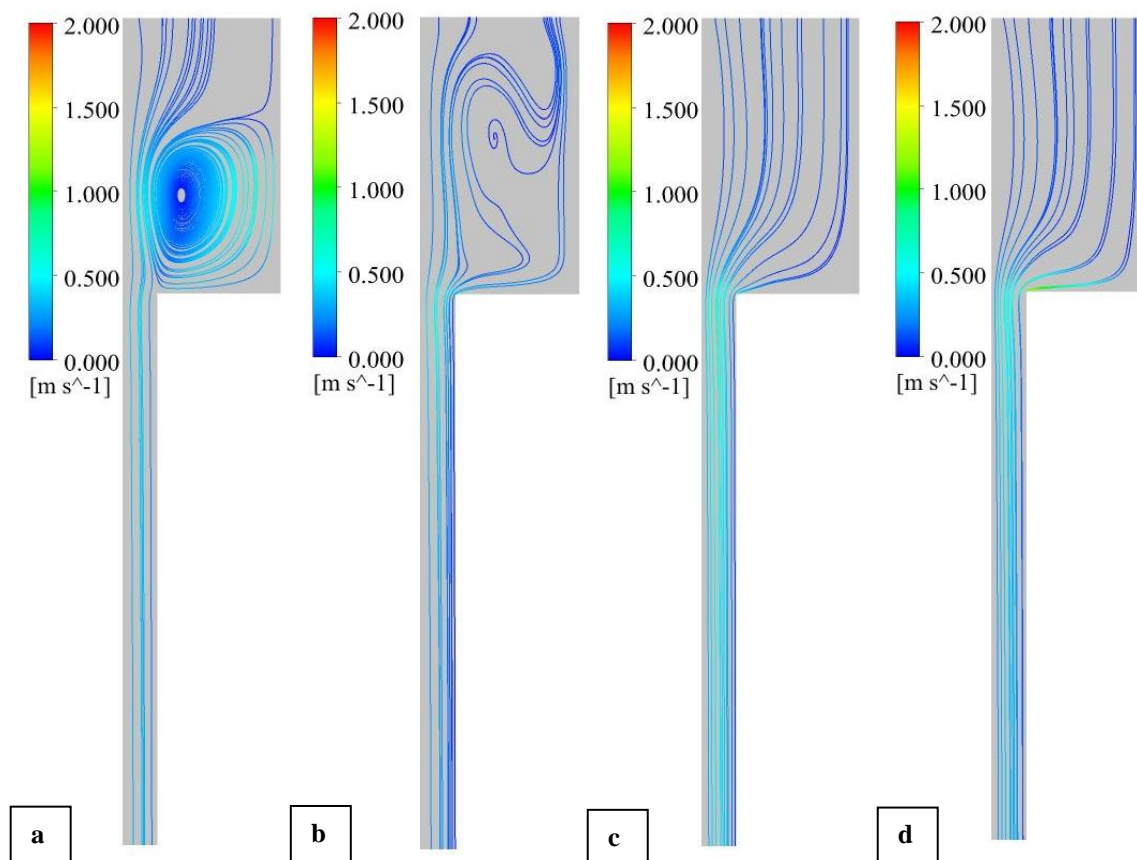
Figure 4.22 Flow field at different values of the total inlet flow rate (a) 10.5, (b) 14 (c) 17.5, and (d) 21 slm with a susceptor rotation rate of 100 rpm, and reactor pressure 300 Torr.

At total flow rate Q=14 slm, there is a recirculation flow occurs near reactor walls at a low rotation rate of the susceptor, as shown in Figure 4.23. When the rotation rate is increased, the forced convection is increased due to the susceptor rotation and thus leading to reduce the effect of the buoyancy-driven flow above the susceptor. The high rotation rate of the susceptor has a significant

effect on the stability of the flow. Thus the buoyancy to inertia ratio can be defined as $\frac{Gr}{Re_\omega Re}$.

Increasing the rotation rate of the susceptor leads to a decrease in values of $\frac{Gr}{Re_\omega Re}$, as shown in

Figure 4.24 (a). Reducing the value of $\frac{Gr}{Re_\omega Re}$ enhance the stability of the flow, which improves the

growth rate and uniformity of thin films in MOCVD reactors. The flow mapping approach for some

cases is developed to show the effect of the total inlet flow rate and the rotation rate on the stability

of the flow in a rotating disk MOCVD reactor, as shown in Figure 4.24 (b).
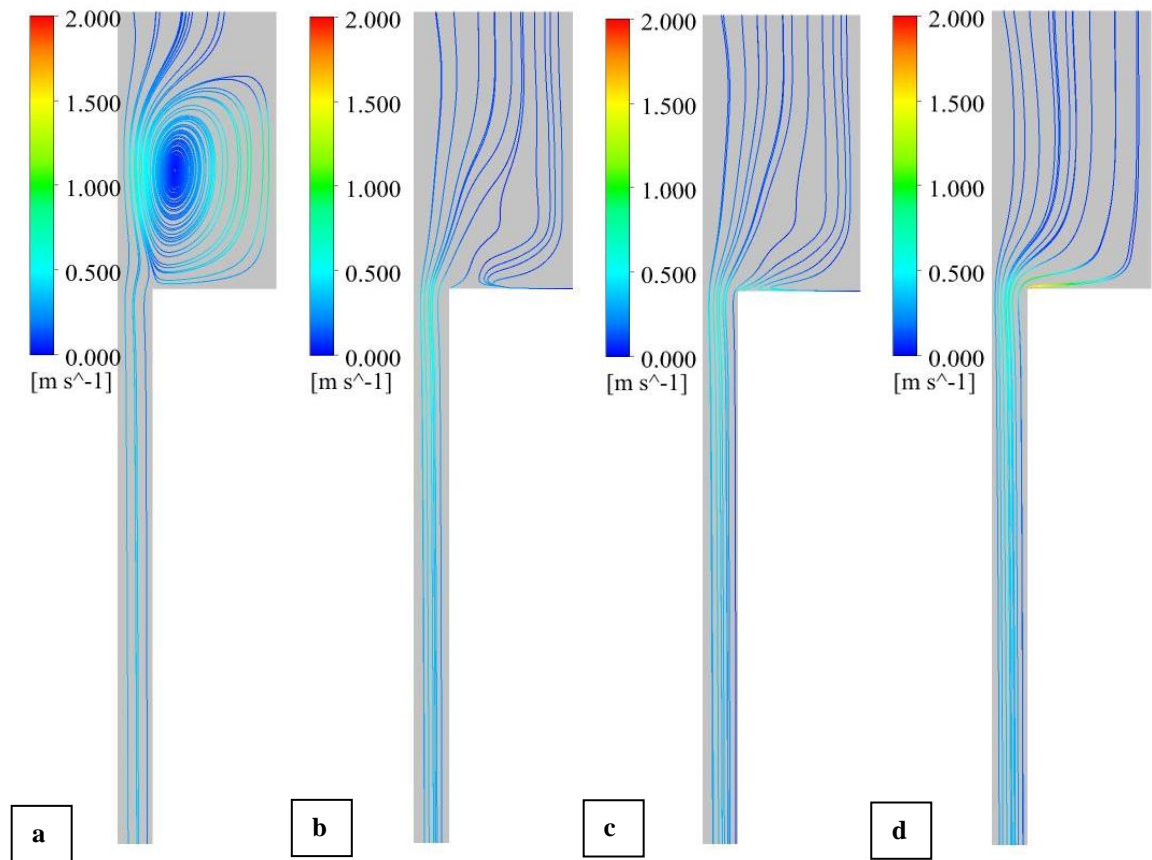
Figure 4.23 Flow field at different values of the susceptor rotation rate (a) 100, (b) 200 (c) 300, and (d) 400 rpm with total inlet flow rate 14 slm, and reactor pressure 300 Torr.
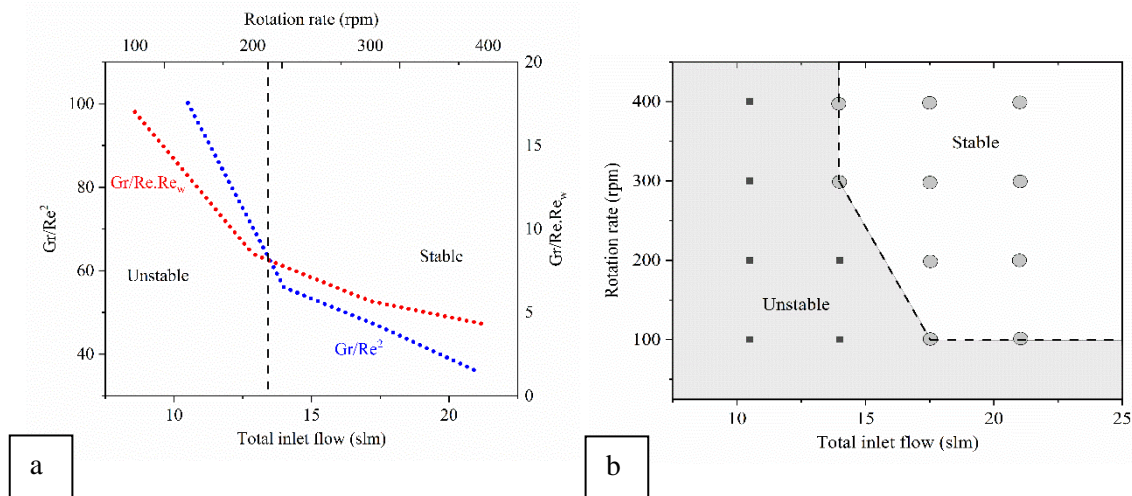
Figure 4.24 (a) Variation of the buoyancy to inertia ratio with total inlet flow and the rotation rate of the susceptor. (b) the flow stability mapping in the rotation rate and total inlet-flow diagram.

One can see that increasing the total flow rate and the rotation rate flow are important parameters in stabilizing the flow in the MOCVD reactor. However, it is difficult to study the flow stability in the MOCVD process due to the chemical reactions. The difficulty arises from the temperature and concentration gradients, geometrical design, and flows pattern in the reactor chamber. As a result, to achieve the high growth rate and better uniformity of the thin film in MOCVD process, these critical value should be considered in the growth process.

4.8 Conclusions

A three-dimensional model has been presented to describe the coupled fluid flow, thermal field, gas phase, and surface reactions in the deposition of GaN thin films. The model gives a further understanding of the effect of growth conditions in a single-wafer MOCVD reactor. The results show that the growth rate of GaN thin films is sensitive to processing conditions such as the rotation rate of the susceptor, the flow rate of TMG, reactor pressure, and the growth temperature. Although the deposition rate increases with increasing rotation rate, reactor pressure, inlet gas velocity, and the flow rate of TMG, the uniformity of GaN thin film is lowered. An inverse behavior is obtained

for the flow rate of NH$_3$; the deposition rate decreases while the uniformity improves. The temperate range of (1220-1350 K) is the most appropriate temperature range for GaN deposition. In summary, the growth rate at mass transport regime is influenced by the boundary layer (BL) thickness, the diffusivity of species through BL, the flow rate of Ga-containing species, at high temperature.

Dimensionless numbers such as Re, Re_ω, and Gr are important parameters in giving a better understanding of flow and thermal field variation in the MOCVD reactor. To show the effect of the total inlet flow rate and the rotation rate on the stability of the flow in a rotating disk MOCVD reactor. The flow mapping approach is developed to indicate the stability of the flow inside the MOCVD reactor without the effect of chemical reactions. Compared to a single-wafer MOCVD reactor, the designing of growth conditions in a multi-wafer MOCVD reactor becomes more difficult since the growth rate and uniformity of GaN thin films are very sensitive to processing parameters and the reactor geometry. In the next chapter, this model will scale up to simulate the growth parameters of the multi-wafer MOCVD reactor used in the experimental study.

Chapter 5

GROWTH BEHAVIOUR IN A MULTI-WAFER REACTOR.

5.1 Introduction

In the previous chapter, a detailed computational model of a small vertical impinging reactor is considered. However, the MOCVD reactor that has an effective usage of precursors, a low operating cost, and high productivity is highly desirable. GaN thin films have the potential for using in various advanced applications in the future. Nevertheless, to this end, it is important to have a long-term cost reduction by increasing the throughput. The cost reduction is based on the number of wafers and the size of the wafer. Nowadays, many different design configurations of MOCVD reactors of manufacturing thin films are available in the industry. In this chapter, the flow characteristics and growth behavior of GaN thin films in multi-wafer MOCVD reactor are investigated.

5.2 MOCVD reactor configuration

The geometrical configuration of the MOCVD reactor plays an important role in controlling the flow characteristics, and the deposition rate to achieve high-quality thin films. Some previous vertical of MOCVD reactor uses a tall cylindrical vessel where the reactant flow is injected from the top towards the rotating susceptor, see Figure 5.1 (a,b). The existing reactor design addresses some problems as follows: (1) inefficient usage of gases and precursors, (2) nonuniform distribution of precursors (3) high manufacturing costs of equipment, and (4) recirculating flow that results in a deposition on internal surfaces of the reactor. Therefore, efforts have been made to design a reactor that allows a uniform gas flow [61], [70], [99]. The geometry of the MOCVD reactor with a flared cone upper surface is proposed by [92]. The design guides gases effectively towards the rotating susceptor surface to use the precursors efficiently. It also improves the stability

of the gas flow pattern inside the reactor and prevents the back-entry gas that forms vortices near to the inlet, as shown in Figure 5.1 (c). In this study, a numerical simulation of the multi-wafer MOCVD reactor has been carried out to analyze the effect of operating conditions and geometrical configuration on the deposition rate and uniformity of GaN thin films.
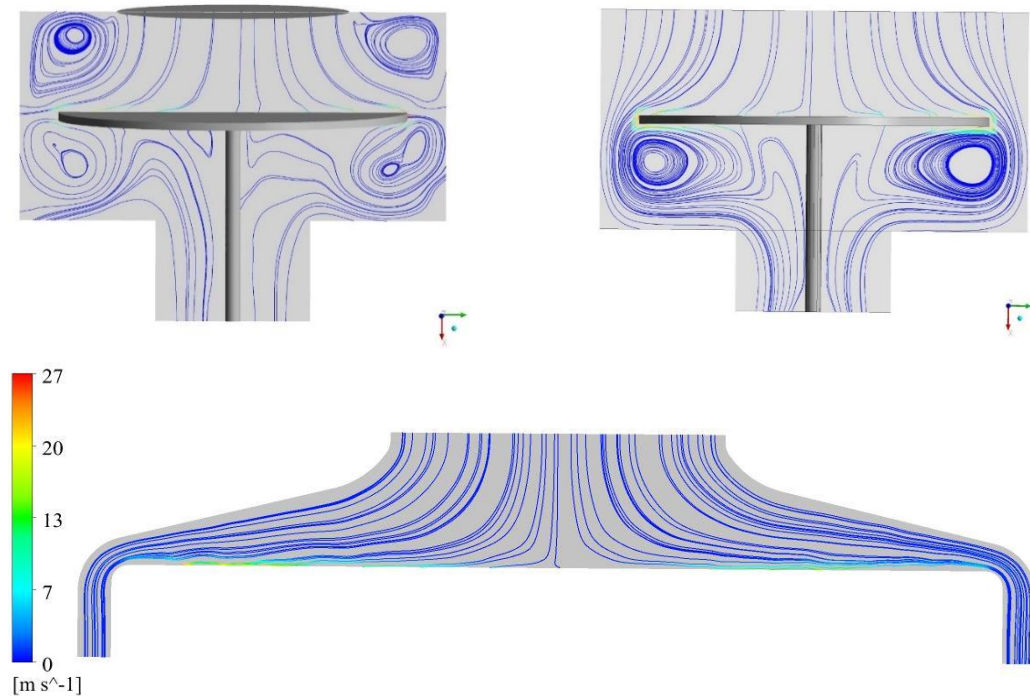
Figure 5.1 Schematic diagram of the multi-wafers MOCVD reactor

Figure 5.2 shows a schematic diagram of the multi-wafers MOCVD reactor considered in the study, adapted from [92]. An eighth of the reactor geometry is modeled due to the axis symmetry. Since this study focuses on the deposition rate and uniformity of GaN thin films, an attempt of reducing the complexity, the reactor components such as gas delivering systems, cooling system, control system, and geometry are simplified without affecting the main reactor chamber to allow the CFD model. A high-density of structured element mesh is considered near the susceptor surface as a large gradient of temperature is expected to arise there. The model employed the chemistry and transport gas properties that are given in the previous chapter under different processing parameters.
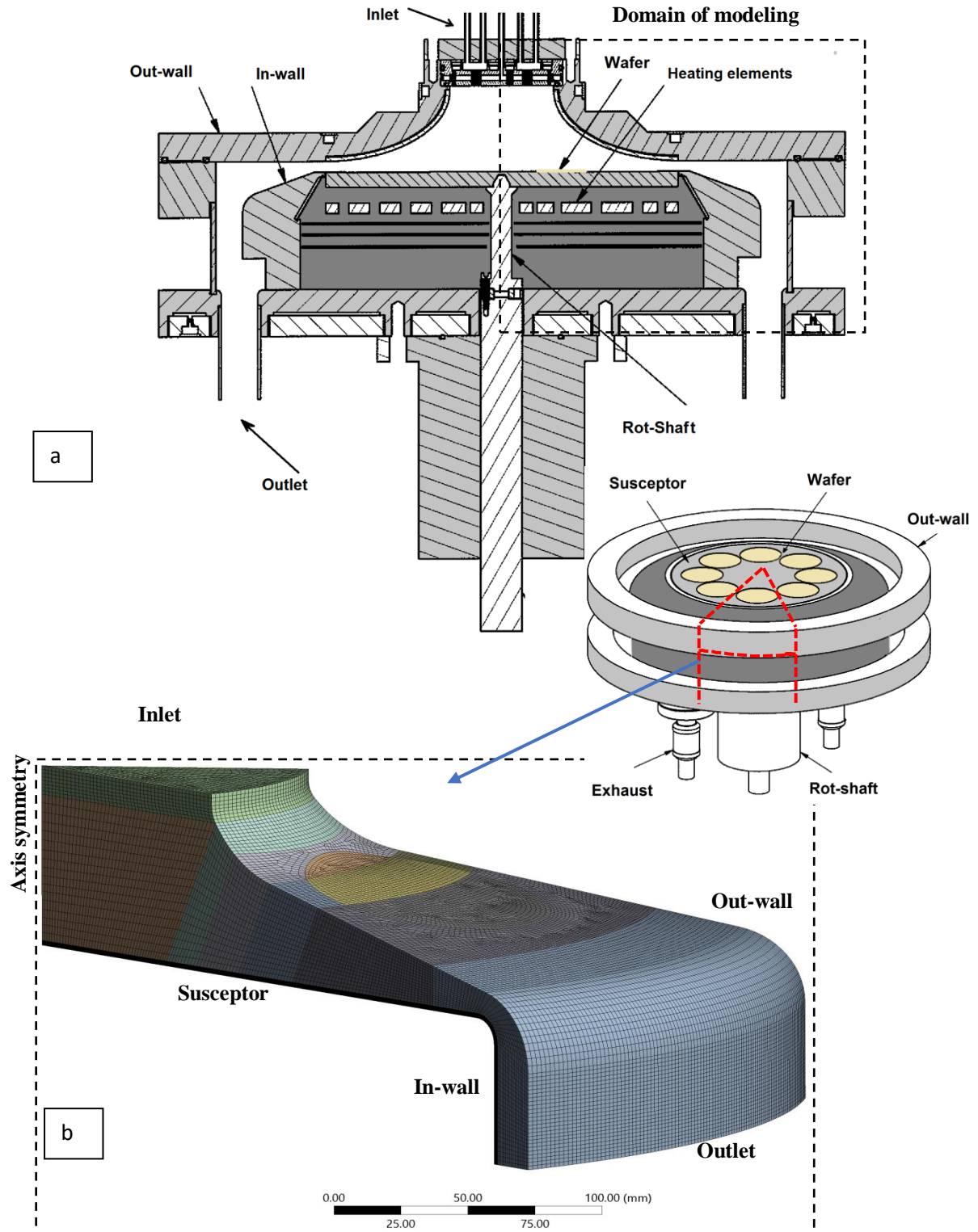
Figure 5.2 (a) Schematic diagram of the multi-wafers MOCVD reactor considered in the study, adapted from [92], and (b) the structured mesh of an eighth of the geometry.

5.3 Results and discussion.

This section presents a comparative study of GaN thin films grown on c-plane sapphire (Al_2O_3) wafers in the multi-wafer MOCVD process. The average radial GaN growth rate is defined as a function of the wafer radius as follows:

$$\text{Average growth}(r) = \int_0^{2\pi} \text{growth rate } (r, \theta). \, d\theta \qquad \text{5-1)}$$

The distribution of the average radial growth in the wafer region bounded by two circles is defined as follows:

$$GR(r) = \frac{\int_{r1}^{r2}\big(\text{growth rate } (r)\big)2\pi r dr}{\pi(r_2^2 - r_1^2)} \qquad \text{5-2)}$$
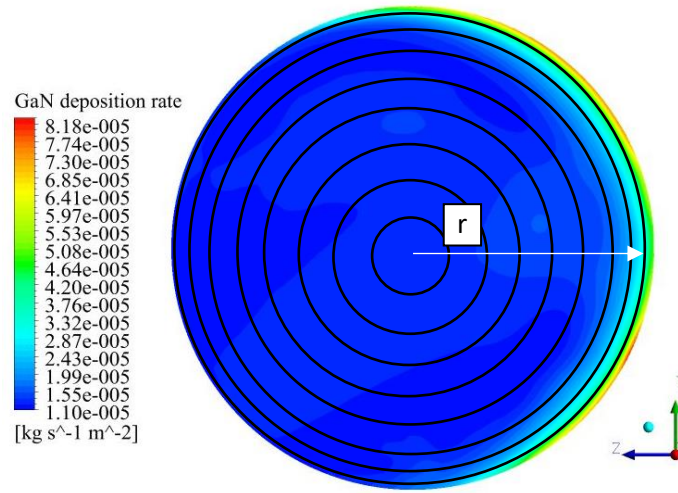
Figure 5.3 GaN deposition rate distribution bounded by two circles along the wafer surface at reference conditions

The deposition rate of GaN thin films over the wafer is averaged on constant ring areas along the wafer radius to capture the radial deposition rate profile. Figure 5.3 shows the deposition rate of GaN thin films bounded by two circles along the wafer surface at reference conditions. Further results are obtained under different processing parameters.

5.3.1 V/III ratio

The effect of varying the V/III ratio on the deposition rate and uniformity of GaN thin films is investigated. Figure 5.4 shows a comparison between the numerical result and the experimental result. The variations in the growth rate are captured by numerical results, which agree quite well with the experimental results. It is observed that high deposition rate arises at the wafer edge while a low deposition rate occurs towards the inner zone of the wafer. The interpretation of that, the velocity increases at the susceptor edge due to the rotation leads to a thin boundary layer. Thus, the diffusivity of reactant species increase, which results in increasing of the deposition rate at the wafer edge.
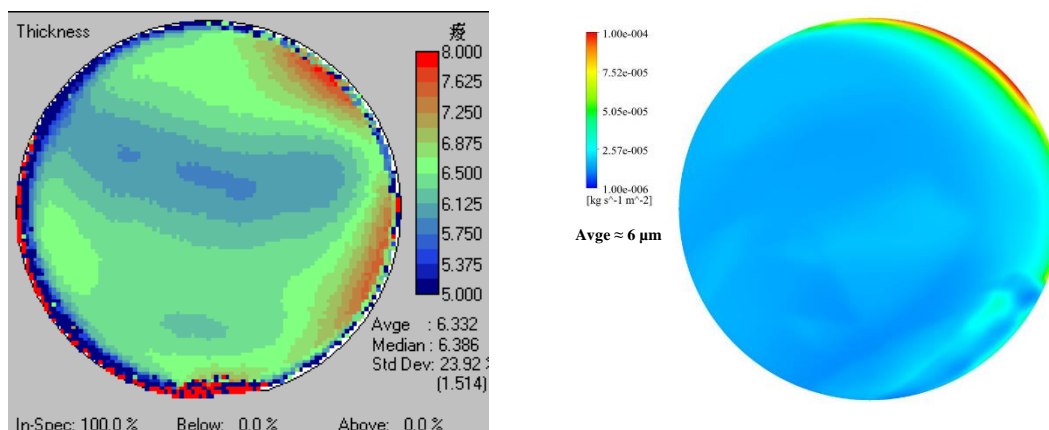
Figure 5.4 Comparison of the GaN deposition rate is obtained (a) the experimental data, and (b) the numerical model at V/III ratio = 615 with reference conditions.

The numerical model shows a similar trend where a high deposition rate occurred at the wafer edge, as shown in Figure 5.4 (b). However, it is observed that there is a difference between the predicted results and the experimental results. The numerical model shows that a higher deposition rate occurs at the wafer edge due to the simplification of reactor design. Also, in the numerical calculations, a high predicted deposition rate takes place at the wafer edge due to the sudden change of surface reactions. The wafer is the only heated surface that consumes the reactant precursors, so the surface reaction beyond the wafer edge falls off to zero to form a singular point. In the

manufacturing process, the average GaN thin film thickness is obtained by excluding 2 mm from the wafer edge. Figure 5.5 shows the variation of the deposition rate and standard deviation profiles along the radial direction of the wafer at different values of the V/III ratio where the NH_3 flow rate is fixed on 17 (slm). At high V/III ratio, less amount of TMG species react with NH_3 species, resulting in a low deposition rate. On the other hand, the average GaN deposition rate increases with decreasing V/III ratio due to the increase in the flow rate of TMG and involving more molecules of TMG in the chemical reaction to form the solid thin film. However, at low V/III ratio, the uniformity of the thin film degrades as the standard deviation increases, as shown in Figure 5.5 (b).
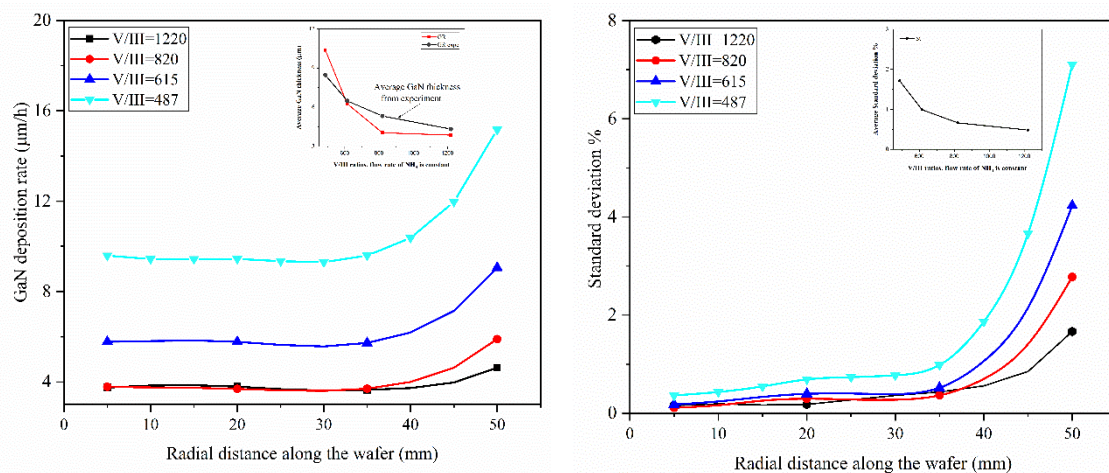
Figure 5.5 Variation of (a) deposition rate and (b) standard deviation profiles along the radial direction of the wafer at different values of the V/III ratio.

The carbon contamination inside the reactor deteriorates the electrical properties of GaN thin films [101]. During the growth rate, the net amount of CH_3 is the primary source of carbon incorporation. It is possible for the CH_3 radical to absorb on or adsorb from the wafer surface[102]. Figure 5.6 shows the distribution of CH_3 and CH_4 mass fractions profiles calculated in a plane apart from the susceptor 1 mm. It can be seen that more mass fraction of CH_3 is accumulated above the substrate that leads to an increase in the carbon concentration, and subsequently, it affects the thin film

quality. The concentration of carbon impurities that originate from decomposed precursors depends on the V/III ratio and reactor pressure. The predicted results show that the mass fraction of CH_4 dominates above the wafer and increase by increasing the TMG flow rate. While the mass fraction of CH_3 shows less amount above the wafer region, and also increases with decreasing the V/III ratio. Hence, more carbon contamination is expected at low V/III ratio.

Figure 5.6 the distribution of the mass fraction of (a) CH_4 and (b) CH_3 gaseous species near the substrate surface along a horizontal line 1 mm above the susceptor.

The results indicated that the deposition rate has a proportional dependence on the TMG flow rate. However, further increasing of TMG flow rate increases the mass fraction of CH_3 and CH_4 above the susceptor. Thus, the carbon concentration can be controlled by decreases the mass fraction of CH_3 by increasing the V/III ratio or adjusting the reactor pressure. At high V/III ratio, low carbon concentration is obtained, but the growth rate is very low. As a result, to get a high deposition rate and less amount of carbon contamination, a proper V/III ratio is required to be addressed.

5.3.2 Reactor pressure

The effect of varying the pressure on the flow characteristics in the reactor and the deposition rate of GaN thin films has been studied. During the growth process, the inlet flow rates of NH_3 and

TMG were maintained as constant as in reference conditions. The precursor mass flow rate and the vacuum pump speed balance to produce the reactor pressure. It is observed that the high reactor pressure strengthens the thermal buoyancy, that leads to flow recirculation in the reactor. As the reactor pressure increased up to 400 Torrs, the buoyancy-driven flow is induced above the hot susceptor and under the reactor wall, as shown in Figure 5.8. The buoyancy force is strong enough to create global natural convection at high reactor pressure. Due to the high temperature of the susceptor, the gases are heated and raised in the center of the reactor and downward along the reactor walls. The streamlines reflect the rising plume at the hot susceptor, compared to the case with low pressure, as shown in Figure 5.8 (b).

The reactor pressure is the most important processing parameter in determining the arrival rate of reactant species at the substrate surface. At high pressure, the gas flow rate in the reactor is low that makes the residence time of the species longer. The residence time (t_{res}) is the duration of reactant gases flowing through the reaction chamber, and the consumption time (t_{con}) is the time to consume available reactant at the growth rate into the depositing film [3]:

$$t_{res} = \frac{VP}{Q} \qquad\qquad\qquad 5\text{-}3)$$

$$t_{con} = \frac{V}{R_s A_s} \qquad\qquad\qquad 5\text{-}4)$$

Where P is reactor pressure, V is the reactor volume, and Q is the input mass flow rate. R_s is the chemical reaction rate, and A_s is the substrate surface area. In the MOCVD reactor, convection and diffusion are the two methods of mass transport [103]. Convective mass transport is occurred due to the bulk motion of the fluid; while diffusive mass transport is the average of the random motions of the individual molecules of the fluid. Residence time has a strong influence on the interactions of chemical reactions in the MOCVD process. It can reflect the transport rate of reactant species inside the MOCVD reactor. At high temperatures, the reaction rate is high enough that nearly all

the precursor injected is consumed [3]. When the residence time is short compared to the consumption time, the film growth is mass transport limited, in which the deposition reaction is high, but the uniformity is likely to be low. The shorter residence time, the higher transport rate of reactant species to the substrate surface, and the higher growth rate.

On the other hand, the long residence time decreases the mass transport rate and enhances the parasitic reaction to form nanoparticles in the gas phase. At high reactor pressure, the gas inlet velocity decreases results in weak forced convection. Thus, a flow recirculation appears that promotes parasitic reactions and hinders precursors to reach the substrate surface efficiently. Further increasing of the reactor pressure near the atmospheric pressure leads to a decrease in the growth rate. The quality of thin-film decreases with increasing depositing of parasitic particles, which also can stick over the reactor walls [70]. Thus, it is crucial to decrease the residence time of the reactant species within the gases reaction chamber to eliminate the undesirable deposition of nanoparticles At high pressure, parasitic reactions enhance adduct formation between TMGa and NH_3, leading to limiting the flux of Ga-containing species at the growing interface.
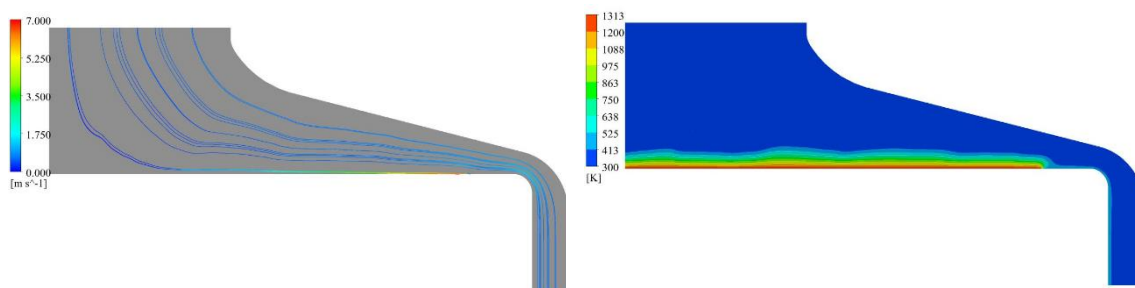
Figure 5.7 Flow and thermal fields with a gas mixture of 40% H_2 and 60% N_2 as the carrier gas at the reactor pressure of 50 Torrs.
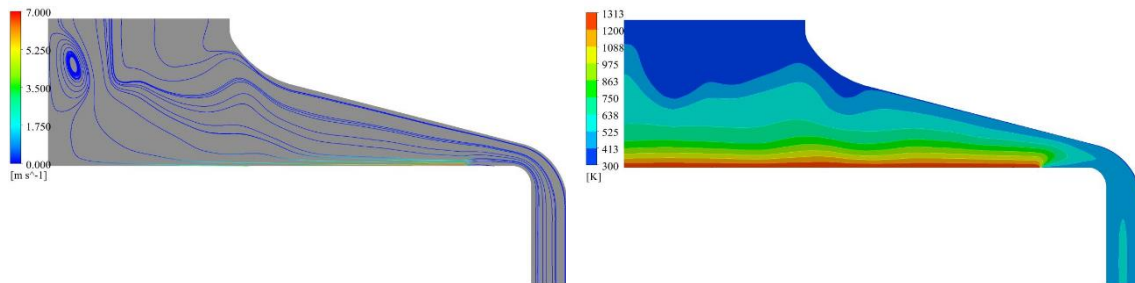
Figure 5.8 Flow and thermal fields with a gas mixture of 40% H_2 and 60% N_2 as the carrier gas at the reactor pressures of 400 Torr.

When the reactor pressure is lowered, the parasitic reaction of the cluster formation in the vapor phase is suppressed. Given that the inlet flow rate is constant, the low pressure produces higher inlet gas velocity and low gas mixture density, which counteract the buoyancy effect and mitigates the natural convection effect. Therefore, the buoyancy-driven flow recirculation is minimized significantly, and it is suppressed effectively.

Figure 5.9 Variation of (a) deposition rate and (b) standard deviation profiles along the radial direction of the wafer at different values of the reactor pressure.

The low reactor pressure has an important effect on the stability of the flow field, which improves the uniformity of GaN thin films. However, too low reactor pressure produces high gas-mixture flow rate, which leads to pumping out most of the metal-organic precursors without reacting

efficiently on the substrate surface. The thin film is more uniform at low reactor pressure, but the deposition rate of GaN thin films is also low. The low deposition rate of GaN thin films arises for the low reactor pressure, as shown in Figure 5.9. The diffusivity of TMG is reduced at high pressure, that results in presenting a radial concentration and resulting in a different rate of deposition along the substrate surface. Species are distributed unevenly in the reactor leads to the high gradient in the diffusion of species to the substrate surface through the boundary layer. Thus, the growth rate is nonuniform along the radial distance of the wafer, as shown in Figure 5.9 (b). Also, at low reactor pressure, the middle zone of the wafer has a lower growth rate than the edges as indicated by the standard deviation.

When the reactor pressure increases, the standard deviation increases leads to low uniformity of the thin film. As aforementioned, the reactor pressure has a significant effect on GaN thin film properties. Provided that the growth pressure is a useful parameter to control the carbon concentration [57]. Ubukata et al. reported that increasing the reactor pressure from 13 kPa (97.5 Torrs) to atmospheric pressure led to decrease the carbon concentration during the growth process of GaN thin films [104]. They used the secondary ion mass spectrometry (SIMS) test to measure the carbon concentrations in the resulted thin film. The predicted results show that the mass fraction of CH_4 increases with increasing the reactor pressure, while the mass fraction of CH_3 decreases with increasing the reactor pressure, as shown in Figure 5.10 shows the distribution of mass fractions of CH_4 and CH_3, respectively. Figure 4.13 (b) shows the variation of CH_3 mass fraction with the reactor pressure; it can be seen from the curve that after the reactor pressure increases to 300 Torrs, the mass fraction of CH_3 decreased. In contrast, the mass fraction of CH_4 increases with increase the reactor pressure to 300 Torrs, then the curve does not change. This result agrees with the experimental results of detecting the carbon concentration using SIMS [104]. Also, the same behavior is obtained in this study, where the carbon incorporation is decreased at the reactor

pressure of 500 Torr with pure N_2 as a carrier gas. It is worth to note that the numerical model can be a useful indicator for the carbon concentration during the GaN deposition.
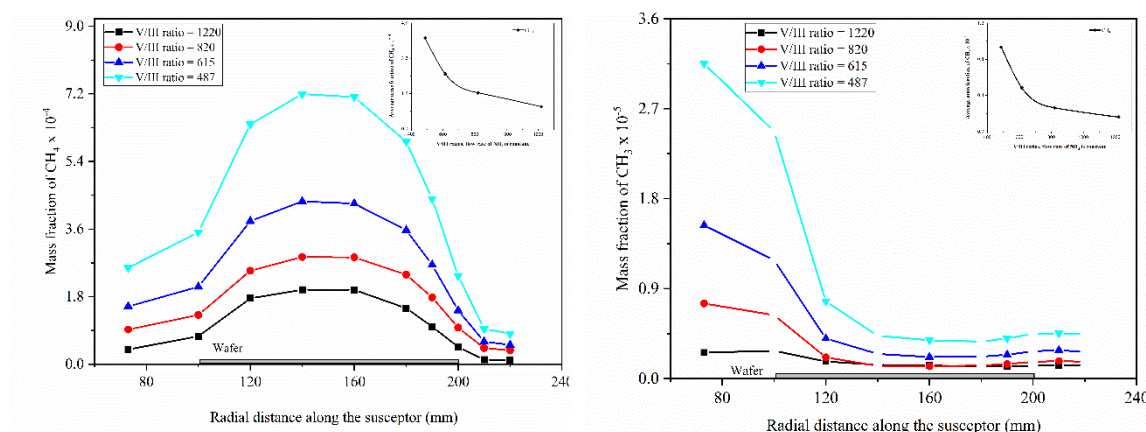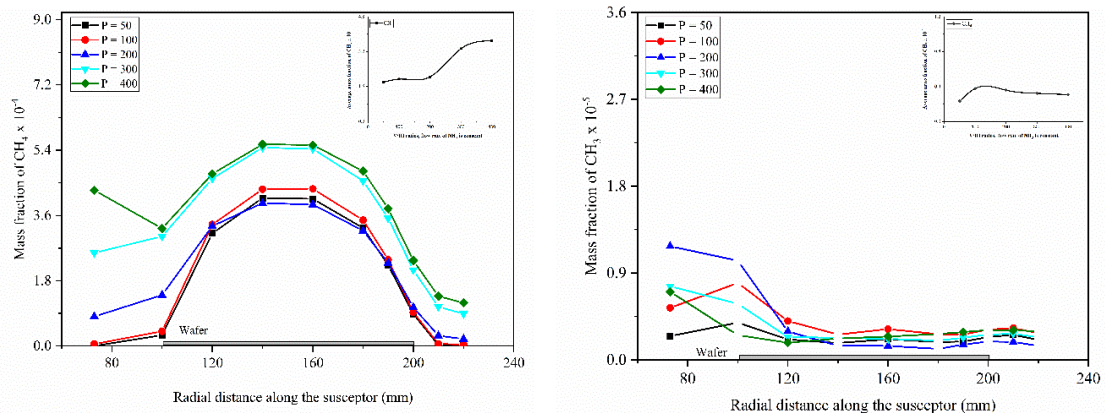

Figure 5.10 the distribution of the mass fraction of (a) CH_4 and (b) CH_3 gaseous species near the substrate surface along a horizontal line 1 mm above the susceptor at different values of the reactor pressure.

The process engineering goal is to tune the reactor pressure so that the growth rate and uniformity of GaN thin films are as high as possible, while the wastage of precursor is minimized. As a result, a proper reactor pressure improves the flow stability inside the reactor. Also, the reactor pressure enhances the diffusivity of TMG species to distribute evenly in the reactor, consequently improving the uniformity of the thin film thickness with a large area of the wafer. It is found that the reactor pressure of 300 Torrs enhances the deposition rate and uniformity of GaN thin films.

5.3.3 Carrier gas

The effect of carrier gas mixture on the deposition rate of GaN thin films and the flow and thermal fields in the reactor is investigated. It is observed that using pure H_2 as the carrier gas results in a smooth streamline and uniform thermal field inside the reactor, as shown in Figure 5.11. On the other hand, using pure N_2 as the carrier gas creates flow recirculation above the susceptor area and increases the buoyancy effects as shown in Figure 5.12.
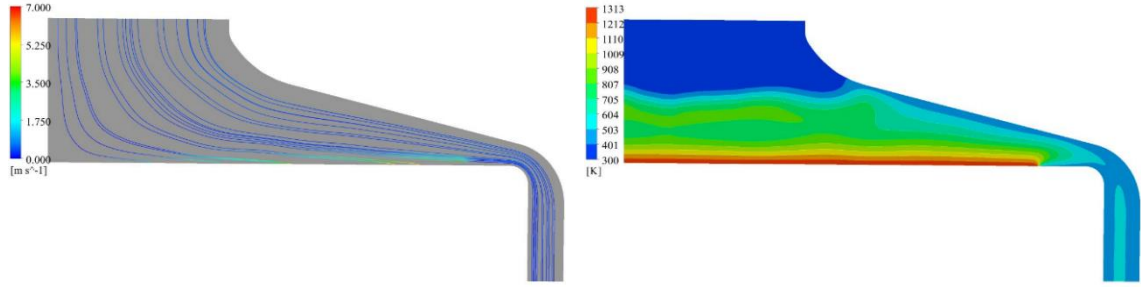
Figure 5.11 Flow and thermal fields with pure H_2 as the carrier gas at a reactor pressure of 200 Torrs.
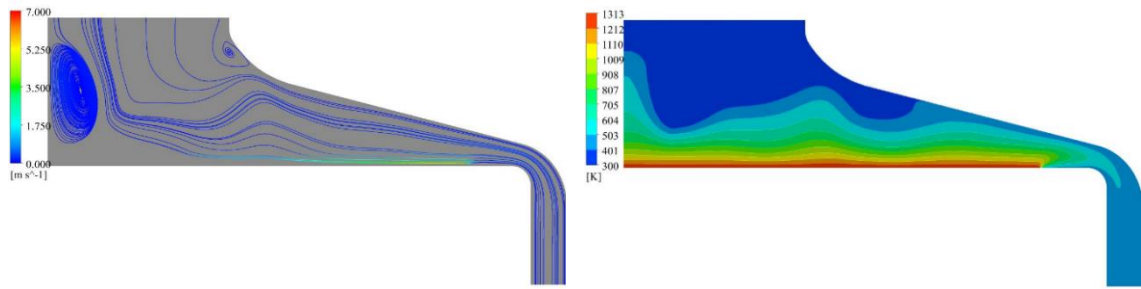
Figure 5.12 Flow and thermal fields with pure N_2 as the carrier gas at a reactor pressure of 200 Torrs.

When the flow rate of N_2 increases, the gas density of gas mixture near the reaction interface is increased, and thus the flow is affected by the heavy N_2 molecule that increases the carrier gas density by increasing N_2. By increasing the concentration of heavier gas in the mixture, the density of the mixture increases causes destabilize the flow. Increasing the density of the mixture leads to an increase in Reynolds number $Re = 2R_s\rho_0 v_0/\mu_0$, and Grashof number $Gr = gH^3\beta_T(T - T_0)\left(\frac{\rho_0}{\mu_0}\right)^2$. Higher values of the Re have the stabilizing effect in the region where the rotation-induce recirculation flow is expected [11]. However, increasing the density of the mixture increases the Gr with a much higher rate than t the Re, results in a buoyancy-driven flow. Flow recirculation inside the reactor causes the temperature variation and influences the uniformity and deposition rate of the GaN thin film. TMG precursors have a higher diffusivity rate in pure H_2 as the carrier gas, that allows the reactants to deposit on the reactor walls. In contrast, the diffusivity rate of TMG

precursors is smaller in pure N_2 as the carrier gas that results in avoiding wall deposition and reducing growth rate along the reactor walls [77]. The deposition rate of GaN thin films at different positions of the wafer using a mixture of H_2 and N_2 as the carrier gas is depicted in Figure 5.13. The results show that using pure N_2 as the carrier gas can affect the uniformity of GaN thin film along the wafer.

Moreover, a low growth rate is obtained when pure N_2 is employed as the carrier gas, at a fixed value of the inlet mass flow rate. Increasing the percentage of N_2 in the gas mixture leads to increasing the inlet velocity and decrease the deposition rate. Wang et al. also observed that using a high ratio of $N_2/(N_2 + H_2)$ led to a rough surface and a decrease in the structural quality of the GaN thin film at atmospheric pressure. In contrast, using pure H_2 as the carrier gas led to mirror-like surface morphology [78]. This result agrees well with the AFM results observed in chapter three in this study, where a smooth surface morphology is obtained. Also, using pure H_2 has significant effects on the growth rate of GaN thin films.

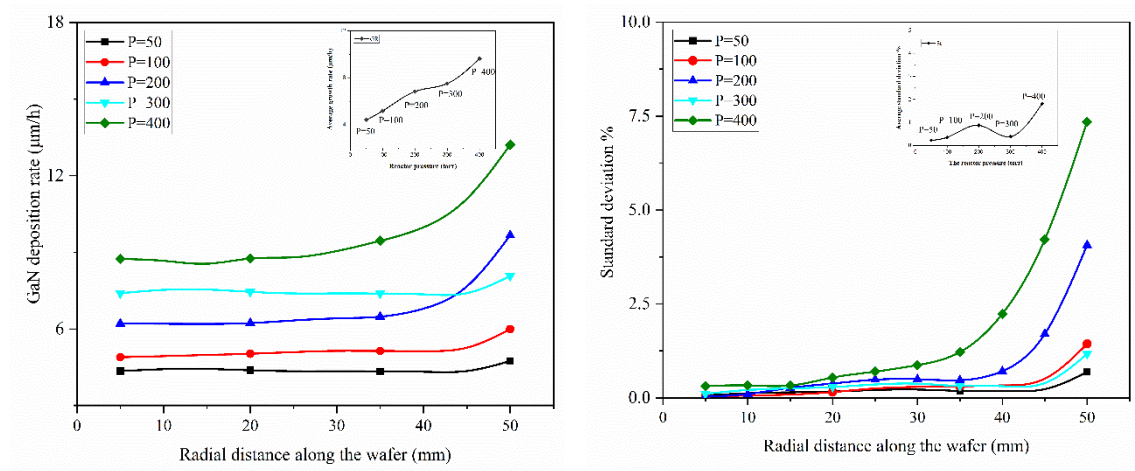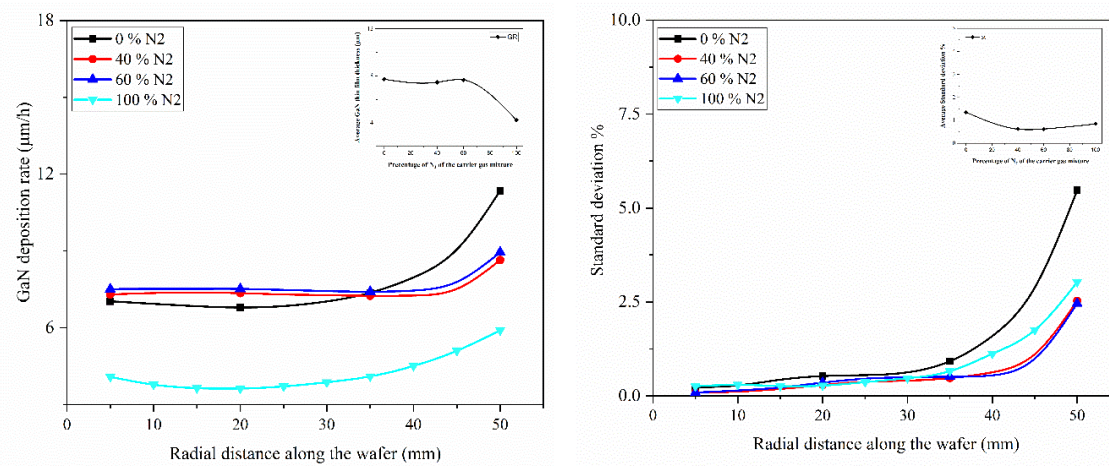Figure 5.13 Variation of (a) deposition rate and (b) standard deviation profiles along the radial direction of the wafer with a mixture of H_2 and N_2 as the carrier gas at a reactor pressure of 200 Torrs.

Pearton et al. [105] stated that H_2 has an important effect on the growth of GaN thin films, as H_2 helps in reducing the activity impurities in the deposition process. However, unintentional incorporation of H_2 can affect the conductivity of the produced thin film. Jian-Li et al. [102] showed that H_2 could enhance the carbon incorporation in GaN epitaxial layer by inhibiting the dissociation of NH_3 and result in more N vacancies. Therefore precise control of H_2 is crucial to get the desired high film quality. The deposition rate along the radial distance of the wafer becomes more uniform when a mixture of N_2 and H_2 used as the carrier gas. As N_2 gas helps to compensate for the effect of H_2 and thus improve the flow characteristics in and out of the chamber, while H_2 gas aids the crystal growth of the GaN thin film. In conclusion, the mixture of the carrier gas affects the flow characteristics as well as the deposition rate and uniformity. Thereby, by using an appropriate mixture of N_2 and H_2 as the carrier gas, the deposition rate and uniformity GaN thin films can be enhanced. The predicted results show using 60% N_2 and 40% H_2 as the carrier gas improves the uniformity and increase the deposition rate of GaN thin films.

5.3.4 Rotation rate

In general, the rotation rate influences the deposition rate and uniformity of thin films. The low rotation rate hinders the layer uniformity and decreases the deposition rate. When the rotation rate increases, streamlines become flatter at a high rate of rotation. High values of flow streamlines are presenting near the susceptor edge at a high rotation rate. As the rotation rate is increased, the thermal boundary thickness decrease and magnitude of the axial velocity increases, leading to a uniform temperature distribution on the susceptor, as shown in Figure 5.14. Moreover, increasing the rotation rate causes to decrease the residence time of precursors in the gas phase reaction zone and an increase in transporting more reactant species to the substrate surface. However, increasing the rotation rate more than 500 rpm leads to induce flow recirculation near the rotating susceptor, and the streamlines start to deflect, as shown in Figure 5.15.
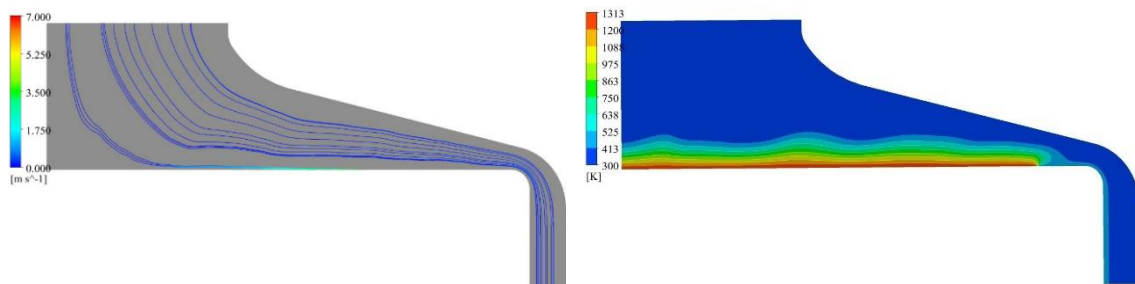
Figure 5.14 Flow and thermal fields with a gas mixture of 40% H_2 and 60% N_2 as the carrier gas at the susceptor rotation rate of 200 rpm.
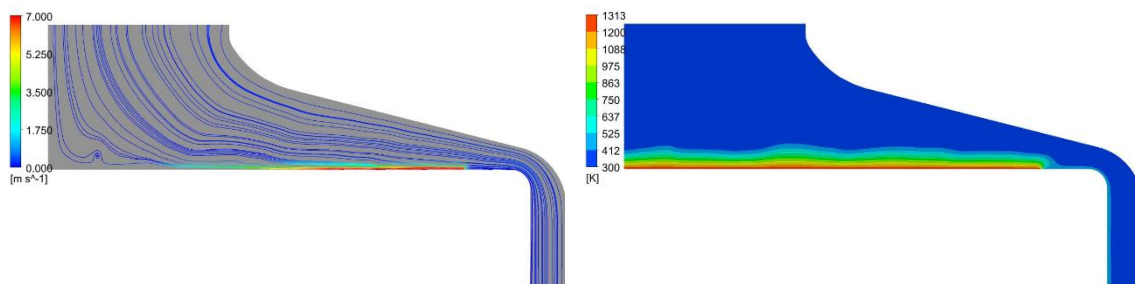
Figure 5.15 Flow and thermal fields with a gas mixture of 40% H_2 and 60% N_2 as the carrier gas at the susceptor rotation rate of 500 rpm.

When the rotational speed is sufficiently high, the momentum boundary due to the rotating susceptor separates from the susceptor surface leading to the formation of inertially driven flow recirculation. The flow recirculation induced by the high susceptor rotation is detrimental to the deposition rate and uniformity of GaN thin films. Nonetheless, the high rotation rate helps to distribute the gas mixture uniformly along with the susceptor surface, and also reduces the boundary layer thickness. So, Ga-containing species can be transported efficiently to the wafer surface. The variation of the deposition rate of GaN thin films along the radial distance of the wafer surface at different rotation rates is shown in Figure 5.16. Rapid rotation rate leads to an increase in the efficiency of reactants usage.

The high rotation rate of the susceptor is beneficial for the improvement of the deposition rate of GaN thin films due to the pumping effect. However, increasing the rate of rotation is prohibitive concerning further process expense. Also, one can see that the standard deviation of the deposition

rate rises gradually, as shown in Figure 5.16 (b). Hence, increasing the rotation can accumulate Ga species contain toward the edges of the susceptor, which results in decreasing the uniformity of GaN thin films.
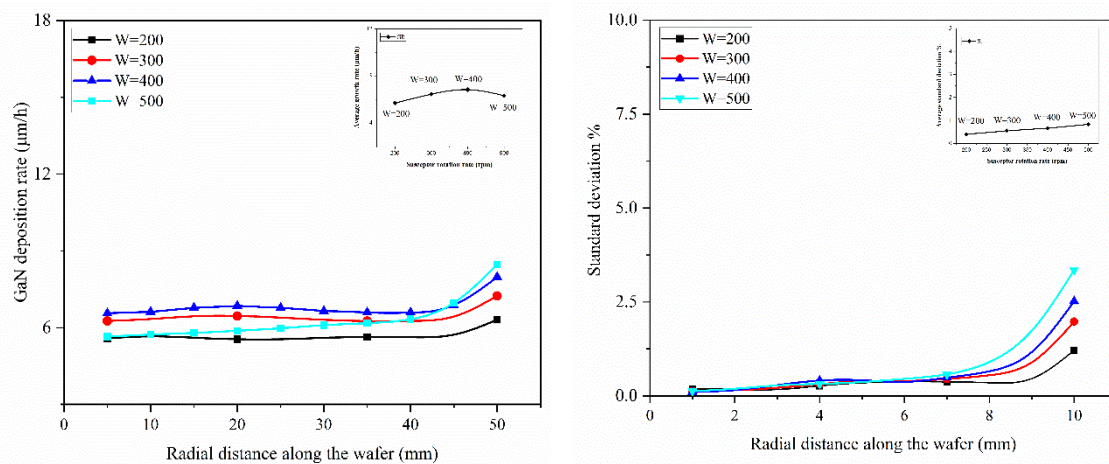
Figure 5.16 Variation of (a) deposition rate and (b) standard deviation profiles along the radial direction of the wafer at different values of the susceptor rotation rate.

The rotation rate has a significant influence on the deposition rate and uniformity of the thin film. It is found that, by increasing the rotation rate of the susceptor to 400 rpm, the deposition rate can be improved; however, the uniformity of GaN thin films has a little improvement.

5.3.5 Gas inlet design

The distribution of Ga-containing species affects the growth rate and uniformity of GaN thin films. Consequently, the inlet design configuration plays an important rule in distributing the metal-organic precursors over the susceptor surface. The gas inlet design has a significant effect on the inlet velocity profile, such as showerhead inlets [3]. Many inlets lead to a uniform flow field inside the reactor. Also, the mesh inlet can cover the entire inlet area, which helps to improve the uniformity of thin films. However, such complex design configuration causes clottings of tiny inlets by adducts formation at the inlet. Thus, the efficiency of the utilization of the precursors is low,

and the maintenance cost is high. Therefore, appropriately adjusting the inlet velocity of precursors, almost help to achieve a uniform and high deposition rate. In previous sections, the gas mixture entered the reactor via a single inlet, producing a uniform plug flow.

In order to focus on transportation of the Ga-containing species to the substrate, the sub-inlet of the metal-organic precursors TMG diluted in a carrier gas (N_2 or H_2) is proposed. The main inlet flow rate of the NH_3 precursors diluted in a gas mixture of N_2 and H_2 as the carrier gas is maintained constant at reference conditions.
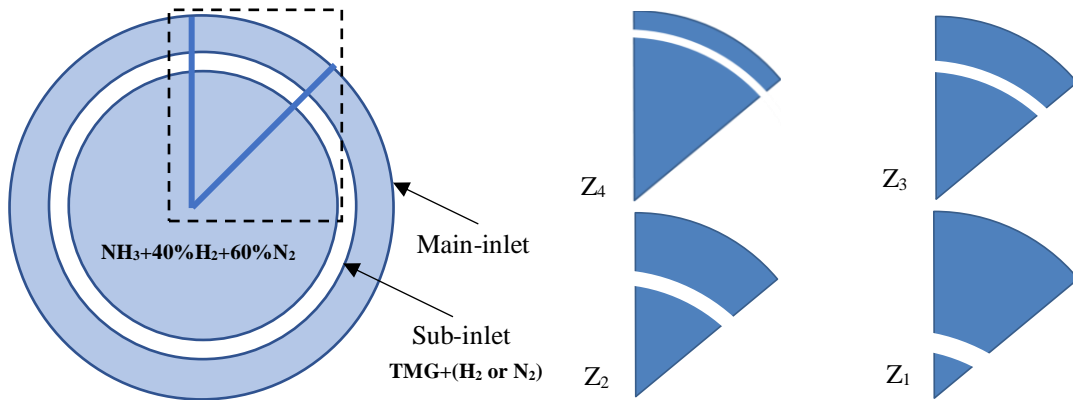
Figure 5.17 Schematic diagram illustrates the location of the sub-inlet for the metal-organic (MO) with a carrier gas along the gas inlet.

The sub-inlet is measured as an annular ring with a constant area of 97.8 mm^2 as follows:

$$A = \pi\left(r_o^2 - r_i^2\right)$$

5-5)

Figure 5.17 shows the sub-inlet configuration at different positions along the main gas inlet. The effect of sub-inlet location on the uniformity and growth rate of GaN thin films is investigated. Figure 5.18 shows the velocity pathlines inside the reactor for different locations of the sub-inlet with pure H_2 as the carrier gas. Location Z_1 shows that the metal-organic precursors transform from the sub-inlet to the susceptor surface in short residence time, which leads to an increase in consumption time of the precursors at the reaction near the substrate surface. Thus, the deposition

rate of GaN thin film increases. On the other hand, the mixture gas transforms fast from the location Z_4 with a proper reaction on the substrate surface and thus decrease of the growth rate. One can note that Ga-containing species reside for a longer time at the substrate surface when it injected from the location Z_1 compare to the location Z_4, as shown in Figure 5.18 (b). The sub-inlet is beneficial for the improvement of the deposition rate due to the transforming Ga-containing species to the substrate surface.
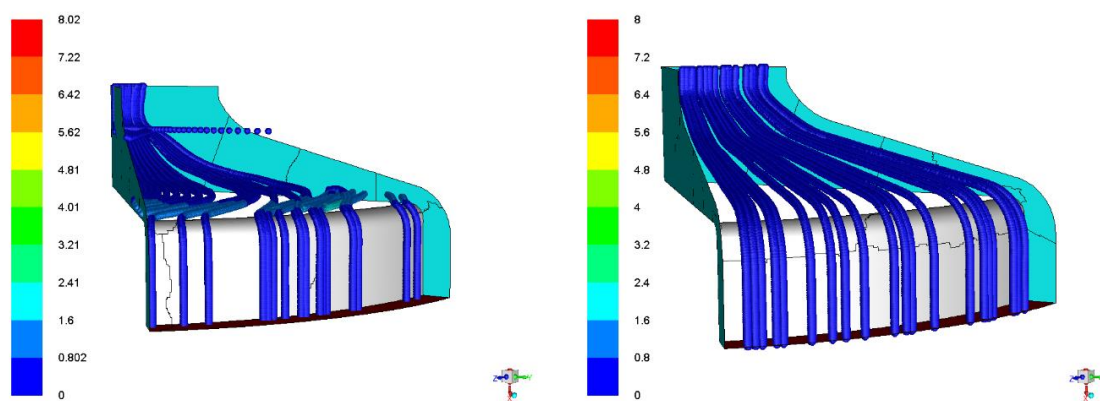
Figure 5.18 Velocity pathline profile with pure H_2 as the carrier gas with MO precursors for the sub-inlet position (a) Z_1 and (b) Z_4 at reference conditions.
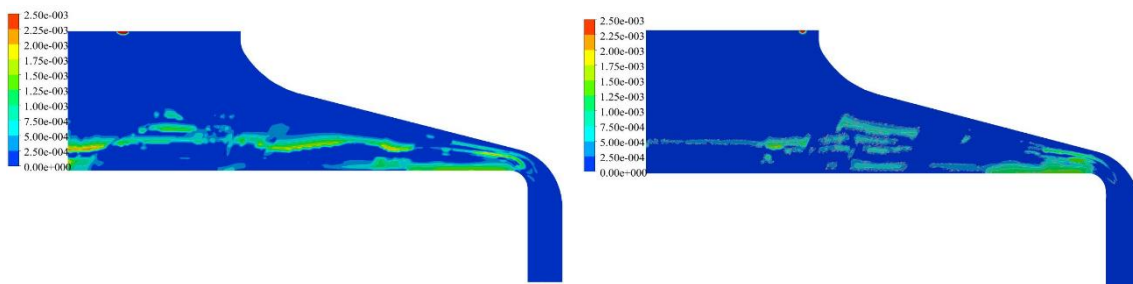
Figure 5.19 Distribution of mass fraction of TMG that is diluted with pure H_2 gas injected from different sub-inlet positions (a) Z_1 and (b) Z_4 at reference conditions.

The effect of the sub-inlet positions is demonstrated to get a spatial variation in the distribution of TMG in the reactor. The TMG precursors is diluted with pure H_2 gas injected from different sub-

inlet locations into the reactor. Figure 5.19 shows the distribution of mass fraction TMG above the susceptor surface for different locations of sub-inlet at reference conditions. TMG precursors decompose rapidly into intermediate species such as MMG that incorporate in reaction to form a sold thin film. The deposition process of GaN thin films is controlled by the diffusion of MMG and MMG:NH_3 species. The distribution of MMG and MMG:NH_3 species above the susceptor are illustrated in Figure 5.20 and Figure 5.21, where TMG precursors injected from the location Z_1 and Z_4, respectively. The results indicate that the sub-inlet location Z_1 aids in distributing the TMG species above the susceptor, which enhances the deposition rate of GaN thin films.
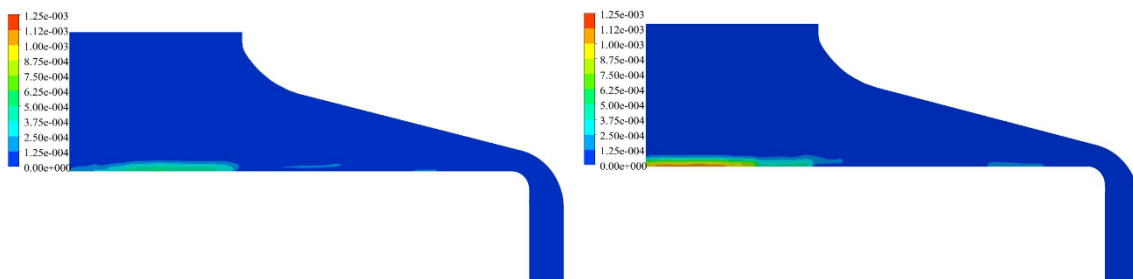
Figure 5.20 Distribution of MMG mass fraction at different locations of sub-inlet (a) Z_1 and (b) Z_4 with pure H_2 as the carrier gas at reference conditions.
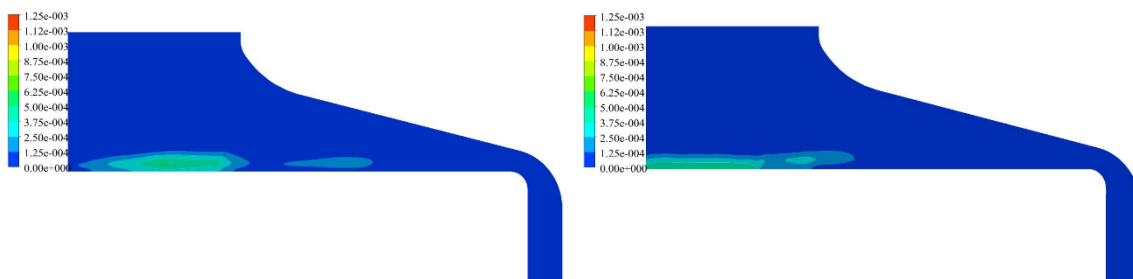
Figure 5.21 Distribution of MMG:NH_3 mass fraction at different locations of sub-inlet (a) Z_1 and (b) Z_4 with pure H_2 as the carrier gas at reference conditions.

A high deposition rate is obtained when the TMG precursors deliver from the location Z_1, as shown in Figure 5.22. The pure H_2 is employed to transport TMG from the sub-inlet at location Z_1, while the main inlet employees a gas mixture of N_2 and H_2 as the carrier gas at reference conditions.
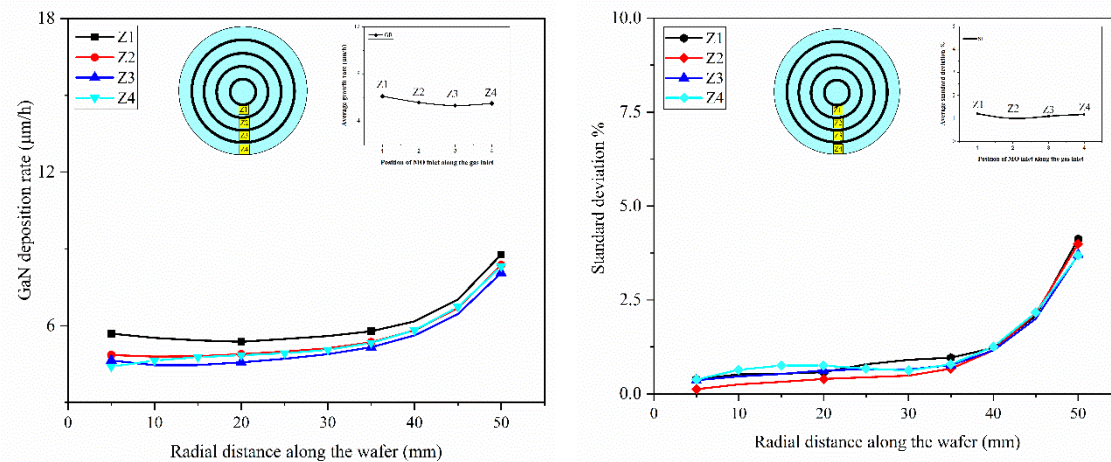
Figure 5.22 Variation of (a) deposition rate and (b) standard deviation profiles along the radial direction of the wafer at different sub-inlet positions with pure H_2 as the carrier gas at reference conditions.

When pure H_2 used to push the metal-organic precursors, the deposition rate decreases slightly by moving the sub-inlet location Z_1 from the center to the location Z_4 at the edge. Thus, H_2 as carrier gas plays little role in transporting the metal-organic species from the gas phase reaction to the substrate surface. Also, changing the location of sub-inlet has a slight effect on the standard deviation profile, as shown in Figure 5.22 (b). On the other hand, using pure N_2 as the carrier gas in the sub-inlet has a significant effect on the deposition rate of GaN thin films.

The pure N_2 has a potential effect of pushing reactant species from the sub-inlet into the reactor towards the substrate surface. Figure 5.23 shows the velocity pathlines inside the reactor for different locations of the sub-inlet with pure N_2 as the carrier gas. At a given fixed gas mixture inlet, the sub-inlet at the location Z_1, which produces a high gas flow to deliver the MO precursors

to the substrate surface. High inlet velocity facilities the transport of the reactant species to reach the substrate surface efficiently, and thus enhances the deposition rate of GaN thin films. Thus, Ga-containing species speeds up the deposition rate.
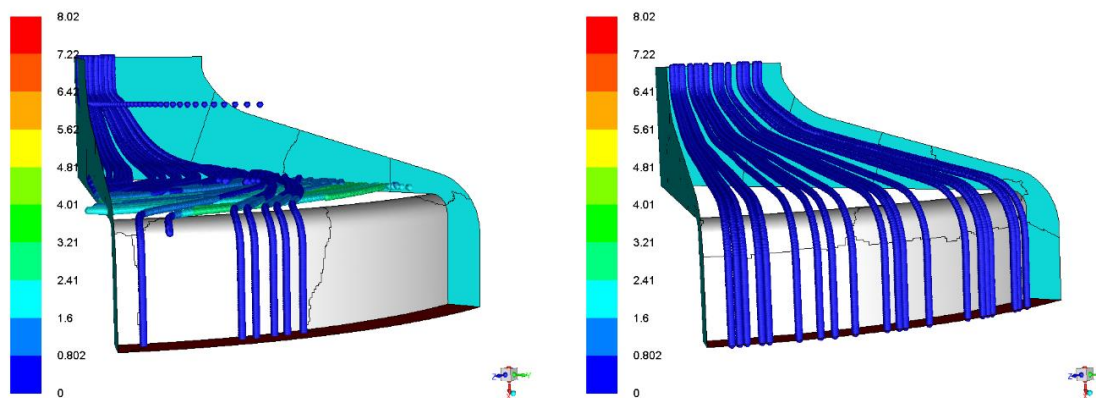
Figure 5.23 Velocity pathlines profile with pure N_2 as the carrier gas with MO precursors for sub-inlet position (a) Z_1 and (b) Z_4 at reference conditions

The growth rate of GaN thin film is affected by the diffusion of Ga-containing species to the substrate surface. Using sub-flow helps to increase the mass flux of Ga-containing species and improves the concentration of Ga-containing species above the susceptor. Figure 5.24 shows the distribution of metal-organic precursors above the susceptor using different positions of the sub-inlet. It shows that TMG species is distributed above the susceptor and high concentration exist near the edge of the rotating susceptor. The results show in case of using pure N_2 in the sub-inlet helps to deliver more metal-organic species to the substrate surface compared with using pure H_2. The heavy N_2 gas pushes Ga-containing species from the inner sub-inlet at location Z_1 towards the rotating susceptor, which leads to distributing TMG species above the susceptor, and more species are accumulated near the susceptor edge. The strong downward flow from the sub-inlet at the location Z_1 facilitates the transport of reactant species to the substrate surface, and it aids these species residing for a long time, leading to high deposition rate.
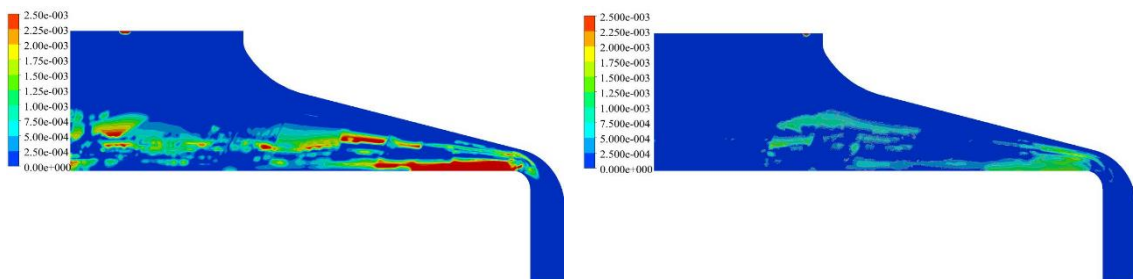
Figure 5.24 Distribution of mass fraction of TMG that is diluted with pure N_2 injected from the sub-inlet at different locations (a) Z1 and (b) Z_4 at reference conditions.

The distribution of MMG and MMG:NH_3 species above the susceptor are illustrated in Figure 5.25 and Figure 5.26, where TMG precursors injected from the location Z_1 and Z_4, respectively. The results indicate that using pure N_2 transport the TMG precursors efficiently from the sub-inlet at the location Z_1 to the substrate surface. Also, pure N_2 aids in distributing the TMG species above the susceptor, which enhances the deposition rate of GaN thin films.
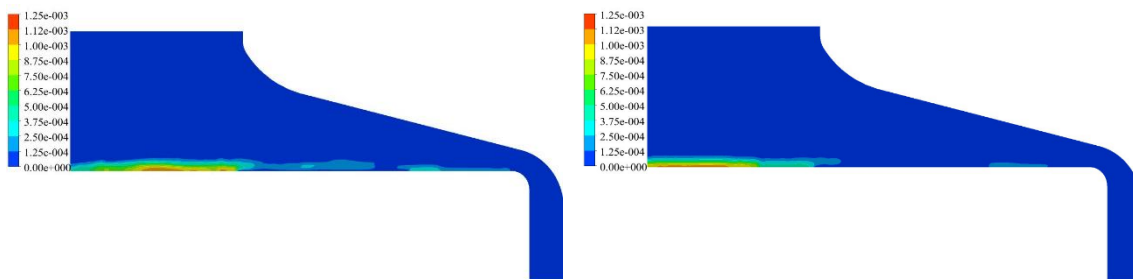
Figure 5.25 Distribution of MMG mass fraction at different locations of sub-inlet (a) Z_1 and (b) Z_4 with pure N_2 as the carrier gas at reference conditions.

A high concentration of MMG:NH_3 presents above the substrate surface as shown in Figure 5.26, which enhances the reaction at the substrate surface. Also, the high rotation rate pulls these reactant species and forces them to stay near the hot substrate surface for a long consumption time, and thus increases the deposition of GaN thin films.
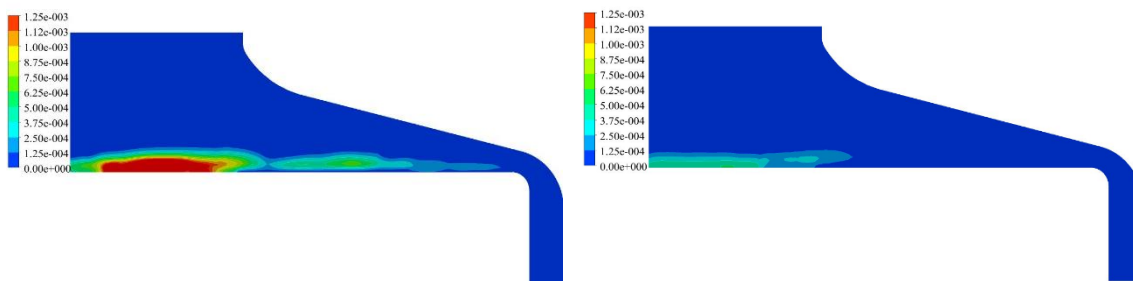
Figure 5.26 Distribution of MMG:NH$_3$ mass fraction at different locations of sub-inlet (a) Z$_1$ and (b) Z$_4$ with pure N$_2$ as the carrier gas at reference conditions.

The variation of deposition rate along the substrate surface under the effect of the sub-inlet is presenting in Figure 5.27. The high deposition rate is obtained when the pure N$_2$ employed to transport TMG from the sub-inlet at location Z$_1$, while the main inlet employees a gas mixture of N$_2$ and H$_2$ as the carrier gas at reference conditions.

Figure 5.27 Variation of (a) deposition rate and (b) standard deviation profiles along the radial direction of the wafer at different sub-inlet positions with pure N$_2$.

A high inlet velocity coming out from the sub-inlet provides the separation of Ga-containing species from NH$_3$, which result in reducing the adduct formation at the inlet. Also, high inlet velocity helps to push the Ga-containing species and reduces the residence time in the gas phase, which results in enhancing the deposition rate. The sub-inlet at the location Z$_1$ shows a high

deposition rate, but there is a higher standard deviation occurs along the radial distance of the wafer surface, as shown in Figure 5.27 (b). Figure 5.28 shows the variation of deposition rate and standard deviation of GaN thin films grown under reference conditions with different carrier gases.
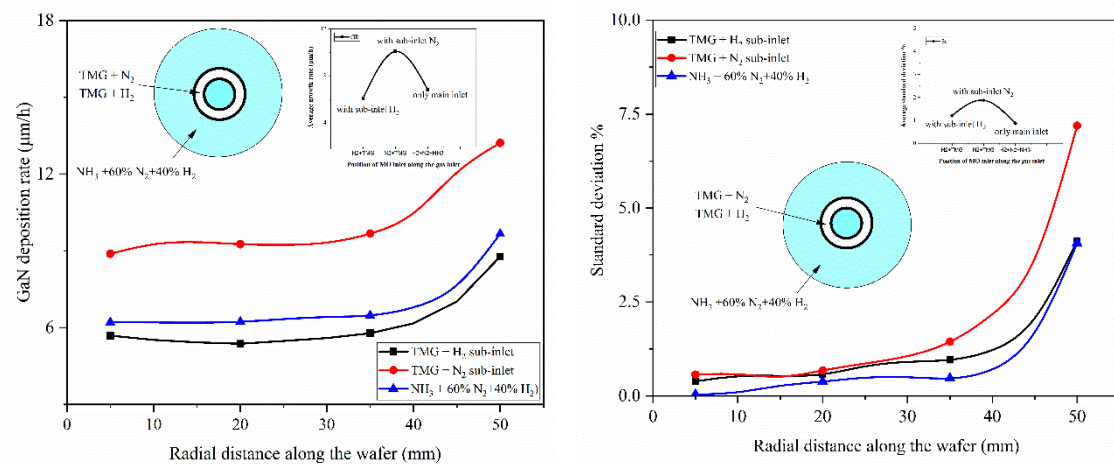
Figure 5.28 Variation of (a) deposition rate and (b) standard deviation profiles along the radial direction of the wafer at Z_1 position.

One can see that the proposed sub-inlet aids to deliver the metal-organic precursors efficiently to the substrate surface, and thus raise the level of the Ga-containing species participating in surface reactions. Therefore, the sub-inlet with pure N_2 has a significant effect on the deposition rate, compared with the main gas inlet without the sub-inlet. The sub-inlet with pure N_2 leads to an increase in the deposition rate, but it decreases the uniformity of the deposition, as shown in Figure 5.28 (b). In conclusion, the location of the sub-inlet has a significant effect on the improvement of the deposition rate and uniformity of GaN thin films.

5.3.6 Wafer carrier design

The metal-organic precursors diluted with N_2 gas injected from the sub-inlet at location Z_1 into the reactor, the gas mixture flows to the susceptor edge. To support the understanding that the distribution of Ga-containing species can essentially improve the deposition rate along the

susceptor surface, growth runs at different wafer locations have been performed. The schematic design of the wafer carrier is illustrated in Figure 5.29.
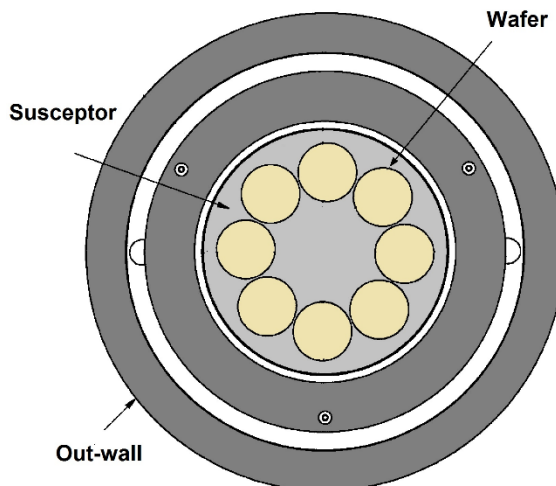
Figure 5.29 Top view schematic diagram of the multi-wafer MOCVD reactor.

Figure 5.30 shows a comparison of the distribution of deposition rates on the wafer surface at different locations along the susceptor surface.
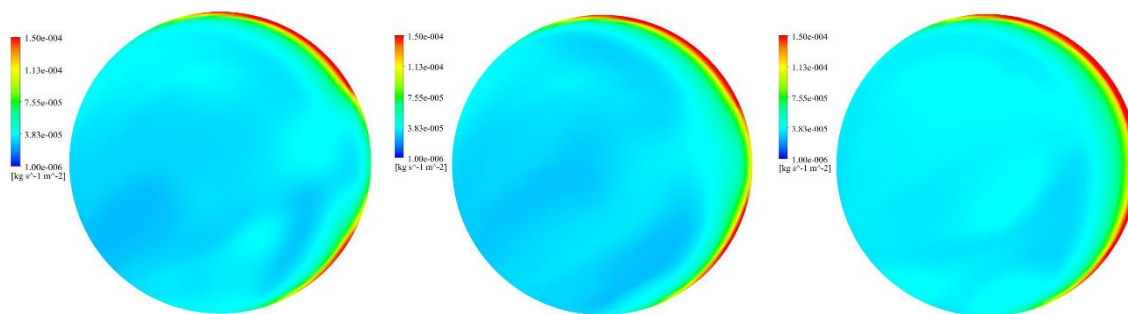
Figure 5.30 Distribution of deposition rate on the wafer surface at different locations from the center of the susceptor (a) W_1, (b) W_2, and (c) W_3 at reference conditions.

It can be seen that the pattern of deposition is the same on each wafer, but that deposition rate of the wafer at the susceptor edge is higher due to the high concentration of TMG species. The variation of deposition rate along the wafer at three distinct distances ($W_1=136$ mm, $W_2=146$ mm,

and W_3=168 mm) from the center along the susceptor is investigated. Results show that the wafer that is located near the susceptor edge has a higher deposition rate than the others, but it is not appropriate for getting a uniform deposition as presenting in Figure 5.31.
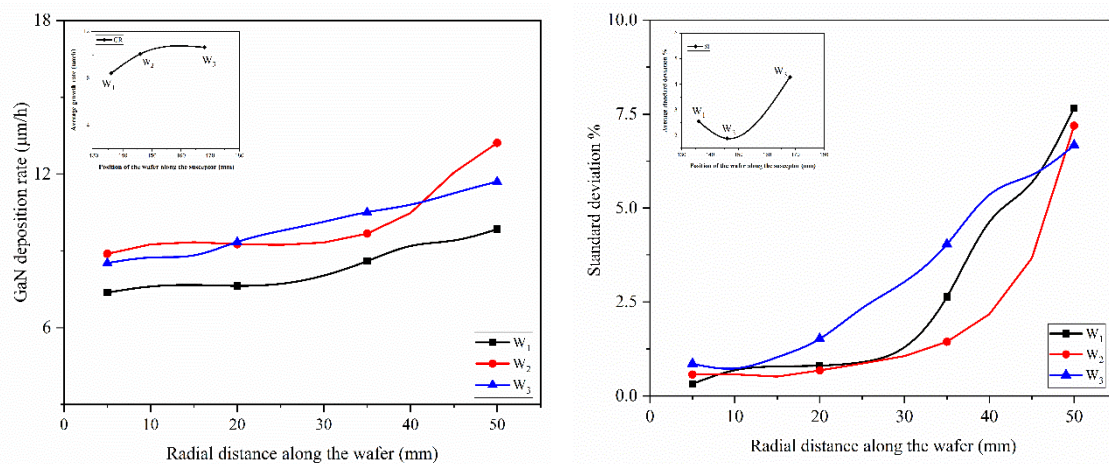
Figure 5.31 Variation of (a) deposition rate and (b) standard deviation profiles along the radial direction of the wafer at different locations with the sub-inlet at location Z_1 with pure N_2 as the carrier gas.

In conclusion, the throughput can be maximized by injecting the metal-organic precursors through the sub-inlet. However, the uniformity of the thin film can be controlled by controlling the flow rate in the sub-inlet to distribute the metal-organic species evenly above the susceptor. Also, consideration in wafer carrier design can enhance the deposition rate of GaN thin films. The location of the wafer at a distance of W_2=146 mm shows the best result.

5.3.7 Reactor height

More precursors are consumed in a reactor that has a considerable distance between the gas inlet and the susceptor. A short distance is sufficient to reduce the reactor volume and consequently, consumes less amount of precursors. At the higher distance between the inlet and susceptor, the natural convection driven by buoyancy forces appears above the substrate
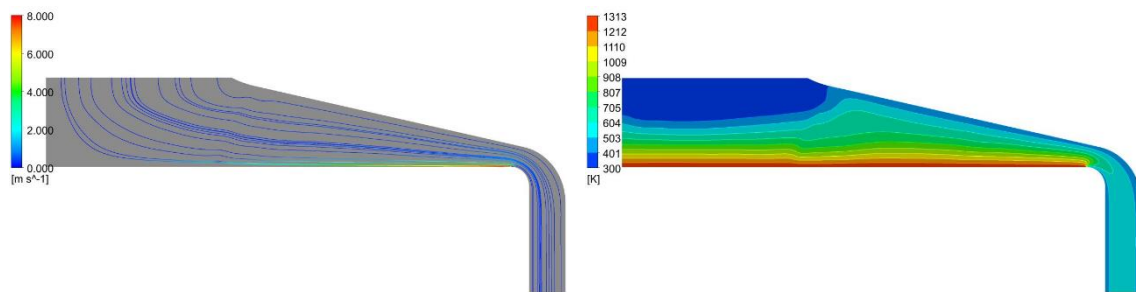
Figure 5.32 Flow and thermal fields with a gas mixture of 40% H_2 and 60% N_2 as the carrier gas at the reactor height of 45 mm.
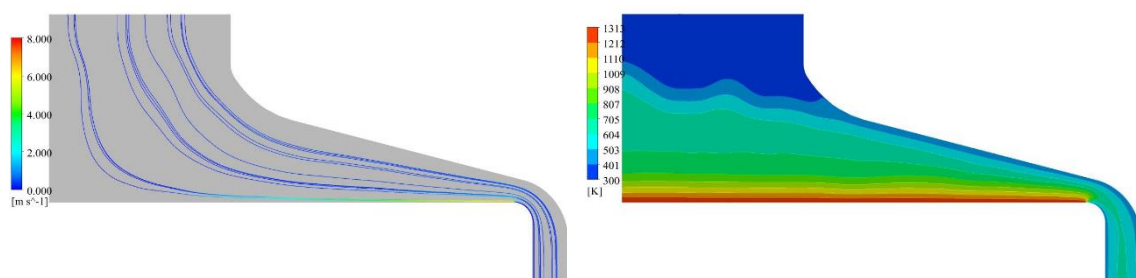
Figure 5.33 Flow and thermal fields with a gas mixture of 40% H_2 and 60% N_2 as the carrier gas at the reactor height of 90 mm.

Figure 5.33 shows the distribution of temperature at H=45 mm and H=90 mm, respectively. When the reactor height is reduced, the spatial distribution of the temperature field is changing according to the patterns of gas flow. Figure 5.34 shows the deposition rate profile versus the distance between the inlet and the susceptor at reference conditions. The deposition rate decreases with increasing the distance from H=45 mm to H=90 mm, as shown in Figure 5.34 (a). It is found that the deposition rate along the radial distance decreases with increases the distance between the inlet and the susceptor to H=90 mm.

As the distance between the inlet and the susceptor increases, the residence time of precursors transforming from the inlet to the substrate surface becomes longer. Thus, the reactants precursors stay for a long time in gas phase reactions, which leads to consumption of the reactant precursors and decrease the growth rate. The higher growth rate is obtained for the smaller distance of H = 45

mm, but the uniformity of GaN thin films is decreased. At a low distance, the gas velocity increases near the substrate surface, leading to reduce the thin film boundary, which increases the deposition rate. However, reducing the distance between the inlet and the susceptor leads to a decrease in the uniformity of the thin film.

On the other hand, increasing the distance aids in decreasing the temperature gradient between the gas inlet and susceptor, which makes more reactant to be mixed before reach the substrate surface and thus cause pre-reaction, which affects the growth rate. According to the Grashof number, increasing the distance further leads to an increase in the natural convection, which could cause flow recirculation inside the reactor and affect the growth rate.
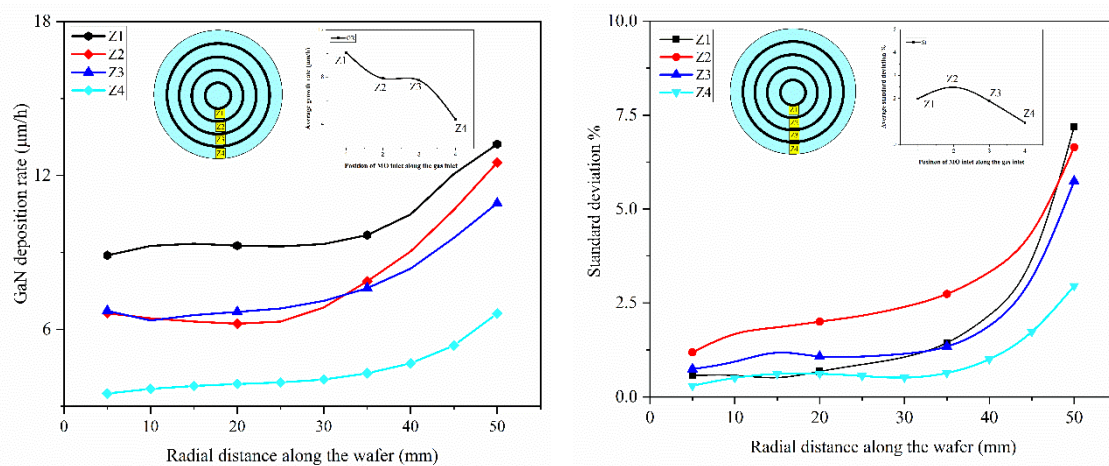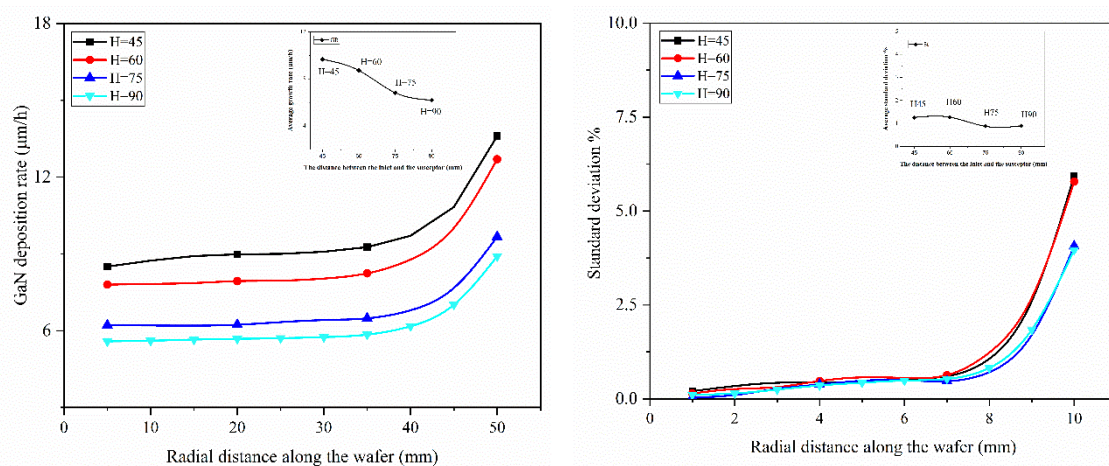

Figure 5.34 Variation of (a) deposition rate and (b) standard deviation profiles along the radial direction of the wafer at different values of the reactor height.

At the reference conditions, forced convection in the reactor includes the gas inlet flow and susceptor rotation rate, which are kept constant. Thus, strong natural convection results in a nonuniform distribution of reactant species above the rotating susceptor and consequently decrease the growth rate. Nonetheless, increasing the distance to H=90 mm, improves the uniformity of GaN thin films, as shown in Figure 5.34 (b). As a result, the distance between the inlet and the susceptor is an important processing factor. Therefore, an appropriate distance H=75 has been obtained for

growing thin films with high-quality. The variation tendency of the uniformity of GaN thin films versus the distance between the inlet and the susceptor is parabolic.

5.4 Conclusions

The numerical simulation is carried out for the growth rate and flow characteristics in the multi-wafer reactor. The effects of processing parameters and reactor design configuration on the uniformity and growth rate of GaN thin film have been investigated. The numerical results show that appearing of recirculating flow at high reactor pressure can affect the deposition rate and uniformity of GaN thin films. In strong flow recirculation, the precursors are trapped and not reach the susceptor effectively. Also, increasing the V/III ratio can lower the incorporation of carbon impurities, especially CH_3, and CH_4 in the growth rate. The composition of carrier gas has an important effect on flow characteristics, so using a mixture of N_2 and H_2 gases can help to take advantages of both properties of N_2 and H_2 for a large scale production system.

The inlet design has a significant effect on improving the reactant species utilization and increases the growth rate. Also, the wafer carrier design can affect the deposition rate and uniformity of GaN thin films. The proper distance between the inlet and the susceptor aids to decrease the temperature gradient and improve the stability of the flow above the rotating susceptor. The predicted results have significant reference values for guiding role and parameter optimization of GaN growth in MOCVD reactor. A unique advantage can be resulted by optimizing the boundary conditions to produce a uniform thin film with a higher growth rate. Consequently, reducing the manufacturing cost and save resources.

Chapter 6

OPTIMIZATION WITH SURROGATE MODEL

6.1 Introduction

In engineering design, the direct optimization based on the numerical simulation is inefficient since iterative analyses require enormous iterations and high computational cost during the optimization [106]. Thus, the surrogate-based optimization is an effective technique to alleviate the expensive computation experiments with fewer sample points. In this chapter, the response of the numerical modeling of GaN deposition in the MOCVD process is represented in a surrogate-based model. Figure 6.1 illustrates the construction of the surrogate-based model which involves three stages: (i) design of experiments (DOE); (ii) construction or training of the surrogate model; and (iii) model validation.
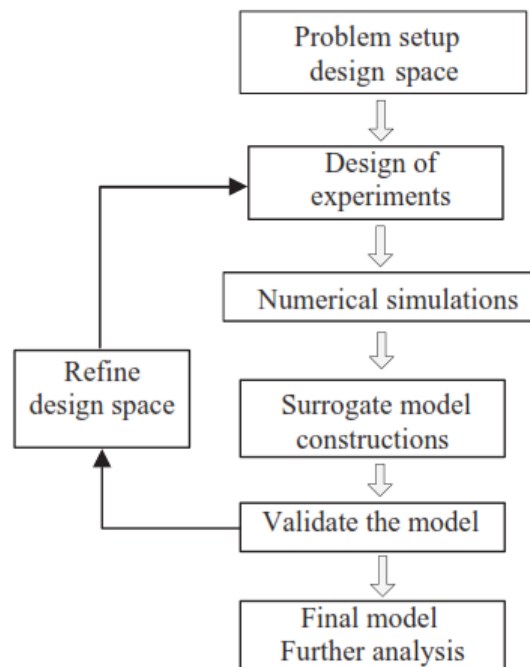
Figure 6.1 Flowchart of building surrogate-model, adapted from [106]

Response surface models are generated for the growth rate and uniformity of GaN thin films concerning typical design variables. Then the deterministic optimization and optimization under uncertainty are performed to find a set of optimal solutions.

6.2 Design of experiments

Design of experiments (DOE) determines multiple combinations of the controlled parameters points in the design space. Several sampling techniques are available to distribute the sample points to provide adequate coverage of the design space without variation. Full factorial design of experiments is given by every possible combination of the factor values $N = L^c$, where L and c represent levels and parameters, respectively [107]. When the number of design variables is big, the use of the full factorial method is required more design points. For example, it requires 15625 design points to study the deposition rate and uniformity of GaN thin films under the effect of six operating parameters; each parameter has five levels. The optimal Latin hypercube (LHC) method generates initial sample data. It is ensuring for each variable; all points are distributed randomly in the design space [108]. Table 6-1lists processing parameters considered in the design of the experiment.

Table 6-1) Processing parameters of GaN deposition in the MOCVD system

Symbol	Factors	Initials	Range
ω	Susceptor rotating rate (rpm)	1200	0 – 1400
T	Wafer temperature (k)	1273	1073 – 1473
u	Velocity inlet of the mixture (m/s)	0.127	0.0254-0.225
P	Pressure (Torr)	140	20-500
NH$_3$	NH3 Flow rate (slm)	6	2 – 10
TMG	TMG Flow rate (slm)	0.003	0.001 - 0.005

6.3 Correlation of parameters

Practical work usually involves many factors, which requires multi-factor analysis. When the number of input variables is increased, the analysis becomes more and more intractable. Therefore,

it is required to exclude unimportant input parameters to reduce additional sampling points. A set of design points (DPs) in the design space given in Table 6-1. The number of DPs is determined according to the convergence of the output parameters. Measuring of linear dependency for each pair of design variables are calculated using the average of non-dimensional slop as follows:

$$X = [x_1, x_2, x_3, \dots, x_N]$$
$$Y = [y_1, y_2, y_3, \dots, y_N]$$
$$m_n = \frac{(y_n - y_{n-1})/(1/N) + (y_{n+1} - y_n)/(1/N)}{2}$$

$$\bar{\bar{m}}_{X-Y} = \frac{\sum_{n=1}^{N} m_n}{n}$$

	P	T	w	u	NH$_3$	TMG
GR	$\bar{\bar{m}}_{P-GR}$	$\bar{\bar{m}}_{T-GR}$	$\bar{\bar{m}}_{w-GR}$	$\bar{\bar{m}}_{u-GR}$	$\bar{\bar{m}}_{NH3-GR}$	$\bar{\bar{m}}_{TMG-GR}$
St	$\bar{\bar{m}}_{P-St}$	$\bar{\bar{m}}_{T-St}$	$\bar{\bar{m}}_{w-St}$	$\bar{\bar{m}}_{u-St}$	$\bar{\bar{m}}_{NH3-St}$	$\bar{\bar{m}}_{TMG-St}$

	P	T	w	u	NH$_3$	TMG
GR	3.22	1.83	0.99	0.79	0.31	8.87
St	0.82	0.14	0.20	0.07	0.18	0.68

Figure 6.2 Correlation matrix of design variables

The correlation matrix given in Figure 6.2 shows the effects of design variables on the growth rate and uniformity of GaN thin films, respectively. It is observed that the flow rate of TMG and reactor pressure P have direct correlations to the growth rate (GR) and standard deviation (St). The same behavior is observed for the susceptor temperature, but it has less influence on Gr, St, and Un, respectively. These operating conditions are considered in the optimization study to increase the deposition rate and uniformity of GaN thin films in the range of the design space.

6.4 Surrogate models

The objective of the surrogate model is to construct an approximate mathematical model based on sampled points to predict the relationship between inputs and outputs of the process. The surrogate-based model is classified into two types:

➢ The exact fitting creates a smooth curve that passes through all data points. It is an accurate and useful technique for a small amount of data.

➢ The best-fitting provides the best prediction of the response behavior. The best-fitting does not necessarily pass through any of the data points. It is beneficial for a large amount of data.

Many techniques have been developed to achieve either exact or best fitting with single or multiple variables [109]. The most common surrogate models of creating response surface are:

6.4.1 Polynomial response surface

It is one of the simplest and most commonly used surrogate models. It employs a polynomial approximation to explore the relationship between input parameters and estimated response. The regression formulation for small-scale models is given as follows:

$$\mathbf{F(s)} \cong \mathbf{w}.\mathbf{B(s)}$$

<div align="right">6-1)</div>

Where w is a vector of the regression coefficients, and B(s), is a linear combination of the modeling monomials.

6.4.2 Kriging model

Kriging method is an interpolating method, where the generated response surface passes through all the initial sampling points. Spatial prediction is based on minimizing the error variance between observed and estimated value [110].

Kriging method is used for better capturing of high nonlinearity parametric modeling [111]. Estimated value $Z(s_0)$, can be obtained by linear combined of available samples $Z(s_i)$, at the nth known locations, and weighting coefficients w_I that its sum equals 1, to ensure that the estimate is unbiased.

$$Z(s_0) = \sum_{i=1}^{N} w_i Z(s_i) \qquad \text{6-2)}$$

The estimated values are then determined by minimizing the error variance between estimated function and the experimental results. Optimal weights coefficient w_I can be calculated as below:

$$w_i = C_{ij}^{-1} C_{j0} + \left[\frac{1 - 1_i C_{ij}^{-1} C_{j0}}{1_i C_{ij}^{-1} 1_j} \right] C_{ij}^{-1} 1_j \qquad \text{6-3)}$$

Where s_0 denotes investigated variables; C_{ij} and C_{i0} are the covariance matrix and vector, respectively. The choice of the functional form of the covariance is important since it influences the predictive ability of the method [108]. In this paper, a Gaussian kernel function is employed to compute C_{ij} and C_{i0}.

$$C_{ij} = COV(s_i, s_j) \equiv exp\left[-\gamma \| s_i - s_j \|^2 \right] \qquad \text{(6-4)}$$

$$C_{i0} = COV(s_i, s_0) \equiv exp[-\gamma \| s_i - s_0 \|^2] \qquad \text{(6-5)}$$

Where $|s_i - s_j|$ is Euclidean distance between the two points, and γ is a positive constant parameter that describes how the data are correlated. The Kriging model used to estimate unknown value $F(s_0)$ as follow:

$$F(s_0) = \sum_{i=1}^{N} w_i F(s_i) \qquad \text{(6-6)}$$

where F is a vector of experimental results at known locations.

The approximation function F(s) is defined by the product of weighting coefficients and covariance function.

$$F(s) \cong w_i \sum_{i=1}^{q} COV\ (s_0, s_i) \tag{6-7}$$

Where s is a design sampling point, and q is the dimension of the polynomial space.

6.5 Optimization of the MOCVD process

The growth rate and uniformity of GaN thin films should be maximized, while the standard deviation of growth rate should be minimized to obtain high productivity. The non-uniformity factor of the deposition rate is proposed to evaluate the uniformity of the GaN thin film. It is defined as the ratio of maximum variation in the deposition rate to the average deposition rate of GaN thin films across the wafer surface as follows:

$$U_n = \frac{GR_{Max} - GR_{Min}}{GR_{Avg}} \tag{6-8}$$

The non-uniformity factor is obtained, after removing the points near the wafer edge, which are not feasible. Two sets of design variables are considered in this section as follows:

(1) The reactor pressure and the flow rate of TMG.

(2) The susceptor temperature and the flow rate of TMG.

Effects of varying the reactor pressure and susceptor temperature on the growth rate, standard deviation, and non-uniformity factor of GaN thin films with different values of the flow rate of TMG, are shown in Figure 6.3, Figure 6.4, and Figure 6.5. Results indicate that the growth rate and standard deviation increase with increasing the reactor pressure, while the nonuniformity factor is varying with reactor pressure. It is observed at low-pressure, increasing the flow rate of TMG

results in a high value of nonuniformity factor along the wafer surface. Though a uniform deposition rate is obtained at low pressure, there is a high deposition rate on the wafer edge, which affects the uniformity factor. In contrast, increasing the reactor pressure results in a decrease in the non-uniformity factor, which offers the possibility to improve GaN thin film quality at moderate values of the reactor pressure.

The effect of the susceptor temperature has been investigated. It is observed that there was a slight increase in the growth rate when the temperature increased from 1073 to 1473K with different values of the TMG flow rate, as shown in Figure 6.3(b). Moreover, results show in Figure 6.4 (b) that the standard deviation increases linearly with increasing the temperature at different values of the TMG flow rate. It is indicated that the growth rate in this temperature range depends only on the mass transport rate of reactive species to the substrate surface. Also, as long as the reactor pressure is kept constant at 140 Torr, changing the susceptor temperature has a marginal influence on the uniformity factor, as shown in Figure 6.4 (b).
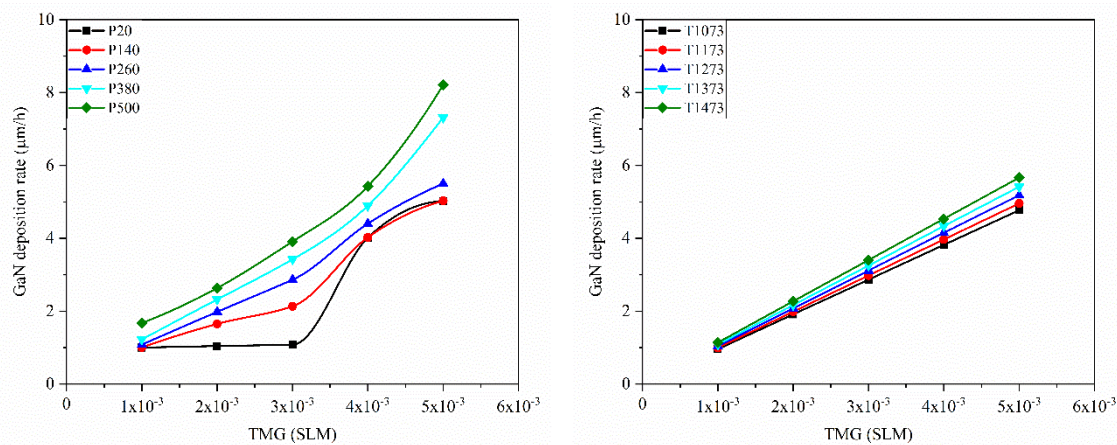
Figure 6.3 Varying the deposition rate of GaN thin films with the flow rate of TMG at different values of (a) the reactor pressure, (b) the susceptor temperature, respectively.
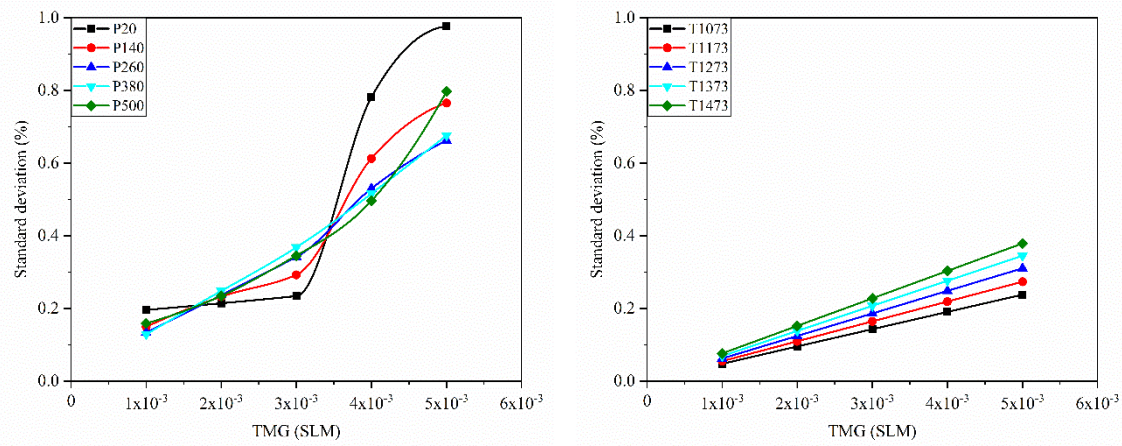
Figure 6.4 Varying the standard deviation of GaN thin films with the flow rate of TMG at different values of (a) the reactor pressure, (b) the susceptor temperature, respectively.
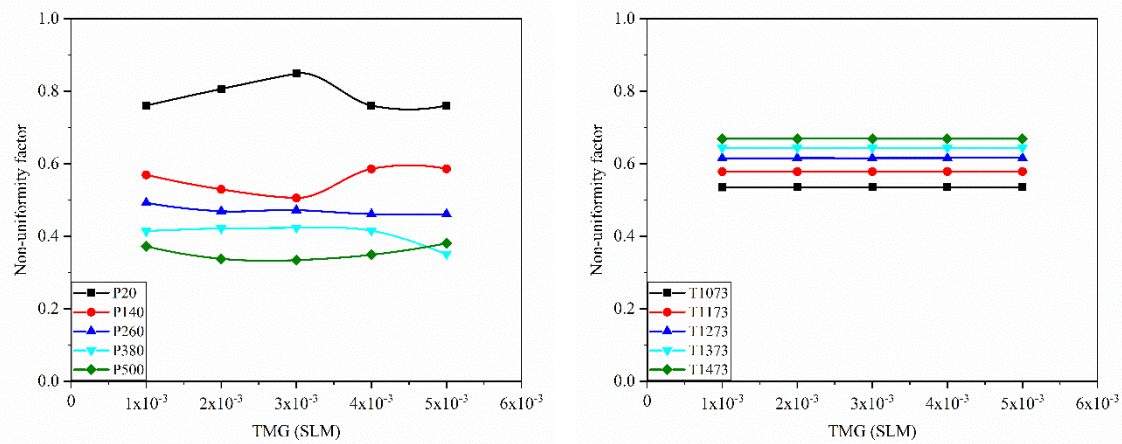
Figure 6.5 Varying the nonuniformity factor with the flow rate of TMG at different values of (a) the reactor pressure, (b) the susceptor temperature, respectively.

The objective is to increase the growth rate and uniformity of GaN thin films grown on the sapphire wafer and correspondingly decrease the production cost. As a result, the response surface of the deposition rate and uniformity in terms of these design variables are generated and discussed later. Then further results are obtained in the optimization problem.

6.6 Generated response surfaces

Response surfaces are generated in different methods to validate and compare the quality of the approximated models. Figure 6.6 shows a comparison of response surfaces created by Kriging and

polynomial method. Results show that the responses are highly nonlinear, Kriging method has more accuracy than the polynomial method to create response surfaces, as shown in Figure 6.6-c. Kriging method is employed to generate response surfaces based on predicted results from the numerical model with different design variables. The average deposition rate (GR), standard deviation (St), and nonuniformity factor (Un) are used to evaluate the growth rate and uniformity of GaN thin films in the MOCVD reactor. The nonuniformity factor (Un) is given in equation ((6-8); it is used to evaluate the uniformity of the thin film along the wafer surface, after removing the points near the edge. Five levels of each design variable are considered for the experiment. There are 25 design points for each set of design variables considered in generating response surface, as shown in Figure 6.7, Figure 6.8, and Figure 6.9, respectively.
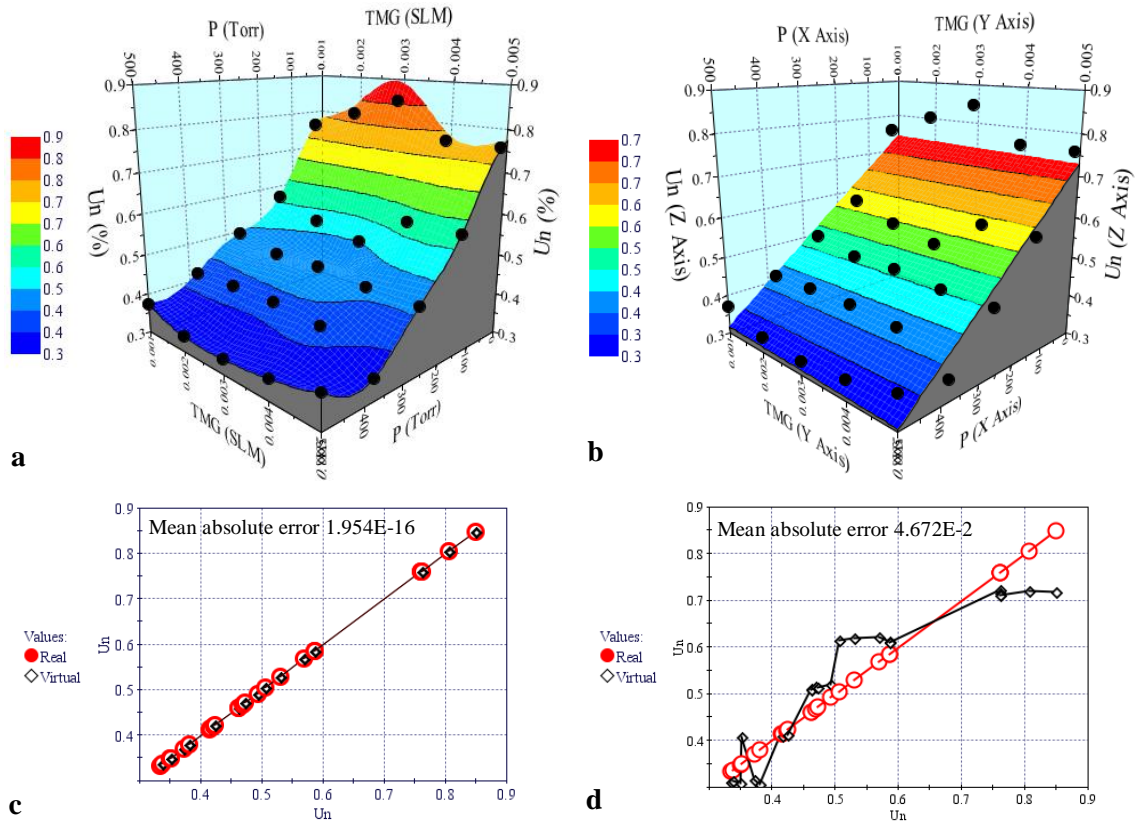
Figure 6.6: Response surfaces of nonuniformity factor created by (a) Kriging method, (b) Polynomial method, and the mean absolute error (c) Kriging method, (d) Polynomial method.
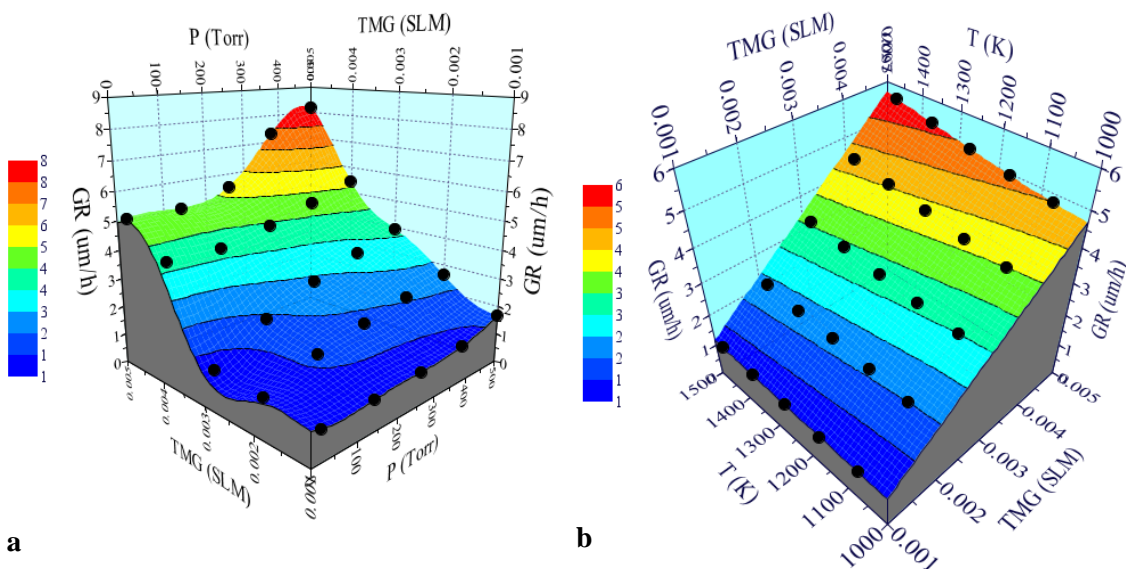
Figure 6.7 Response surface of the growth rate (GR) of GaN thin films grown with different values of TMG flow rates at different values of (a) the reactor pressure, and (b) the susceptor temperature respectively.
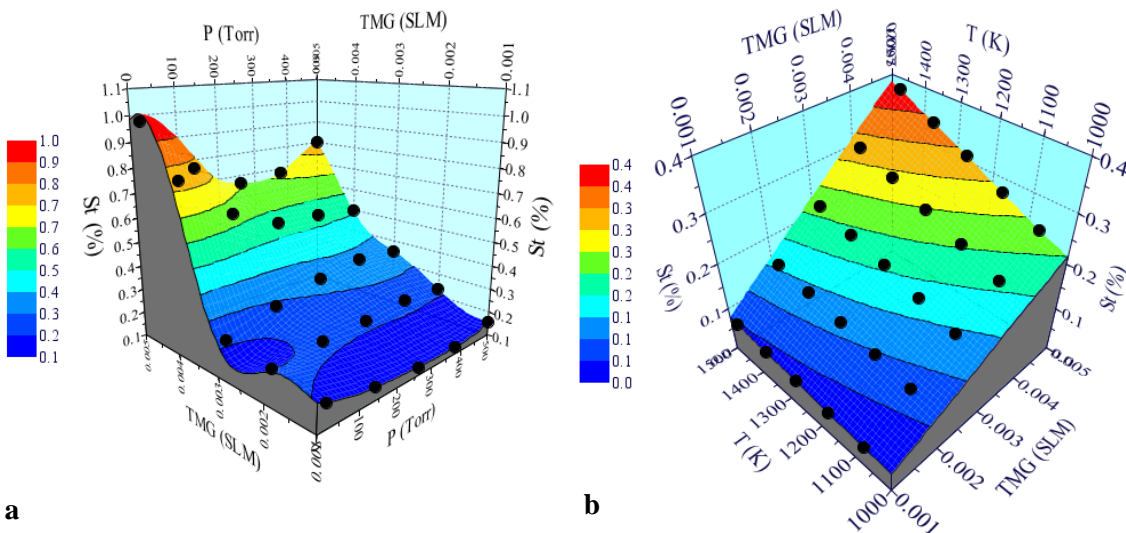
Figure 6.8 Response surface of the standard deviation (St) of GaN thin films grown with different values of the TMG flow rate at different values of (a) the reactor pressure, and (b) the susceptor temperature.
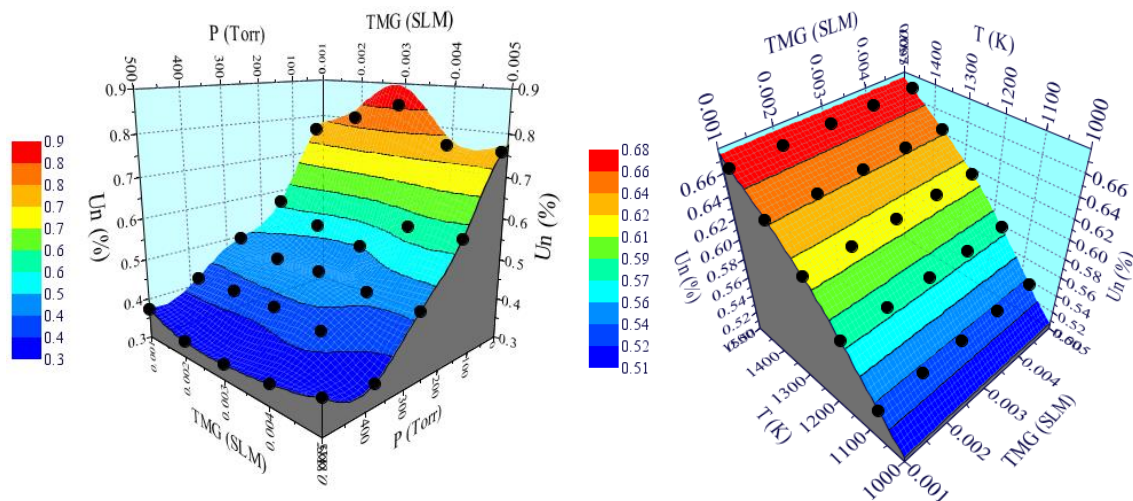
Figure 6.9 Response surface of the nonuniformity factor (Un) of GaN thin films grown with different values of the TMG flow rate at different values of (a) the reactor pressure, and (b) the susceptor temperature.

Results show that at a low value of the TMG flow rate, increasing the reactor pressure has a slight influence on GR; in contrast, it has a significant influence on St and Un. At a high value of the TMG flow rate, increasing the reactor pressure in the range of (260 -400) Torr leads to increase in the growth rate of GaN thin films, and improves both St and Un. On the other hand, the susceptor temperature shows slight increase in GR, and St, while there is no effect on Un as indicated in response surfaces shown in   Figure 6.7 (b), Figure 6.8(a), and Figure 6.9(b) respectively. The accuracy of the response surface model is verified by comparing results from numerical simulation and estimated results from the response surface model, as shown in Table (6-2). The error percentage (ε) between simulations results and the surrogate model results. For the average deposition, the error percentage (ε_{GR}) is less than 8% , the error percentage (ε_{St}) is less than 10% for standard deviation, which indicate good validation. Results are satisfying the feasibility of using response surface models in formulating the optimization study of GaN thin films over the range of design variables in the MOCVD process.

Table (6-2) Verification of the surrogate-based model solution.

No	u (m/s)	ω (rpm)	T (K)	NH$_3$ (slm)	TMG (slm)	P (Torr)	GR (μm/h)	St (μm/h)	GR* (μm/h)	St* (μm/h)	ε_{GR} %	ε_{St} %
1	0.025	1000	1073	6	0.002	170	1.783	0.235	1.93	0.247	7.6	4.85
2	0.025	1000	1073	6	0.005	425	7.96	0.712	7.37	0.648	7.19	9.87
3	0.025	1000	1180	6	0.003	260	2.826	0.166	2. 681	0.185	5.41	9.74
4	0.025	1000	1360	6	0.003	260	3.233	0.211	3.452	0.243	6.32	7.81

6.7 Deterministic optimization

In general, the high productivity of the MOCVD process is increased by increasing the growth rate and decreasing the standard deviation of GaN thin films. Therefore, the objective function is to maximize GR and minimized St subjected to the constraint of allowable values of Un. Most of the practical applications are modeled as multi-objective optimization problems because they have multiple objectives [113]. It would be more practical to form a multi-objective optimization problem instead of optimizing GR and St individually. Deterministic multi-objective optimization of GaN deposition formulated as follows:

$$\underset{x}{Max} f(s) = GR(s)$$

$$\underset{x}{Min} f(s) = St(s)$$

$$s.t \quad g_1(s) = Un(s) \leq 0.4$$

$$s_l \leq s \leq s_u$$

6-9)

Where s_l, s_u are lower and upper tolerance limits of the system parameter, respectively. $f(s)$ is continuous but not necessarily differentiable. Figure 6.10 illustrates the flowchart of optimization using the surrogate-based model.
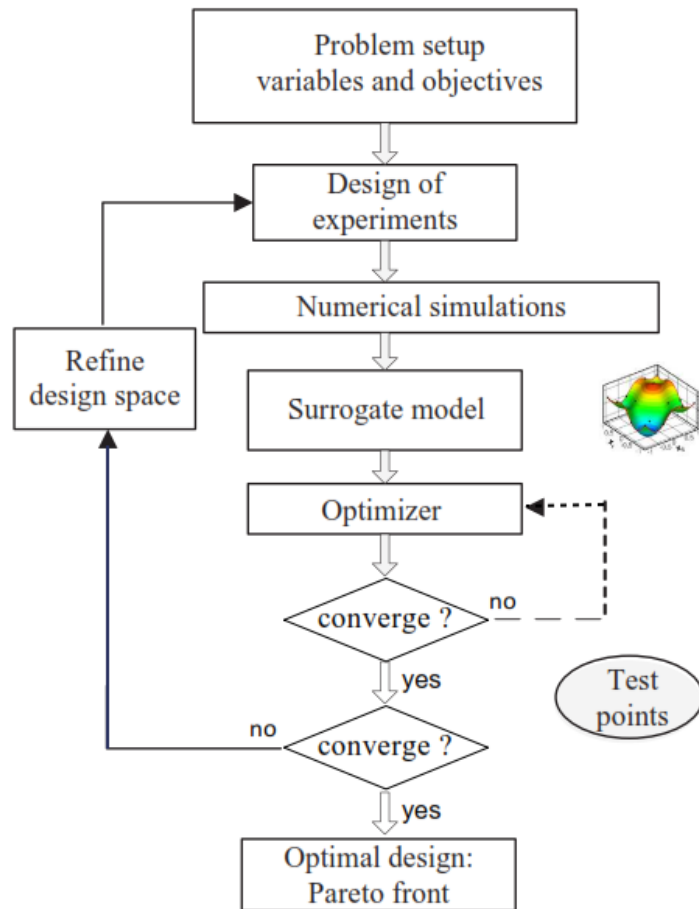
Figure 6.10 Flow chart of the surrogate-based optimization.

Multi-objective optimization problems aim is to find all possible trade-offs among multiple objective functions, that are usually conflicting. It is challenging to choose a single solution for a multi-objective optimization problem without iterative interaction with the decision-maker. A general approach is to show decision-makers a set of optimal solutions [114]. Pareto frontier provides a set of optimal solutions of design variables. However, solving multi-objective optimization problems is not easy due to theoretical and computational challenges. Genetic algorithm (GA) such as Multi-objective genetic algorithm (MOGA-II) is a good choice to achieve this goal [115].

Two sets of design variables are considered, the reactor pressure and the flow rate of TMG and the susceptor temperature and the flow rate of TMG. The response function of deposition rate and uniformity of GaN thin films in terms of these two sets of design variables are generated and discussed in this section. Three optimization formulations are proposed. The first one is to maximize the growth rate (GR) with constraints on the non-uniformity factor (Un). The second one is to minimize the standard deviation (St) with the same constraints on Un. Finally, multiobjective optimization of both GR and St subjected to the same constraint of Un. The solution of the optimization problem is implemented in commercial software modeFRONTIER [113].

6.7.1 Design Variables: the reactor pressure and the flow rate of TMG.

In practical needs for high productivity of optoelectronic devices, the maximization of the GR is an essential factor. Maximize GR can be formulated as follows:

$$\underset{P,TMG}{Max\, GR}$$

$$s.t \quad Un(s) \leq 0.4$$

$$P_l \leq P \leq P_u$$

$$TMG_l \leq TMG \leq TMG_u$$

6-10)

Where the bounds of the design variables are given in Table 6-1. The chosen bounds $P_l = 20$ and $P_u = 500$ Torr, and $TMG_l = 0.001$ and $TMG_u = 0.005$ slm, respectvlly. Figure 6.11 shows the location, which marked by the blue circle of the optimal solution. The optimal solution indicates that the reactor pressure is a significant factor in the control of the growth rate and uniformity of GaN thin films.
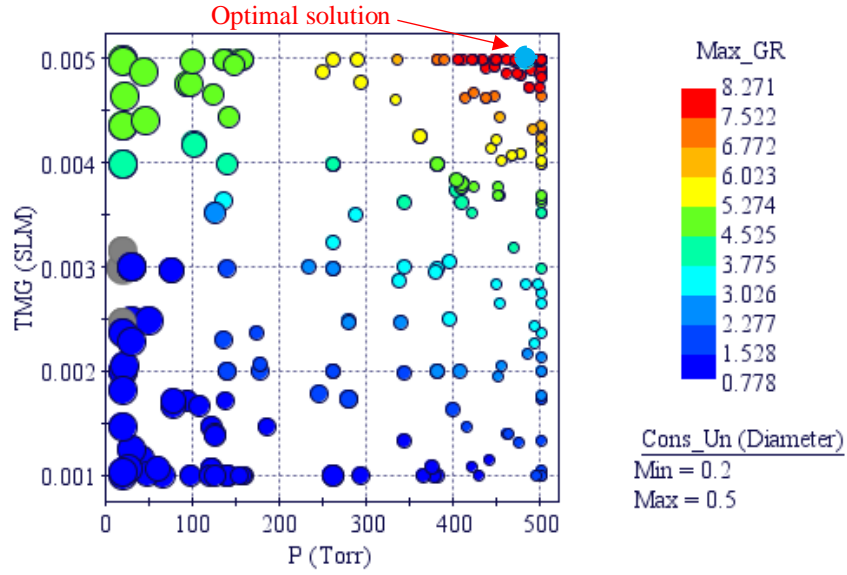
Figure 6.11: The location of the optimal solution of maximizing the growth rate of GaN thin films under constraint.

It is a desirable objective of production GaN thin films to have a high average growth rate with a high level of uniformity of the thin film. It is more practical to get high-quality thin film for semiconductor industrial applications [6]. The uniformity of GaN thin film can be controlled within certain bounds by minimizing the standard deviation (St). The mathematical form of minimizing St is expressed as follows:

$$\underset{P,TMG}{Min}\ St$$

$$s.t \quad Un(s) \leq 0.4$$

$$P_l \leq P \leq P_u$$

$$TMG_l \leq TMG \leq TMG_u$$

6-11)

The location of the optimal solution is shown in Figure 6.12. Both the reactor pressure and the flow rate of TMG are important in minimizing the standard deviation. At a low value of TMG, increasing the reactor pressure up to 375 Torr improves the uniformity of GaN thin films. However, getting

the minimum standard deviation results in a low deposition rate. Thus, an improvement in the uniformity requires degradation the growth rate due to the inverse relationship between these two objectives. A multi-objective formulation is considered to find a set of nondominated solutions by compromising between objectives of design variables.

Figure 6.12: The location of the optimal solution of minimizing the standard deviation of GaN thin films under constraint.

Multi-objective formulation of maximizing GR and minimizing St with the constraint of nonuniformity factor is given as follows:

$$\underset{P,TMG}{Max\ GR}$$

$$\underset{P,TMG}{Min\ St}$$

$$s.t \quad Un(s) \leq 0.4$$

$$P_l \leq P \leq P_u$$

$$TMG_l \leq TMG \leq TMG_u$$

6-12)

Instead of optimizing the growth rate (GR) and standard deviation (St) individually, multiobjective optimization would be more practical for the production of GaN thin films. Figure 6.13 and Figure 6.14 show that the Pareto frontier captures the trade-off behavior between the growth rate and uniformity of GaN thin films for the flow rate of TMG and the reactor pressure, respectively. Pareto frontier provides a set of optimal solutions and offers more flexibility than single-objective formulations for decision-makers.

Thus, a suitable set of the flow rate of TMG and reactor pressure can be select to deposit GaN thin films in the MOCVD reactor. The high growth rate of GaN thin films is obtained at a high flow rate of TMG, as shown in Figure 6.13. Pareto frontier profile moves to the right with higher GR. The same behavior is obtained with increasing the reactor pressure, as shown in Figure 6.14. Applying the physical constraint of uniformity Un = 0.5 narrows the design domain for the deposition rate and uniformity of GaN thin films. Values of optimal solutions are given in Results are satisfying the feasibility of using response surface models in the study of the optimization.

Table (6-3). The FLUENT simulations have verified the feasibility of obtained optimal solutions of design variables.

Figure 6.13: Pareto frontier for the optimization of GaN thin films with different values of the TMG flow rate.

Figure 6.14: Pareto frontier for the optimization of GaN thin films with different values of the reactor pressure.

Results are satisfying the feasibility of using response surface models in the study of the optimization.

Table (6-3) Optimal solutions and the verification responses by CFD model solution.

No	P (Torr)	TMG (SLM)	St (μm/h)	GR (μm/h)	St* (μm/h)	GR* (μm/h)	ε_{St} %	ε_{GR} %
1	482.99	0.005	0.7844	8.271	0.683	7.314	12.9	11.5
2	376.66	0.001	0.1288	1.2171	0.1285	1.382	2.3	11.9

6.7.2 Design Variables: the susceptor temperature and the flow rate of TMG.

The impact of the susceptor temperature and TMG flow rate on the optimization of GaN thin films is presented. It is desirable to maximize the growth rate (GR) of GaN thin films subject to the same

constraints described previously. Where the lower and upper bound of the susceptor temperature are considered as $T_l = 1073\ K$ and $T_u = 1473\ K$, respectively.

$$\underset{T,TMG}{Max\,GR}$$

$$s.t \quad Un(s) \le 0.4$$

$$T_l \le T \le T_u$$

$$TMG_l \le TMG \le TMG_u$$

6-13)

Figure 6.15 shows the location of the optimal solution, where a maximum growth rate (GR) is obtained. The optimal solution is found at T=1183 K and TMG =0.005 SLM subjected to the constraint of the nonuniformity Un=0.4. This confirms that increase the susceptor temperature with a high flow rate of TMG degrades the uniformity of the thin film. Thus, it is advisable to set the susceptor temperature in the diffusion limit regime.
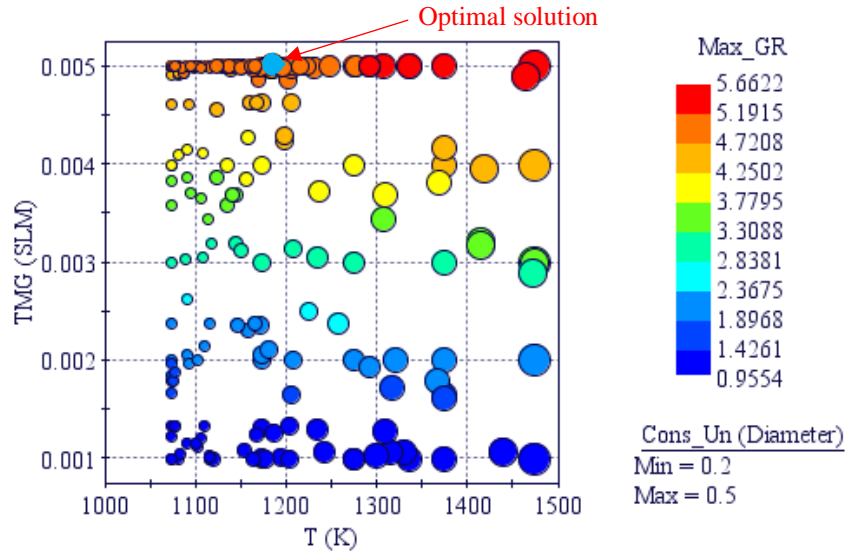
Figure 6.15: The location of the optimal solution of minimizing the standard deviation of GaN thin films under constraint.

However, the focus is on finding a high uniformity of GaN thin films by minimizing the standard deviation (St). The objective function of minimizing St is formulated as follows:

$$\underset{T,TMG}{Min \, St}$$

$$s.t \quad Un(s) \leq 0.4$$

$$T_l \leq T \leq T_u$$

$$TMG_l \leq TMG \leq TMG_u$$

6-14)

The optimal solution is found respect to the flow rate and susceptor temperature. Low susceptor temperature and low TMG flow rate provide the lowest standard deviation, as shown in **Error! R eference source not found.**. However, they lead to the lowest growth rate of 0.95 (µm/h).
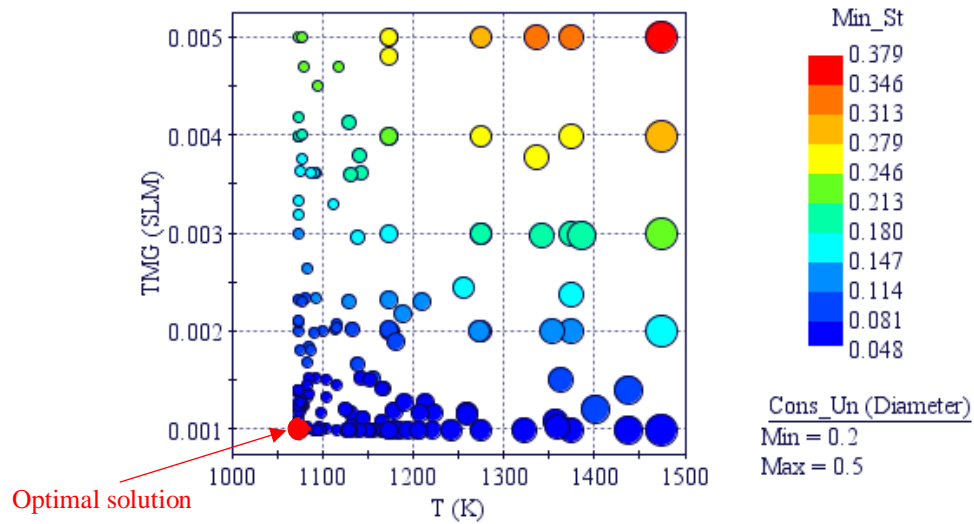
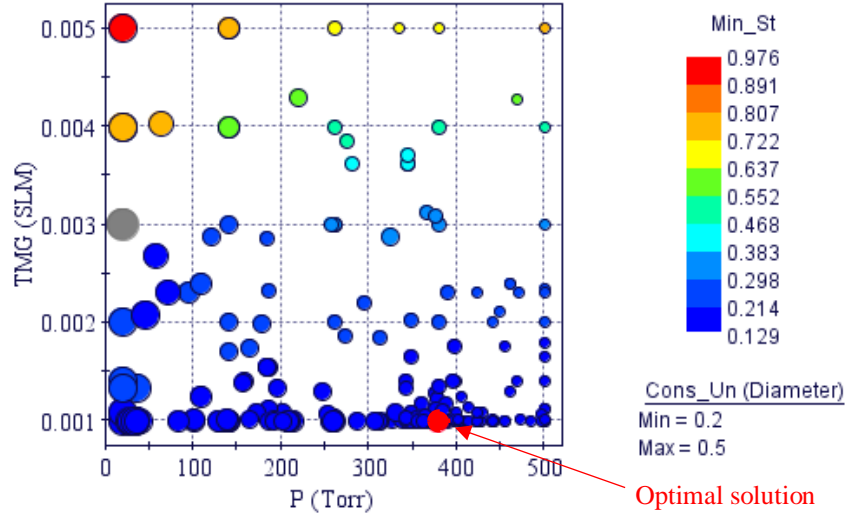Figure 6.16: The location of the optimal solution of minimizing the standard deviation of GaN thin films under constraint.

The multi-optimization formulation is given in Equ. (6-15). It is to maximize the growth rate and minimize the standard deviation simultaneously subjected to the same constraints of the nonuniformity factor.

$$\underset{T,TMG}{Max}\,GR$$

$$\underset{T,TMG}{Min}\,St$$

$$s.t \quad Un(s) \leq 0.4$$

$$T_l \leq T \leq T_u$$

$$TMG_l \leq TMG \leq TMG_u$$

6-15)

Since a multi-objective optimization is employed, the optimal solution is a compromised solution between the growth rate and the standard deviation. The trade-off behavior between the growth rate and standard deviation is given by the Pareto frontier, as shown in Figure 6.16 and Figure 6.17, respectively. The variation in the Pareto frontier under the flow rate of TMG, as shown in Figure 6.17. Figure 6.18 shows a reduced range of optimal solutions due to sensitivity to variation in susceptor temperature subjected to nonuniformity factor Un=0.4. Thus, it is preferable to choose the part of Pareto frontier where a high growth rate and acceptable uniformity is achieved.
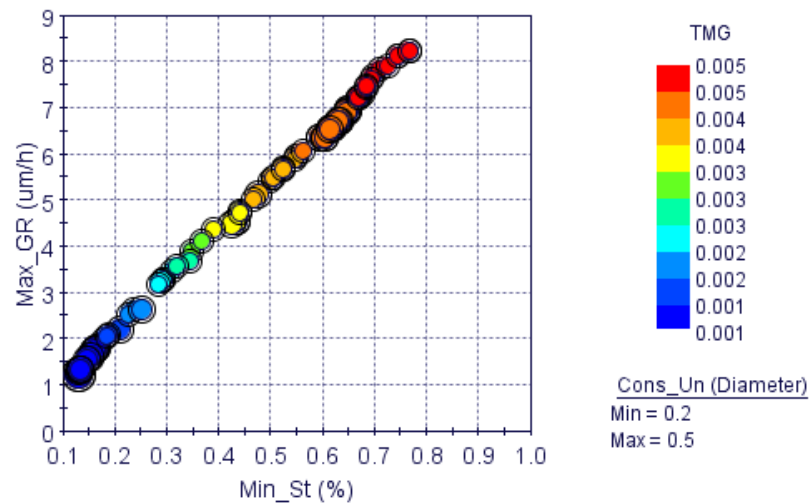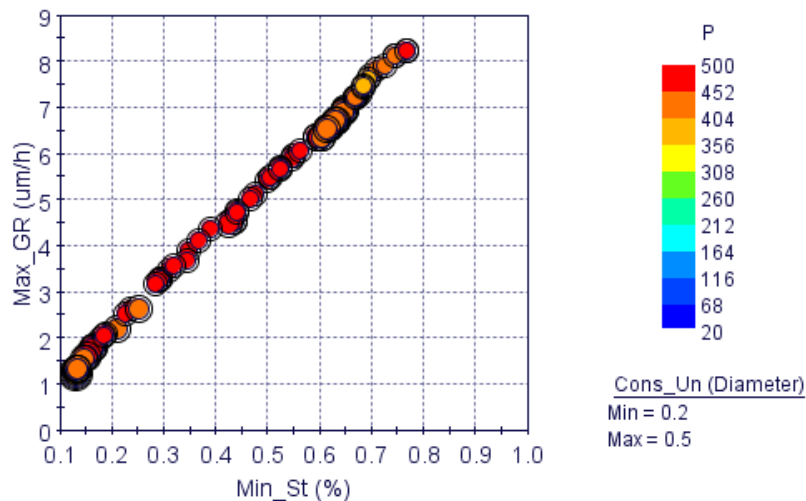

Figure 6.17: Pareto frontier for the optimization of GaN thin films with different values of the reactor pressure.
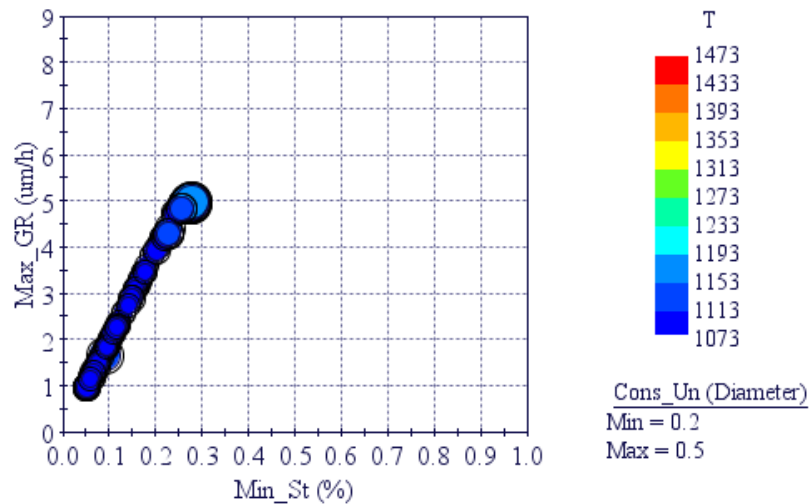
Figure 6.18: Pareto frontier for the optimization of GaN thin films with different values of the reactor pressure.

Values of optimal solutions are given in Table Table (6-4). The FLUENT simulations have verified the feasibility of obtained optimal solutions of design variables.

Table (6-4) Optimal solutions and the verification responses by CFD model solution.

No	T (K)	TMG (SLM)	GR^* (μm/h)	St (μm/h)	GR (μm/h)	St^* (μm/h)	ε_{GR} %	ε_{St} %
1	1183	0.005	4. 729	0.27712	4.248	0.3281	10.17	15.54
2	1073	0.001	0.95544	0.04971	0.9127	0.0613	4.46	18.2

Results are satisfying the feasibility of using response surface models in the study of the optimization.

6.8 Optimization under uncertainty

The optimization of GaN deposition in the MOCVD process is performed as a deterministic problem, and the uncertainty associated with operating conditions is neglected. However, under such circumstances, even a small deviation in operating conditions from the optimal solution could result in a violation of the constraints and detortion of the optimal solution. The optimization under

uncertainty refers to the optimization of design by taking into consideration the uncertain input parameters and the corresponding output response statics [116]. Thus, the deterministic optimization might not do well in the practical deposition of GaN thin films. Operating conditions such as the reactor pressure, flow rate of precursors, and the susceptor temperature do not tend to be deterministic in the MOCVD process. To this end; robust design optimization is applied for the growth rate and uniformity of GaN thin films to enhance the performance of the MOCVD process. Thus, the MOCVD system responds to variation in its operating conditions with minimal error or damage to output results. Table (6-5 lists uncertain design variables of the MOCVD process considered in the robust optimization. These design variable are assumed to be distributed normally with a mean and standard deviation values.

Table (6-5) Uncertain design variables of GaN deposition in the MOCVD system

parameter	Range in variation			
Input	Upper	Lower	mean	Standard deviation
T	1073	1473	1273	25
P	20	500	260	20
TMG	0.001	0.005	0.003	0.0005

The optimization of GaN deposition consider uncertain design variables is formulated as follows:

6.8.1 Design Variables: P and TMG under uncertainty.

When the design variables, the reactor pressure and flow rate of TMG have some design uncertainties, they can affect the response of growth rate and standard deviation, as shown in Figure 6.19 and Figure 6.20 respectively. Table (6-6) lists the optimal solution of design variables for deterministic optimization and optimization under uncertainty. Results show that the response of robust optimization has a lower optimal solution for growth rate and higher for the standard deviation. It indicates that the variation of the reactor pressure has a significant effect on growth rate and uniformity of GaN thin films. It is observed that the application of variation in operating

conditions makes the optimal solution more realistic, and shift Pareto frontier slightly, as shown in Figure 6.21 and Figure 6.22, respectively. Moreover, the reactor pressure is restricted in a smaller range of high values to achieve the multi-objective and under nonuniformity constraint.
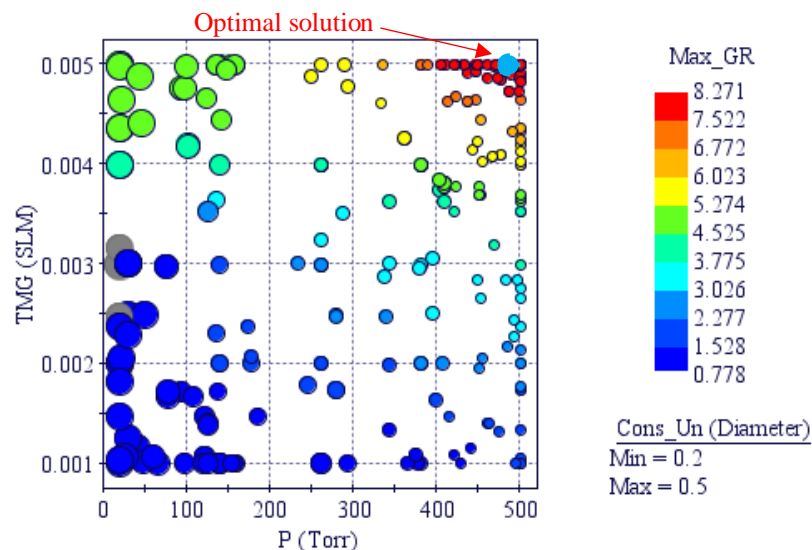
Figure 6.19: The location of the optimal solution of maximizing the growth rate of GaN thin films under uncertainty.
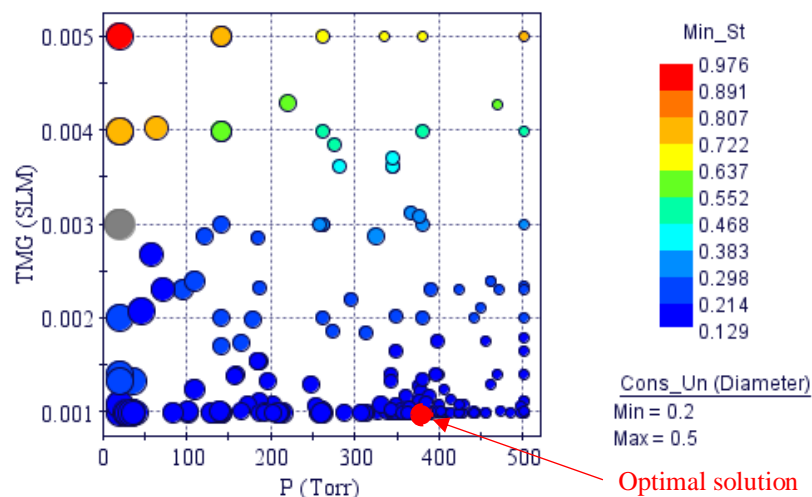
Figure 6.20: The location of the optimal solution of minimizing the standard deviation of GaN thin films under uncertainty.
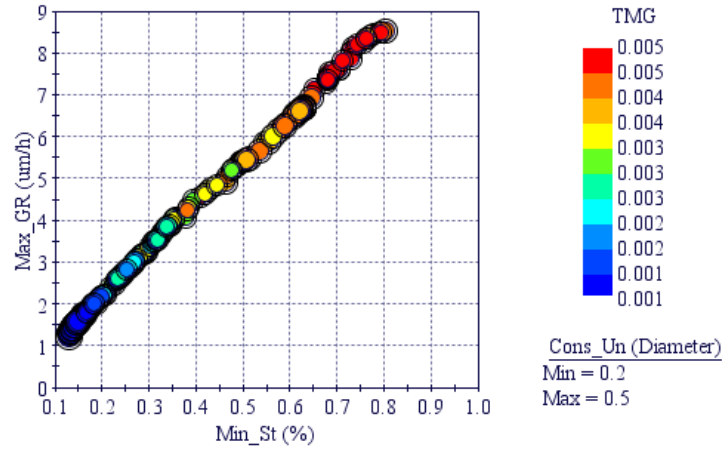
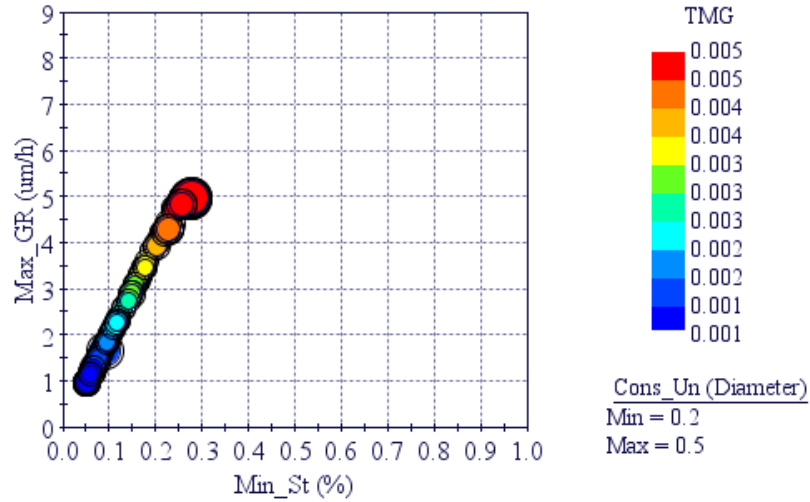Figure 6.21: Pareto frontier for the optimization of GaN thin films with different values of the TMG flow rate under uncertainty.
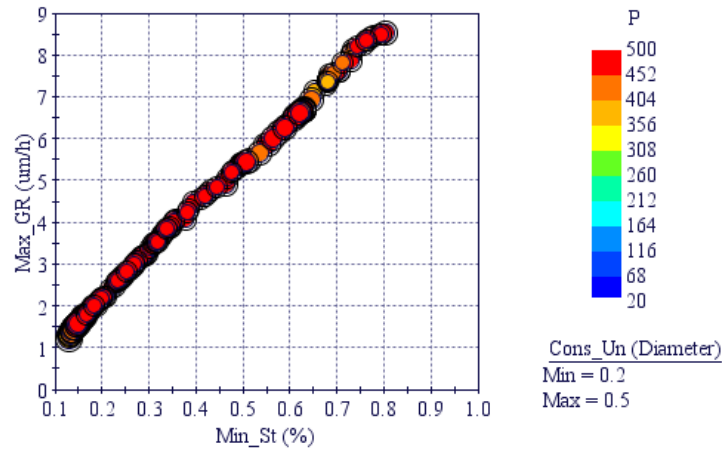
Figure 6.22: Pareto frontier for the optimization of GaN thin films with different values of the reactor pressure under uncertainty.

Table (6-6) Optimal solutions of deterministic and optimization under uncertainty.

Optimization.	P (Torr)	TMG (SLM)	St (μm/h)	GR (μm/h)	ε_{St} %	ε_{GR} %
Determinstic	482.99	0.005	0.7844	8.271	0	0
Under uncertanity	455.71	0.005	0.7356	7.946	-3.93	-6.22
Determinstic	376.66	0.001	0.1288	1.2171	0	0
Under uncertanity	358.19	0.001	0.1576	1.429	22.3	17.4

6.8.2 Design Variables: T and TMG under uncertainty.

The susceptor temperature and flow rate of TMG have a significant effect on the growth rate and uniformity of GaN thin film. However, results show a slight change in the response of growth rate and standard deviation values toward the variation in the susceptor temperature.
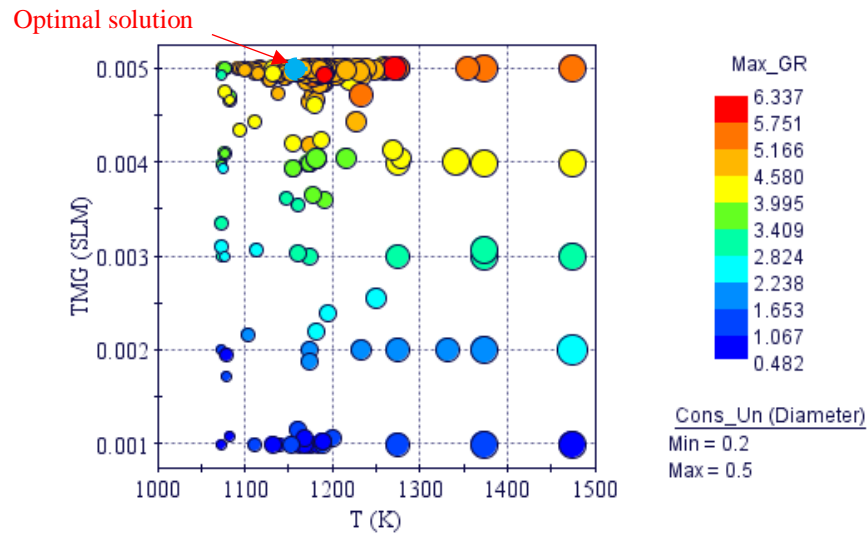
Figure 6.23: The location of the optimal solution of minimizing the standard deviation of GaN thin films under uncertainty.
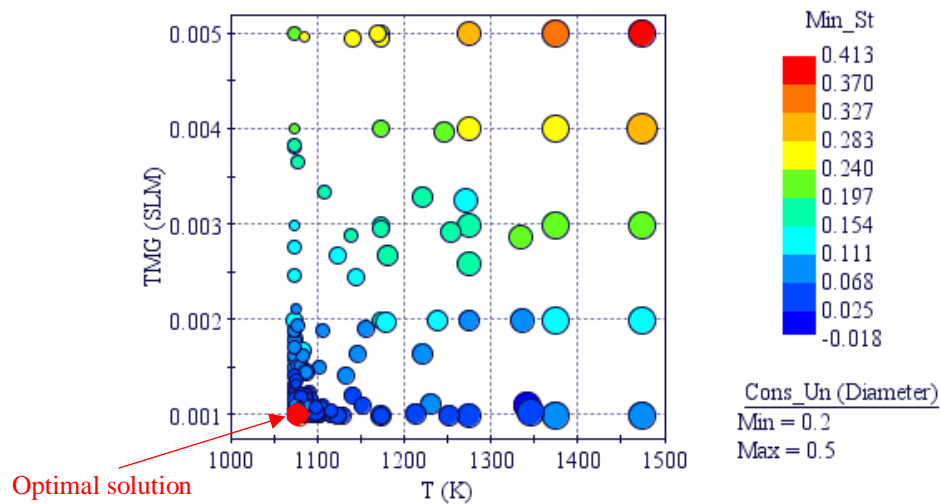
Figure 6.24: The location of the optimal solution of minimizing the standard deviation of GaN thin films under uncertainty.

Figure 6.23 and Figure 6.24 show the location of optimal solutions under design uncertainty for the growth rate and standard deviation, respectively. Compared to determinist optimization, it is observed that the location of optimal solutions under uncertainty has a small shift, as indicated in The impact of variation of design variables on growth rate and the standard deviation is illustrated in Pareto frontier, as shown in Figure 6.25 and Figure 6.26, respectively. The application of variation in operating conditions restricts the optimal solution to the smaller range for the susceptor temperature. The susceptor temperature is restricted in a smaller range of low values to meet the objective under nonuniformity constraint. In contrast, Pareto frontier less restricted to the variation in the flow rate of TMG, as shown in Figure 6.25.

Table (6-7). On the other hand, results show that the response of robust optimization has increased the range of optimal solution of the multi-objective formulation.
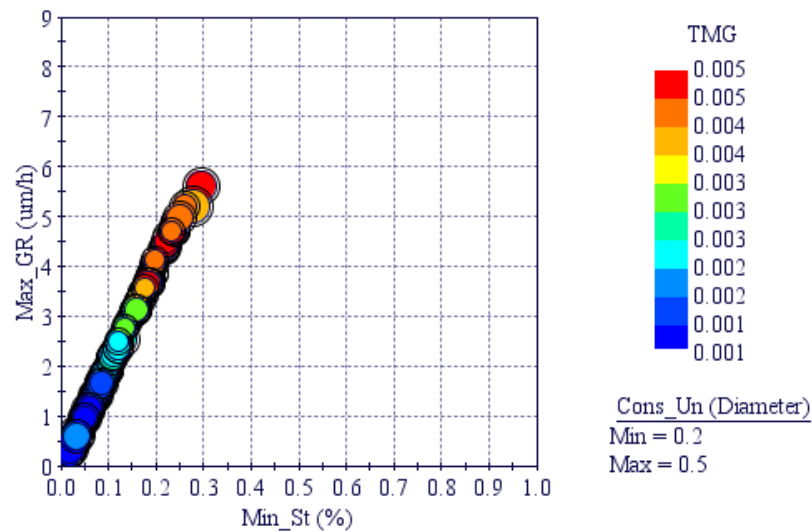
Figure 6.25: Pareto frontier for the optimization of GaN thin films with different values of the TMG flow rate.
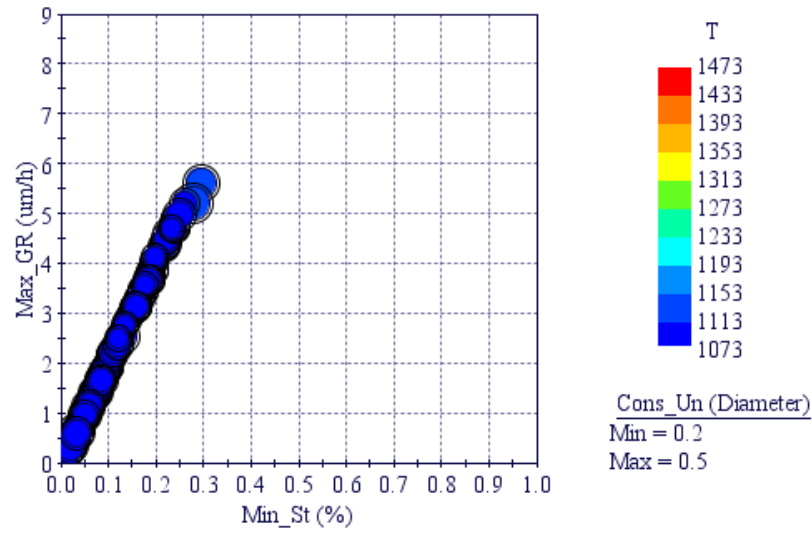
Figure 6.26: Pareto frontier for the optimization of GaN thin films with different values of the susceptor temperature.

The impact of variation of design variables on growth rate and the standard deviation is illustrated in Pareto frontier, as shown in Figure 6.25 and Figure 6.26, respectively. The application of variation in operating conditions restricts the optimal solution to the smaller range for the susceptor temperature. The susceptor temperature is restricted in a smaller range of low values to meet the objective under nonuniformity constraint. In contrast, Pareto frontier less restricted to the variation in the flow rate of TMG, as shown in Figure 6.25.

Table (6-7) Optimal solutions and the verification responses by CFD model solution.

No	T (K)	TMG (SLM)	St (μm/h)	GR (μm/h)	ε_{St} %	ε_{GR} %
deterministic	1183	0.005	0.27712	4.9791	0	0
Under uncertainty	1179.2	0.00494	0.2727	4.917	-1.587	-1.385
deterministic	1073	0.001	0.04759	0.95544	0	0
Under uncertainty	1079	0.001	0.04818	0.9608	1.239	0.005

6.9 Conclusions

In this chapter, the deterministic and robust optimization of the growth of GaN thin films grown in a vertical rotating disk MOCVD reactor are performed. The influence of operating conditions is simulated based on the 3D CFD model, which has developed earlier in this study. Kriging model is employed to create the response surface of the growth rate, standard deviation, and nonuniformity respectively of GaN thin films. Predicted response surfaces are used in the deterministic optimization and optimization under uncertainty of the MOCVD process. Two sets of design variables in the MOCVD process are considered TMG flow rate with the reactor pressure, and TMG flow rate with temperature susceptor. Results show that TMG flow rate and the reactor pressure have a significant effect on growth rate and uniformity of GaN thin films. It is observed that results from the robust optimization are more realistic than the results of the deterministic optimization. The results reveal that the proposed optimization formulation can generate Pareto frontier of conflicting objectives, thus providing reliable solutions for decision-makers.

Chapter 7

CONCLUSIONS AND FUTURE WORKS

7.1 Conclusions

It must be stressed that the quality and uniformity of GaN thin films have significant effect on the performance of optoelectronic devices. The effect of operating parameters including the (V/III) ratio, which represents ammonia (NH_3) flow rate to trimethylgallium (TMG) flow rate, reactor pressure, and carrier gas type on the GaN growth rate and film uniformity, is investigated. The epitaxial growth of GaN thin films was carried out in two commercial MOCVD systems, a vertical rotating disk MOCVD reactor, and a close-coupled showerhead MOCVD reactor. The results indicate that the average deposition rate increases with increase the reactor pressure, but it decreases with increasing the precursor concentration ratio. A high-quality thin film is obtained when pure H_2 is used as a carrier gas.

On the other hand, utilizing a high flow rate of pure N_2 as a carrier gas enhances the deposition rate. However, it decreases the uniformity of the thin film, and also it promotes carbon contamination in the thin film. It is worth to note that using an appropriate mixture of H_2 and N_2 as a carrier can improve the deposition rate and quality of GaN thin films.

Material characterizations of the specimens, including the crystal quality and surface morphology, have carried out. At high V/III, AFM results indicate that a smooth surface of the GaN thin film. Also, Raman scattering results show that GaN thin films that are grown at high V/III ratio have less residual stress and high crystalline quality. On the other hand, XRD results show that GaN thin films grown at low V/III ratio have high dislocation density, and that can affect the quality of the thin film. Moreover, SEM results show some-micro cracks on the cross-sectional of GaN thin films.

The study has successfully developed a three-dimensional CFD model for single wafer and multi-wafer reactors to describe various operating conditions and design parameters. The model gives a further understanding of the effect of growth conditions in the MOCVD process. Results show that the growth rate of GaN thin films is sensitive to processing conditions such as the rotation rate of the susceptor, the flow rate of TMG, reactor pressure, and susceptor temperature. Higher deposition rate occurs with increasing the rotation rate, reactor pressure, inlet gas velocity, and the flow rate of TMG. When the flow rate of NH_3 is increased, the deposition rate is decreased while the uniformity is improved. The temperate range of (1200-1350 K) is the most appropriate temperature range for GaN deposition. Dimensionless numbers, including Reynolds and Grashoff, give a better understanding of flow and thermal field behavior in the MOCVD reactor. A flow mapping approach is developed to indicate the stability of gas flow inside the MOCVD reactor without the effect of chemical reactions on the deposition rate. It is observed that increasing the total flow rate and the rotation rate flow enhance the flow stability.

Compared to a single-wafer MOCVD reactor, the designing of growth conditions in a multi-wafer MOCVD reactor becomes more difficult since the growth rate and uniformity of GaN thin films are very sensitive to processing parameters and the reactor geometry. Results show at high reactor pressure; recirculating flow appears which can trap the precursors to reach the susceptor surface effectively. Also, the high pressure promotes chemical reactions between TMG and NH_3 in the gas phase. Thus, the deposition rate and uniformity of GaN thin films are affected. When the V/III ratio has increased, the incorporation of carbon impurities, especially CH3, and CH4 in the growth rate, is decreased. The composition of carrier gas has an important effect on flow characteristics and quality of the GaN thin film, so using a mixture of N_2 and H_2 gases can help to take advantages of both properties of N_2 and H_2 for a large scale production system.

The inlet design has a significant effect on improving the reactant species utilization and increases the growth rate. Also, the wafer carrier design can affect the deposition rate and uniformity of GaN

thin films. The proper distance between the inlet and the susceptor aids to decrease the temperature gradient and improve the stability of the flow above the rotating susceptor. The predicted results have significant reference values for guiding role and parameter optimization of GaN growth in MOCVD reactor.

A unique advantage can be resulted by optimizing the boundary conditions to produce a uniform thin film with a higher growth rate. In this study, optimization-based surrogate models are employed to predicate optimal operating parameters for high deposition rate and high uniformity of GaN thin films. The surrogate-based model demonstrates the feasibility of optimizing a complex process such as MOCVD based on design variables. It is used to perform both deterministic optimization and optimization under uncertainty of the MOCVD process, then predicted results of two approaches are compared. It is observed that results from the robust optimization are more realistic than the results of the deterministic optimization. The results reveal that the proposed optimization formulation can generate Pareto frontier of conflicting objectives, thus providing reliable solutions for decision-makers. This study establishes guidelines for the optimization of the deposition of GaN thin films in the MOCVD process.

7.2 Future work

In the future study of the CVD process, study the optimization of GaN thin films growth at the microscopic level using kinetic Monte Carlo scheme combined with the computational fluid dynamics method. This study has investigated the effect of reactor geometry on the growth rate and uniformity. However, the proposed CFD model, combined with the surrogate model, can be utilized to find the optimal operating conditions in different geometrical configurations of MOCVD reactors. Also, study the growth behavior of GaN thin films by scaling up the wafer size to increase the throughput.

REFERENCES

[1]   D. Gerthsen, B. Neubauer, C. Dieker, R. Lantier, A. Rizzi, and H. Lüth, "Molecular beam epitaxy (MBE) growth and structural properties of GaN and AlN on 3C-SiC(001) substrates," *J. Cryst. Growth*, vol. 200, no. 3, pp. 353–361, Apr. 1999.

[2]   R. D. Vispute *et al.*, "Growth of epitaxial GaN films by pulsed laser deposition," *Appl. Phys. Lett.*, vol. 71, no. 1, pp. 102–104, Jul. 1997.

[3]   M. L. Hitchman and A. C. Jones, *Chemical Vapour Deposition: Precursors, Processes and Applications*. Royal Society of Chemistry, 2009.

[4]   K. Hiramatsu *et al.*, "Growth mechanism of GaN grown on sapphire with AlN buffer layer by MOVPE," *J. Cryst. Growth*, vol. 115, no. 1, pp. 628–633, Dec. 1991.

[5]   W.-C. Huang *et al.*, "Investigations of GaN growth on the sapphire substrate by MOCVD method with different AlN buffer deposition temperatures," *Mater. Sci. Semicond. Process.*, vol. 45, no. Supplement C, pp. 1–8, Apr. 2016.

[6]   B. Mitrovic, A. Gurary, and W. Quinn, "Process conditions optimization for the maximum deposition rate and uniformity in vertical rotating disc MOCVD reactors based on CFD modeling," *J. Cryst. Growth*, vol. 303, no. 1, pp. 323–329, May 2007.

[7]   W. T. Cheng, H. C. Li, and C. N. Huang, "Simulation and optimization of silicon thermal CVD through CFD integrating Taguchi method," *Chem. Eng. J.*, vol. 137, no. 3, pp. 603–613, Apr. 2008.

[8]   A. Elhaddad, "Growth of SiC by High Temperature CVD and Application of Thermo-gravimetry for an In-situ Growth Rate Measurement - Google Search," Duisburg-Essen, Germany, 2010.

[9]   M. N. R. Ashfold, P. W. May, C. A. Rego, and N. M. Everitt, "Thin film diamond by chemical vapour deposition methods," *Chem. Soc. Rev.*, vol. 23, no. 1, p. 21, 1994.

[10]   J. Meng and Y. Jaluria, "Numerical Simulation of GaN Growth in a Metalorganic Chemical Vapor Deposition Process," *J. Manuf. Sci. Eng.*, vol. 135, no. 6, pp. 061006–061013, Nov. 2013.

[11]   B. Mitrovic, A. Gurary, and L. Kadinski, "On the flow stability in vertical rotating disc MOCVD reactors under a wide range of process parameters," *J. Cryst. Growth*, vol. 287, no. 2, pp. 656–663, Jan. 2006.

[12]   B. Wu, R. Ma, and H. Zhang, "Epitaxy growth kinetics of GaN films," *J. Cryst. Growth*, vol. 250, no. 1, pp. 14–21, Mar. 2003.

[13]   F. A. Ponce and D. P. Bour, "Nitride-based semiconductors for blue and green light-emitting devices," *Nature*, vol. 386, no. 6623, p. 386351a0, Mar. 1997.

[14]   W. Wang, H. Yang, and G. Li, "Growth and characterization of GaN-based LED wafers on La 0.3 Sr 1.7 AlTaO 6 substrates," *J. Mater. Chem. C*, vol. 1, no. 26, pp. 4070–4077, 2013.

[15]   S. Nakamura and M. R. Krames, "History of Gallium-Nitride-Based Light-Emitting Diodes for Illumination," *Proc. IEEE*, vol. 101, no. 10, pp. 2211–2220, Oct. 2013.

[16]   S. Nakamura, M. Senoh, N. Iwasa, and S. Nagahama, "High-Brightness InGaN Blue, Green and Yellow Light-Emitting Diodes with Quantum Well Structures," *Jpn. J. Appl. Phys.*, vol. 34, no. 7A, pp. L797–L799, Jul. 1995.

[17]   "How Metal Organic Chemical Vapor Phase Deposition (MOCVD) Works," *AZoM.com*, 28-Nov-2014. [Online]. Available: https://www.azom.com/article.aspx?ArticleID=11585. [Accessed: 12-Apr-2018].

[18]   Y. Taniyasu and M. Kasu, "Improved emission efficiency of 210-nm deep-ultraviolet aluminum nitride light-emitting diode," *NTT Tech Rev*, vol. 8, no. 8, 2010.

[19]   A. A. Bergh, "Blue laser diode (LD) and light emitting diode (LED) applications," *Phys. Status Solidi A*, vol. 201, no. 12, pp. 2740–2754, Sep. 2004.

[20] K.-J. Cui *et al.*, "Blue laser diode-initiated photosensitive resins for 3D printing," *J. Mater. Chem. C*, vol. 5, no. 46, pp. 12035–12038, 2017.

[21] Y.-H. Ra *et al.*, "The influence of the working pressure on the synthesis of GaN nanowires by using MOCVD," *J. Cryst. Growth*, vol. 312, no. 6, pp. 770–774, Mar. 2010.

[22] A. K. Pattanaik and V. K. Sarin, "Basic Principles of CVDThermodynamics and Kinetics," in *Chemical Vapor Deposition*, 1st ed., vol. 2, Ohio, USA: ASM International, Materials Park, 2001, pp. 23–43.

[23] R. L. Mahajan, "Transport Phenomena in Chemical Vapor-Deposition Systems," in *Advances in Heat Transfer*, vol. 28, Supplement C vols., D. Poulikakos, Ed. Elsevier, 1996, pp. 339–425.

[24] C. R. Kleijn, "Transport phenomena in chemical vapor deposition reactors," PhD, Delft University of Technology, Netherlands, 1991.

[25] Y. Fu, "RESIDUAL STRESS IN GALLIUM NITRIDE FILMS GROWN ON SILICON SUBSTRATES BY METALORGANIC CHEMICAL VAPOR DEPOSITION," Ohio University, 2000.

[26] M. H. Grabow and G. H. Gilmer, "Molecular Dynamics Studies of Semiconductor Thin Films and Interfaces," *MRS Online Proc. Libr. Arch.*, vol. 94, ed 1987.

[27] P. Kidd, *XRD of gallium nitride and related compounds: strain, composition and layer thickness (booklet).* .

[28] A. Dadgar *et al.*, "MOVPE growth of GaN on Si – Substrates and strain," *Thin Solid Films*, vol. 515, no. 10, pp. 4356–4361, Mar. 2007.

[29] D. Zhu, D. J. Wallis, and C. J. Humphreys, "Prospects of III-nitride optoelectronics grown on Si," *Rep. Prog. Phys.*, vol. 76, no. 10, p. 106501, Oct. 2013.

[30] R. Loganathan, M. Jayasakthi, K. Prabakaran, R. Ramesh, P. Arivazhagan, and K. Baskar, "Studies on dislocation and surface morphology of AlxGa1−xN/GaN heterostructures grown by MOCVD," *J. Alloys Compd.*, vol. 616, no. Supplement C, pp. 363–371, Dec. 2014.

[31] Y. Chen, R. Schneider, S. Y. Wang, R. S. Kern, C. H. Chen, and C. P. Kuo, "Dislocation reduction in GaN thin films via lateral overgrowth from trenches," *Appl. Phys. Lett.*, vol. 75, no. 14, pp. 2062–2063, Sep. 1999.

[32] S. Nakamura, M. Senoh, N. Iwasa, S. Nagahama, T. Yamada, and T. Mukai, "Superbright Green InGaN Single-Quantum-Well-Structure Light-Emitting Diodes," *Jpn. J. Appl. Phys.*, vol. 34, no. 10B, p. L1332, Oct. 1995.

[33] C. Hemmingsson and G. Pozina, "Optimization of low temperature GaN buffer layers for halide vapor phase epitaxy growth of bulk GaN," *J. Cryst. Growth*, vol. 366, no. Supplement C, pp. 61–66, Mar. 2013.

[34] M. J. Kappers, R. Datta, R. A. Oliver, F. D. G. Rayment, M. E. Vickers, and C. J. Humphreys, "Threading dislocation reduction in (0001) GaN thin films using SiNx interlayers," *J. Cryst. Growth*, vol. 300, no. 1, pp. 70–74, Mar. 2007.

[35] X. Ni, "Growth and characterization of non-polar GaN materials and investigation of efficiency droop in InGaN light emitting diodes," Virginia Commonwealth University, 2010.

[36] R. Chierchia, T. Böttcher, H. Heinke, S. Einfeldt, S. Figge, and D. Hommel, "Microstructure of heteroepitaxial GaN revealed by x-ray diffraction," *J. Appl. Phys.*, vol. 93, no. 11, pp. 8918–8925, May 2003.

[37] P. Fini *et al.*, "The Effect of Growth Environment on the Morphological and Extended Defect Evolution in GaN Grown by Metalorganic Chemical Vapor Deposition," *Jpn. J. Appl. Phys.*, vol. 37, no. 8R, p. 4460, Aug. 1998.

[38] I. Grzegory and S. Porowski, "GaN substrates for molecular beam epitaxy growth of homoepitaxial structures," *Thin Solid Films*, vol. 367, no. 1, pp. 281–289, May 2000.

[39] G. Kamler, J. L. Weyher, I. Grzegory, E. Jezierska, and T. Wosiński, "Defect-selective etching of GaN in a modified molten bases system," *J. Cryst. Growth*, vol. 246, no. 1, pp. 21–24, Dec. 2002.

[40] M. A. Moram and M. E. Vickers, "X-ray diffraction of III-nitrides," *Rep. Prog. Phys.*, vol. 72, no. 3, pp. 1–39, 2009.

[41] H. Kang *et al.*, "X-Ray Diffraction Analysis of GaN and AlGaN," *MRS Online Proc. Libr. Arch.*, vol. 743, Jan. 2002.

[42] L. Lu *et al.*, "Morphology of threading dislocations in high-resistivity GaN films observed by transmission electron microscopy," *J. Appl. Phys.*, vol. 102, no. 3, p. 033510, Aug. 2007.

[43] W. C. Lan, C. D. Tsai, and C. W. Lan, "The effects of shower head orientation and substrate position on the uniformity of GaN growth in a HVPE reactor," *J. Taiwan Inst. Chem. Eng.*, vol. 40, no. 4, pp. 475–478, Jul. 2009.

[44] H. Yin, X. Wang, G. Hu, J. Ran, H. Xiao, and J. Li, "Operational optimization of GaN thin film growth employing numerical simulation in a showerhead MOCVD reactor," in *2008 9th International Conference on Solid-State and Integrated-Circuit Technology*, 2008, pp. 710–713.

[45] E. V. Yakovlev, R. A. Talalaev, Yu. N. Makarov, B. S. Yavich, and W. N. Wang, "Deposition behavior of GaN in AIX 200/4 RF-S horizontal reactor," *J. Cryst. Growth*, vol. 261, no. 2, pp. 182–189, Jan. 2004.

[46] S. Surender, K. Prabakaran, R. Loganathan, S. Pradeep, S. Singh, and K. Baskar, "Effect of growth temperature on InGaN/GaN heterostructures grown by MOCVD," *J. Cryst. Growth*, vol. 468, no. Supplement C, pp. 249–251, Jun. 2017.

[47] Y. Xian *et al.*, "Effects of growth pressure on the properties of p-GaN layers," *J. Cryst. Growth*, vol. 325, no. 1, pp. 32–35, Jun. 2011.

[48] S. Suresh, S. Lourdudoss, G. Landgren, and K. Baskar, "Studies on the effect of ammonia flow rate induced defects in gallium nitride grown by MOCVD," *J. Cryst. Growth*, vol. 312, no. 21, pp. 3151–3155, Oct. 2010.

[49] H. X. Wang, H. D. Li, Y. Amijima, Y. Ishihama, and S. Sakai, "Influence of rotation speed of substrate on the growth mechanism of InGaN/GaN multiple quantum wells grown by six-wafer metal organic chemical vapor deposition system," *J. Cryst. Growth*, vol. 235, no. 1, pp. 183–187, Feb. 2002.

[50] R. Niebuhr, K. Bachem, K. Dombrowski, M. Maier, W. Pletschen, and U. Kaufmann, "Basic studies of gallium nitride growth on sapphire by metalorganic chemical vapor deposition and optical properties of deposited layers," *J. Electron. Mater.*, vol. 24, no. 11, pp. 1531–1534, Nov. 1995.

[51] Z. J. Yu, B. S. Sywe, A. U. Ahmed, and J. H. Edgar, "The growth and characterization of GaN on sapphire and silicon," *J. Electron. Mater.*, vol. 21, no. 3, pp. 383–387, Mar. 1992.

[52] D. Sengupta, "Does the Ring Compound [(CH3)2GaNH2]3 Form during MOVPE of Gallium Nitride? Investigations via Density Functional and Reaction Rate Theories," *J. Phys. Chem. B*, vol. 107, no. 1, pp. 291–297, Jan. 2003.

[53] A. Hirako, K. Kusakabe, and K. Ohkawa, "Modeling of reaction pathways of GaN growth by metalorganic vapor-phase epitaxy using TMGa/NH3/H2 system: a computational fluid dynamics simulation study," *Jpn. J. Appl. Phys.*, vol. 44, no. 2R, p. 874, 2005.

[54] F. H. Yang, "Modern metal-organic chemical vapor deposition (MOCVD) reactors and growing nitride-based materials," *Nitride Semicond. Light-Emit. Diodes LEDs Mater. Technol. Appl.*, pp. 27–65, 2014.

[55] L. PENG, "MOCVD growth and characterization of wide band gap group III-nitride semiconductors," Thesis, 2003.

[56] M. Dauelsberg *et al.*, "Modeling and process design of III-nitride MOVPE at near-atmospheric pressure in close coupled showerhead and planetary reactors," *J. Cryst. Growth*, vol. 298, no. Supplement C, pp. 418–424, Jan. 2007.

[57] K. Matsumoto *et al.*, "Opportunities and challenges in GaN metal organic chemical vapor deposition for electron devices," *Jpn. J. Appl. Phys.*, vol. 55, no. 5S, p. 05FK04, Apr. 2016.

[58] O. Briot, J. P. Alexis, S. Sanchez, B. Gil, and R. L. Aulombard, "Influence of the VIII molar ratio on the structural and electronic properties of MOVPE grown GaN," *Solid-State Electron.*, vol. 41, no. 2, pp. 315–317, Feb. 1997.

[59] M. Meyyappan, Ed., "Chemical vapor deposition process," in *Computational modeling in semiconductor processing*, 1 st., Boston: Artech House, 1995, pp. 97–191.

[60] C. Y. Soong, C. H. Chyuan, and R. Y. Tzong, "Thermo-Flow Structure and Epitaxial Uniformity in Large-Scale Metalorganic Chemical Vapor Deposition Reactors with Rotating Susceptor and Inlet Flow Control," *Jpn. J. Appl. Phys.*, vol. 37, no. 10R, pp. 5823–5834, Oct. 1998.

[61] D. I. Fotiadis, S. Kieda, and K. F. Jensen, "Transport phenomena in vertical reactors for metalorganic vapor phase epitaxy: I. Effects of heat transfer characteristics, reactor geometry, and operating conditions," *J. Cryst. Growth*, vol. 102, no. 3, pp. 441–470, May 1990.

[62] Sun Jingxi, Redwing J. M., and Kuech T. F., "Transport and Reaction Behaviors of Precursors during Metalorganic Vapor Phase Epitaxy of Gallium Nitride," *Phys. Status Solidi A*, vol. 176, no. 1, pp. 693–698, Nov. 1999.

[63] C. Theodoropoulos, T. J. Mountziaris, H. K. Moffat, and J. Han, "Design of gas inlets for the growth of gallium nitride by metalorganic vapor phase epitaxy," *J. Cryst. Growth*, vol. 217, no. 1, pp. 65–81, Jul. 2000.

[64] D. Sengupta, S. Mazumder, W. Kuykendall, and S. A. Lowry, "Combined ab initio quantum chemistry and computational fluid dynamics calculations for prediction of gallium nitride growth," *J. Cryst. Growth*, vol. 279, no. 3, pp. 369–382, Jun. 2005.

[65] C. K. Hu, C. J. Chen, and T. C. Wei, "A Simplified and Universal Mechanism Model for Prediction of Gallium Nitride Thin Film Growth Through Numerical Analysis," *NextGen Res.*, vol. 2, no. 7, pp. 07–15, 2016.

[66] Z. Zhang, H. Fang, H. Yan, Z. Jiang, J. Zheng, and Z. Gan, "Influencing factors of GaN growth uniformity through orthogonal test analysis," *Appl. Therm. Eng.*, vol. 91, no. Supplement C, pp. 53–61, Dec. 2015.

[67] P. George, H. C. Gea, and Y. Jaluria, "Optimization of Chemical Vapor Deposition Process," in *IDETC/CIE 2006*, Pennsylvania, USA, 2006, pp. 309–316.

[68] Z.-H. Han and K.-S. Zhang, "Surrogate-based optimization," in *Real-World Applications of Genetic Algorithms*, In-Tech, 2012, pp. 341–360.

[69] Y. Cheng *et al.*, "High uniform growth of 4-inch GaN wafer via flow field optimization by HVPE," *J. Cryst. Growth*, vol. 445, pp. 24–29, Jul. 2016.

[70] S. Hu, S. Liu, Z. Zhang, H. Yan, Z. Gan, and H. Fang, "A novel MOCVD reactor for growth of high-quality GaN-related LED layers," *J. Cryst. Growth*, vol. 415, no. Supplement C, pp. 72–77, Apr. 2015.

[71] C.-C. Wang, K.-C. Chen, C.-D. Tsai, J.-C. Chian, C.-L. Chao, and Y.-J. Lin, "Development of a novel gas spray module for MOCVD systems," p. 4.

[72] k-Space Associates, Inc., "Real-Time-Process-Monitoring-by-kSA-ICE-for-GaN-and-AlGaN-on-Si-App-Note-07JAN16.pdf," 2016. .

[73] M. Ali *et al.*, "Analysis of threading dislocations in void shape controlled GaN re-grown on hexagonally patterned mask-less GaN," *J. Cryst. Growth*, vol. 344, no. 1, pp. 59–64, Apr. 2012.

[74] D. Ehrentraut, E. Meissner, and M. Bockowski, *Technology of gallium nitride crystal growth*, vol. 133. Springer Science & Business Media, 2010.

[75] T. Sasaki and T. Matsuoka, "Analysis of two-step-growth conditions for GaN on an AlN buffer layer," *J. Appl. Phys.*, vol. 77, no. 1, pp. 192–200, Jan. 1995.

[76] E. J. Tarsa, B. Heying, X. H. Wu, P. Fini, S. P. DenBaars, and J. S. Speck, "Homoepitaxial growth of GaN under Ga-stable and N-stable conditions by plasma-assisted molecular beam epitaxy," *J. Appl. Phys.*, vol. 82, no. 11, pp. 5472–5479, Dec. 1997.

[77] O. Schön, B. Schineller, M. Heuken, and R. Beccard, "Comparison of hydrogen and nitrogen as carrier gas for MOVPE growth of GaN," *J. Cryst. Growth*, vol. 189–190, pp. 335–339, Jun. 1998.

[78] H. X. Wang, Y. Amijima, Y. Ishihama, and S. Sakai, "Influence of carrier gas on the morphology and structure of GaN layers grown on sapphire substrate by six-wafer metal organic chemical vapor deposition system," *J. Cryst. Growth*, vol. 233, no. 4, pp. 681–686, Dec. 2001.

[79] P. F. Fewster, *X-Ray scattering from semiconductors and other materials*. World Scientific, 2015.

[80] D.-J. Kim, Y.-T. Moon, K.-S. Ahn, and S.-J. Park, "In situ normal incidence reflectance study on the effect of growth rate of nucleation layer on GaN by metalorganic chemical vapor deposition," *J. Vac. Sci. Technol. B Microelectron. Nanometer Struct. Process. Meas. Phenom.*, vol. 18, no. 1, pp. 140–143, Jan. 2000.

[81] H. Z. Xi, B. Y. Man, C. S. Chen, M. Liu, J. Wei, and S. Y. Yang, "Effects of annealing temperature on amorphous GaN films formed on Si(1 1 1) by pulsed laser deposition," *Semicond. Sci. Technol.*, vol. 24, no. 8, p. 085024, 2009.

[82] U. Haboeck, H. Siegle, A. Hoffmann, and C. Thomsen, "Lattice dynamics in GaN and AlN probed with first- and second-order Raman spectroscopy," *Phys. Status Solidi C*, vol. 0, no. 6, pp. 1710–1731, Sep. 2003.

[83] H. Harima, "Properties of GaN and related compounds studied by means of Raman scattering," *J. Phys. Condens. Matter*, vol. 14, no. 38, p. R967, 2002.

[84] H. Zhang *et al.*, "Growth of high quality GaN on a novel designed bonding-thinned template by HVPE," *CrystEngComm*, vol. 14, no. 14, pp. 4777–4780, Jun. 2012.

[85] J. Liu *et al.*, "Strain and microstructures of GaN epilayers with thick InGaN interlayer grown by MOCVD," *Mater. Sci. Semicond. Process.*, vol. 60, pp. 66–70, Mar. 2017.

[86] M. W. C. Jr., *NIST-JANAF Thermochemical Tables*, 4th ed., 2 vols. Maryland, USA, 1998.

[87] O. Köksoy and T. Yalcinoz, "Robust Design using Pareto type optimization: A genetic algorithm with arithmetic crossover," *Comput. Ind. Eng.*, vol. 55, no. 1, pp. 208–218, Aug. 2008.

[88] K. Kuo, "Principles of Combustion," *John Wiley & Sons, Inc.*, 2005. .

[89] R. P. Parikh and R. A. Adomaitis, "An overview of gallium nitride growth chemistry and its effect on reactor design: Application to a planetary radial-flow CVD system," *J. Cryst. Growth*, vol. 286, no. 2, pp. 259–278, Jan. 2006.

[90] H. Zhang, R. Zuo, and G. Zhang, "Effects of reaction-kinetic parameters on modeling reaction pathways in GaN MOVPE growth," Nov. 2017.

[91] M. E. Coltrin, R. J. Kee, and F. M. Rupley, "Surface chemkin: A general formalism and software for analyzing heterogeneous chemical kinetics at a gas-surface interface," *Int. J. Chem. Kinet.*, vol. 23, no. 12, pp. 1111–1128, Dec. 1991.

[92] M. E. Coltrin, R. J. Kee, and J. A. Miller, "A mathematical model of the coupled fluid mechanics and chemical kinetics in a chemical vapour deposition reactor," *J Electrochem Soc*, pp. 425–434, 1984.

[93] Inc. ANSYS, "ANSYS Fluent User's Guide," Pennsylvania, USA, 2016.

[94] S. V. Patankar, *Numerical Heat Transfer and Fluid Flow*, First. USA: Taylor & Francis, 1980.

[95] M. E. Coltrin, R. J. Kee, and G. H. Evans, "A Mathematical Model of the Fluid Mechanics and Gas-Phase Chemistry in a Rotating Disk Chemical Vapor Deposition Reactor," *J. Electrochem. Soc.*, vol. 136, no. 3, pp. 819–829, 1989.

[96] M. H. J. M. de Croon, "Chemical Boundary Layers in CVD," *J. Electrochem. Soc.*, vol. 137, no. 9, p. 2867, 1990.

[97] M. Meyyappan, *Computational Modeling in Semiconductor Processing*, 1st ed. Norwood, MA, USA: Artech House, Inc., 1994.

[98] K. Harafuji *et al.*, "Complex Flow and Gas-Phase Reactions in a Horizontal Reactor for GaN Metalorganic Vapor Phase Epitaxy," *Jpn. J. Appl. Phys.*, vol. 39, no. 11R, p. 6180, Nov. 2000.

[99] C.-F. Tseng, T.-Y. Tsai, Y.-H. Huang, M.-T. Lee, and R.-H. Horng, "Transport phenomena and the effects of reactor geometry for epitaxial GaN growth in a vertical MOCVD reactor," *J. Cryst. Growth*, vol. 432, pp. 54–63, Dec. 2015.

[100] M. J. Begarney and F. J. Campanale, "Chemical vapor deposition reactor," US8778079B2, 15-Jul-2014.

[101] A. C. Jones, "Metalorganic precursors for vapour phase epitaxy," *J. Cryst. Growth*, vol. 129, no. 3, pp. 728–773, Apr. 1993.

[102] Z. Jian-Li, L. Jun-Lin, P. Yong, F. Wen-Qing, Z. Meng, and J. Feng-Yi, "Effects of Carrier Gas on Carbon Incorporation in GaN," *Chin. Phys. Lett.*, vol. 31, no. 3, p. 3, 2014.

[103] H. Li, "Mass transport analysis of a showerhead MOCVD reactor," *J. Semicond.*, vol. 32, no. 3, p. 033006, Mar. 2011.

[104] A. Ubukata, Y. Yano, H. Shimamura, A. Yamaguchi, T. Tabuchi, and K. Matsumoto, "High-growth-rate AlGaN buffer layers and atmospheric-pressure growth of low-carbon GaN for AlGaN/GaN HEMT on the 6-in.-diameter Si substrate metal-organic vapor phase epitaxy system," *J. Cryst. Growth*, vol. 370, pp. 269–272, May 2013.

[105] S. J. Pearton *et al.*, "The incorporation of hydrogen into III-V nitrides during processing," *J. Electron. Mater.*, vol. 25, no. 5, pp. 845–849, May 1996.

[106] A. Messac, *Optimization in Practice with MATLAB®: For Engineering Students and Professionals*, 1st ed. New York, USA: Cambridge University Press, 2105.

[107] G. E. Box, S. Hunter, and W. Gordon, *Statistics for Experimenters: Design, Innovation, and Discovery*, 2nd ed. Hoboken, New Jersey: John Wiley & Sons. Inc, 2005.

[108] J.-P. Costa, L. Pronzato, and E. Thierry, "A Comparison Between Kriging And Radial Basis Function Networks For Nonlinear Prediction," presented at the Nonlinear Signal and Image Processing, Antalya, Turkey, 1999, pp. 1–5.

[109] A. Forrester, A. Sobester, and A. Keane, "Engineering Design via Surrogate Modelling: A Practical Guide," *John Wiley & Sons, UK, pp 33-76*, 2008. .

[110] S. Sakata, F. Ashida, and M. Zako, "An efficient algorithm for Kriging approximation and optimization with large-scale sampling data," *Comput. Methods Appl. Mech. Eng.*, vol. 193, no. 3–5, pp. 385–404, 2004.

[111] L. Lebensztajn, C. A. R. Marretto, M. C. Costa, and J. L. Coulomb, "Kriging: a useful tool for electromagnetic device optimization," *IEEE Trans. Magn.*, vol. 40, no. 2, pp. 1196–1199, Mar. 2004.

[112] M. Buhmann, *Radial Basis Functions: Theory and Implementations*. Cambridge, UK: Cambridge University Press, 2004.

[113] A. Clarich, R. Russo, and M. Carriglio, "Multi-Objective Optimization with Modefrontier Interfaces For Ansa And Metapost," presented at the 4th ANSA & μETA International Conference, Thessaloniki, Greece, 2011, pp. 1–16.

[114] Q. Long, C. Wu, T. Huang, and X. Wang, "A genetic algorithm for unconstrained multi-objective optimization," *Swarm Evol. Comput.*, vol. 22, no. Supplement C, pp. 1–14, Jun. 2015.

[115] T. Murata and H. Ishibuchi, "MOGA: multi-objective genetic algorithms," in *Proceedings of 1995 IEEE International Conference on Evolutionary Computation*, 1995, vol. 1, pp. 289–294.

[116] K. K. Bodla, J. Y. Murthy, and S. V. Garimella, "Optimization Under Uncertainty Applied to Heat Sink Design," 2012.

[117] P. T. Lin, "Parametric modeling and optimization of thermal systems with design uncertainties," Rutgers University - School of Enginnering, New Brunswick, New Jersey, 2010.

[118] R. Lopez and A. Beck, "Reliability-Based Design Optimization Strategies Based on FORM: A Review," *J. Braz. Soc. Mech. Sci. Eng.*, vol. 34, pp. 506–514, Dec. 2012.

[119] A. M. Hasofer and N. C. Lind, "Exact and Invariant Second-Moment Code Format," *J. Eng. Mech. Div.*, vol. 100, no. 1, pp. 111–121, 1974.

[120] J. Tu, K. K. Choi, and Y. H. Park, "A New Study on Reliability-Based Design Optimization," *J. Mech. Des.*, vol. 121, no. 4, pp. 557–564, Dec. 1999.

[121] B. D. Youn and K. K. Choi, "An Investigation of Nonlinearity of Reliability-Based Design Optimization Approaches," *J. Mech. Des.*, vol. 126, no. 3, pp. 403–411, May 2004.

[122] B. D. Youn, K. K. Choi, and Y. H. Park, "Hybrid Analysis Method for Reliability-Based Design Optimization," *J. Mech. Des.*, vol. 125, no. 2, pp. 221–232, Jun. 2003.

[123] Y. Aoues and A. Chateauneuf, "Benchmark study of numerical methods for reliability-based design optimization," *Struct. Multidiscip. Optim.*, vol. 41, no. 2, pp. 277–294, Mar. 2010.